

Università degli Studi di Napoli Federico II
Scuola Politecnica e delle Scienze di Base



Dottorato di Ricerca in
Ingegneria Strutturale, Geotecnica e Rischio Sismico
XXXVI ciclo

DOCTORAL THESIS

**STRUCTURAL ANALYSIS AND
BEHAVIOUR OF COMPLEX
MONUMENTAL BUILDINGS IN SEISMIC
AREAS:
THE ST. DOMENICO MAGGIORE
CONVENT IN NAPLES**

Paola Sorrentino

Thesis Advisor:
Prof. Antonello De Luca

December 2023

Cadendo, la goccia scava la pietra, non per la sua forza ma per la sua costanza.

Tito Lucrezio Caro

*“A te che non sei parte dell’immenso
ma è l’immenso che fa parte solo di te”*

E.G.

Negramaro, L’immenso

**STRUCTURAL ANALYSIS AND BEHAVIOUR OF COMPLEX
MONUMENTAL BUILDINGS IN SEISMIC AREAS:
THE ST. DOMENICO MAGGIORE CONVENT IN NAPLES**

Ph.D. Thesis presented
for the fulfilment of the Degree of Doctor of Philosophy
in Ingegneria Strutturale, Geotecnica e Rischio Sismico

by

Paola Sorrentino

December 2023

Università degli Studi di Napoli Federico II



Ph.D. Program in
Ingegneria Strutturale, Geotecnica e Rischio Sismico

XXXVI ciclo

Chairman: Prof. Iunio Iervolino

Thesis Advisor: Prof. Antonello De Luca

Acknowledgement

I would like to express my deep appreciation for the assistance and support I received from a number of individuals throughout the course of this research.

First and foremost, I extend my deepest gratitude to Prof. De Luca for providing me with the unique opportunity to study these remarkable Convents. His guidance and encouragement were invaluable, and I am profoundly grateful for the privilege of being his PhD student.

A sincere acknowledgment goes to Eng. Antonio L'Arciprete for his indispensable support during the modelling and analysis phases of the project. His expertise played a crucial role in the success of this research.

A special note of gratitude is reserved for Prof. Santiago Huerta for generously hosting me at the University of Madrid during this research.

I am particularly grateful to Arch. Orsola Foglia, Arch. Giuseppe Longobardi, Eng. Michele Candela and Prof. Claudio Grimellini for sharing their valuable experiences regarding the interventions on the Convent. Their insights and the wealth of information provided were instrumental in conducting a comprehensive historical analysis. Additionally, I extend my gratitude for the graphical drawings that proved instrumental during the survey phase.

I would also like to express my gratitude to Arch. Marianna Pedalino (Città Metropolitana di Napoli, Dirigente della Direzione Tecnica Scuole) and Arch. Annarita Marciano (Città Metropolitana di Napoli, Direzione Tecnica Scuole, Responsabile del Procedimento per l'intervento in oggetto) for granting permission to publish the results presented in this dissertation.

Paola Sorrentino

Abstract

This dissertation deals with the nonlinear structural behaviour of the Saint Domenico Convent, paradigmatic example of a Complex Monumental Building. Located in the historical centre of Naples, it consists of eight constructions built in different periods, ranging from the 8th to the 17th century, and having distinct features in terms of structural typology. Similar to many masonry buildings of this type, the convent has undergone a significant evolution over the years, with the addition of structural portions to existing ones, resulting in a highly complex configuration. The thesis, mainly devoted to the nonlinear behaviour of masonry structures, also provides an analysis of the historical evolution, along with alterations and changes in use. The analysis of such buildings has led to the proposal of a definition for complex monumental buildings. Even if characterized by a certain unity, these buildings differ from monumental buildings, like the Reggia di Caserta, Palazzo Farnese, or ecclesiastical monuments, that has an unity even if their construction spans over the years. Additionally, they cannot be assimilated to aggregate buildings, as first proposed by A. Giuffrè (1993) and later developed by numerous researchers, where the addition of structural portions to existing ones over the years is necessary to provide unity to urban development. In this dissertation, nonlinear analyses of the convent are carried out using a methodology intended for all complex buildings, that includes the analysis of the single structures, by neglecting the interaction with the others, and of the entire convent. In addition, it considers the analysis of the incremental addition of constructions. Nonlinear analyses conducted for seismic vulnerability assessment provide insights into the historical evolution and the impact of irregularities. The comparison of nonlinear behaviours and seismic vulnerability assessments in compliance with the N2 method provides results and methodologies that, in the author's opinion, can be extended to so-called complex monumental buildings. The results are also extended to another building analysed in the thesis, the San Carlo all'Arena convent in Naples. In conclusion, based on the results of the analyses presented in this dissertation, the author strongly advises a methodology for the analysis of complex monumental buildings that includes the analyses of the single constructions, of the entire convent and of the incremental addition of constructions.

Keywords: complex monumental buildings, nonlinear static analysis, N2 method, SAM method.

Sintesi in lingua italiana

Nella presente tesi viene affrontato lo studio del comportamento sismico del convento di San Domenico Maggiore a Napoli, paradigmatico esempio di edificio monumentale particolarmente articolato. L'edificio, come molti altri complessi dello stesso tipo, si è sviluppato nel tempo mediante successive addizioni e quindi presenta un'articolazione particolarmente complessa. Nella tesi viene presentato lo studio dell'evoluzione storica, unitamente alle manomissioni ed alterazioni, nonché alle diverse destinazioni d'uso. Tutto viene riguardato analizzando il comportamento non lineare delle strutture in muratura. L'analisi di edifici di questo tipo ha permesso nelle conclusioni di proporre la definizione di edifici monumentali complessi. Tali edifici, pur mantenendo una loro unitarietà, non possono identificarsi con edifici monumentali, quali ad esempio la Reggia di Caserta, Palazzo Farnese oppure monumenti di tipo ecclesiastico, dove la unitarietà dell'edificio la si riconosce, anche se la costruzione si è prolungata in più di un secolo. Al tempo stesso, pur non potendosi analizzare alla stessa maniera di questi edifici, essi presentano un'unitarietà che si differenzia dal concetto di edilizia in aggregato, proposto per la prima volta da A. Giuffrè (1993) e sviluppato successivamente da tanti ricercatori, dove l'aggregazione avviene per successive addizioni, solitamente necessaria per dare unità e continuità ad uno sviluppo urbanistico. Nella tesi vengono sviluppate le analisi non lineari del complesso con una metodologia, che si propone di utilizzare per tutti gli edifici complessi, che passa dall'analisi del singolo corpo di fabbrica, a quello della fabbrica nel suo complesso. Inoltre, tale metodologia include anche l'analisi strutturale dei corpi addizionati uno alla volta. Le analisi sviluppate per la valutazione della vulnerabilità sismica forniscono spunti sugli effetti dello sviluppo nel tempo di questi edifici e sugli effetti delle irregolarità. Il confronto, sia dei comportamenti non lineari che delle verifiche di vulnerabilità condotte secondo il metodo N2, fornisce sia risultati che metodologie che, a parere dell'autrice, possono essere estesi ad edifici cosiddetti complessi. I risultati vengono estesi anche ad un ulteriore edificio analizzato nella tesi di dottorato, il complesso di San Carlo all'Arena a Napoli. In conclusione, sulla base delle analisi presentate nella tesi, l'autrice raccomanda fortemente per l'analisi degli edifici monumentali complessi una metodologia che prevede l'analisi del singolo corpo di fabbrica, dell'intero edificio e dell'addizione dei vari corpi.

Parole chiave: edifici monumentali complessi, analisi statica non lineare, metodo N2, metodo SAM.

Contents

Introduction.....	23
1 The case study: St. Domenico Maggiore Convent in Naples.....	29
1.1 Description of the case study.....	29
1.1.1 Construction 0: Saint Thomas’s Dormitory	31
1.1.2 Construction 1: Master Dormitory.....	32
1.1.3 Construction 2: granaries	32
1.1.4 Construction 4.....	33
1.1.5 Construction 4’.....	33
1.1.6 Construction 5.....	34
1.1.7 Construction 6: the new novitiate	35
1.1.8 Construction 7: Saint Domenico’s cloister	35
1.2 Different occupancy of the convent.....	45
2 Historical evolution of the complex	51
2.1 The construction phases as outlined in Bianco et al. (2016).....	51
2.2 The 17th-century structural interventions	58
2.3 The modifications and alterations of the 19th and 20th centuries	58
2.4 The conservative restoration of the 21st century	59
2.5 The earthquakes experienced by the convent over the years	61
3 Preliminary considerations: the rules of art.....	63
3.1 Structural system: preliminary considerations	64

3.2	On the stability of the masonry walls as suggested in Rondelet (1802)	66
3.3	In-plan area ratio A_w/A_{tot}	70
3.4	On the arrangement of the openings	80
4	Structural analysis of masonry vaults	83
4.1	On the material to be used for the vaults as suggested in Breyman (1885)	84
4.2	On the construction methods as described in Breyman (1885).....	93
4.2.1	Barrel vaults	93
4.2.2	Cross vaults	95
4.2.3	Lowered cloister vaults	98
4.3	On the thickness of the vaults and piers as suggested by Colombo (1887)	100
4.4	Structural analysis of the vaults of Saint Domenico Maggiore Convent.....	103
4.4.1	Construction 0: barrel vault V^{0,A_2} (mezzanine floor)	104
4.4.2	Construction 0: cross vault $V^{0,2_2}$ (second floor).....	109
4.4.3	Construction 0: lowered cloister vault V^{0,T_2} (ground floor)	114
5	Structural modelling of complex masonry buildings	125
5.1	Strategies for modelling of masonry structures	126
5.1.1	One-dimensional macro-models	129
5.1.2	Two-dimensional macro-models.....	131
5.2	The SAM method.....	135
5.2.1	The pier element	135
5.2.2	The spandrel element	138
5.3	Simplified method in the framework of limit analysis.....	139
5.3.1	The simple portal	139
5.3.2	The multi-span masonry portal frames.....	141
5.3.3	The multi-bay multi-storey wall.....	143
6	Structural modelling of St. Domenico Convent in Naples.....	147

6.1	The strategy of modelling adopted for the St. Domenico Convent	148
6.2	Simplifications introduced in the structural models.....	148
6.3	Mechanical properties of material.....	150
6.4	Reference system	151
7	Non-linear behavior under horizontal loads	153
7.1	Non-linear Static Analysis of single Construction.....	154
7.2	Non-linear Static Analysis of entire Convent.....	201
7.3	Comparison between the single Construction and the entire Convent	206
8	Seismic vulnerability assessment of St. Domenico Convent	211
8.1	The N2 method: historical overview and procedure	211
8.2	Seismic Vulnerability Assessment of the Convent.....	215
8.2.1	Seismic vulnerability assessment of the single constructions	216
8.2.2	Seismic vulnerability assessment of the entire convent ..	227
8.3	Comparison of the results	230
9	Discussion	235
9.1	The procedure adopted for the seismic vulnerability assessment.	236
9.2	The extension of the procedure on the Saint Carlo all’Arena Convent in Naples	236
9.3	Non-linear behavior of the constructions of St. Domenico Maggiore Convent.....	247
9.4	Seismic vulnerability assessment of St. Domenico Convent	253
9.5	Simplified method to check the non-linear static analysis through the Limit Analysis.....	256
9.6	The impact of irregularities on the seismic vulnerability assessment	260
9.7	Proposal of definition of complex monumental building.....	270
	Conclusive Remarks	271

Appendix	
A1 The earthquake experienced by the convent over the years	273
A2 Wall alignments	281
A3 The Case Study of St. Carlo all’Arena Convent in Naples	297
A3.1 Description of the Case Study.....	298
A3.2 Historical evolution of the Convent.....	303
A3.2.1 The construction phases as outlined in Polcari (2018) ...	303
A3.2.2 The period following the 2016 Norcia Earthquake	306
A3.2.3 The different occupancy of the Convent.....	306
A3.3 Preliminary considerations: the rules of art.....	311
A3.3.1 Structural system: preliminary considerations	311
A3.3.2 On the stability of the masonry walls as suggested in Rondelet (1802).....	312
A3.3.3 In-plan area ratio A_W/A_{tot}	314
A3.3.4 On the arrangement of the openings.....	317
A3.4 Structural modelling of the convent.....	317
A3.4.1 Simplifications introduced in the structural models.....	318
A3.4.2 Mechanical properties of material	318
A3.4.3 Reference system.....	320
A3.5 Seismic vulnerability assessment.....	320
A3.5.1 Capacity curves.....	320
A3.5.2 Seismic vulnerability indexes.....	327
A3.5.3 Non-linear static analysis of 2D walls.....	335
A4 St. Carlo all’Arena Convent: Wall alignments	340
A5 The application of L.A. to check non-linear analysis through SAM method	347
A5.1 Application to a regular masonry wall.....	348
A5.2 Sensitivity analysis: compressive strength.....	350
A5.3 Application to generic masonry wall	352
Bibliography	397

List of Figures

Figure I.1. Saint Domenico Convent in Naples.	26
Figure I.2. Author's delineation and denomination of the structures.	27
Figure 1.1. Case study: Construction 0 (a), Construction 1 (b), Construction 2 (c), Construction 4 (d), Construction 4' (e), Construction 5 (f), Construction 6 (g), Construction 7 (h).	30
Figure 1.2. Construction 0: plan of the ground floor and cross section.	37
Figure 1.3. Construction 1: plan and cross section.	38
Figure 1.4. Construction 2: plan and cross section.	39
Figure 1.5. Construction 4: plan, cross section and frontal view.	40
Figure 1.6. Construction 4': plan and cross section.	41
Figure 1.7. Construction 5: plan and cross sections.	42
Figure 1.8. Construction 6: plan and cross section.	43
Figure 1.9. Construction 7: plan and cross section.	44
Figure 1.10. Different occupancy: ground floor.	46
Figure 1.11. Different occupancy: first floor.	47
Figure 1.12. Different occupancy: mezzanine floor.	48
Figure 1.13. Different occupancy: second floor.	49
Figure 2.1. Construction phases as outlined in Bianco (2012) and Bianco et al. (2016).	54
Figure 2.2. Lafrery maps (1566).	55
Figure 2.3. Braun and Hogenberg maps (1572).	56
Figure 2.4. Carafa maps (1775).	57

Figure 2.5. Chains in Refectory (a) and in Chapter Room (b).	58
Figure 2.6. Crack pattern following the 1980 Irpinia Earthquake (2001)..60	
Figure 2.7. Intensity of the seismic events experienced by the convent (https://emidius.mi.ingv.it/CPTI15-DBMI15/query_place/).....	62
Figure 3.1. Comparison between maximum slenderness and the limit suggested by Rondelet (1802).	70
Figure 3.2. A_w/A_{tot} ratio computed by Rondelet (1802).	71
Figure 3.3. In-plan ratio: Construction 0.	73
Figure 3.4. In-plan ratio: Construction 1.	74
Figure 3.5. In-plan ratio: Construction 2.	75
Figure 3.6. In-plan ratio: Construction 4.	76
Figure 3.7. In-plan ratio: Construction 6.	77
Figure 3.8. In-plan ratio: Construction 7.	79
Figure 4.1. Vaults' labels and location endoscopic analyses: Construction 0 – ground floor.	85
Figure 4.2. Vaults' labels and location endoscopic analyses: Construction 0 – mezzanine floor.	86
Figure 4.3. Vaults' labels and location endoscopic analyses: Construction 0 – second floor.	87
Figure 4.4. Vaults' labels and location endoscopic analyses: Construction 1 – ground floor.	88
Figure 4.5. Vaults' labels and location endoscopic analyses: Construction 1 – first floor.	89
Figure 4.6. Lowered cloister vault V^{0,T_2} : Endoscopic Analysis.	90
Figure 4.7. Barrel vault V^{0,A_2} : Endoscopic Analysis.	90
Figure 4.8. Cross vault $V^{0,2_2}$: Endoscopic Analysis.	91
Figure 4.9. Barrel vault V^{1,T_1} : Endoscopic Analysis.	91
Figure 4.10. Lowered cloister vault $V^{1,1_2}$: Endoscopic Analysis.	92
Figure 4.11. Cross vault $V^{1,1_1}$: Endoscopic Analysis.	92
Figure 4.12. Different arrangement of barrel vault: longitudinal (a) and herringbone arrangement (b); additional brick pattern for barrel vault (c) [8].	95

Figure 4.13. Cross vault: connection details [8].	96
Figure 4.14. Cross vault of construction 0 after the 1980 Irpinia Earthquake: herringbone arrangement.	98
Figure 4.15. Lowered cloister vault: herringbone arrangement [8].	99
Figure 4.16. Barrel vault V^{0,A_2} : Plan and Cross-Section.	105
Figure 4.17. Barrel vault V^{0,A_2} : Discretization.	106
Figure 4.18. Barrel vault V^{0,A_2} : Definition of Horizontal Thrust.	107
Figure 4.19. Barrel vault V^{0,A_2} : thrustline (a) and funicular polygon (b)..	108
Figure 4.20. Cross vault $V^{0,2_2}$: Plan and Cross-Section.	110
Figure 4.21. Cross vault $V^{0,2_2}$: Discretization.	111
Figure 4.22. Cross vault $V^{0,2_2}$: Definition of Horizontal Thrust.	112
Figure 4.23. Cross vault $V^{0,2_2}$: thrustline (a) and funicular polygon (b)...	113
Figure 4.24. Lowered cloister vault V^{0,T_2} : Plan and Cross-Section.	115
Figure 4.25. Lowered cloister vault V^{0,T_2} : Discretization.	116
Figure 4.26. Lowered cloister vault V^{0,T_2} : Definition of Horizontal Thrust.	117
Figure 4.27. Lowered cloister vault V^{0,T_2} : thrustline (a) and funicular polygon (b).	118
Figure 4.28. Lowered cloister vault V^{0,T_2} - minimum thrust: thrustline (a) and funicular polygon (b).	119
Figure 4.29. Lowered cloister vault $V^{0,T_2} - H = 23$ kN: thrustline (a) and funicular polygon (b).	120
Figure 4.30. Lowered cloister vault $V^{0,T_2} - H = 26$ kN: thrustline (a) and funicular polygon (b).	121
Figure 4.31. Lowered cloister vault $V^{0,T_2} - H = 29$ kN: thrustline (a) and funicular polygon (b).	122
Figure 5.1. Modelling strategies for masonry structures: (a) detailed micro-modelling; (b) simplified micro-modelling; and (c) macro-modelling [19].	127
Figure 5.2. Model proposed by Calderoni, 1987.	130
Figure 5.3. SAM model.	131

Figure 5.4. Braga and Liberatore model (1990).	132
Figure 5.5. D’Asdia and Viskovic method (1995).	133
Figure 5.6. Kinematic model for the macro-element (Gambarotta and Lagomarsino, 1996).	133
Figure 5.7. The basic macro-element proposed by Calìo et a. (2012): (a) undeformed configuration; and (b) deformed configuration.	134
Figure 5.8. Main in-plane failure mechanisms of a masonry portion: (a) flexural failure; (b) shear-diagonal failure; and (c) shear-sliding failure.	134
Figure 5.9. Simulation of the main in-plane failure mechanisms of a macro-element proposed by Calìo et al. (2012): (a) flexural failure; (b) shear-diagonal failure; and (c) shear sliding failure.	134
Figure 5.10. Definition of effective height proposed by Dolce (1989). ..	136
Figure 5.11. Piers failure mechanisms: diagonal cracking, sliding and bending failure/rocking.	137
Figure 5.12. Simple portal.	139
Figure 5.13. Possible crack pattern.	140
Figure 5.14. Collapse Mechanisms.	141
Figure 5.15. Multispan Masonry portal frame.	141
Figure 5.16. Multi-bay multi-storey wall	143
Figure 5.17. Frame mechanism: impossible collapse mechanism.	143
Figure 5.18. Global collapse mechanism: hypothesis of Como and Grimaldi.	144
Figure 5.19. Generic masonry wall: Condition loads.	145
Figure 5.20. Values of coefficient α for different condition loads.	146
Figure 6.1. Structural models of each Construction.	152
Figure 6.2. Structural model of the Convent.	152
Figure 7.1. <i>Construction 0</i> – Distribution of forces proportional to masses: capacity curves in terms of (a) forces vs displacements; (b) Forces divided by weight vs displacements divided by total height of the structure.	159
Figure 7.2. <i>Construction 0</i> – Distribution of forces proportional to the first vibration mode: capacity curves in terms of (a) forces vs	

displacements; (b) Forces divided by weight vs displacements divided by total height of the structure.	160
Figure 7.3. <i>Construction 0</i> – Failure Mechanism in (a) x and (b) y direction.	161
Figure 7.4. <i>Construction 0</i> – Capacity curves in terms of forces vs displacements of (a) 2D walls in x direction; (b) comparison between capacity curve of 2D walls and 3D structure in x direction. Capacity curves in terms of forces vs displacements of (c) 2D walls in y direction; (d) comparison between capacity curve of 2D walls and 3D structure in y direction.	163
Figure 7.5. <i>Construction 0</i> – Capacity curves in terms of Forces divided by weight vs displacements divided by total height of the structure of (a) 3D structure; (b) 2D walls; (c) comparison between capacity curve of 2D walls and 3D structure.....	165
Figure 7.6. <i>Construction 0 (wall 3x)</i> – Failure mechanisms and comparison between the simplified formula and the pushover curve in term of Forces divided by weight vs displacements divided by total height of the structure.....	166
Figure 7.7. <i>Construction 1</i> – Distribution of forces proportional to masses: capacity curves in terms of (a) forces vs displacements; (b) Forces divided by weight vs displacements divided by total height of the structure.....	167
Figure 7.8. <i>Construction 1</i> – Distribution of forces proportional to the first vibration mode: capacity curves in terms of (a) forces vs displacements; (b) Forces divided by weight vs displacements divided by total height of the structure.	168
Figure 7.9. <i>Construction 1</i> – Failure Mechanism in (a) x and (b) y direction.	169
Figure 7.10. <i>Construction 1</i> – Capacity curves in terms of forces vs displacements of (a) 2D walls in x direction; (b) comparison between capacity curve of 2D walls and 3D structure in x direction. Capacity curves in terms of forces vs displacements of (c) 2D walls in y direction; (d) comparison between capacity curve of 2D walls and 3D structure in y direction.	171
Figure 7.11. <i>Construction 1</i> – Capacity curves in terms of Forces divided by weight vs displacements divided by total height of the structure of	

	(a) 3D structure; (b) 2D walls; (c) comparison between capacity curve of 2D walls and 3D structure.	173
Figure 7.12.	<i>Construction 2</i> – Distribution of forces proportional to masses: capacity curves in terms of (a) forces vs displacements; (b) Forces divided by weight vs displacements divided by total height of the structure.	174
Figure 7.13.	<i>Construction 2</i> – Distribution of forces proportional to the first vibration mode: capacity curves in terms of (a) forces vs displacements; (b) Forces divided by weight vs displacements divided by total height of the structure.	175
Figure 7.14.	<i>Construction 2</i> – Failure Mechanism in (a) x and (b) y direction.	176
Figure 7.15.	<i>Construction 2</i> – Capacity curves in terms of forces vs displacements of (a) 2D walls in x direction; (b) comparison between capacity curve of 2D walls and 3D structure in x direction. Capacity curves in terms of forces vs displacements of (c) 2D walls in y direction; (d) comparison between capacity curve of 2D walls and 3D structure in y direction.	178
Figure 7.16.	<i>Construction 2</i> – Capacity curves in terms of Forces divided by weight vs displacements divided by total height of the structure of (a) 3D structure; (b) 2D walls; (c) comparison between capacity curve of 2D walls and 3D structure.	180
Figure 7.17.	<i>Construction 4</i> – Distribution of forces proportional to masses: capacity curves in terms of (a) forces vs displacements; (b) Forces divided by weight vs displacements divided by total height of the structure.	181
Figure 7.18.	<i>Construction 4</i> – Distribution of forces proportional to the first vibration mode: capacity curves in terms of (a) forces vs displacements; (b) Forces divided by weight vs displacements divided by total height of the structure.	182
Figure 7.19.	<i>Construction 4</i> – Failure Mechanism in (a) x and (b) y direction.	183
Figure 7.20.	<i>Construction 4</i> – Capacity curves in terms of forces vs displacements of (a) 2D walls in x direction; (b) comparison between capacity curve of 2D walls and 3D structure in x direction. Capacity curves in terms of forces vs displacements of (c) 2D walls in y direction; (d) comparison between capacity curve of 2D walls and 3D structure in y direction.	185

Figure 7.21. <i>Construction 4</i> – Capacity curves in terms of Forces divided by weight vs displacements divided by total height of the structure of (a) 3D structure; (b) 2D walls; (c) comparison between capacity curve of 2D walls and 3D structure.....	187
Figure 7.22. <i>Construction 6</i> – Distribution of forces proportional to masses: capacity curves in terms of (a) forces vs displacements; (b) Forces divided by weight vs displacements divided by total height of the structure.....	188
Figure 7.23. <i>Construction 6</i> – Distribution of forces proportional to the first vibration mode: capacity curves in terms of (a) forces vs displacements; (b) Forces divided by weight vs displacements divided by total height of the structure.	189
Figure 7.24. <i>Construction 6</i> – Failure Mechanism in (a) x and (b) y direction.	190
Figure 7.25. <i>Construction 6</i> – Capacity curves in terms of forces vs displacements of (a) 2D walls in x direction; (b) comparison between capacity curve of 2D walls and 3D structure in x direction. Capacity curves in terms of forces vs displacements of (c) 2D walls in y direction; (d) comparison between capacity curve of 2D walls and 3D structure in y direction.	192
Figure 7.26. <i>Construction 6</i> – Capacity curves in terms of Forces divided by weight vs displacements divided by total height of the structure of (a) 3D structure; (b) 2D walls; (c) comparison between capacity curve of 2D walls and 3D structure.....	194
Figure 7.27. <i>Construction 7</i> – Distribution of forces proportional to masses: capacity curves in terms of (a) forces vs displacements; (b) Forces divided by weight vs displacements divided by total height of the structure.....	195
Figure 7.28. <i>Construction 7</i> – Distribution of forces proportional to the first vibration mode: capacity curves in terms of (a) forces vs displacements; (b) Forces divided by weight vs displacements divided by total height of the structure.	196
Figure 7.29. <i>Construction 7</i> – Failure Mechanism in (a) x and (b) y direction.	197
Figure 7.30. <i>Construction 7</i> – Capacity curves in terms of forces vs displacements of (a) 2D walls in x direction; (b) comparison between capacity curve of 2D walls and 3D structure in x direction. Capacity	

curves in terms of forces vs displacements of (c) 2D walls in y direction; (d) comparison between capacity curve of 2D walls and 3D structure in y direction.	199
Figure 7.31. <i>Construction 7</i> – Capacity curves in terms of Forces divided by weight vs displacements divided by total height of the structure of (a) 3D structure; (b) 2D walls; (c) comparison between capacity curve of 2D walls and 3D structure.	201
Figure 7.32. Structural model of the Constructions C0-1-2-6-7.	202
Figure 7.33. <i>Constructions 0-1-2-6-7</i> – Distribution of forces proportional to masses: capacity curves in terms of (a) forces vs displacements; (b) Forces divided by weight vs displacements divided by total height of the structure.	203
Figure 7.34. <i>Constructions 0-1-2-6-7</i> – Distribution of forces proportional to the first vibration mode: capacity curves in terms of (a) forces vs displacements; (b) Forces divided by weight vs displacements divided by total height of the structure.	204
Figure 7.35. <i>Construction 0-1-2-6-7</i> : Failure Mechanism in (a) x and (b) y direction.	205
Figure 7.36. <i>Mass (x direction)</i> . Comparison between capacity curve of single construction and the entire convent in terms of (a) forces vs displacements; (b) Forces divided by weight vs displacements divided by total height of the structure.	207
Figure 7.37. <i>Mass (y direction)</i> . Comparison between capacity curve of single construction and the entire convent in terms of (a) forces vs displacements; (b) Forces divided by weight vs displacements divided by total height of the structure.	208
Figure 7.38. <i>Mode (x direction)</i> . Comparison between capacity curve of single construction and the entire convent in terms of (a) forces vs displacements; (b) Forces divided by weight vs displacements divided by total height of the structure.	209
Figure 7.39. <i>Mode (y direction)</i> . Comparison between capacity curve of single construction and the entire convent in terms of (a) forces vs displacements; (b) Forces divided by weight vs displacements divided by total height of the structure.	210
Figure 8.1. Idealization of the force-displacement relationship of the equivalent SDOF system into an elasto – plastic form.	215
Figure 8.2. Seismic demand for (a) $T * > T_c$ (a) and (b) $T * < T_c$	215

Figure 8.3. <i>Construction 0</i> : ADRS Spectrum in (a) x and (b) y direction. .	217
Figure 8.4. <i>Construction 1</i> : ADRS Spectrum in (a) x and (b) y direction. .	218
Figure 8.5. <i>Construction 2</i> : ADRS Spectrum in (a) x and (b) y direction. .	219
Figure 8.6. <i>Construction 4</i> : ADRS Spectrum in (a) x and (b) y direction. .	220
Figure 8.7. <i>Construction 6</i> : ADRS Spectrum in (a) x and (b) y direction. .	221
Figure 8.8. <i>Construction 7</i> : ADRS Spectrum in (a) x and (b) y direction. .	222
Figure 8.9. <i>Construction 0</i> : Seismic Vulnerability Indexes.	224
Figure 8.10. <i>Construction 1</i> : Seismic Vulnerability Indexes.	224
Figure 8.11. <i>Construction 2</i> : Seismic Vulnerability Indexes.	225
Figure 8.12. <i>Construction 4</i> : Seismic Vulnerability Indexes.	225
Figure 8.13. <i>Construction 6</i> : Seismic Vulnerability Indexes.	226
Figure 8.14. <i>Construction 7</i> : Seismic Vulnerability Indexes.	226
Figure 8.15. <i>Construction 7</i> : ADRS Spectrum in (a) x and (b) y direction.	228
Figure 8.16. <i>Constructions 0-1-2-6-7</i> : Seismic Vulnerability Indexes.	229
Figure 8.17. Comparison between Seismic Vulnerability Indexes of the single construction and the entire convent.	231
Figure 8.18. Comparison between Seismic Vulnerability Indexes of the single construction and the entire convent: x direction.	232
Figure 8.19. Comparison between Seismic Vulnerability Indexes of the single construction and the entire convent: y direction.	232
Figure 9.1. San Carlo all’Arena Convent in Naples.	237
Figure 9.2. Plan of the first floor.	238
Figure 9.3. Structural models of each construction.	239
Figure 9.4. Structural model of the Convent.	239
Figure 9.5. <i>Mass (x direction)</i> . Comparison between capacity curve of single construction and the entire convent in terms of (a) forces vs displacements; (b) Forces divided by weight vs displacements divided by total height of the structure.	241
Figure 9.6. <i>Mass (y direction)</i> . Comparison between capacity curve of single construction and the entire convent in terms of (a) forces vs	

displacements; (b) Forces divided by weight vs displacements divided by total height of the structure.	242
Figure 9.7. <i>Mode (x direction)</i> . Comparison between capacity curve of single construction and the entire convent in terms of (a) forces vs displacements; (b) Forces divided by weight vs displacements divided by total height of the structure.	243
Figure 9.8. <i>Mode (y direction)</i> . Comparison between capacity curve of single construction and the entire convent in terms of (a) forces vs displacements; (b) Forces divided by weight vs displacements divided by total height of the structure.	244
Figure 9.9. Comparison between Seismic Vulnerability Indexes of the single construction and the entire convent.	245
Figure 9.10. <i>Mass (x direction)</i> . The impact of adding new structures to the existing ones on the capacity curves in terms of (a) forces vs displacements; (b) Forces divided by weight vs displacements divided by total height of the structure.	249
Figure 9.11. <i>Mass (y direction)</i> . impact of adding new structures to the existing ones on the capacity curves in terms of (a) forces vs displacements; (b) Forces divided by weight vs displacements divided by total height of the structure.	250
Figure 9.12. <i>Mode (x direction)</i> . The impact of the addition of Constructions on the capacity curve in terms of (a) forces vs displacements; (b) Forces divided by weight vs displacements divided by total height of the structure.	251
Figure 9.13. <i>Mode (y direction)</i> . The impact of adding new structures to the existing ones on the capacity curves in terms of (a) forces vs displacements; (b) Forces divided by weight vs displacements divided by total height of the structure.	252
Figure 9.14. The effect of the addition of Constructions on the seismic vulnerability indexes.	254
Figure 9.15. Comparison between Seismic Vulnerability Indexes in x direction.	255
Figure 9.16. Comparison between Seismic Vulnerability Indexes in y direction.	255
Figure 9.17. Horizontal collapse multipliers: (a) Construction 0; (b) Construction 1 and (c) San Carlo all’Arena.	258

Figure 9.18. Scatter between the proposed formula and the pushover analysis.....	259
Figure 9.19. Variation of forces in the x direction (blue line) and y direction (red line), and weight variation (green line) at the fifth floor due to the addition of constructions.....	263
Figure 9.20. Analised wall: 8y.	264
Figure 9.21. Evolution of plastic hinges of the wall 8y of the C0.	267
Figure 9.22. Evolution of plastic hinges of the wall 8y of the C0: comparison between the analysis of C0 and of C0-1-2-6-7.....	268
Figure 9.23. Collapse mechanism of the wall 8y of the C0: comparison between the analysis of C0 and of C0-1-2-6-7.....	269
Figure A2.1. <i>Construction 0</i> : wall alignments – plan.....	281
Figure A2.2. <i>Construction 0</i> : wall alignments – x direction.	282
Figure A2.3. <i>Construction 0</i> : wall alignments – y direction.....	284
Figure A2.4. <i>Construction 1</i> : wall alignments – plan.....	285
Figure A2.5. <i>Construction 1</i> : wall alignments.....	287
Figure A2.6. <i>Construction 2</i> : wall alignments – plan.....	288
Figure A2.7. <i>Construction 2</i> : wall alignments.....	288
Figure A2.8. <i>Construction 4</i> : wall alignments – plan.....	289
Figure A2.9. <i>Construction 4</i> : wall alignments.....	289
Figure A2.10. <i>Construction 6</i> : wall alignments – plan.....	290
Figure A2.11. <i>Construction 6</i> : wall alignments – x direction.	291
Figure A2.12. <i>Construction 6</i> : wall alignments – y direction.....	292
Figure A2.13. <i>Construction 7</i> : wall alignments – plan.....	293
Figure A2.14. <i>Construction 7</i> : wall alignments.....	296
Figure A3.1. San Carlo all’Arena Convent in Naples.....	298
Figure A3.2. Plan (a) and Cross-Sections A-A(b) and B-B (c).....	301
Figure A3.3. Façade facing Via Foria: the adjacent constructions.....	302
Figure A3.4. Dome of the church: internal (a) and external view (b).	302
Figure A3.5. Connection between the Convent and the Church.	303

Figure A3.6. Façade on via Foria (De Cesare F., 1837. <i>Sull'origine delle lesioni della chiesa di San Carlo Borromeo in Napoli e suo progetto di ricostruzione</i>) (a); Current state of the Façade on via Foria (b).	304
Figure A3.7. Historical evolution of the Convent: plan (a) and façade (b).	305
Figure A3.8. Newspaper articles: il Corriere del Mezzogiorno (8/11/2016) (a) Metronapoli.it (14/12/2017).....	306
Figure A3.9. Different occupancy: ground floor (a); mezzanine floor (b); first floor (c); mezzanine floor (d); second floor (e); third floor (f); and façade (g).	310
Figure A3.10. Comparison between maximum slenderness and the limit suggested by Rondelet (1802).....	313
Figure A3.11. In-plan ratio.....	316
Figure A3.12. Wall 18y: the issue of the added openings.	317
Figure A3.13. Structural models of each construction.	319
Figure A3.14. Structural model of the Convent.	319
Figure A3.15. <i>Mass (x direction)</i> . Comparison between capacity curve of single construction and the entire convent in terms of (a) forces vs displacements; (b) Forces divided by weight vs displacements divided by total height of the structure.	323
Figure A3.16. <i>Mass (y direction)</i> . Comparison between capacity curve of single construction and the entire convent in terms of (a) forces vs displacements; (b) Forces divided by weight vs displacements divided by total height of the structure.	324
Figure A3.17. <i>Mode (x direction)</i> . Comparison between capacity curve of single construction and the entire convent in terms of (a) forces vs displacements; (b) Forces divided by weight vs displacements divided by total height of the structure.	325
Figure A3.18. <i>Mode (y direction)</i> . Comparison between capacity curve of single construction and the entire convent in terms of (a) forces vs displacements; (b) Forces divided by weight vs displacements divided by total height of the structure.	326
Figure A3.19. Comparison between Seismic Vulnerability Indexes of the single construction and the entire convent.....	329
Figure A3.20. <i>Construction 1</i> . ADRS Spectrum in (a) x and (b) y direction.	330

Figure A3.21. <i>Construction 2</i> . ADRS Spectrum in (a) x and (b) y direction.	331
Figure A3.22. <i>Construction 3</i> . ADRS Spectrum in (a) x and (b) y direction.	332
Figure A3.23. <i>Construction 4</i> . ADRS Spectrum in (a) x and (b) y direction.	333
Figure A3.24. <i>Complex</i> . ADRS Spectrum in (a) x and (b) y direction.	334
Figure A3.25. <i>X direction</i> : Capacity curve of 2D walls in terms of (a) forces vs displacements; comparison between capacity curve of 2D walls and 3D structure in terms of (b) forces vs displacements; (c) Forces divided by weight vs displacements divided by total height of the structure.....	337
Figure A3.26. <i>Y direction</i> : Capacity curve of 2D walls in terms of (a) forces vs displacements; comparison between capacity curve of 2D walls and 3D structure in terms of (b) forces vs displacements; (c) Forces divided by weight vs displacements divided by total height of the structure.....	338
Figure A3.27. <i>Y direction</i> : Capacity curve of 2D walls in terms of forces vs displacements: zoom.	339
Figure A4.1. <i>San Carlo all’Arena Convent</i> : wall alignments – plan.....	340
Figure A4.2. <i>San Carlo all’Arena Convent</i> : wall alignments – x direction. .	343
Figure A4.3. <i>San Carlo all’Arena Convent</i> : wall alignments – y direction...	346
Figure A5.1. Analysed masonry wall.	348
Figure A5.2. Pushover curves (continue red line) and comparison with the simplified formula (dashed red line), B_{min}/H (dashed blue line) and B_{max}/H (dashed green line): regular wall.	349
Figure A5.3. Pushover curves in terms of $F - d$ (a) and comparison between the pushover curves and the simplified formula (dashed red line), B_{min}/H (dashed blue line) and B_{max}/H (dashed green line) for different values of fd	351
Figure A5.4. Scatter between the results obtained with the pushover analysis and the simplified formula.	352
Figure A5.5. Analysed walls: San Domenico Maggiore – Construction 0.	356

Figure A5.6. Analysed walls: San Domenico Maggiore – Construction 1.	358
Figure A5.7. Analysed walls: San Carlo all’Arena.....	362
Figure A5.8. <i>Construction 0</i> . Pushover curves and comparison with the simplified formula (dashed red line), $B_{\min}/\alpha H$ (dashed blue line) and $B_{\max}/\alpha H$ (dashed green line): (a) 3x; (b) 4x; (c) 5x; (d) 6x.	370
Figure A5.9. <i>Construction 1</i> . Pushover curves and comparison with the simplified formula (dashed red line), $B_{\min}/\alpha H$ (dashed blue line) and $B_{\max}/\alpha H$ (dashed green line): (a) 1x; (b) 2x; (c) 3x; (d) 4x.	378
Figure A5.10. <i>San Carlo all’Arena</i> . Pushover curves and comparison with the simplified formula (dashed red line), $B_{\min}/\alpha H$ (dashed blue line) and $B_{\max}/\alpha H$ (dashed green line): (a) 1x; (b) 2x; (c) 3x; (d) 4x; (e) 12x; (f) 13x; (g) 14x; (h) 15x; (i) 16x.	396

List of Tables

Table 1.1. Different occupancy of the convent.	50
Table 3.1. Comparison between wall thickness and the rules of art: C0. ..	68
Table 3.2. Comparison between wall thickness and the rules of art: C1. ..	68
Table 3.3. Comparison between wall thickness and the rules of art: C2. ..	68
Table 3.4. Comparison between wall thickness and the rules of art: C4. ..	68
Table 3.5. Comparison between wall thickness and the rules of art: C6. ..	69
Table 3.6. Comparison between wall thickness and the rules of art: C7. ..	69
Table 3.7. In-plan ratios for analysed structures.	80
Table 4.1. Keystones at the crown and springers at the impost for barrel vault supporting floors with ordinary loads.	100
Table 4.2. Keystones at the crown and springers at the impost for cross vault and lowered cloister vault supporting ordinary loads.	101
Table 4.3. Keystones at the crown.	102
Table 4.4. Width of piers.	102
Table 4.5. Barrel vault V^{0,A_2} : Weights of voussoirs.	106
Table 4.6. Cross vault $V^{0,2}$: Weights of voussoirs.	111
Table 4.7. Weights of voussoirs.	116
Table 4.8. Summary of results.	124
Table 6.1. Height of the floors considered for the structural models.	150
Table 6.2. Mechanical properties of the tuff.	150
Table 7.1. <i>Distribution of forces proportional to the masses</i> : Maximum values of forces and displacement and of F/W and d/H ratios in x and y direction.	158

Table 7.2. <i>Distribution of forces proportional to the first vibration mode</i> : Maximum values of forces and displacement and of F/W and d/H ratios in x and y direction.....	158
Table 7.3. <i>Distribution of forces proportional to the masses</i> : Maximum values of forces and displacement and of F/W and d/H ratios in x and y direction.	202
Table 7.4. <i>Distribution of forces proportional to the masses</i> : Maximum values of forces and displacement and of F/W and d/H ratios in x and y direction.	202
Table 8.1. Seismic Vulnerability Indexes of single constructions.....	227
Table 8.2. Seismic Vulnerability Indexes of Construction C0-1-2-6-7.	229
Table 8.3. Comparison between Seismic Vulnerability Indexes of the single construction and the entire convent.....	233
Table 9.1. Scatter between the proposed formula and the pushover analysis.	259
Table 9.2. Modal forces at various floors: C0.....	261
Table 9.3. Modal forces at various floors: C0-1.	261
Table 9.4. Modal forces at various floors: C0-1-7.....	262
Table 9.5. Modal forces at various floors: C0-1-6-7.	262
Table 9.6. Modal forces at various floors: C0-1-2-6-7.....	262
Table A1.1 – Earthquake experienced by the convent from 13th century.	274
Table A3.1. Different occupancy of St. Carlo all’Arena convent.	311
Table A3.2. Comparison between wall thickness and the rules of art.	313
Table A3.3. In-plan ratios for the analysed structure.	314
Table A3.4. Mechanical properties of the tuff.....	318
Table A3.5. <i>Distribution of forces proportional to the masses</i> : Maximum values of forces and displacement and of F/W and d/H ratios in x and y direction.	322
Table A3.6. <i>Distribution of forces proportional to the first vibration mode</i> : Maximum values of forces and displacement and of F/W and d/H ratios in x and y direction.....	322
Table A3.7. Seismic Vulnerability Indexes.....	327

Table A5.1. Regular wall: width of pier (the minimum in bold and the maximum in italics) and weighted average of the width in meters.	349
Table A5.2. Regular wall: weights expressed in tons, equivalent height in meters and the simplified proposed formula in comparison with the minimum and the maximum ratio.	349
Table A5.3. Mechanical properties of the masonry.	350
Table A5.4. <i>Construction 0</i> . Wall weights, coefficient α , overall height and equivalent height.	353
Table A5.5. <i>Construction 1</i> . Wall weights, coefficient α , overall height and equivalent height.	353
Table A5.6. <i>San Carlo all’Arena</i> . Wall weights, coefficient α , overall height and equivalent height.	353
Table A5.7. <i>Construction 0</i> . Minimum, maximum and weighted average value and the outcomes of the simplified formula.	354
Table A5.8. <i>Construction 1</i> . Minimum, maximum and weighted average value and the outcomes of the simplified formula.	354
Table A5.9. <i>San Carlo all’Arena</i> . Minimum, maximum and weighted average value and the outcomes of the simplified formula.	354

Introduction

This dissertation deals with the nonlinear structural behaviour of the Saint Domenico Convent in Naples (Figure I.1). Situated within the historical centre of Naples, the convent case study represents a seminal case of Complex Masonry Buildings. Similar to many masonry buildings of this type, the convent has undergone a significant evolution over the years, resulting from the addition of various constructions in different periods, ranging from the 8th to the 17th century. Specifically, the convent comprises eight constructions, each characterized by distinct features in terms of structural typology. Figure I.2 visually presents the author's delineation and denomination of these structures, a fundamental framework serving as the basis for the ensuing analyses showcased in this dissertation.

The thesis, mainly devoted to the nonlinear behaviour of masonry structures, also provides an analysis of the historical evolution, along with alterations and changes in use. The plan is the following.

In Chapter 1, a comprehensive depiction of the case study is offered. A description of each individual construction is presented, highlighting the interconnections between each structural entity and the overall convent. Additionally, an overview of the various function and uses within the convent, coupled with the evolution of these uses over the years, is provided.

In Chapter 2, the historical evolution that the convent has experienced, starting from the 8th century, when the original structure was built, and extending through the 20th century, is outlined. Specifically, a detailed account of the construction phases, as outlined in Bianco et al. (2016), is provided and all the modifications and alterations that the complex has undergone over the years are documented.

In Chapter 3, some preliminary considerations about the structural layout of the constructions are offered based on the analysis of geometrical data, as the architectural plan and perspective view of the walls. These considerations aim to the analysis of the construction quality of the convent, that is evaluated in terms of its adherence to “the rules of art”, delineated in significant ancient treatise, as the treatise by Rondelet (1802), Breyman (1885), Cavalieri San Bertolo (1839) and Leon Battista Alberti (1452).

In Chapter 4, the structural analysis of the masonry vaults of the Saint Domenico Maggiore Convent in Naples is provided. The analysis focuses

on assessing adherence to the guidelines outlined in Breymann's treatise (1885) regarding materials and construction methods for vaults, along with compliance with Colombo's Manual of Engineer (1887) prescriptions concerning vault and pier thickness. Following the evaluation of vault adherence to the "rules of art", the analysis of the stability of the vaults under vertical loads is presented, according to Méry's method (1840).

In Chapter 5, a brief description of the main strategies for modelling of masonry structures is presented, with a specific focus on the SAM approach. This approach is implemented into the CDS-Win software used for nonlinear static analyses of the Convent. Additionally, the Chapter outlines the simplified method developed by the research group within the framework of limit analysis. In particular, the simplified formulas proposed to predict the horizontal capacity of various structures, including single portal frames (Giordano et al., 2007), multi-bay masonry portals (Giordano et al., 2006), and multistorey unreinforced masonry frames (Lucibello, 2013, and Mazziotti, 2015), are briefly discussed.

Due to the complexity of the Convent and to gain a deeper understanding of the structural behaviour, nonlinear analyses are performed using a methodology intended for all complex buildings. This procedure includes the analysis of the single construction, by neglecting the interaction with the others, and the analysis of the entire convent as a unified structure, assuming perfect interaction among all the constructions. In addition, 2D walls analyses within each construction are performed, with the aim to identify the weakest wall alignment that lead to the collapse of the structure and the local crises.

In Chapter 6, a comprehensive description of the structural models of the Saint Domenico Convent in Naples is outlined. Initially, the chosen modelling strategy is discussed, followed by an exploration of the simplifications applied to the structural models of each construction and the entire convent. This section also provides the mechanical properties of the materials and information on the reference systems used for each structural model.

In Chapter 7, the results of nonlinear static analyses of each construction and of the entire convent are provided in terms of capacity curves and failure mechanisms. Additionally, a comparative analysis between the capacity curve of the 3D structure and the 2D walls is provided. To validate the results obtained with nonlinear static analysis through the SAM method, the analysis of 2D walls are compared with the results obtained with the simplified formula proposed by the research group in the framework of limit analysis.

In Chapter 8, the results in terms of Seismic Vulnerability Indexes for the analysed constructions are given. In particular, The graphical representation of the application of the N2 method by Fajfar is presented, along with seismic vulnerability indexes for both individual constructions and the entire convent.

In Chapter 9, a discussion of the results presented in this dissertation is outlined. The comparison of nonlinear behaviours and seismic vulnerability assessments in compliance with the N2 method provides results and methodologies that, in the author's opinion, can be extended to so-called complex monumental buildings. The results are also extended to another building analysed in the thesis, the San Carlo all'Arena convent in Naples.

In conclusion, a proposal of definition of complex monumental buildings is formulated, accompanied by an identification of their typical complexities. Even if characterized by certain unity, these buildings differ from monumental buildings, such as the Reggia di Caserta, Palazzo Farnese, or ecclesiastical monuments, that has an unity even if their construction spans over the years. Moreover, they cannot be assimilated to aggregate buildings, as first proposed by A. Giuffrè (1993) and subsequently developed by various researchers, where the addition of structural portions over the years is necessary to provide unity to urban development.



(a)



(b)

Figure I.1. Saint Domenico Convent in Naples.

Chapter 1

The case study: St. Domenico Maggiore Convent in Naples

The present dissertation deals with the nonlinear structural behaviour of the Saint Domenico Convent in Naples. Located in the historical centre of Naples, the convent consists of eight constructions, built in different periods, spanning from the 8th to the 17th century, and having different features in terms of structural typology.

Within this chapter, a comprehensive depiction of the case study is offered. In particular, the description of each individual construction is presented, highlighting the interconnections between each structural entity and the overall convent. Furthermore, an overview of the various function and uses within the convent is provided.

1.1 Description of the case study



(a)



(b)



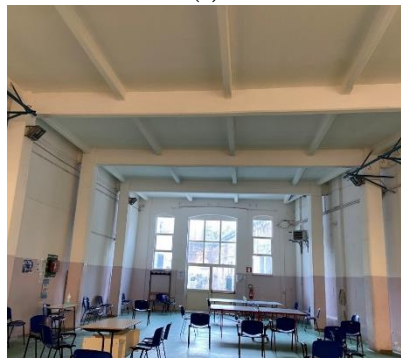
(c)



(d)



(e)



(f)



(g)



(h)

Figure 1.1. Case study: Construction 0 (a), Construction 1 (b), Construction 2 (c), Construction 4 (d), Construction 4' (e), Construction 5 (f), Construction 6 (g), Construction 7 (h).

1.1.1 Construction 0: Saint Thomas's Dormitory

The Saint Thomas Dormitory (Figure 1.1a) is characterized by a rectangular plan, approximately 87m x 17m, and consists of four storeys above the ground level, including a mezzanine, and a basement below. The overall building height is 23.16m. The walls are made of Neapolitan yellow tuff, varying in thickness from 285cm, at the ground floor, to 30cm thick at the 4th level. The horizontal floors are marked by different typologies of vault, including barrel, cross, sail and lowered cloister vaults.

The Construction 0 is linked for a length of 11m to the Northeast with the Construction 1, consisting of three storeys above the ground level and a basement level. On its Southern side, it joins with Construction 6, having three storeys above the ground level and a basement level, for a length of 15.0m. To the North, it connects to a part of Construction 7, characterized by four storeys above the ground level, including a mezzanine, for a length of 24.50m. Furthermore, it is linked to East with the Saint Domenico cloister (Construction 7), having two storeys above the ground level, for a length of 40m.

The first two levels and the basement of the Constructions 0 and 1, built in the same period, exhibit similar characteristics with floors at the same height. In particular, both the ground floor, located at a height of +38.50 m.a.s.l., and the first floor, at a height of +44.00 m.a.s.l., are constructed with tuff masonry and are characterized by various types of vaults (barrel, sail, and lowered cloister vaults). However, the third level of Construction 1, although built during the same period as Construction 0, shows differences in both construction type and floor height. Specifically, the third level of Construction 1 is made of tuff masonry, featuring r.c. frames and floor of steel beams, and has a floor height of +50.15 m.a.s.l.. The interstorey-height is 4.50m. In contrast, the third level of Construction 0 is made of tuff masonry, and its floors consist of various typologies of vaults (lowered cloister vaults for the classrooms, cross vaults for the central corridor). This level is located at a height of +52.95 m.a.s.l. and has a interstorey-height of 4.55m in the classrooms and 7.46 meters in the central corridor.

The part of Construction 7 to the North, adjacent to Construction 0, shows variations in floor heights compared to the latter: it has a ground floor at a lower height of +36.25 m.a.s.l., the first-floor level at the same height of +44.00 m.a.s.l., a mezzanine floor at a slightly lower height of +48.77 m.a.s.l. (compared to +48.85 m.a.s.l. for the mezzanine floor of Construction 0), the second-floor level at the same height of +52.95

m.a.s.l., and a roof at a higher height than the adjacent part of the classrooms, measuring +58.90 m.a.s.l. (compared to +58.15 m.a.s.l. for the side part of Construction 0).

Similarly, the adjacent Construction 6 has floors at different height compared to the Construction 0. Specifically, its ground floor is located at a height of +40.15 m.a.s.l., the first floor at +44.35 m.a.s.l., the mezzanine at +48.80 m.a.s.l., and the roof at +53.10 m.a.s.l.

Plan and cross section are plotted in Figure 1.2.

1.1.2 Construction 1: Master Dormitory

The Master Dormitory (Figure 1.1b) is characterized by a rectangular plan, approximately 81m x 11m, and consists of three storeys above the ground level, and a basement below. The overall building height is 17.50m. The walls are made of Neapolitan yellow tuff, varying in thickness from 140cm, at the ground floor, to 35cm thick at the 3rd level. The horizontal floors are marked by different typologies of vault on the first two floor, including barrel, cross and lowered cloister vaults. The 3rd floor is characterized by r.c. frames, with columns and beams having sections of 30x30 and 30x70 respectively. The roof is composed of steel beams.

The Construction 1 is linked for a length of 11m to the Northeast with the Construction 0, consisting of four storeys above the ground level, including a mezzanine, and a basement level. On its Southern side, it joins with Construction 2, having one storeys above the ground level and a basement level, for a length of 7.0m. To the North, it connects to a part of Construction 7, characterized by three storey above the ground level, for a length of 21.0m.

As described in the previous section, the first two levels and the basement of the Constructions 0 and 1, built in the same period, exhibit similar characteristics with floors at the same height. However, the third level of Construction 1, although built during the same period as Construction 0, shows differences in both construction type and floor height.

The part of Construction 7, adjacent to Construction 1, has floor at the same height.

Plan and cross section are plotted in Figure 1.3.

1.1.3 Construction 2: granaries

The Construction 2 (Figure 1.1c), originally the granaries of the convent, is characterized by trapezoidal plan with a length of approximately 40m, a

shorter base of about 7m, and a longer base of about 14m, resulting in a total area of 428m². The structure consists of two levels, one of which is a basement level facing the courtyard of the Casanova Institute, and an above-ground level facing Via San Sebastiano. The overall height of the building is equal to 6.85m, of which 5.25m pertain to the upper floor. The walls are made of Neapolitan yellow tuff and exhibit varying thickness, ranging from 135cm to 60cm thick. The central columns are made of red brick with a cross-section of 80x80cm. The roof is composed of steel beams.

The Construction 2 is connected for a length of 7m to the North with the Construction 1, consisting of three storeys above the ground level and a basement level. On its Southern side, it adjoins with Construction 4', having one storey above the ground level, for a length of 3.10m.

The ground level of the Construction 2 is located at a height of +38.95 m.a.s.l., differing from the ground floor of the neighbouring Construction 4', which aligns with the courtyard height at +37.35 m.a.s.l.

Plan, cross section and frontal view are plotted in Figure 1.4.

1.1.4 Construction 4

The Construction 4 (Figure 1.1d) is characterized by a rectangular plan, approximately 46mx9m, resulting in a total area of 423m². The structure consists of one level, with an overall height of 6.0m. The walls are made of Neapolitan yellow tuff with a thickness of 50cm. The roof is composed of steel beams.

The Construction 4 is connected for a length of 4.70m to the South with the Construction 4' and for a length of 19.45m to the East with the Construction 5, both consisting of one storey above the ground level.

The ground level of the Construction 4 is aligned with the courtyard height at +37.35 m.a.s.l., as the neighbouring Construction 4'. In contrast, the adjacent Construction 5 is characterized by a ground floor at a higher height equal to +37.85 m.a.s.l.

Plan, cross section and frontal view are plotted in Figure 1.5.

1.1.5 Construction 4'

The Construction 4' (Figure 1.1e) is a mixed masonry-r.c. building characterized by a rectangular plan, with an area of 135m². The structure consists of one level, with an overall height of 6.15m. The walls are made of Neapolitan yellow tuff, with variable thickness ranging from 135cm to

45cm. The r.c. frames are arranged in both orthogonal directions, with a distance between axes ranging from 3.70 m to 5.03m. The columns have a cross-section of 40x40cm, while the beams exhibit cross-sectional dimensions of 25x35 cm in the transverse direction and 20x25 cm longitudinally. The floor consists of r.c. slab with a thickness of 10 cm.

Construction 4' is connected for a length of 4.70m to the North with Construction 4, which consists of one storey above the ground level, and for a length of 3.10m to the West with Construction 2, having one storey above the ground level and a basement level.

The ground level of Construction 4' is aligned with the courtyard height at +37.35 m.a.s.l., as the neighbouring Construction 4. In contrast, the adjacent Construction 2 is characterized by a ground floor at a higher height equal to +38.95 m.a.s.l.

Plan and cross sections are plotted in Figure 1.6.

1.1.6 Construction 5

The Construction 5 (Figure 1.1f) is a mixed masonry - r.c. building characterized by a trapezoidal plan with a length of approximately 20m, a shorter base of about 9m, and a longer base of about 13m, resulting in a total area of 210m². The structure consists of one level, with an overall height of 6.15m. The walls are made of Neapolitan yellow tuff, with variable thickness ranging from 70cm to 35cm. The r.c. frames are arranged only in transversal direction, with a distance between axes ranging from 3.40m and 3.80m and variable span from 7.50 m to 10.0m. The columns have a cross-section of 40x40cm, while the beams exhibit cross-sectional dimension of 20x60cm. The floor consists of r.c. slab with a thickness of 20 cm.

Construction 5 is connected for a length of 19.25m to the Southeast with Construction 6, which consists of three storey above the ground level and a basement level, and for a length of 19.45m to the West with Construction 4, having one storey above the ground level.

Construction 5 is characterized by a ground floor at a higher height than the courtyard, equal to +37.85 m.a.s.l.. The ground floor of the neighbouring Construction 4 is aligned with the courtyard height at +37.35 m.a.s.l. while the adjacent Construction 6 have a ground floor at a higher height equal to +40.15 m.a.s.l..

Plan and cross sections are plotted in Figure 1.7.

1.1.7 Construction 6: the new novitiate

The New Novitiate (Figure 1.1g) is characterized by a rectangular plan, approximately 43mx15m, and consists of three storeys above the ground level and a basement below. The overall building height is 15.35m. The walls are made of Neapolitan yellow tuff, varying in thickness from 95cm, at the ground floor, to 50cm thick at the 3rd level. The horizontal floors are composed of steel beams, while at the basement level, there are barrel vaults, and at the 3rd level, two cross vaults can be found.

The Construction 6 is linked for a length of 15m to the North with Construction 0, consisting of four storeys above the ground level, including a mezzanine, and a basement below. Towards the Northeast, it is adjacent to Construction 5, having one storey above the ground level, for a length of 19.15m.

The floors of Construction 6 differ in height from those of the adjacent Construction 0. Specifically, the ground floor is located at a height of +40.15 m.a.s.l., the first floor at +44.35 m.a.s.l., the mezzanine floor at +48.80 m.a.s.l., and the roof at +53.10 m.a.s.l. In contrast, for Construction 0, the ground floor is at a height of +38.50 m.a.s.l., the first floor at +44.00 m.a.s.l., the mezzanine floor at +48.85 m.a.s.l., the second floor at +52.95 m.a.s.l., and the roof of the side sections at +58.15 m.a.s.l.

Plan and cross sections are plotted in Figure 1.8.

1.1.8 Construction 7: Saint Domenico's cloister

The Construction 7 (Figure 1.1h) is characterized by an irregular plan, with an area of 2,150m² and consists of four storeys above the ground level, including a mezzanine. The overall height of the structure is approximately 23m. The walls are made of Neapolitan yellow tuff, varying in thickness from 170cm, at the ground floor, to 35cm thick at the 4th level. The horizontal floors are marked by different typologies of vault, including barrel, cross, sail and lowered cloister vaults. An exception is the Consistory, which boasts a truss as its roofing design, distinct from the other vaulted structures.

The Construction 7 is linked for a length of 24.50m to the South with Construction 0, consisting of four storeys above the ground level, including a mezzanine, and a basement below. Towards the East, it is adjacent to Construction 1, having three storeys above the ground level and a basement below, for a length of 21m.

The floors of Construction 7 differ in height from those of the adjacent Construction 0, except for the 2nd and the 4th level (first and second floor). Specifically, the ground floor is located at a height of +36.45 m.a.s.l., the first floor at +44.00 m.a.s.l., the mezzanine floor at +48.77 m.a.s.l., the second floor at +52.95 m.a.s.l. with an interstorey of 5.70m. In contrast, for the adjacent Construction 0, the ground floor is at a height of +38.50 m.a.s.l., the first floor at +44.00 m.a.s.l., the mezzanine floor at +48.85 m.a.s.l., the second floor at +52.95 m.a.s.l., and the roof of the side sections at +58.15 m.a.s.l.

Plan and cross sections are plotted in Figure 1.9.

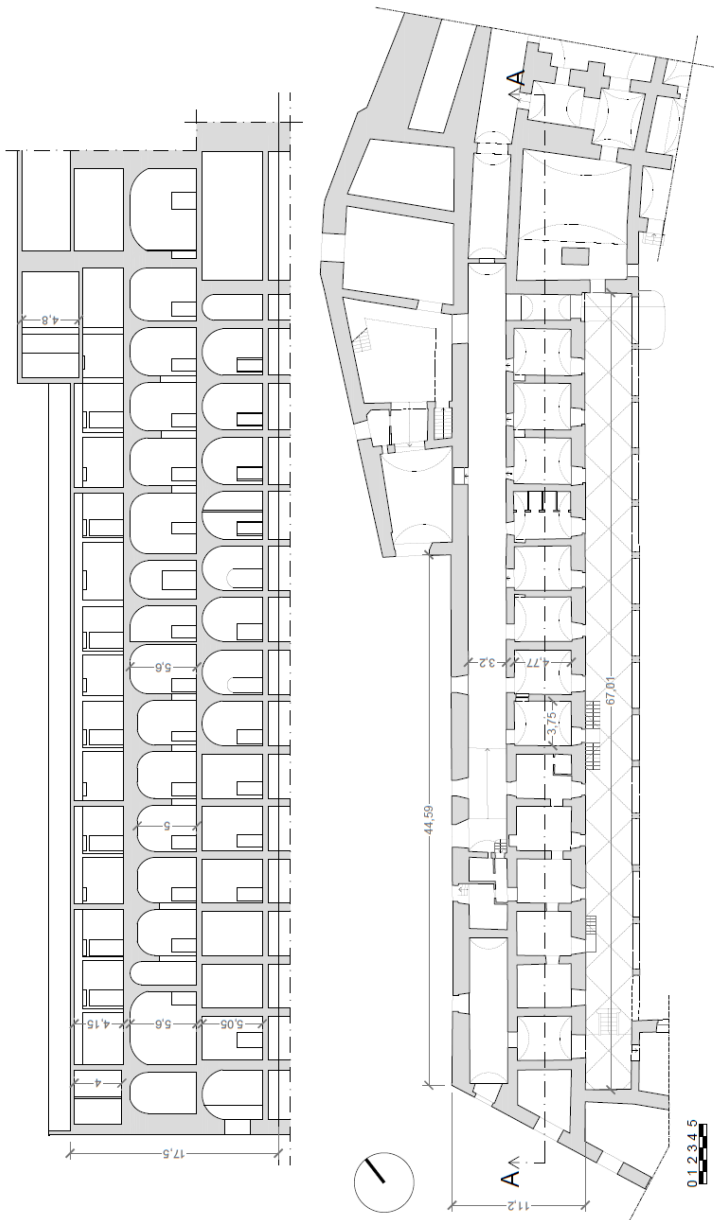


Figure 1.3. Construction 1: plan and cross section.

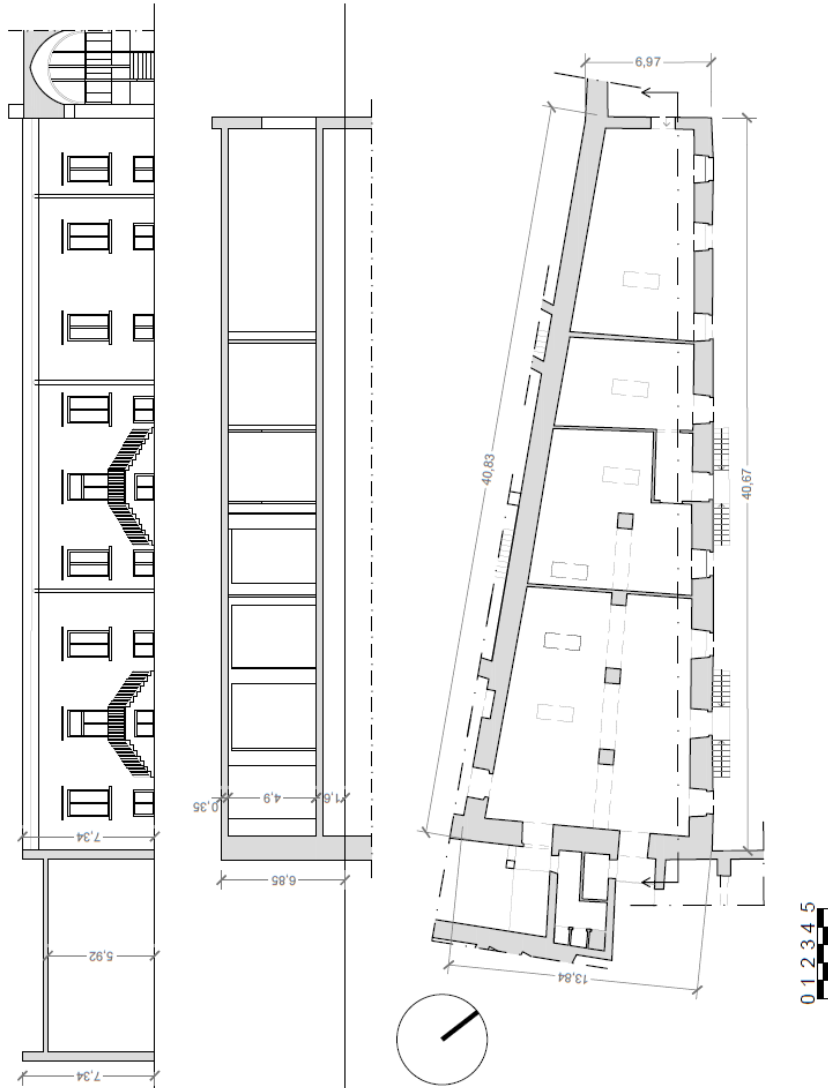


Figure 1.4. Construction 2: plan and cross section.

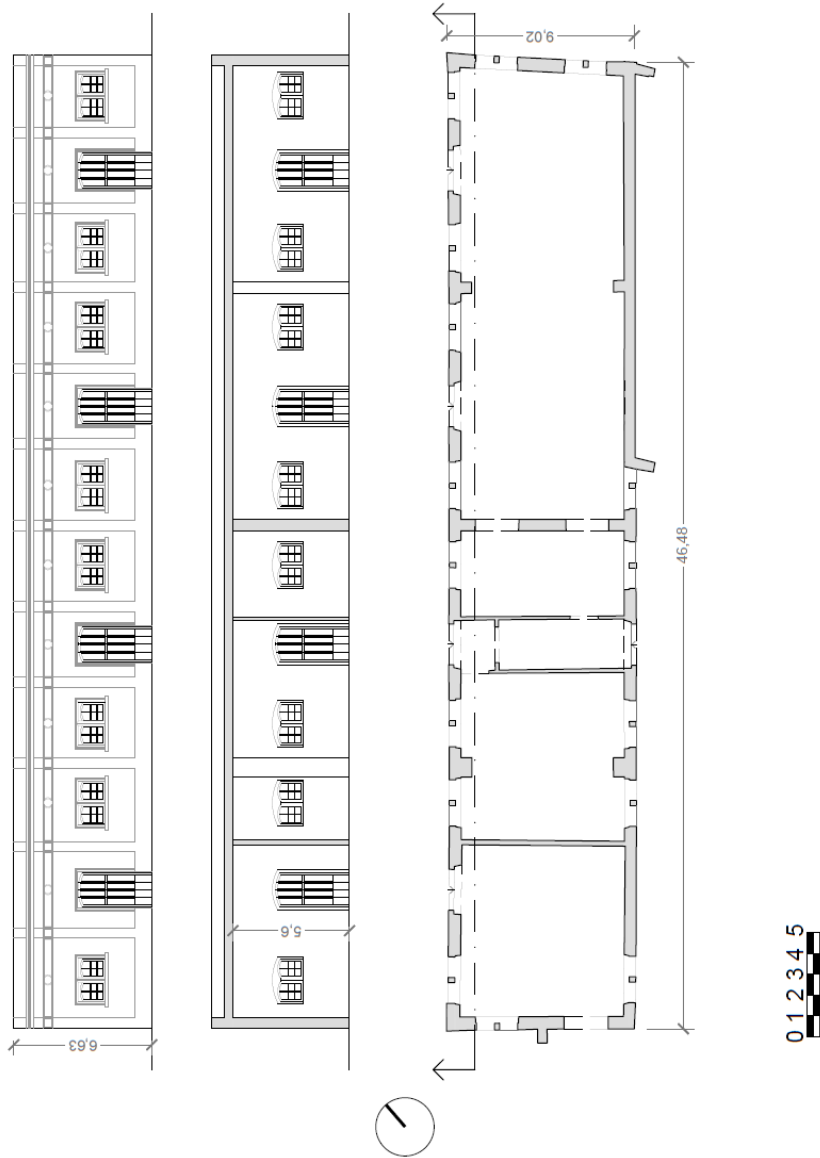


Figure 1.5. Construction 4: plan, cross section and frontal view.

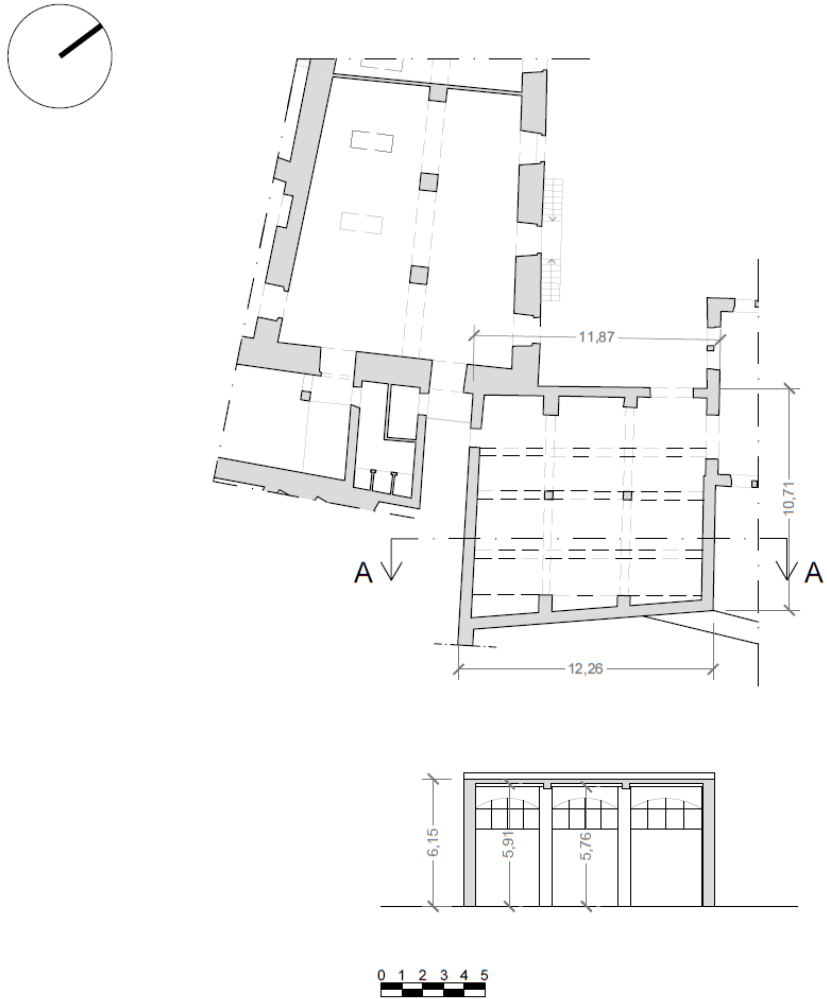


Figure 1.6. Construction 4': plan and cross section.

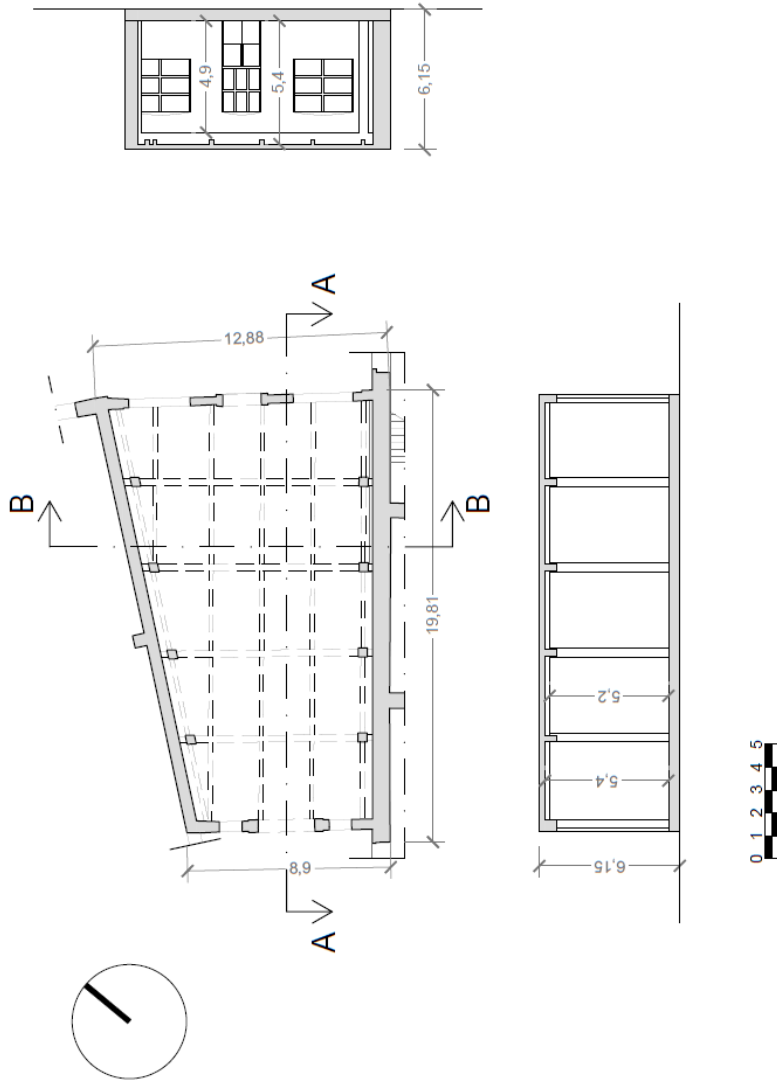


Figure 1.7. Construction 5: plan and cross sections.

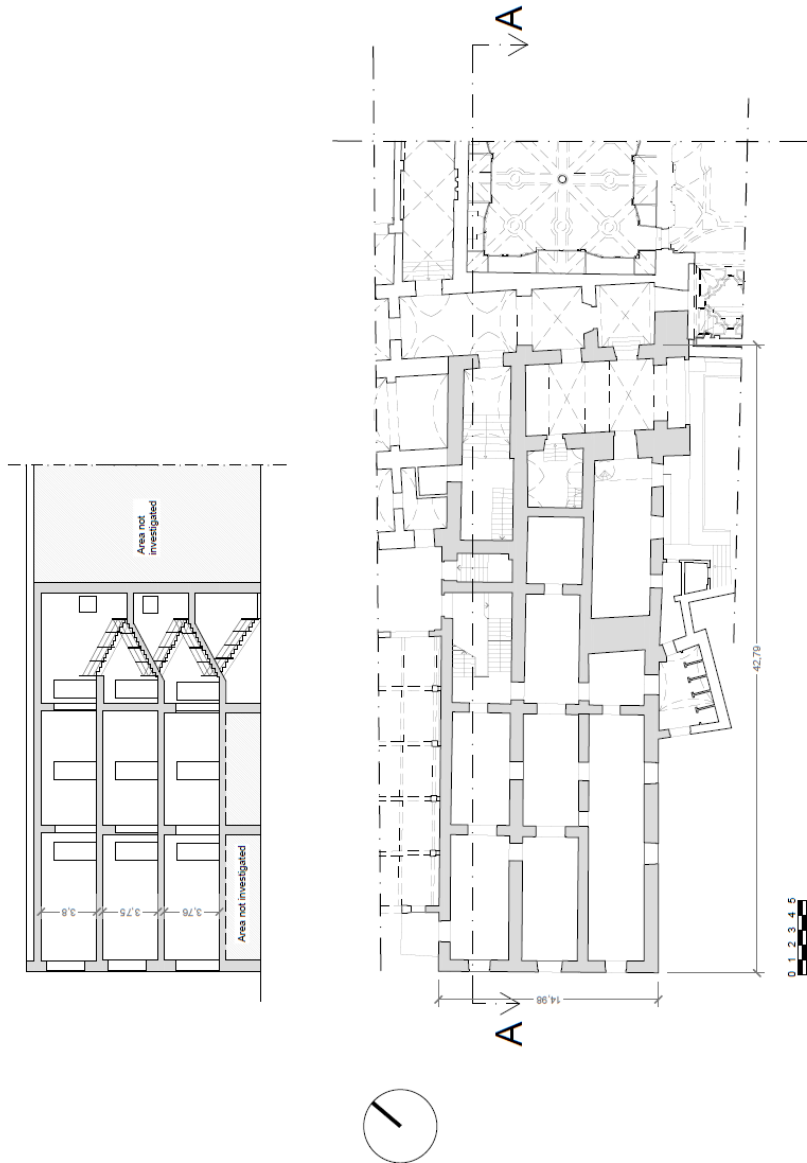


Figure 1.8. Construction 6: plan and cross section.

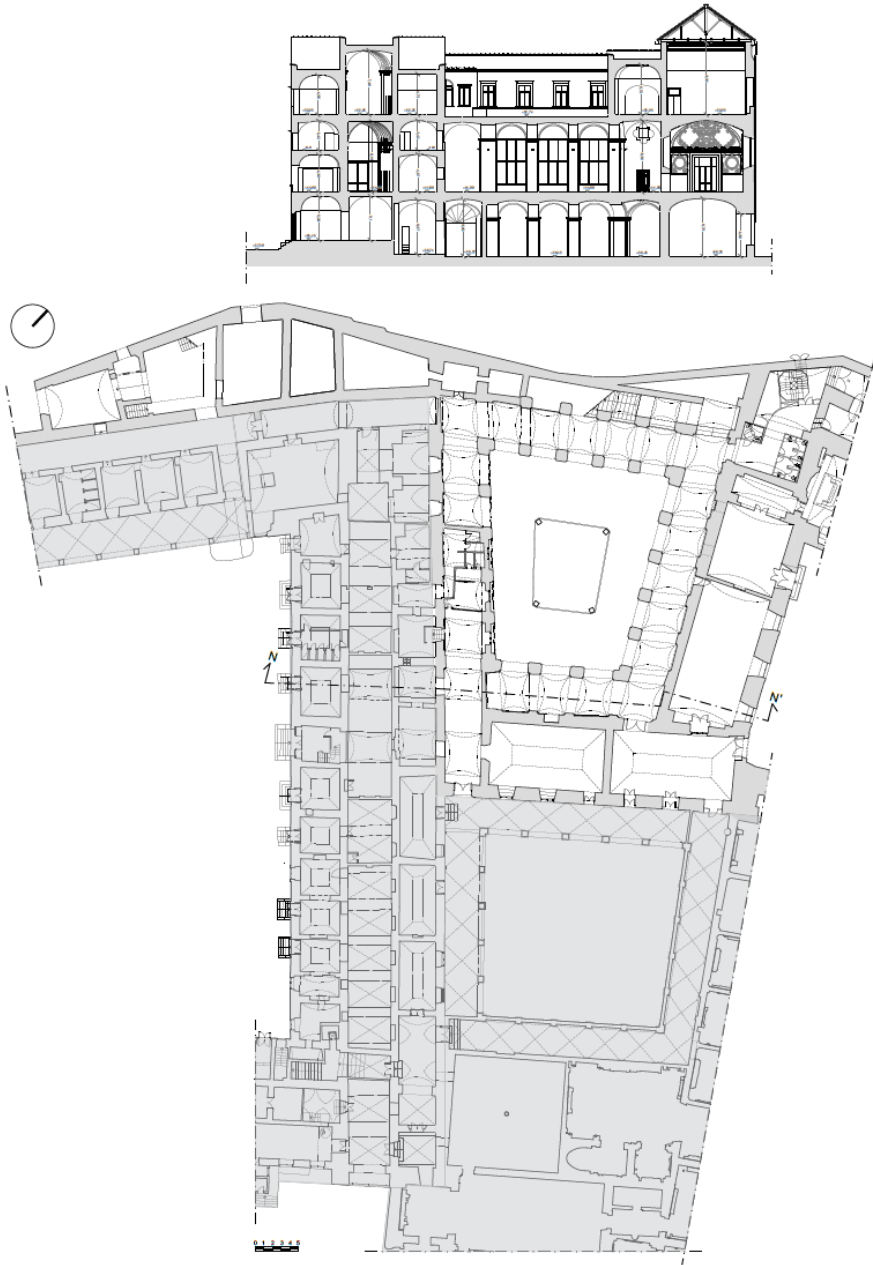


Figure 1.9. Construction 7: plan and cross section.

1.2 Different occupancy of the convent

Over the years, St. Domenico convent has undergone various changes in terms of its occupancy. In its early years, it served as a Convent for the Dominican Order. However, since the suppression of monasteries in 1865, the convent has been partitioned among several different institutions. A comprehensive account of the convent's historical evolution, including changes in occupancy from the first suppression of monasteries of 1809 to recent years, is presented in Chapter 2 of this dissertation.

Nowadays, the convent continues to be occupied by various institutions, each with different purposes. A graphical representation of the institutions occupying different floors within the convent is provided in Figures 1.10-13. As it can be observed, the *Casanova Institute* (depicted in red) dominates the use of the convent, extending its presence across a significant portion of the architectural complex. In particular it occupies nearly the entirety of the Construction 0 (the majority of ground floor, the wing that faces the central courtyard on the first and mezzanine floor, and a substantial portion of the second floor), the Construction 1, Construction 2, Construction 4, Construction 4', Construction 5, Construction 6, and finally the second floor of the Construction 7.

Virtus Parteneopea (highlighted in green) occupies a small portion of the Construction 0, comprising five spaces, and two spaces of the Construction 7.

Dominican Father (indicated in blue) maintain their presence within the convent occupying three spaces of the Construction 0 on the ground floor, a portion of the corridor on the first floor, the Southeastern side on the mezzanine floor, a small part on the second floor.

Lastly, the *Museo DoMa* (highlighted in pink) occupies a half of the first floor of the Construction 0 and the first three level of the Construction 7 (ground, first and mezzanine floor).

Table 1.1 provides a comprehensive account of the area occupied by each institution on the various floors of the convent. Upon analyzing the data, it becomes evident that the Casanova Institute significantly dominates the utilization of the convent space.

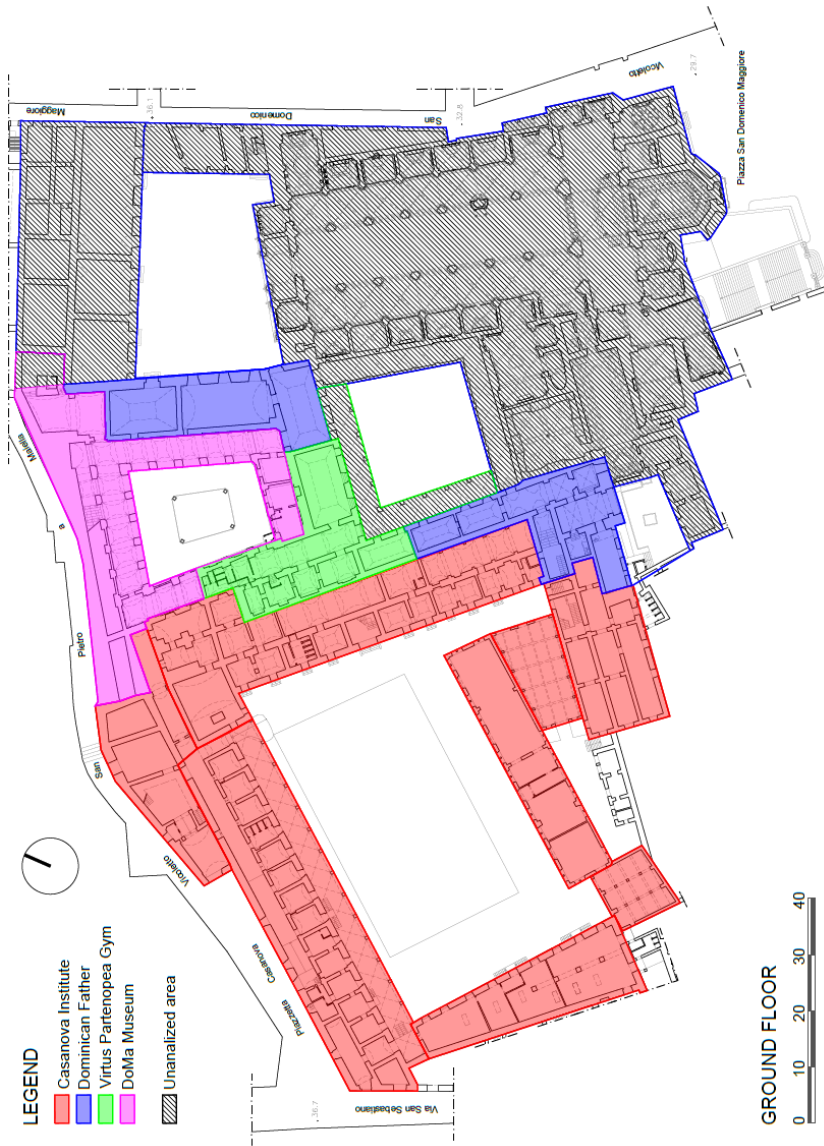


Figure 1.10. Different occupancy: ground floor.

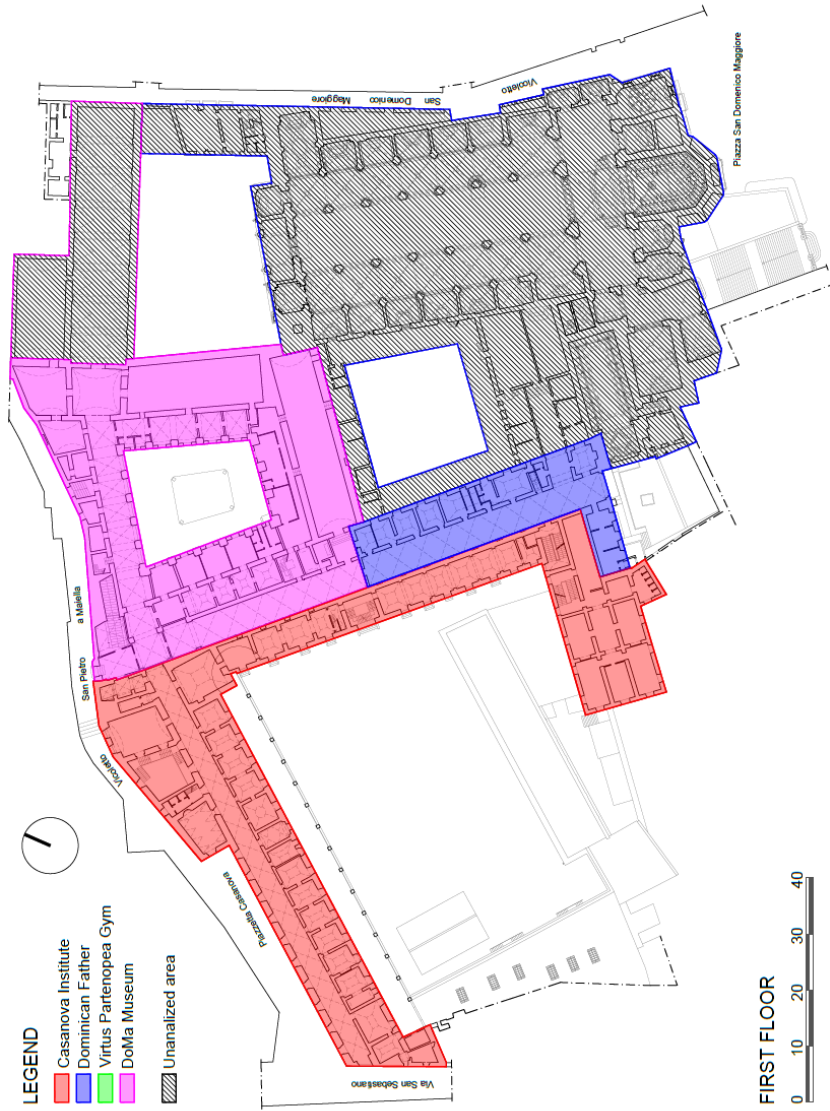


Figure 1.11. Different occupancy: first floor.

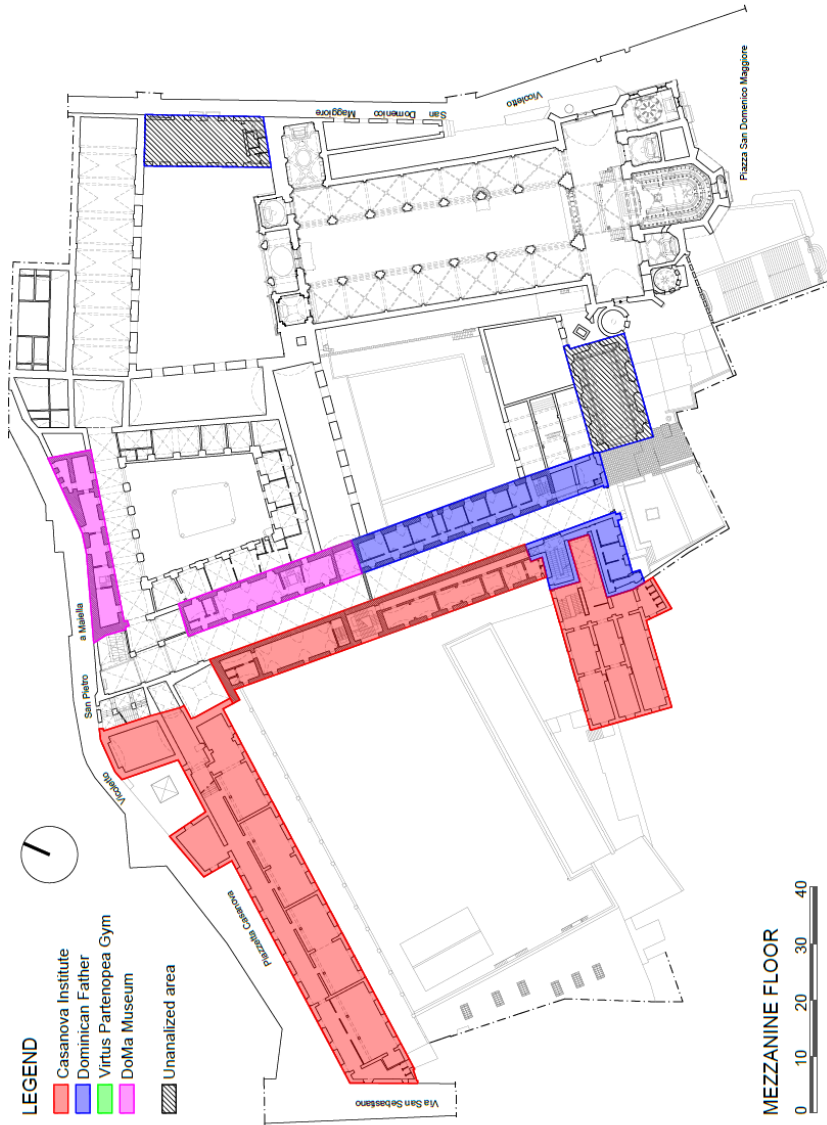


Figure 1.12. Different occupancy: mezzanine floor.

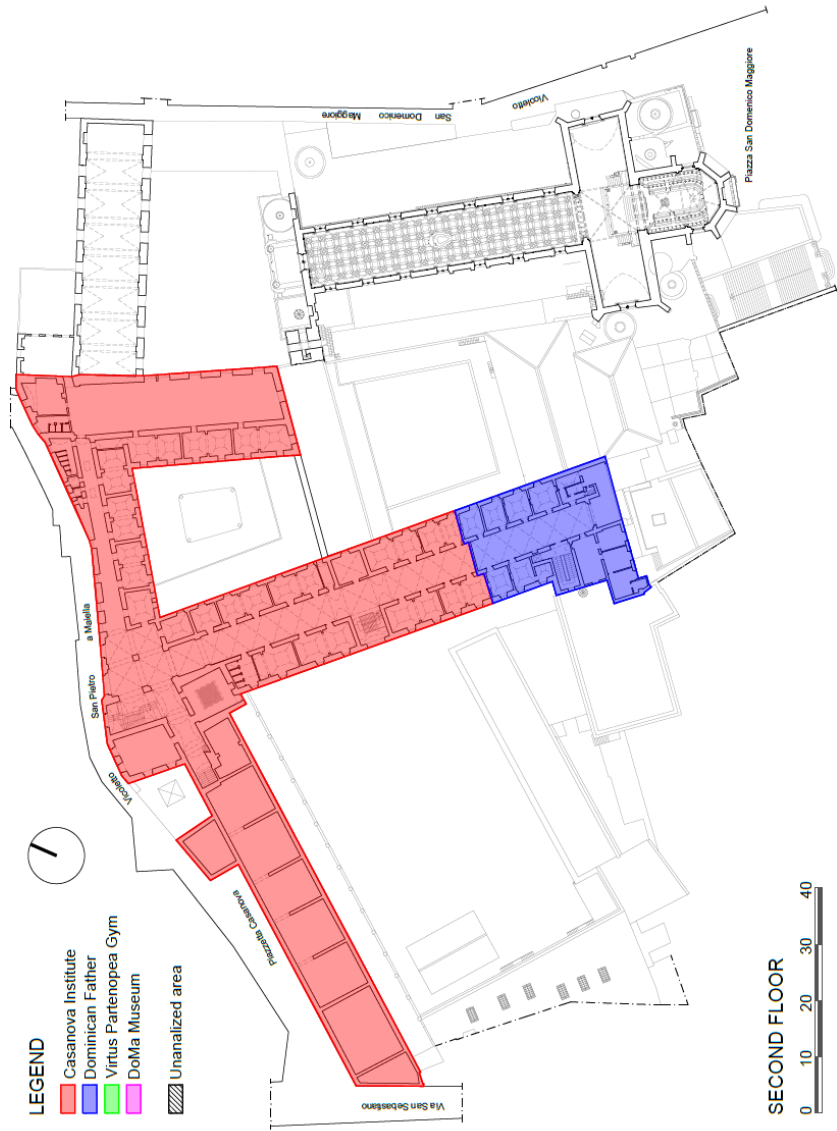


Figure 1.13. Different occupancy: second floor.

Table 1.1. Different occupancy of the convent.

Occupancy	Ground Floor	First Floor	Mezzanine Floor	Second Floor	TOT
	<i>[m²]</i>	<i>[m²]</i>	<i>[m²]</i>	<i>[m²]</i>	<i>[m²]</i>
Casanova Institute	4073.65	2182.17	1822.18	3300.91	11378.91
Dominican Father	901.75	598.93	431.74	557.89	2490.31
Virtus Partenopea Gym	508.73	0.00	0.00	0.00	508.73
DoMa Museum	938.52	2181.65	375.66	0.00	3495.83
TOT	6422.65	4962.75	2629.58	3858.80	17873.78

Chapter 2

Historical evolution of the complex

Over the years, the convent has undergone a significant evolution; some topical moments in the history of the building were marked by noteworthy earthquakes that hit the city of Naples from the 13th century, including: 1456 Central Italy Earthquake (Mw=7.19), 1688 Sannio Earthquake (Mw= 7.06), 1857 Great Neapolitan Earthquake (Mw= 7.12) and 1980 Irpinia Earthquake (Mw= 6.81).

This chapter deals with the historical evolution that the convent has experienced, starting from the 8th century, when the original structure was built, and extending through the 20th century. Specifically, it provides a detailed account of the construction phases, as outlined in Bianco et al. (2016 [1]), and documents all the modifications and alterations that the complex has undergone over the years. These changes were notably influenced by the earthquakes that struck the city of Naples, as well as the suppression of monasteries in 1809 and 1867. As a result of the latter, the Dominican order vacated the convent, making way for the establishment of the Casanova Institute, which significantly transformed the convent.

2.1 The construction phases as outlined in Bianco et al. (2016)

This section focuses on the construction phases as outlined in Bianco (2012 [2]) and Bianco et al. (2016). The construction of the convent has been divided into five distinct phases, spanning from the 8th century to the 20th century. The following list presents these phases in chronological order.

- *First Phase: 8th – 10th century.* The original foundation of the complex dates back to a period between the 8th and 10th centuries, and despite undergoing significant transformations in the 13th century, several elements from this early era were remarkably preserved. However, in the present configuration, large portions attributable to this period are no longer prominent. The remaining traces are limited to certain surviving parts, such as the ancient church of San Michele Arcangelo in Morfisa, the Treasure Room, the Chapel of the Crucifix, and the Chapel of San Carlo Borromeo. The latter chapel has a walled access, along with two mullioned windows and a walled arch, all of which are visible in the Saint Thomas's cloister.
- *Second Phase: 12th century.* The following portions of the current configuration of the Monastery are attributed to this second phase (1283-1320 approx.): the granaries, the Church of Saint Domenico Maggiore, the Dormitory of Saint Thomas (two floors), the Master Dormitory (two floors). During this period, the convent had already expanded significantly, occupying a substantial portion of the available land. In fact, it extended to the very boundaries of the lot, abutting the adjacent roads and surrounding private buildings.
- *Third Phase: 15th – 16th century.* In the subsequent years (the period following the 1456 Central Italy Earthquake), three types of interventions were implemented: the first focused on creating new building structures to expand the complex, the second involved utilizing spaces with interventions that resulted in duplicating volumes, the third centered around working with pre-existing volumes. The following portions are attributed to this phase: new novitiate, the porch of the Master Dormitory, Saint Thomas' cloister.
- *Fourth Phase: 17th century (1669 – 1673).* The fourth phase marks a crucial milestone in the history of the monastery, as it took on the shape and formal configuration that still characterizes it to this day. As in the third phase, due to the limited availability of free space within the lot, the decision was made to proceed with the occupation of any available vacant areas. The following portions belong to this period: Saint Domenico's cloister, Chapter Room (first level).

- *Fifth Phase: 17th century (1678 – 1682).* The following portions of the current configuration of the Monastery are attributed to this period: third floor for the Masters Dormitory, third floor for the Saint Thomas's Dormitory, the second floor of the novitiate.

A graphical representation of the phases outlined above is given in Figure 2.1.

In Figures 2.2-4, historical maps of the city of Naples are shown, illustrating the transformations undergone by the convent over the centuries. In particular:

- Lafrery maps (1566) and the Braun and Hogenberg maps (1572) allow to reflect on the original configuration of the convent and the "insula";
- The cartographic survey curated by Giovanni Carafa, Duke of Noja (1775), attests to the expansion of the complex, occupying the entire "insula."



Figure 2.2. Lafrery maps (1566).



Figure 2.3. Braun and Hogenberg maps (1572).

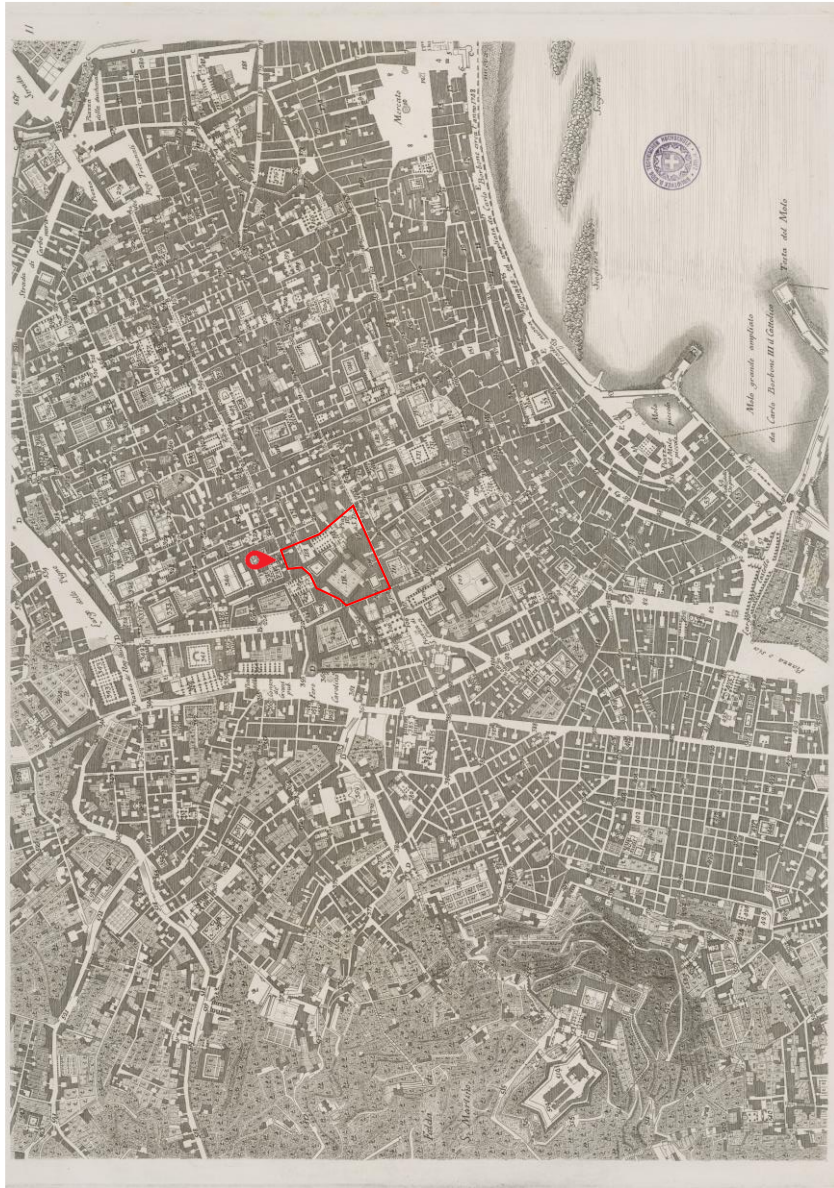


Figure 2.4. Carafa maps (1775).

2.2 The 17th-century structural interventions

In 1686, the architect Francesco Antonio Picchiatti faced significant structural issues. In particular, the Refectory (Figure 2.5a) and the Chapter Room (Figure 2.5b), built by Ruffo, exhibited cracks due to the additions of the upper floor made by Presti. The solution implemented involved reinforcing the vault with brick arches and two chains in each arch, which are still visible today. Furthermore, he also intervened in response to the 1688 Sannio Earthquake and the 1694 Irpinia Earthquake, which caused damage to the convent. Specifically, he carried out consolidations of the walls using a local rebuilding methodology (“scuci-cuci”) and installed chains in the vaults (Picone, 2016 [3]).

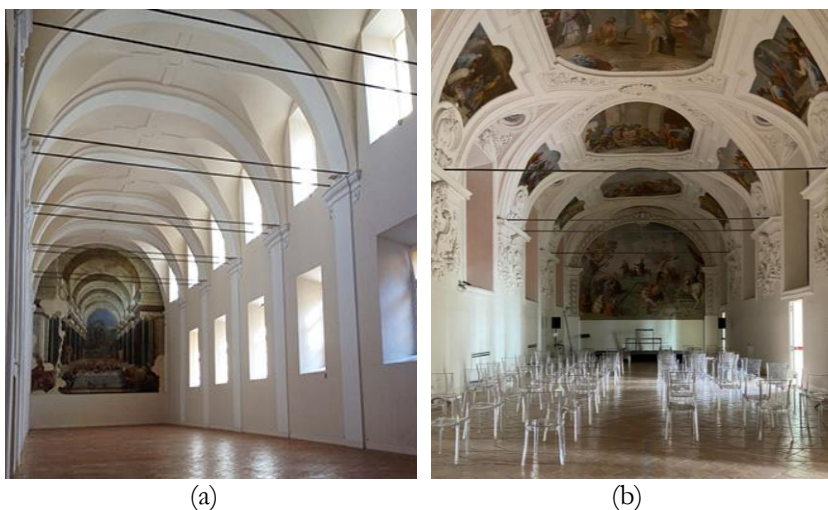


Figure 2.5. Chains in Refectory (a) and in Chapter Room (b).

2.3 The modifications and alterations of the 19th and 20th centuries

In 1809 the Dominicans were forced to leave the convent, due to the suppression of monasteries by Murat. For a decade, the entire convent was converted into a barracks. However, in 1820, the Dominicans reoccupied the church, only to face another suppression of monasteries in 1865, which compelled them to abandon the convent once more. This measure led to

significant alterations within the convent, including (1) modifications of openings, (2) change to staircases, and (3) the installation of sanitary facilities, unfortunately causing irreparable damage to important artworks. The convent was divided among several institutions. In 1869, the Casanova Institute was given possession of the entire northwest wing of the convent. The porticoed wing surrounding the garden, now transformed into a gym, was allocated for classrooms, while the ground floor dormitories and granaries were repurposed as laboratories. These laboratories rapidly expanded, occupying two more spacious areas adjacent to the old novitiate. The wing of St. Thomas was transformed into a technical school for drawing, while the adjacent areas of the St. Thomas cloister were used as a gym, known as “Virtus Partenopea” since 1890. The entire novitiate building and a part of the main dormitory provided accommodation for art dealers. Additionally, the offices of the San Giuseppe district court were located on the second floor. The Library, Chapter Room and Refectory were occupied by the Assizes court. The second floor housed an administration office and the Flavio Gioia technical school. The different utilization of the spaces damaged the entire structure. The Casanova Institute made significant modifications to the two main staircases and also altered the layout of the old rooms. In fact, the rooms were combined in pairs and are now functioning as classrooms (Salerno, 1997 [4]). The Flavio Gioia technical school, which is no longer housed in S. Domenico, left a notable impact on the structure: it added a large elevated volume, serving as a drawing classroom, situated above the Chapter Room. Furthermore, the Assizes court modified the Chapter Room by installing a false ceiling, resulting in the reduction of the fresco. Additionally, the space was divided with the security cells (Lumaga [5]). In the 20th century, there were no significant interventions. The most significant alteration occurred in the 1950s when the truss in the Masters Dormitory was removed.

2.4 The conservative restoration of the 21st century

The Saint Domenico Maggiore convent suffered significant damage during the 1980 Irpinia Earthquake. In Figure 2.6, a series of pictures from a survey conducted in 2001 by Città Metropolitana di Napoli illustrates a part of the crack pattern observed in the convent after the seismic event. Specifically,

the photos highlight the crack pattern of the cross vaults, revealing fractures in the keystone of the perimetral arches. As it can be observed, during that period, the vaults lacked reinforcement ties. However, in a more recent survey conducted by the author, these reinforcement ties were found to be in place. Their inclusion was part of long and difficult conservative restoration started in the early 2000s and concluded by 2010, as described in detail below. The lack of a significant crack pattern in the more recent surveys provides strong evidence for the effectiveness of the interventions.

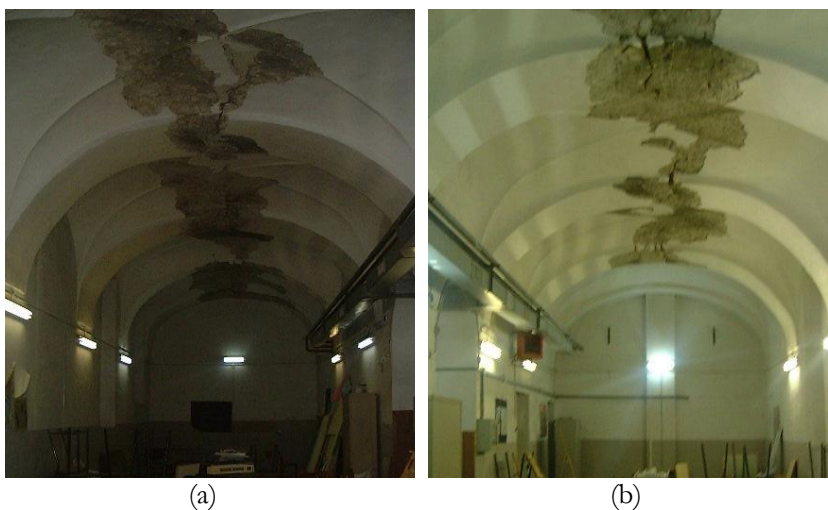


Figure 2.6. Crack pattern following the 1980 Irpinia Earthquake (2001).

A clear and exhaustive account of the interventions carried out by the Soprintendenza per i Beni Ambientali e Architettonici di Napoli during that year is provided by Foglia et al.. The area involved in the restoration were:

- The Chapter Room, Library and the first floor and the mezzanine floor of Saint Thomas Dormitory;
- The Saint Domenico cloister.

The interventions involved:

- Construction of a new steel-framed suspended ceiling, replacing the existing masonry vault in the Library.
- Extensive demolition of alterations, floors, arch fillings, partitions. Notably, the entire mezzanine floor, consisting of steel floors and vaults in the Saint Domenico cloister, was demolished. This restoration effort successfully restored the cloister's original first-

floor layout. Additionally, the prison cells in the Small Refectory were removed, as well as the partitions inside the Consistory Room that fragmented its space.

- Demolition of the building extension on the side of the Library, which had been added in the mid-20th century.
- Reopening of the cell entrances facing the San Tommaso corridor, which were transformed into classrooms and laboratories for the Casanova Institute.
- Restoration of a direct connection with the Library by demolishing a masonry wall on the San Tommaso corridor side, as well as the mezzanine floor.
- Restoration of the original dimensions and features of the mezzanine openings, with “Roman-style” balconies vertically aligned with the cell entrances.
- Demolition of a masonry structure with a SAP floor, previously used as a classroom for the Casanova Institute, located on the extrados of the barrel vaults with lunettes of the Small Refectory (Foglia et al., 2016 [6]).

Additionally, extensive interventions to reduce thrust of vaults on the bearing walls were implemented, involving the widespread application of ties in the Saint Thomas Dormitory, the Saint Domenico cloister and the Master Dormitory.

2.5 The earthquakes experienced by the convent over the years

In Figure 2.7 the Intensity (MCS) of the earthquakes experienced by the convent starting from the 13th century up to the current year is given. This graph is based on data provided by the Database Macrosismico Italiano of INGV and included in the **Appendix 1** of this dissertation. As evident from the graph, the Intensity values range between 3 and 8. In particular, among the strong earthquakes that hit the city of Naples and exhibited the higher Intensity value, it can be mentioned: the 1456 Central Italy Earthquake ($M_w=7.19$), the 1688 Sannio Earthquake ($M_w= 7.06$), the 1857 Great Neapolitan Earthquake ($M_w= 7.12$) and the 1980 Irpinia Earthquake ($M_w= 6.81$). These earthquakes severely damaged the convent and marked pivotal moments in its historical evolution, as described in previous sections.

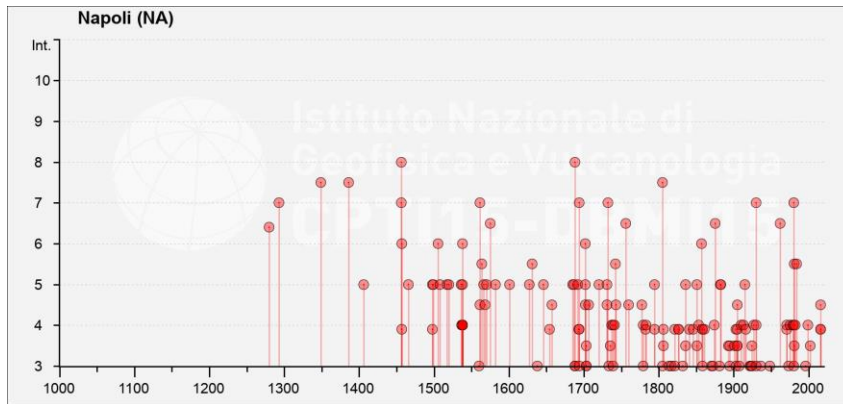


Figure 2.7. Intensity of the seismic events experienced by the convent (https://emidius.mi.ingv.it/CPTI15-DBMI15/query_place/).

Chapter 3

Preliminary considerations: the rules of art

This Chapter provides some preliminary considerations about the structural layout of the buildings case study based on the analysis of geometrical data, as the architectural plan and prospective view of the walls of the building. These considerations are finalized to the analysis of the construction quality of the convent, that is evaluated in terms of its adherence to “the rules of art”, delineated in significant ancient treatise, as the treatise by Rondelet, Breyman, Cavalieri San Bertolo and Leon Battista Alberti, and in the Italian Building Code (NTC 18). Specifically, in the following sections, initially general observations on the structural layout of the analysed structures will be delineated. Following this, it will be analysed the compliance with the rules suggested in his treatise by Rondelet on the stability of the walls and on the ratio between the in-plan area of the walls and the total area and with the recommendations by Lourenco, EC8 and Italian Building Code about the ratio between the area of the walls in each main direction and the total in-plan area of the building. This will be followed by the analysis of the adherence to the principles listed by Cavalieri San Bertolo in his treatise regarding the regularity of the arrangement of the openings and the rules by Breyman about the lowered cloister vaults. These considerations affect the performance of the structure significantly, as described in detail in the following sections and aim to define if the structures are well conceived.

3.1 Structural system: preliminary considerations

In this Section some general considerations on the structural system for each analysed construction are listed, aiming to define if the structures are well conceived.

About the structural system of *Construction 0*, the following observations are made.

- The building has rectangular plan, approximately 87mx17m.
- It consists of four storeys above the ground level, including a mezzanine, and a basement below with an overall building height of 23.16m. The central corridor has a higher height than the two lateral portions of the structure.
- The thicknesses of the walls at various levels are respectful of the rules of arts, see Sections 3.2 and 3.3.
- The construction exhibits a regular arrangement of the openings with a vertical alignment in longitudinal direction, but this regularity is not observed in the transverse direction. Furthermore, in transverse direction, the structure is characterized by the presence of walls supported by vaults. See Section 3.4 for a detailed analysis.
- The spacing between transverse walls on the ground floor is within the limits set by the Italian Building Code (NTC 18) [7], which prescribes distances not exceeding 7m. On the first floor, in the two lateral sections containing classrooms, these distances don't exceed the 7m, whereas in the central part, the corridor, these walls are entirely absent. On the mezzanine floor, the transverse walls have a spacing greater than 10 meters, and they are nearly absent. On the second floor, similar to the first floor, these walls are absent in the central corridor area and have a spacing of less than 7m in the lateral sections occupied by classrooms. It's important to note that these walls feature minimal dimensions for the resistant sections of the masonry piers, resulting in low rigidity and providing minimal seismic resistance.

Construction 1

- The building has rectangular plan, approximately 81m x 11m.
- It consists of three storeys above the ground level and a basement below with an overall height of 17.50m.
- The thicknesses of the walls at various levels are respectful of the rules of arts, see Sections 3.2 and 3.3.
- The construction exhibits a regular arrangement of the openings with a vertical alignment. See Section 3.4.
- The transverse walls are arranged with regular spacing, not exceeding 7m, especially on the ground floor and the first floor in the section occupied by classrooms (North-East side). Nevertheless, in the corridor section (North-West side), these walls are entirely absent.
- The lowered cloister vaults of the first floor are not respectful of the rule suggested by Breyman [8] which recommends that they should remain unloaded. This is due to the addition of another level occupied by the laboratories of the Casanova Institute in later years.

Construction 2

- The building has a trapezoidal plan with a length of approximately 40m, a shorter base of about 7m, and a longer base of about 14m, resulting in a total area of 428m².
- It consists two levels, one of which is a basement level facing the courtyard of the Casanova Institute, and an above-ground level facing Via San Sebastiano. The overall height of the building is equal to 6.85m.
- The thicknesses of the walls are such that they result in strong stability, in accordance with Rondelet's rule, see Sections 3.2 and 3.3.
- The transverse walls are entirely absent.

Construction 4

- The building has rectangular plan, approximately 46m x 9m.
- It consists of one single level with an overall height of 6.0m.
- The thicknesses of the walls are such that they result in low stability, in accordance with Rondelet's rule, see Sections 3.2 and 3.3.

- The spacing between transverse walls exceed the limits outlined in the Italian Building Code (NTC 18) of 7m, reaching 20m.

Construction 6

- The building has rectangular plan, approximately 43mx15m.
- It consists three storeys above the ground level and a basement below with an overall height of 15.35m.
- The thicknesses of the walls at various levels are respectful of the rules of arts, see Sections 3.2 and 3.3.
- The construction exhibits a regular arrangement of the openings with a vertical alignment. See Section 3.4.
- The transverse walls are arranged with regular spacing, not exceeding 7m, except for one classroom on the ground floor, where the transverse walls are positioned with a distance of 17 meters.

Construction 7

- The building has by an irregular plan, with an area of 2,150m².
- It consists of four storeys above the ground level, including a mezzanine, with an overall height of 23.0m.
- The thicknesses of the walls at various levels are respectful of the rules of arts, see Sections 3.2 and 3.3.
- In both directions, the construction exhibits an irregular arrangement of the openings, with variations in vertical alignment and variations in pier widths. Furthermore, the structure is characterized by the presence of walls supported by vaults. See Section 3.4.
- The transverse walls are arranged with an irregular spacing, exceeding 7m.

3.2 On the stability of the masonry walls as suggested in Rondelet (1802)

In his treatise [9], Rondelet suggests distinct limits for the slenderness of the wall, defined as the ratio between free deflection height of the wall (h_0) and the thickness (t), classifying them into three categories: $h_0/t= 8$ for wall

with strong stability; $h_0/t= 10$ for wall with medium stability and $h_0/t= 12$ for wall with low stability.

“Si possono distinguere, nella costruzione degli edifici tre gradi di stabilità, uno massimo, uno medio ed uno minimo.

Quindi dietro le osservazioni fatte sopra una grandissima quantità d'edifici di tutti i generi, risulta che un muro avrà una forte stabilità, se ha per spessore l'ottava parte della sua altezza; che la decima parte procurerà ad esso una stabilità media, e la dodicesima il minore grado di stabilità ch'esso può avere.”

(Rondelet, 1802. *Traité teorique et pratique de l'Art de Batir*)

These established limits are also reiterated in several treatise and manuals of engineer of 19th century, including the treatise by Cavalieri – San Bertolo (1839) [10] and the Manual of Engineer by Colombo (1887) [11]. Furthermore, the latter manual suggests minimum wall thicknesses for different building typologies, including buildings with slab, vaults and industrial buildings, and with a particular distinction between external and internal walls.

Tables 3.1-6 offer a comparative analysis of the slenderness of the walls of the analysed Constructions in relation to the limit proposed by Rondelet for walls with low stability. Additionally, comparisons between the wall thicknesses and the minimum values suggested by Colombo in his Manual of Engineer are given. In particular, it can be observed that the slenderness of the walls on various floors of each construction is lower or equal to the value recommended by Rondelet for wall with low stability. However, only in few cases the values exceed this limit, specifically on the second floor of Construction 0, the mezzanine floor of Construction 1 and the ground floor and second floor of the Construction 7, standing at 17, 13, 16 and 17 respectively (see Figure 3.1). Regarding wall thickness, distinctions are made between internal (t_{int}) and external walls (t_{ext}). In few instances, the thickness of walls is not respectful of the rules suggested by Colombo, with differences ranging from 5cm (evident on the ground floor of Construction 0 and the first floor of Construction 1) to 15cm (found on the first and second floor of Construction 0 and on the ground, first, and mezzanine floors of Construction 7).

Table 3.1. Comparison between wall thickness and the rules of art: C0.

Level	Construction 0				Rondelet (1802)	Colombo (1877)	
	t_{int}	t_{ext}	h_0	h_0/t	$(h_0/t)_{low}$	t_{int}	t_{ext}
<i>[-]</i>	<i>[cm]</i>	<i>[cm]</i>	<i>[cm]</i>	<i>[-]</i>	<i>[-]</i>	<i>[cm]</i>	
Ground Floor	50-115	95-285	557	11-2	12	55	75
First Floor	40-130	80-145	485	12-3		55	65
Mezzanine Floor	35-130	80-145	410	12-3		45	55
Second Floor	30-95	80-145	515	17-4		45	45

Table 3.2. Comparison between wall thickness and the rules of art: C1.

Level	Construction 1				Rondelet (1802)	Colombo (1877)	
	t_{int}	t_{ext}	h_0	h_0/t	$(h_0/t)_{low}$	t_{int}	t_{ext}
<i>[-]</i>	<i>[cm]</i>	<i>[cm]</i>	<i>[cm]</i>	<i>[-]</i>	<i>[-]</i>	<i>[cm]</i>	
Ground Floor	45-80	110-140	550	12-4	12	55	75
First Floor	50-135	70-125	615	12-5		55	65
Mezzanine Floor	35-135	70-75	450	13-3		45	55

Table 3.3. Comparison between wall thickness and the rules of art: C2.

Level	Construction 2				Rondelet (1802)	Colombo (1877)	
	t_{int}	t_{ext}	h_0	h_0/t	$(h_0/t)_{low}$	t_{int}	t_{ext}
<i>[-]</i>	<i>[cm]</i>	<i>[cm]</i>	<i>[cm]</i>	<i>[-]</i>	<i>[-]</i>	<i>[cm]</i>	
Ground Floor	-	60-135	525	9-4	12	35	35

Table 3.4. Comparison between wall thickness and the rules of art: C4.

Level	Construction 4				Rondelet (1802)	Colombo (1877)	
	t_{int}	t_{ext}	h_0	h_0/t	$(h_0/t)_{low}$	t_{int}	t_{ext}
<i>[-]</i>	<i>[cm]</i>	<i>[cm]</i>	<i>[cm]</i>	<i>[-]</i>	<i>[-]</i>	<i>[cm]</i>	
Ground Floor	50	50	605	12-2	12	35	35

Table 3.5. Comparison between wall thickness and the rules of art: C6.

Level	Construction 6				Rondelet (1802)	Colombo (1877)	
	t_{int}	t_{ext}	h_0	h_0/t	$(h_0/t)_{low}$	t_{int}	t_{ext}
<i>[-]</i>	<i>[cm]</i>	<i>[cm]</i>	<i>[cm]</i>	<i>[-]</i>	<i>[-]</i>	<i>[cm]</i>	
Ground Floor	60-95	75-90	420	7-4		45	55
First Floor	55-90	70-80	415	8-5	12	45	45
Mezzanine Floor	50-75	65-75	430	9-6		35	35

Table 3.6. Comparison between wall thickness and the rules of art: C7.

Level	Construction 7				Rondelet (1802)	Colombo (1877)	
	t_{int}	t_{ext}	h_0	h_0/t	$(h_0/t)_{low}$	t_{int}	t_{ext}
<i>[-]</i>	<i>[cm]</i>	<i>[cm]</i>	<i>[cm]</i>	<i>[-]</i>	<i>[-]</i>	<i>[cm]</i>	
Ground Floor	50-150	100-170	810	16-5		55	75
First Floor	50-120	70-155	480	10-3	12	55	65
Mezzanine Floor	50-120	70-155	415	8-3		45	55
Second Floor	35-110	70-130	594	17-5		45	45

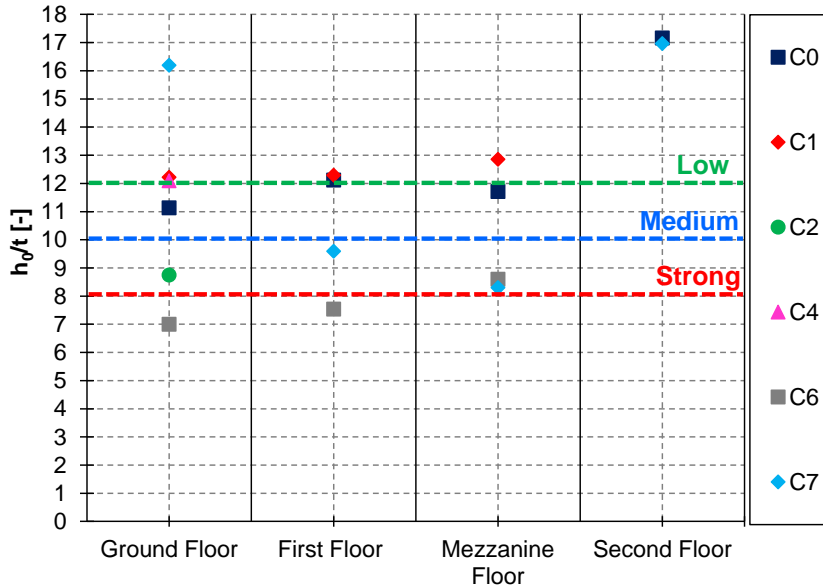


Figure 3.1. Comparison between maximum slenderness and the limit suggested by Rondelet (1802).

3.3 In-plan area ratio A_w/A_{tot}

A geometric parameter that provides a simple means to assess the efficiency of a masonry structure is the ratio between the area of the walls (A_w) and the total in-plan area of the building (A_{tot}). This parameter affects the mean vertical stress values significantly. In his treatise, Rondelet [9] computed these ratios for several famous masonry monuments, aiming to provide some reference values (see Figure 3.2).

Tavola che indica il rapporto dei muri e dei punti d'appoggio di molti edifici, colla superficie totale da essi occupata.

NOMI DEGLI EDIFICI	SUPERFICIE TOTALE		SUPERFICIE DEI PUNTI		Rapporto in mil. delle superficie totali
	IN		D'APPOGGIO IN		
	metri	tese	metri	tese	
Cupola degl'Invalidi di Parigi . . .	2695.4	709 1/2	724.0	190 1/2	0.268
Chiesa di S. Pietro in Roma . . .	21103.1	5553 4/9	5511.0	1450 1/2	0.261
Panteon di Roma . . .	3182.0	837 7/18	739.2	194 1/4	0.232
Tempio antico detto Galluzzo a Roma.	855.6	225 1/6	201.4	53. 0	0.226
Progetto della chiesa di S. Pietro di Bramante . . .	19843.0	5222. 0	4354.8	1146. 0	0.219
Chiesa di Santa Sofia a Costantinopoli.	9591.1	2524. 0	2097.3	552. 0	0.217
Chiesa di Santa Maria de' Fiori a Firenze.	7881.2	2074. 0	1582.7	416 1/2	0.201
Tempio della Concordia a Girgenti . .	636.6	167 1/2	123.6	32 1/2	0.194
Edificio in mezzo alle terme di Caracalla.	25604.4	6798. 0	4499.2	1184. 0	0.176
Gran tempio di Pesto . . .	1426.9	375 1/2	24.6	64 3/4	0.172
Chiesa di S. Paolo di Londra . . .	7809.0	2055. 0	1330. 0	350. 0	0.170
Edificj nel mezzo delle Terme di Diocleziano	32680.0	8600. 0	5464.4	1438. 0	0.167
Tempio di Giunone Lucina a Girgenti.	634.0	166 3/4	103.2	27 1/6	0.163
Cattedrale di Milano . . .	11696.4	3078. 0	1985.6	522 1/4	0.161
Chiesa di S. Vitale a Ravenna . . .	676.2	178. 0	106.1	28. 0	0.157
Chiesa di S. Pietro in Vinculis a Roma.	2000.0	529 2/3	311.6	82. 0	0.155
Chiesa di Santa Genevieffa . . .	5593.6	1472. 0	861.4	226 3/4	0.154
Chiesa di S. Sulpicio . . .	5646.8	1486. 0	848.2	223 1/5	0.151
Chiesa di S. Domenico a Palermo . .	3173.2	835 1/18	463.6	122. 0	0.146
Chiesa di Nostra Signora a Parigi . .	6258.6	1647. 0	816.4	230 2/1	0.140
Chiesa di S. Giuseppe a Palermo . .	2420.6	637. 0	335.6	88 1/3	0.139

Figure 3.2. A_w/A_{tot} ratio computed by Rondelet (1802).

The significance of this ratio and the necessity of drawing lessons from historical examples are also highlighted by Cavalieri (1839) in his own treatise [10]:

Nell'arte di fabbricare sono sempre da valutarsi tutte quelle riprove della stabilità degli edifici che vengono desunte dal confronto del subbietto con quei monumenti dell'arte i quali hanno dato lungo saggio della solida loro costituzione. Per la qual cosa, lungi dall'aversi a riputar vane le scrupolose indagini istituite dal rinomato Rondelet a fine di conoscere l'effettivo rapporto dell'area totale occupata alla somma di quelle delle basi di tutti i muri o piedritti in un buon numero d'edifici di vario genere antichi e moderni di provata stabilità, dobbiamo anzi saperli buon grado che coi risultati all'accurate sue osservazioni ci ha somministrato un mezzo opportuno onde poter mettere ad un esame comparativo, e quasi di fatto, la stabilità, direm così, basamentale di qualunque grand'edificio.

(Cavalieri – San Bertolo, 1839. Istituzioni di architettura statica e idraulica)

In addition to the in-plan ratio that affects the mean vertical stress values significantly, another geometric parameter useful to assess the seismic performance of a masonry structure with a simplified method is the ratio between the area of the walls in each main direction and the total in-plan area of the building. According to Lourenco et al. [12], it is recommended a minimum value of 10% for historical masonry buildings. Eurocode 8 [13] suggests values of up to 2% for structures with a rigid floor diaphragms, while the Italian Building Code (NTC 18) [7] advises values up to 3.5%.

Figures 3.2-7 give histograms containing the values of the in-plan ratios A_w/A_{tot} , $A_{w,x}/A_{tot}$, $A_{w,y}/A_{tot}$ for each floor of the analysed structures. By comparing the ratios A_w/A_{tot} (in green) of each construction with those computed by Rondelet for notable monuments, such as Bourse de Commerce, market grain, in Paris (8,4%), Notre Dames in Paris (14%), Basilica of S. Maria del Fiore (20%), the Pantheon (23%) and Dome of Les Invalides (27%), it becomes evident that the analysed constructions are respectful of the rules of art. Additionally, the ratios $A_{w,x}/A_{tot}$ (in red) and $A_{w,y}/A_{tot}$ (in blue) exceed the minimum value prescribed by EC8 (2%) and NTC18 (3.5%), except for the ground floor of Construction 4, that exhibit a value of 3% in transverse direction. However, in some instances, these ratios fall below the minimum value suggested by Lourenco et al. (10%). Specifically:

- The mezzanine and the second floor of the Construction 0 exhibit a minimum value equal to 6% in transverse direction $A_{w,y}/A_{tot}$;
- The mezzanine floor of the Construction 1 shows a minimum value of 6% for the mezzanine floor in transverse direction $A_{w,y}/A_{tot}$;
- The ground floors of Constructions 2 and 4 have values of 5% and 3%, respectively, in transverse direction $A_{w,y}/A_{tot}$;
- The first and the mezzanine floor exhibit values of 9% and 7%, respectively, in transverse direction $A_{w,y}/A_{tot}$.

These results are summarized in Table 3.7, which reports the values of the A_w/A_{tot} , $A_{w,x}/A_{tot}$, $A_{w,y}/A_{tot}$ ratios obtained for each floor of the analysed constructions. In addition, the values lower than the minimum prescribed by Lourenco et al. are highlighted in bold, while values lower than the minimum suggested by EC8 are in italic.

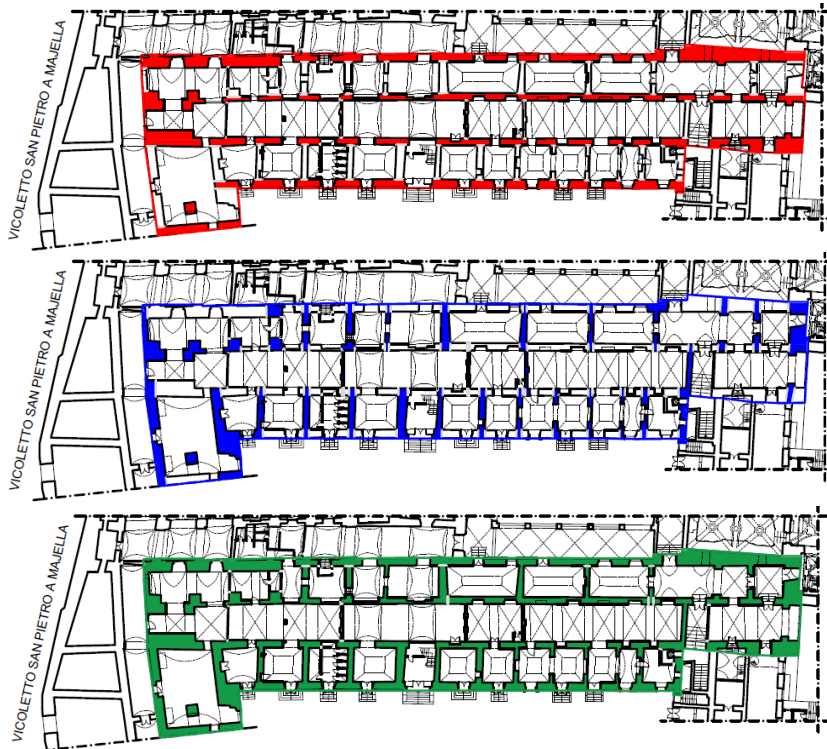
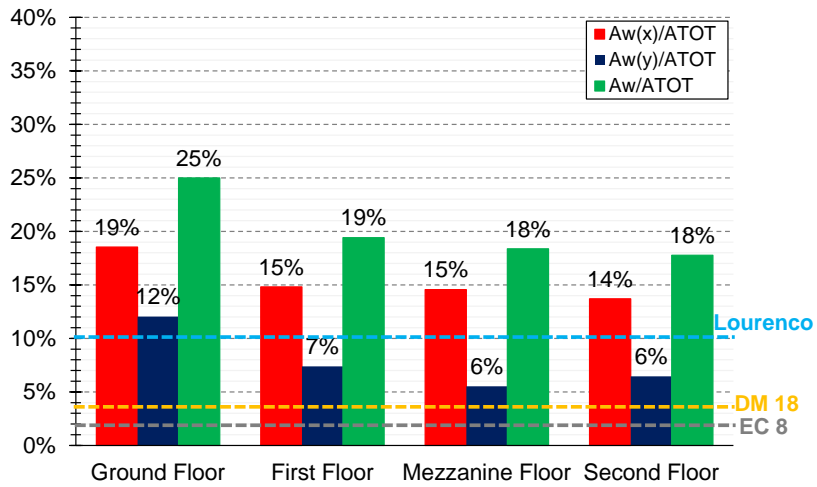


Figure 3.3. In-plan ratio: Construction 0.

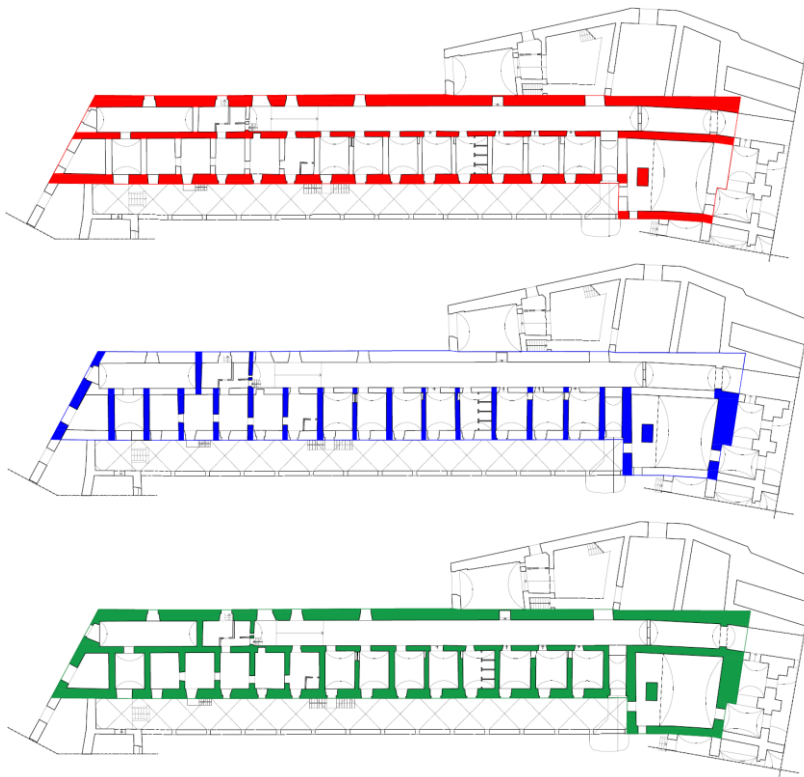
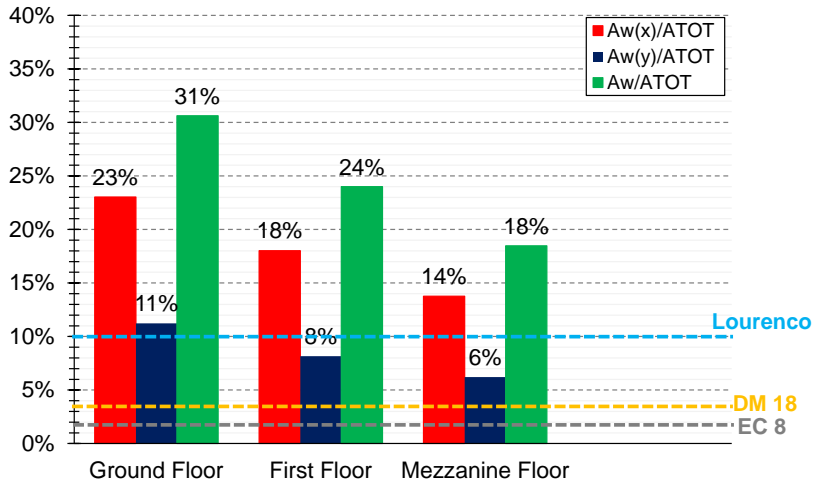


Figure 3.4. In-plan ratio: Construction 1.

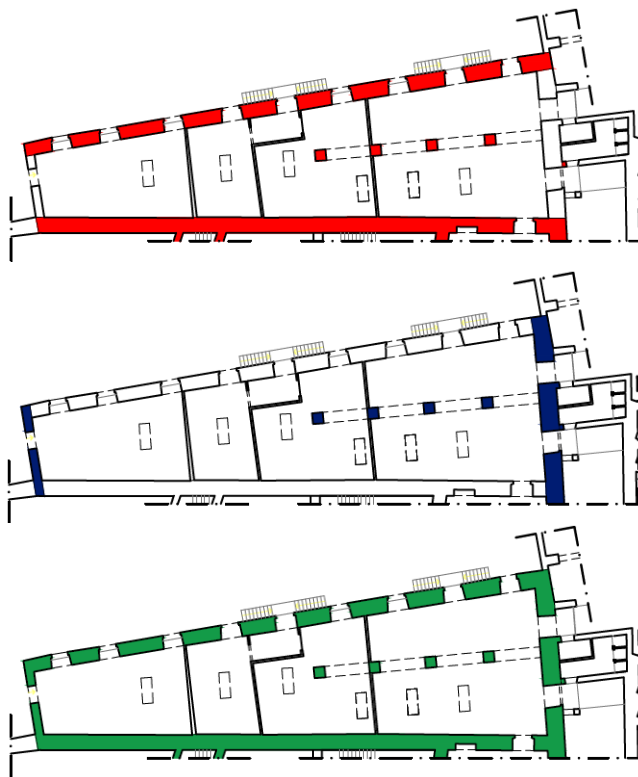
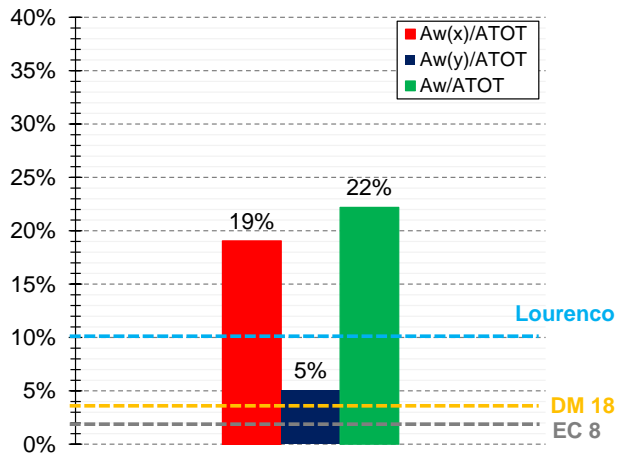


Figure 3.5. In-plan ratio: Construction 2.

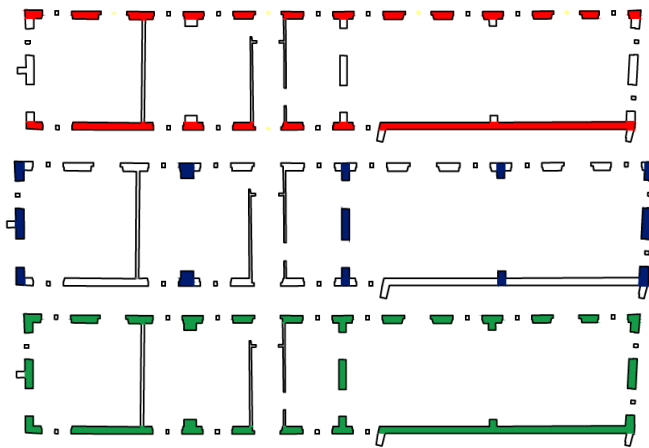
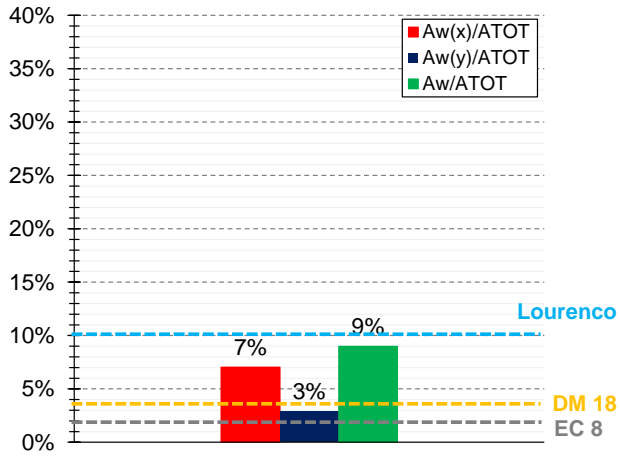


Figure 3.6. In-plan ratio: Construction 4.

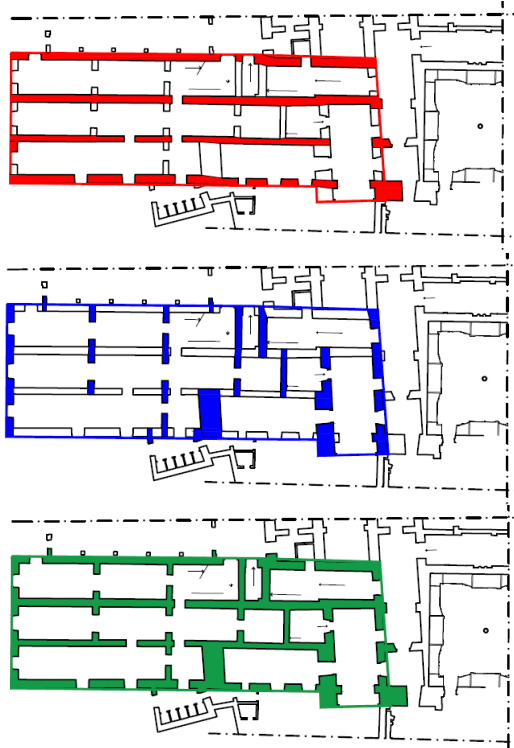
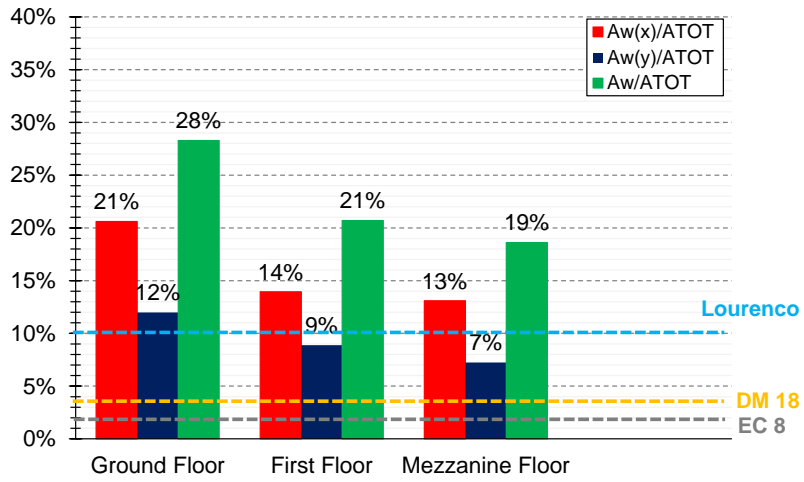


Figure 3.7. In-plan ratio: Construction 6.

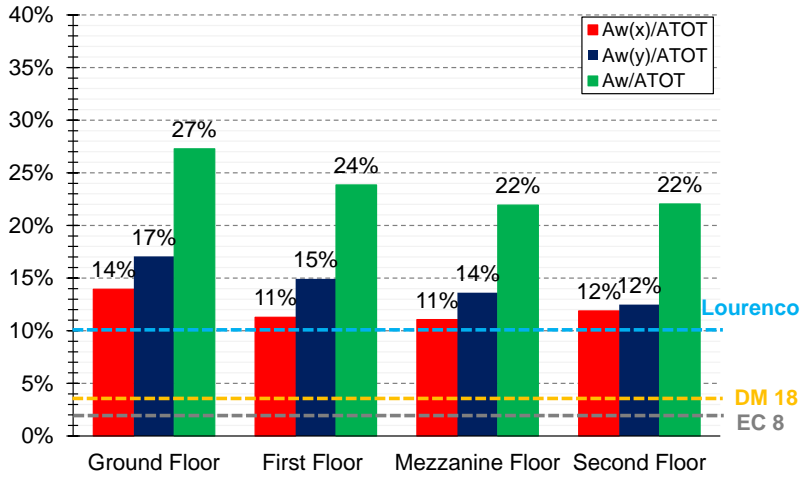




Figure 3.8. In-plan ratio: Construction 7.

Table 3.7. In-plan ratios for analysed structures.

Construction	Level	A_{tot}	A_w	A_w/A_{tot}	$A_{w,x}$	$A_{w,x}/A_{tot}$	$A_{w,y}$	$A_{w,y}/A_{tot}$
$[-]$	$[-]$	$[m^2]$	$[m^2]$	$[\%]$	$[m^2]$	$[\%]$	$[m^2]$	$[\%]$
C0	Ground Floor	1566	391	25%	290	19%	188	12%
	First Floor	1493	290	19%	221	15%	110	7%
	Mezzanine Floor	1493	274	18%	217	15%	83	6%
	Second Floor	1493	265	18%	205	14%	96	6%
C1	Ground Floor	1000	306	31%	230	23%	112	11%
	First Floor	951	228	24%	171	18%	78	8%
	Mezzanine Floor	952	176	18%	131	14%	59	6%
C2	Ground Floor	428	95	22%	81	19%	22	5%
C4	Ground Floor	425	38	9%	30	7%	12	3%
C6	Ground Floor	649	183	28%	134	21%	78	12%
	First Floor	617	128	21%	86	14%	55	9%
	Mezzanine Floor	617	115	19%	81	13%	45	7%
C7	Ground Floor	2153	587	27%	300	14%	367	17%
	First Floor	2153	514	24%	243	11%	321	15%
	Mezzanine Floor	2044	448	22%	226	11%	278	14%
	Second Floor	1470	324	22%	175	12%	183	12%

3.4 On the arrangement of the openings

In addition to the index discussed in the previous sections, another geometric feature that significantly affects the seismic performance of the masonry structures is the regularity of the arrangement of the openings and their sizes. An irregular arrangement of openings not only reduces the lateral strength and stiffness of the wall but also induces a nonuniform distribution of gravity loads among masonry piers. This irregularity can lead to localized stress concentrations, elevating the risk of premature wall collapse. As a result, the seismic vulnerability of the structure increases significantly (Parisi and Augenti, 2013 [14]). The importance of this issue is also underlined by Cavalieri in his ancient treatise (1839) [10]. Within it, he

outlines four guiding rules for the arrangement of the openings, as listed below [in Italian].

“1° I vani debbono sempre corrispondere verticalmente sui vani, ed i pieni sui pieni. Le trasgressioni di questo precetto producono i così detti posamenti in falso, oignor contrari alla solidità reale ed apparente delle fabbriche.

2° I vani vogliono essere distribuiti a regolari distanze; non troppo spaziosi, né soverchiamente moltiplicati. Osservò il più delle volte ricordato Leon Battista Alberti che nell'opere degli antichi i vani delle facciate non componevano giammai più che la settima, né meno che la nona parte della superficie del muro in cui erano compresi.

3° Siccome le parti basse de' muri sono destinate a sopportare tutto il peso delle parti superiori, così ragion vuole che i vani sieno in esse meno frequenti e meno spaziosi che altrove.

4° I vani debbono tenersi lungi dagli angoli degli edifizzi, i quali ne costituiscono quasi i cardini, ed abbisognano della maggior solidità.”

(Cavalieri – San Bertolo, 1839. Istituzioni di architettura statica e idraulica)

In particular, these principles prescribed: (1) the vertical alignment of the openings, as any deviations from a regular layout can reduce the lateral strength of the walls and can lead to stress concentrations; (2) an uniform distribution of the openings with equal horizontal distance between them; (3) to have fewer and smaller openings in the lower wall section, given the higher vertical loads in these areas; (4) to keep openings away from the corners of buildings, being the corners critical structural points that require greater solidity.

Some considerations regarding the arrangement of the openings of the extracted walls from the analysed structures are listed below. For visual references and detailed plans with labelled wall alignments, please refer to **Appendix 2**.

Construction 0. In longitudinal direction, the masonry walls are characterized by regular arrangement of the openings, showcasing precise vertical alignment and equal horizontal distance between them. However, this regularity is disrupted in the case of wall 5x, where the presence of recesses on the ground floor creates misalignment with the openings on the upper levels. Conversely, in transverse direction, there is an irregular distribution of openings. Additionally, the structure in this direction is characterized by the presence of walls supported by vaults. Furthermore, in x direction, the openings are interspersed with larger-sized masonry piers, defining

unreduced resistant sections. In contrast, in y direction, the walls feature minimal dimensions for the resistant sections of the masonry piers.

Construction 1, 6. The masonry walls are characterized by regular arrangement of the openings, showcasing precise vertical alignment and equal horizontal distance between them. Furthermore, the openings are interspersed with larger-sized masonry piers, defining unreduced resistant sections.

Construction 2, 4. The masonry walls are characterized by regular arrangement of the openings, showcasing equal horizontal distance between them. Furthermore, the openings are interspersed with larger-sized masonry piers, defining unreduced resistant sections.

Construction 7. In both directions, the masonry walls show irregular arrangement of the openings, with variations in vertical alignment and variations in pier widths. Furthermore, the openings are interspersed with larger-sized masonry piers, defining unreduced resistant sections.

Chapter 4

Structural analysis of masonry vaults

This Chapter deals with the structural analysis of the masonry vaults of the St. Domenico Maggiore Convent in Naples. At first, it provides some preliminary considerations finalized to the analysis of the construction quality of the masonry vaults, that is evaluated in terms of their adherence to “the rules of art”. Specifically, the analysis examines compliance with the guidelines from Breyman’s treatise (1885) regarding materials to be used for the construction of the vaults and on their construction methods, as well as adhering to Colombo’s Manual of Engineer (1887) prescriptions concerning vault and pier thickness. This will be followed by the analysis of the stability of the vaults under vertical loads. In particular, the analyses have been conducted through the Méry’s method (1840), for each type of vault found in the convent, including barrel, cross and lowered cloister vaults. According to Méry’s method, the stability of the vaults can be verified through a geometric construction, eliminating the need for extensive calculations. By assuming an arch with three hinges, that is a statically determined structure, the horizontal thrust value is precisely determined. The analysis reveals that the thrust line consistently falls within the middle third, confirming the stability of the analysed vaults, except for the lowered cloister vault. Recognizing that Méry’s method is unsuitable for assessing the stability of this specific vault typology under vertical load, the analysis is extended. This expansion involves discarding the assumption that the thrust line must be contained within the middle third and allowing it to extend throughout the entire thickness of the arch. With the thrust line contained within the arch’s thickness, in accordance with the safety theorem of limit analysis formulated by Heyman (1982), the vault is deemed safe.

4.1 On the material to be used for the vaults as suggested in Breymann (1885)

In his treatise [8], Breymann discusses general principles for constructing vaults, emphasizing the use of lightweight materials to minimize pressures transmitted to the supporting piers. The objective is to enable the construction of thinner piers by opting for lighter materials compared to relatively heavier stones. In particular, Breymann recommends the utilization of bricks, whether solid or hollow, based on the vault span, with a preference for lightweight alternatives. Furthermore, he highlights occasional use of terracotta vessels, tuff, lightweight and porous lava, as well as cement tiles in construction practices.

“In generale si cercherà di adoperare, per la costruzione delle volte, materiale leggero il più possibile perché così le pressioni, che si trasmettono ai piedritti, divengono piccole il più possibile, e per conseguenza si possono costruire questi ultimi più sottili, che se si impiegassero pietre relativamente più pesanti. Siccome la resistenza di un materiale dipende dalla sua densità e questa è in proporzione diretta del suo peso, così nel suo impiego bisogna distinguere bene, se esso ha a servire per volte, che hanno a portare solo il proprio peso, oppure per volte soggette anche a sovraccarico. [...] Ma siccome nell'edilizia raro si ha a fare con volte molto caricate, [...] in genere si impiegano, secondo l'ampiezza della volta, mattoni pieni o vuoti, e leggeri il più possibile. E qualche volta si adoperano pure i vasi di terra cotta, il tufo, la lava leggiera e porosa e le formelle di cemento.”

(Breymann, 1885. Costruzioni in pietra e strutture murali)

These recommendations come to life through their practical implementation in the Convent case study. In the survey phase, the examination of certain vaults was carried out using endoscopic analyses. Figures 4.1 to 4.5, displaying the labels assigned to the vaults, provide a visual guide to the locations of various endoscopic analyses detailed in this dissertation. Specifically, the exact positions of the endoscopies, depicted in the photos from Figures 4.6 to 4.11, are marked with red stars. This meticulous analysis provided insights into the composition of the vaults, revealing both the material used and the underlying stratigraphy. Referencing Figures from 4.6 to 4.11, which depict the endoscopic analyses conducted on some vaults, it becomes evident that these structures are constructed using tuff masonry.

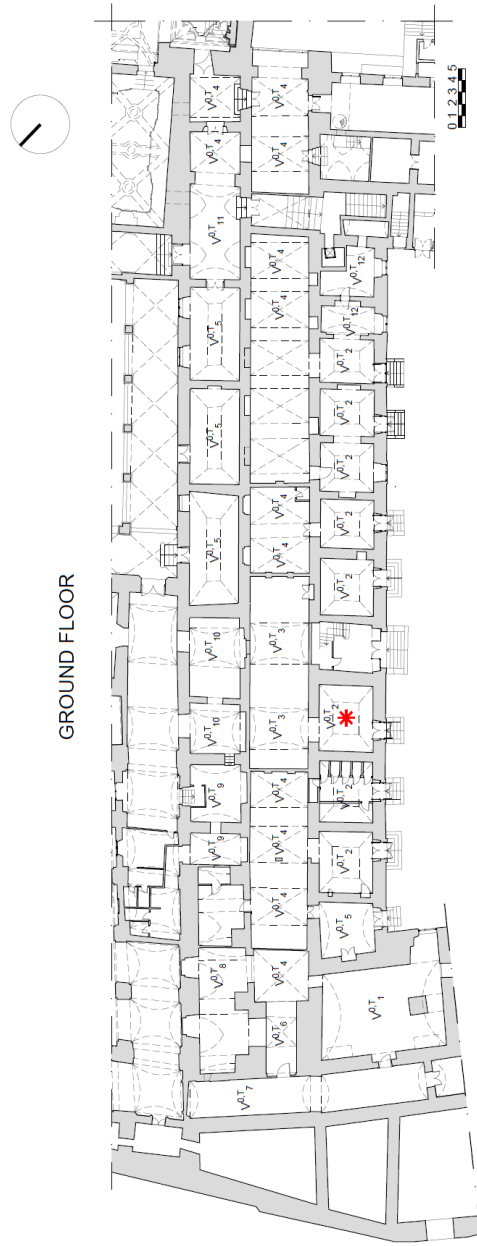


Figure 4.1. Vaults' labels and location endoscopic analyses: Construction 0 – ground floor.

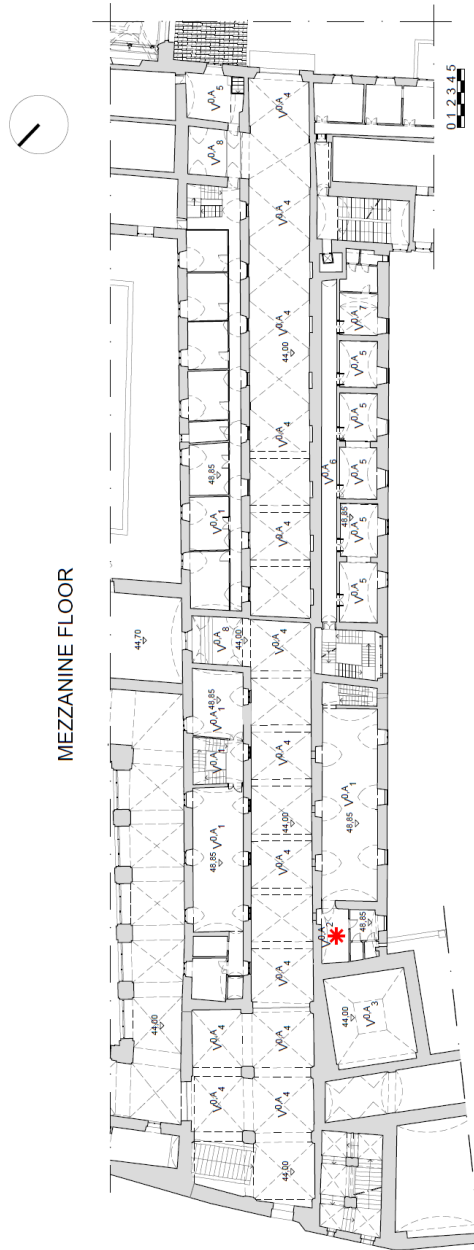


Figure 4.2. Vaults' labels and location endoscopic analyses: Construction 0 – mezzanine floor.

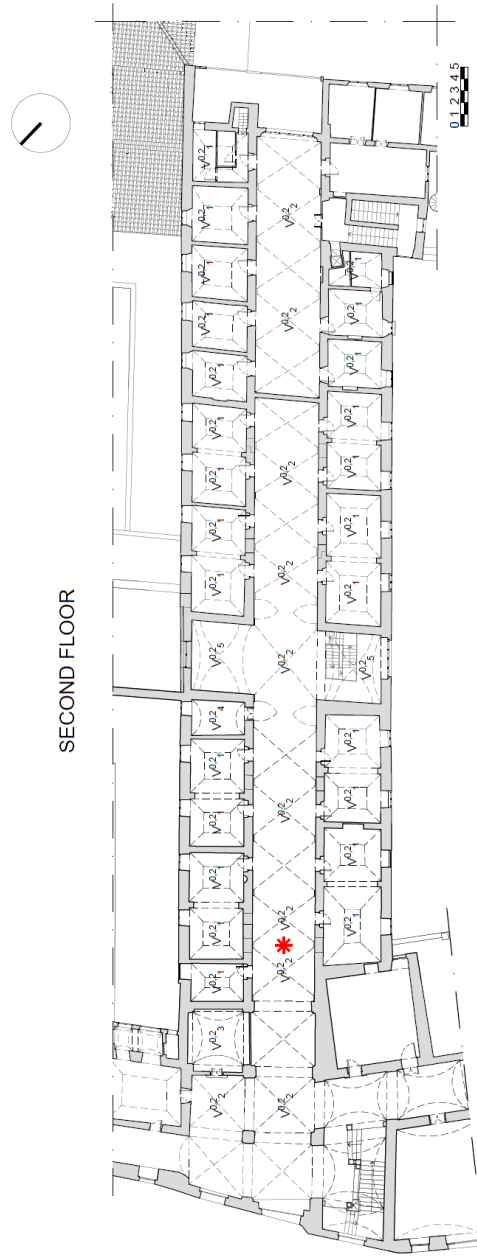


Figure 4.3. Vaults' labels and location endoscopic analyses: Construction 0 – second floor.

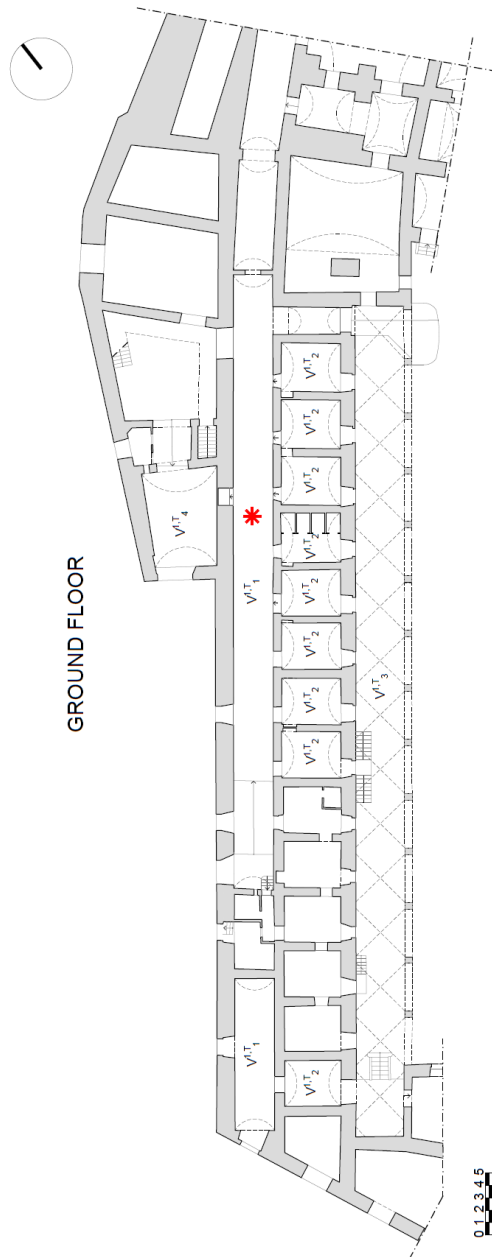


Figure 4.4. Vaults' labels and location endoscopic analyses:
Construction 1 – ground floor.

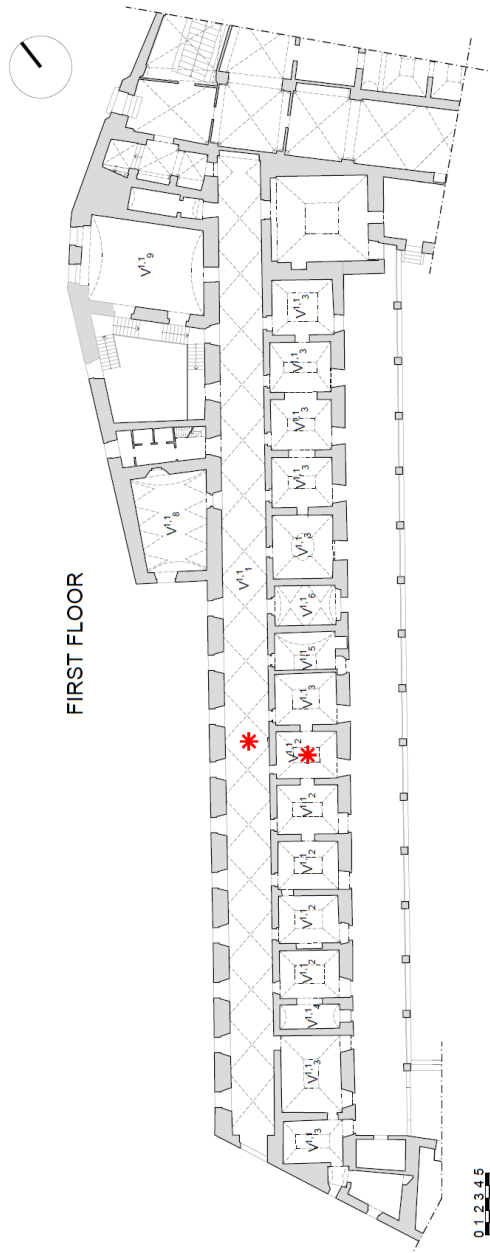


Figure 4.5. Vaults' labels and location endoscopic analyses: Construction 1 – first floor.

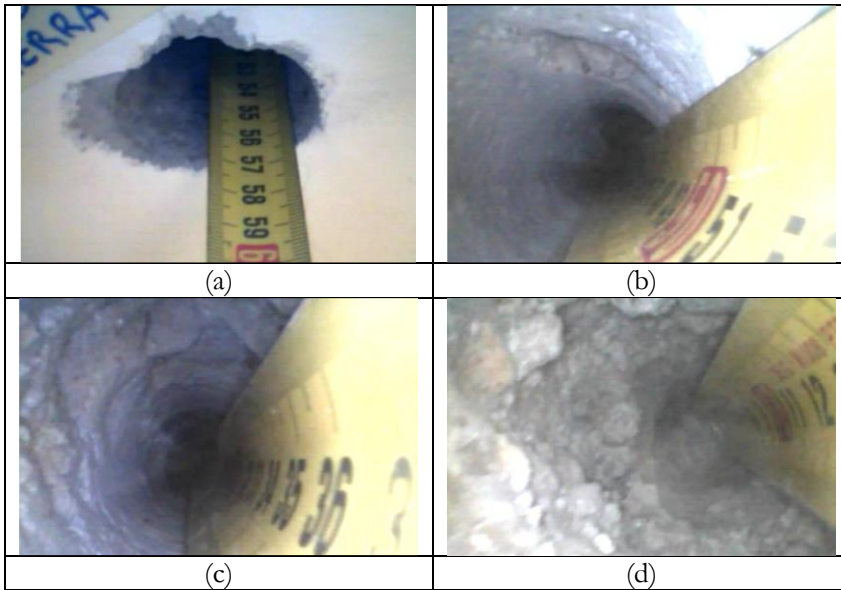


Figure 4.6. Lowered cloister vault V^{0,T_2} : Endoscopic Analysis.

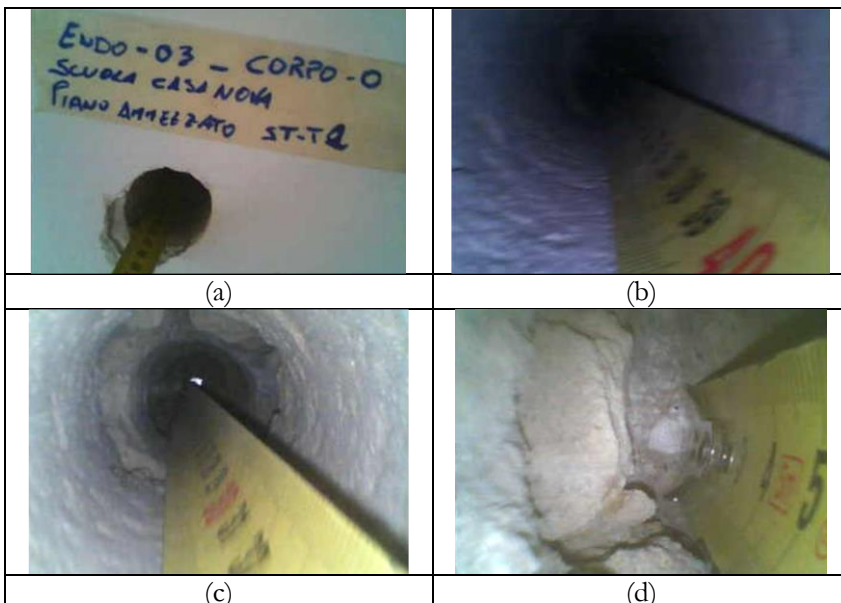


Figure 4.7. Barrel vault V^{0,A_2} : Endoscopic Analysis.

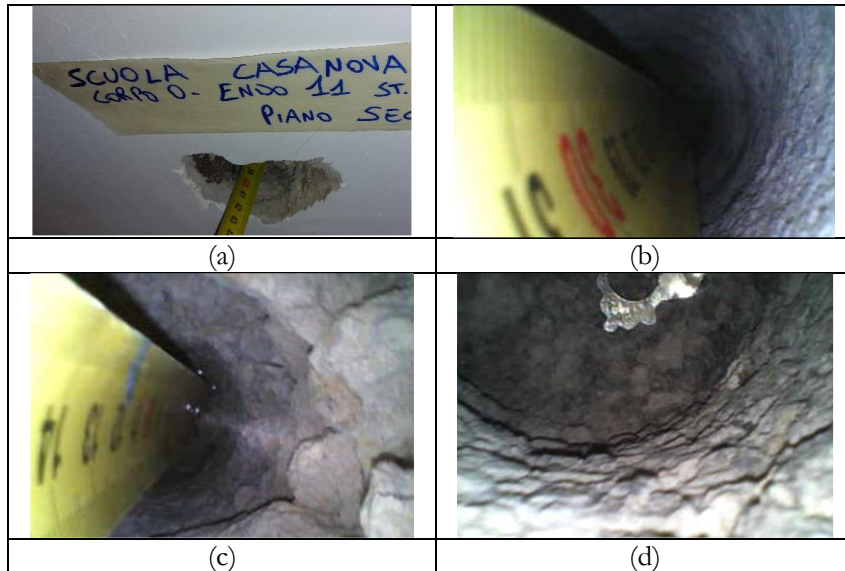


Figure 4.8. Cross vault $V^{0,2}$: Endoscopic Analysis.

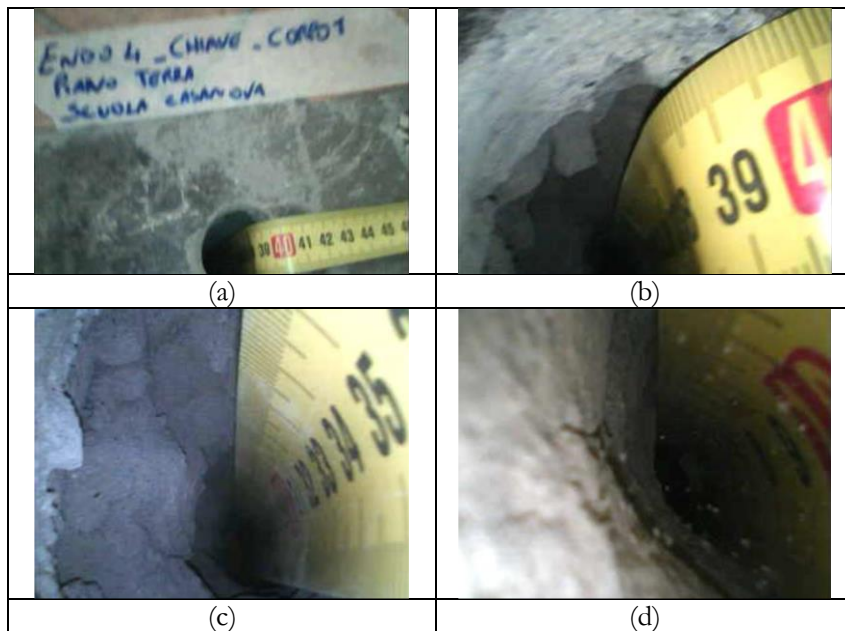


Figure 4.9. Barrel vault V^{1,T_1} : Endoscopic Analysis.

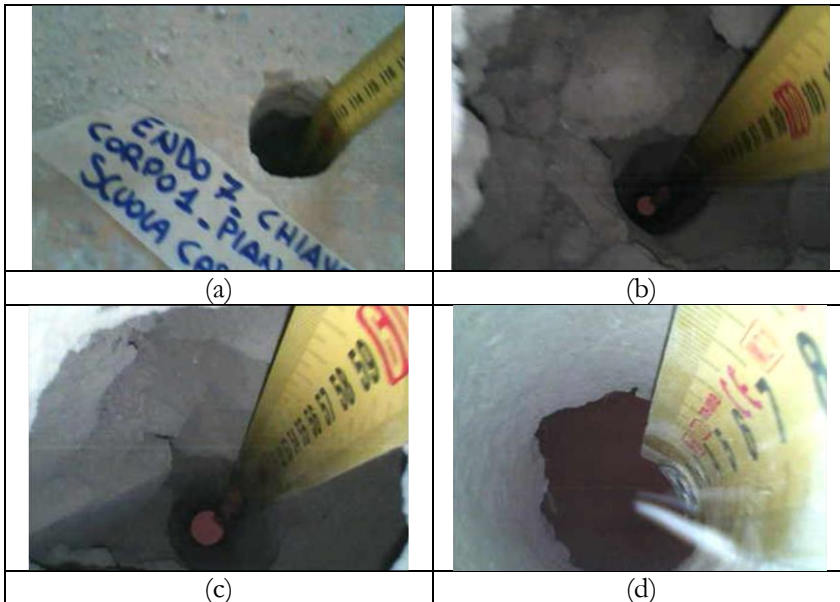


Figure 4.10. Lowered cloister vault $V^{1,12}$: Endoscopic Analysis.

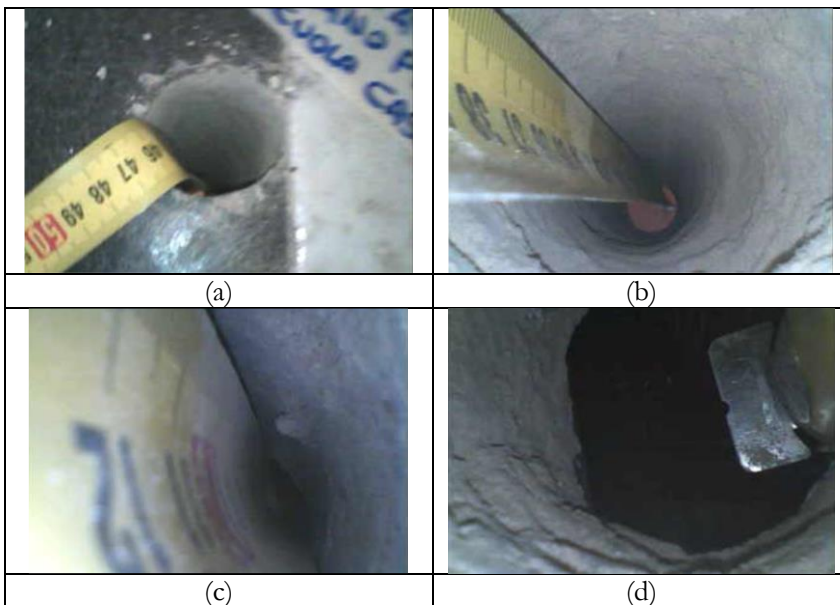


Figure 4.11. Cross vault $V^{1,11}$: Endoscopic Analysis.

4.2 On the construction methods as described in Breyman (1885)

In this Section, the construction methods used in masonry vaults are detailed, focusing particularly on the vault typologies found within the Convent. The discussion highlights different brick patterns employed in barrel, cross, and lowered cloister vaults, outlining the advantages and disadvantages associated with each choice.

4.2.1 Barrel vaults

As described in Breyman (1885) [8], the intrados of barrel vaults is typically arranged in a block pattern (*longitudinal row arrangement*), requiring the use of at least two different and alternating courses of bricks. If the vault is one-brick thick, all bricks are arranged in depth, and the coincidence of joints is easily avoided by starting one course with a full brick and the next with a half brick or a brick and two quarters.

“L’intradosso della volta per solito presenta la disposizione a blocco; si richiedono quindi per formare la disposizione almeno due corsi diversi ed alternati.

Se la volta ha lo spessore di 1 testa, allora tutti i mattoni appaiono disposti in grossezza, e si evita facilmente la coincidenza dei giunti, incominciando un corso si ed uno no, con un mattone due quarti o con un mezzo mattone.”

(Breyman, 1885. Costruzioni in pietra e strutture murali)

This arrangement proves disadvantageous for vaults with large span and a low rise, because the key joints are almost vertical and parallel; consequently, the resistance relies solely on mortar cohesion and is therefore limited. In such instances, an alternative approach was placing the bricks at 45° degrees with respect to the edges of the plan. This arrangement is called *herringbone arrangement*. This method, as detailed by Breyman, initiates construction simultaneously in at least two corners of the space to be vaulted, or more conveniently in all four corners. The vault closure takes place in the middle with a square element. Notably, this technique offers advantages over the previously mentioned method: the pressure of the vault is distributed more on the perimeter walls, where also the front-walls partly act as piers.

“Frequentemente si suole adoperare anche un’altra disposizione, che è detta disposizione a spinapesce. In questa le commisure dei mattoni formano in proiezione orizzontale un angolo di 45 gradi coll’asse della volta.

Il lavoro s'incomincia quindi contemporaneamente almeno in due angoli dell'ambiente da coprirsi con la volta, e con maggiore comodità in tutti e quattro gli angoli, e la chiusura della volta ha luogo nel mezzo con un quadrato. Questo modo di costruire la volta se ne fa ascendere alquanto la linea di chiave dalle due fronti verso il mezzo, offre alcuni vantaggi su quello summentovato e rappresentato nella fig. 347, perché i singoli corsi vi ricevono maggiore sviluppo e la pressione della volta si ripartisce di più sui muri di perimetro, servendo in parte da piedritti anche i muri di fronte."

(Breymann, 1885. Costruzioni in pietra e strutture murali)

The disadvantageous of the longitudinal row arrangement is also confirmed by Formenti in the treatise (1893) [15], which, like Breymann, suggests the herringbone arrangement as an alternative.

"Un tale ordinamento, non è conveniente per le volte reali a botte a tutto sesto, la cui direttrice circolare abbia un raggio grande di curvatura, e per le volte a botte ribassate in genere, nelle quali il rapporto tra la saetta e la corda della direttrice sia piccolo, diventando, in tali volte, e per tale ordinamento minimo il contrasto che si sviluppa tra i materiali dei filari dei mattoni; i filari sono ordinati simmetricamente nelle quattro parti rettangolari in cui è divisa la volta dai piani verticali mediani, ed in ciascuna di queste parti, i filari sono diretti con una inclinazione di 45° per rispetto alle murature di contorno, la quale inclinazione, però, è opposta nei riparti contigui, cosicchè i filari che si proiettano in pianta rettilinei, formano, nella struttura murale della volta, come altrettanti archi zoppi ellittici che si uniscono, con inclinazioni contrarie ed a zig-zag, lungo le due linee di mezzeria della volta, ossia lungo la mezzeria longitudinale rettilinea, e lungo quella trasversale circolare."

(Formenti, 1893. La pratica del fabbricare per l'ingegnere)

Breymann and Formenti describe a third method for constructing vaults with low rise, represented in Figure 4.12c. It stands out from the previously described methods as the courses begin from the center and close at the piers. This method shares the advantages of the herringbone arrangement and additionally provides more convenience and regularity in construction.

When constructing barrel vaults with natural stones, the key to stability lies in the perfect connection of the material with the mortar, requiring primary attention to this aspect.

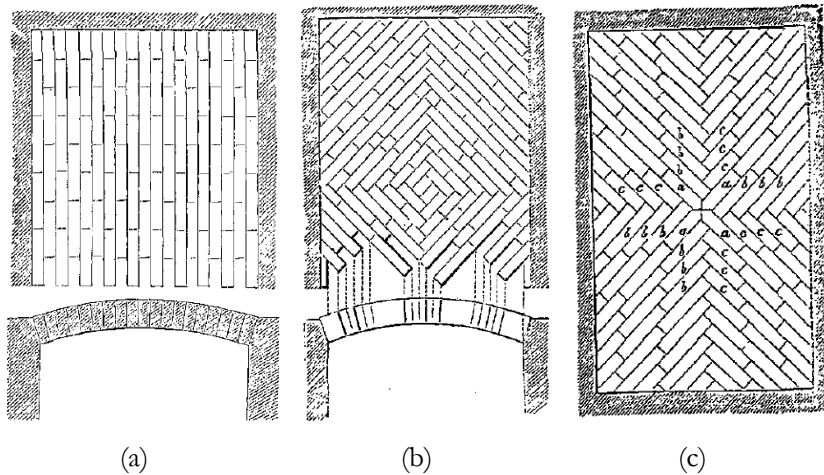


Figure 4.12. Different arrangement of barrel vault: longitudinal (a) and herringbone arrangement (b); additional brick pattern for barrel vault (c) [8].

4.2.2 Cross vaults

The cross vault has a significant static advantage over the other vault types, such as barrel and lowered cloister vaults. Its weight is strategically concentrated at specific points, eliminating the need for continuous surrounding walls as required by other vault types.

As outlined in Breymann, treatise (1885) [8], the construction process of the cross vault involves the installation of centering corresponding to the arches, corners, and ribs. A notable feature is the erection of a vertical support structure, known as the “monk”, positioned at the intersection of diagonals in a quadrilateral or at the center of gravity of regular or irregular polygons. This “monk” provides crucial support for the converging centering elements.

Following centering installation, the vault construction initiates from the corners. In the case of brick material, the cross vault employs a herringbone arrangement. The thickness of the fillings is determined by the span length, typically receiving the thickness of one brick for spans between 4.5 m and 5.5 m. Connection details for fillings of different thicknesses are illustrated in Figure 4.13. The construction process closely aligns with principles outlined for barrel vaults.

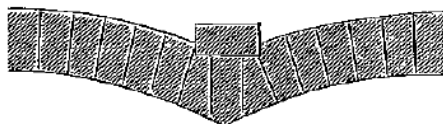


Fig. 396.

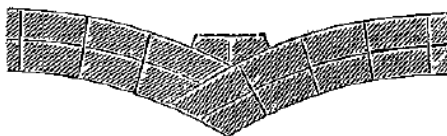


Fig. 397.



Fig. 398.

Figure 4.13. Cross vault: connection details [8].

“La costruzione della volta a crociera richiede essa pure l’impianto di centine in corrispondenza agli archi di testa, agli spigoli ed alle costole.

[...]

Nel punto di incontro delle diagonali della pianta quadrilatera, o nel centro di gravità del poligono regolare od irregolare si eleva un ritto, il così detto monaco, al quale si appoggiano le centine ivi concorrenti.

[...]

All'impianto delle centine tien dietro la costruzione delle volte, che naturalmente si deve incominciare dagli angoli.

[...]

Se il materiale è costituito di mattoni, allora alla volta si costruisce con disposizione a spinapesce, per cui i filari di due ripieni attigui vengono a trovarsi in un piano, e la pressione della volta, che agisce secondo gli spigoli, si trasmette normalmente ai corsi dei ripieni. Con questa disposizione è pure possibile rinforzare il collegamento dei ripieni con gli spigoli, sui quali i singoli ripieni trovano peduccio. L'ingrossamento degli spigoli in confronto allo spessore dei ripieni è almeno di una testa. I ripieni per solito, quando hanno la corda da 4, 5 m a 5,5 m ricevono lo spessore di una testa, ed allora lo spessore degli spigoli si fa di due teste. Con spessore maggiore di 2 teste i ripieni non si possono costruire bene, ed allora agli spigoli si assegna lo spessore di 3 teste. le fig. 396 – 398 mostrano il modo di collegamento per ripieni grossi 1 e 2 teste, con spigoli rinforzati di 1 testa, in sezione normale a questi ultimi.

(Breyman, 1885. Costruzioni in pietra e strutture murali)

From the available photos dating back to the period following the 1980 Irpinia earthquake, it is evident that the cross vaults in Construction 0 of the Convent of San Domenico Maggiore feature a herringbone brick arrangement (Figure 4.14), adhering to the principles outlined by Breyman in his treatise.

However, for the other Constructions of the convent, more detailed investigations were not feasible, preventing the identification of the specific brick arrangement type.



Figure 4.14. Cross vault of construction 0 after the 1980 Irpinia Earthquake: herringbone arrangement.

4.2.3 Lowered cloister vaults

As outlined in Breymann (1885) [8], for the construction of the horizontal central part of the lowered cloister vaults, opting for a gently rounded profile is preferable to a flat structure. When utilizing bricks, a herringbone arrangement is recommended for optimal construction. To ensure the successful execution of this pattern, it is suggested to maintain a profile flatter than a quarter of a circle in the section near the perimeter of the vault. Alternatively, the adoption of the herringbone arrangement exclusively to the horizontal central part of the vault can be chosen. For added structural support, it is advisable to strategically position resilient, high-quality natural stones, particularly at point “a” in the corners (Figure 4.15).

“Per costruirla si richiede un manto completo, e non si ha altro ad osservare circa il medesimo, se non che la parte centrale che forma lo specchio anche in questo caso, non deve essere piana, ma bensì un po’ arrotondata. Se si adoperano i mattoni per materiale, si costruisce una volta collo spessore di 1 testa con disposizione a spinapesce. Le parti prossime ai muri di perimetro ed appartenenti alla volta a padiglione od a conca tengono più schiacciate di un quarto di circolo, perché altrimenti non si potrebbe eseguire bene la disposizione a spinapesce. Ma se si vuol tenere la costruzione, che si rileva dalla sezione

trasversale alla fig. 444, allora le parti arcuate si trattano come una volta a padiglione, e si adotta la disposizione a spinapesce per la sola parte centrale. E' da raccomandarsi di porre in a, negli angoli, pietre naturali di qualità resistente, per impostarvi la parte di volta costrutta a spinapesce."

(Breyman, 1885. Costruzioni in pietra e strutture murali)

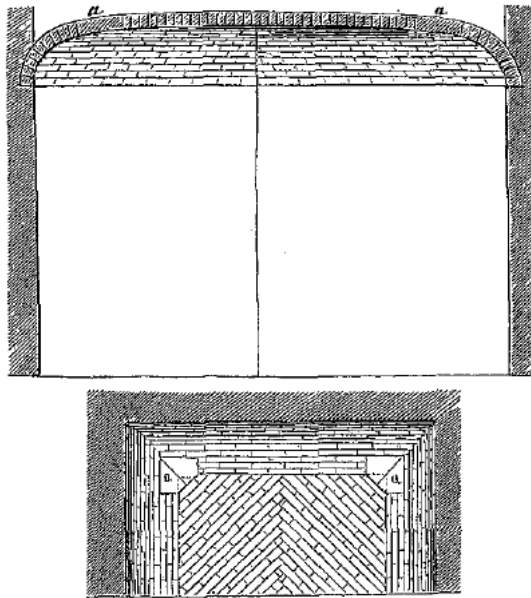


Fig. 444.

Figure 4.15. Lowered cloister vault: herringbone arrangement [8].

For this specific vault typology, any external loads beyond the self-weight must be avoided. The overall success of the entire structure only depends on the use of excellent mortar. Indeed, the central horizontal part of the vault is characterized by a certain level of security only when it can be regarded as a unified with the mortar.

“Anche alla volta specchio non si può assolutamente addossare sovraccarico. Perché, sebbene la sua resistenza si possa ritenere un po' meno piccola di quella di una piattabanda, pure il successo di tutto l'insieme dipende solo dall'impiego di una eccellente malta: infatti la parte centrale della volta a specchio accorda solo una certa sicurezza, quando la si può considerare come un sol tutto riunito insieme dalla malta”.

(Breyman, 1885. Costruzioni in pietra e strutture murali)

For this particular vault type in the convent case study, more comprehensive investigations proved unfeasible, impeding the identification of the specific brick arrangement type and detailed information about the characteristics of the mortar.

Furthermore, the lowered cloister vaults on the ground and first floor of Construction 0 and on the first floor of Construction 1 deviate from Breyman's recommended rule, which suggests they should remain unloaded. This deviation is attributed to the later addition of other levels, occupied by the laboratories of the Casanova Institute in subsequent years.

4.3 On the thickness of the vaults and piers as suggested by Colombo (1887)

In his Manual of Engineer [11], Colombo (1887) outlines guidelines for the construction of various type of vaults, including barrel vaults, cross vaults and lowered cloister vaults, with specific considerations for their dimensions and supporting structures. The prescribed number of keystones and springers, as well as the thickness of piers, varies based on the span of the vault. Additionally, the thickness of piers is influenced by the height of the structure.

For *barrel vaults supporting floors with ordinary loads*, the number of keystones at the crown and springers at the impost varies depending on the span of the vault. In particular, for spans from 4 to 5 m, 1 keystone and 2-3 springers are advised; for spans between 5 and 8, 2 keystones and 3-4 springers are prescribed (Table 4.1). The width of piers is detailed based on the height of the structure and the type of arch used. For heights up to 3 m, the suggested width for piers is $1/6$ – $2/11$ of the span and $2/7$ – $2/9$ of the span for semicircular and segmental arches, respectively. For height higher than 3 m, the pier's width is increased of $1/6$ – $1/8$ of the height.

Table 4.1. Keystones at the crown and springers at the impost for barrel vault supporting floors with ordinary loads.

Barrel vault supporting floors with ordinary loads		
Span	up to 4-5 m	5-8 m
keystones at the crown	1	2
springers at the impost	2-3	3-4

“Groschezza delle spalle, fino a 3 m di altezza, 1/6 – 2/11 della luce per archi a tutto sesto; 2/7 – 2/9 per archi scemi con saetta da 1/8 a 1/3 della corda. Per altezze > 3 m, la groschezza si aumenta di 1/6 – 1/8 dell’altezza.”

Similarly, for *cross vaults and lowered cloister vaults supporting ordinary loads*, the prescribed number of keystones and springers varies with the span dimension of the vault. Specifically, for spans up to 3.5 - 4 m, one keystone and 1-2 springers are suggested; for spans between 4 and 6 m, two keystones and 2-3 springers are prescribed; and for spans between 6 and 8 m, two keystones and 3-4 springers are recommended (Table 4.2). The width of piers is discussed concerning the structure’s height, with distinct recommendations for various vault heights:

1. For Heights < 3 m:
 - In cross vaults, the width of piers should be between 1/4 and 1/6 of the diagonal.
 - In lowered cloister vaults, the width should range from 1/4 to 1/5 of the span.
2. For Heights > 3 m:
 - An additional thickness is advised, increasing the previous measurement from 1/8 to 1/10 of the height.

Table 4.2. Keystones at the crown and springers at the impost for cross vault and lowered cloister vault supporting ordinary loads.

Cross vault and lowered cloister vault supporting ordinary loads			
Span	up to 3.5-4 m	4-6 m	5-8 m
keystones at the crown	1	2	2
springers at the impost	1-2	2-3	3-4

“Groschezza delle spalle o piedritti.

- *per altezze < 3 m lo spessore delle spalle è di 1/4 - 1/6 della diagonale nelle volte a crociera, 1/4 - 1/5 dell’ampiezza in quelle a schifo, 1/7 – 1/8 del diametro in quelle a tazza.*
- *Per altezze > 3 m, si aumenta il precedente spessore di 1/8 – 1/10 dell’altezza.”*

Finally, the treatise touches on simple covering vaults without additional loads, suggesting the use of bricks, solid or hollow, laid flat for small spans

and providing thickness recommendations for keystones and shoulders for both small and large spans.

“Volte di semplice copertura senza sopraccarico si possono fare con mattoni, pieni o vuoti, messi a piatto, per piccole ampiezze; per grandi ampiezze (volte delle chiese etc.) lo spessore in chiave = 1/40 – 1/60, la gross. dei piedritti = 1/7 -1/9 dell’ampiezza.”

Tables 4.3 and 4.4 present a comparative analysis of keystone dimensions at the crown and pier widths for selected vaults in the analysed constructions, in relation to the prescriptions by Colombo. In particular, the thicknesses at the crown align with Colombo’s guidelines, with the exception of the barrel vault, which deviates with a lower value. In terms of pier widths, it is evident that the observed values fall below Colombo’s prescribed standards outlined in his Manual, except for the cross vault whose values align with the prescriptions.

Table 4.3. Keystones at the crown.

Vault	Span	Colombo (1887) keystones at crown			
		[m]	[n]	[cm]	[cm]
Barrel vault	V ^{0,A} ₂	4.73	1	12	23
Cross vault	V ^{0,2} ₂	5.37	2	24	22
Cloister vault	V ^{0,T} ₂	4.50	2	24	24

Table 4.4. Width of piers.

Vault	Span	Height	Colombo (1887) Width of piers			
			[m]	[m]	[cm]	[cm]
Barrel vault	V ^{0,A} ₂	4.73	1.82	79	- 86	74
Cross vault	V ^{0,2} ₂	5.37	5.04	56	- 72	70
Cloister vault	V ^{0,T} ₂	4.50	3.42	124	- 147	92

4.4 Structural analysis of the vaults of Saint Domenico Maggiore Convent

In this Section, the structural analysis of the vaults for vertical loads in the Convent of San Domenico Maggiore in Naples is presented. The analyses are performed using Méry's method (1840) [16], considering each type of vault found in the convent, including barrel vaults, cross vaults, and lowered cloister vaults.

Méry observed that actual arches have a thickness greater than strictly necessary for mathematical equilibrium. This characteristic permits the tracing of infinite thrust lines without accurately determining the true one. To find an unique equilibrated solution among these infinite possibilities, he assumed the arch with three hinges, representing a statically determined structure (isostatic structure). In particular, the hypotheses adopted by Méry are:

- 1) The subject of the study is the symmetric masonry arch, modelled as a system of rigid bodies (voussoirs), subjected to a symmetric load;
- 2) The collapse mechanism of Mascheroni is considered, involving the formation of three plastic hinges – two on the intrados of the arch at the 30° sections and one at the arch crown;
- 3) Finite friction and infinite compressive strength for the masonry are assumed. However, in the latter part of Méry's essay, this hypothesis is revisited, and the effect of limited compressive strength is examined.

The arch with three hinges, being a statically determined structure, allows the solution to be derived solely from equilibrium equations. However, Méry's method employs a graphical representation, devoid of complex calculations, to determine the horizontal thrust value and the thrust line.

To account for the finite compressive strength of the masonry, the middle third is regarded as the limit of the thrust line. If the thrust line remains within this middle third, all sections experience compression, ensuring the stability of the arch.

4.4.1 Construction 0: barrel vault V^{0,A_2} (mezzanine floor)

The barrel vault V^{0,A_2} of the Construction 0 (Figure 4.16) sets on a trapezoidal plan, whose main dimensions are 4.73 and 4.83 m. The cross-section of the vault reveals a segmental arch characterized by a rise (f) of 165 cm and a span ($2L$) of 473 cm, resulting in a f/L ratio of 0.70. The arch has a distinctive radius of 263 cm and a thickness of 23 cm, assumed to be constant along the cross-section.

For the structural analysis, a portion of 1 m has been considered, in longitudinal direction. Due to the arch's symmetry, the study has focused on one half of the structure. The arch has been subdivided into 9 ideal voussoirs to discretise the calculation of the load due to self-weight and the additional loads (Figure 4.17). A specific weight of the masonry and filling equal to 16 kN/m^3 and an additional load of 3 kN/m^3 (Cat. C of the NTC18) have been considered. The total weight of the vault, estimated summing the self-weight $W_i = 40.98 \text{ kN}$ and the additional loads $W_{es} = 7.04 \text{ kN}$, is equal to $W_{tot} = 48.02 \text{ kN}$. Table 4.5 provides a comprehensive overview of the weight of each voussoir and the total weight of the middle arch.

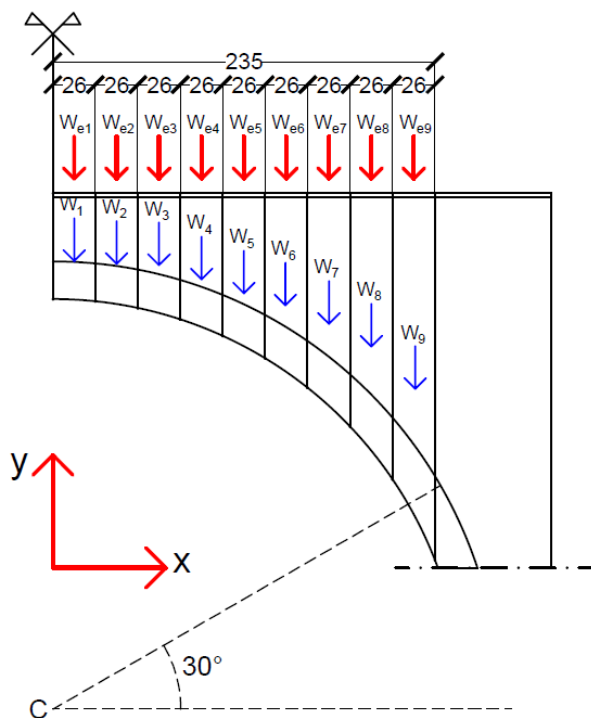


Figure 4.17. Barrel vault V^{0,A_2} : Discretization.

Table 4.5. Barrel vault V^{0,A_2} : Weights of voussoirs.

n.	x	x_G	A	s	Q_{es}	W_i	W_{es}	W_{tot}
(-)	(m)	(m)	(m ²)	(m)	(kN/m ²)	(kN)	(kN)	(kN)
1	0.00	0.13	0.17	1.00	3.00	2.73	0.78	3.52
2	0.26	0.39	0.18	1.00	3.00	2.85	0.78	3.63
3	0.52	0.65	0.19	1.00	3.00	3.08	0.78	3.86
4	0.78	0.92	0.21	1.00	3.00	3.43	0.78	4.22
5	1.04	1.18	0.25	1.00	3.00	3.93	0.78	4.71
6	1.30	1.44	0.29	1.00	3.00	4.59	0.78	5.38
7	1.56	1.70	0.34	1.00	3.00	5.46	0.78	6.24
8	1.83	1.96	0.41	1.00	3.00	6.62	0.78	7.40
9	2.09	2.22	0.52	1.00	3.00	8.28	0.78	9.06
TOT						40.98	7.04	48.02

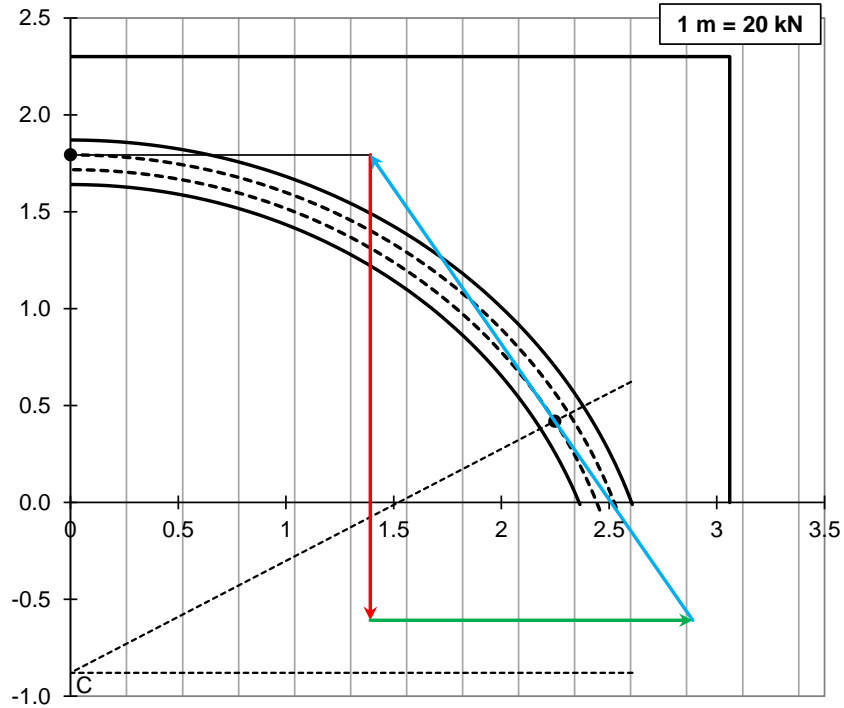
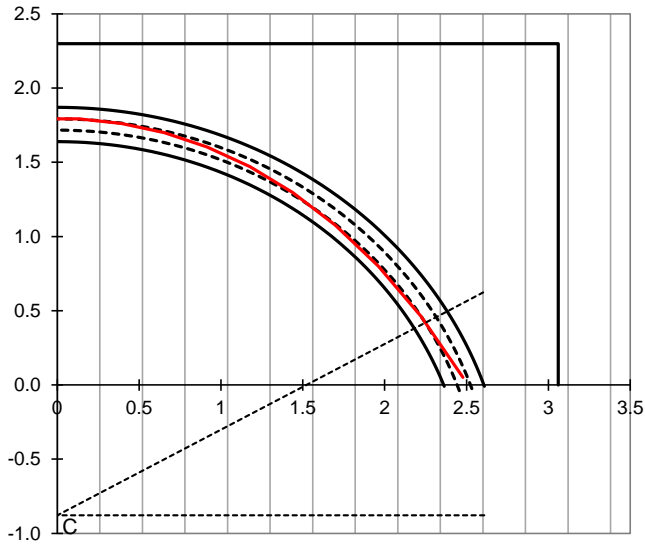


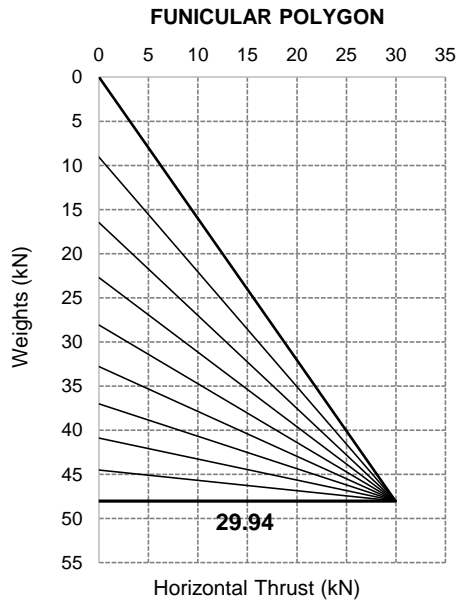
Figure 4.18. Barrel vault V^{0,A_2} : Definition of Horizontal Thrust.

Considering the weights of the voussoirs, the position of the resultant of the weight (in red), the value obtained for the horizontal thrust with Méry's construction is $H=29.94$ kN (in green) (Figure 4.18).

The analysis carried out graphically in Figure 4.19 shows that the thrust line lies within the middle third, confirming the stability of the vault.



(a)



(b)

Figure 4.19. Barrel vault V^{0,A_2} : thrustline (a) and funicular polygon (b).

4.4.2 Construction 0: cross vault $V^{0,2_2}$ (second floor)

The cross vault $V^{0,2_2}$ of the Construction 0 (Figure 4.20) sets on a rectangular plan, whose dimensions are 5.37 and 4.24 m. The cross-section of the vault reveals a segmental arch characterized by a rise (f) of 243 cm and a span ($2L$) of 537 cm, resulting in a f/L ratio of 0.91. The arch has a distinctive radius of 281 cm and a thickness of 22 cm, assumed to be constant along the cross-section.

For the structural analysis, a portion of 1 m has been considered. Due to the arch's symmetry, the study has focused on one half of the structure. The arch has been subdivided into 9 ideal voussoirs to discretise the calculation of the load due to self-weight and the additional loads (Figure 4.21). A specific weight of the masonry and filling equal to 16 kN/m^3 and an additional load of 0.5 kN/m^3 (Cat. H of the NTC18) have been considered. The total weight of the vault, estimated summing the self-weight $W_i = 46.59 \text{ kN}$ and the additional loads $W_{es} = 1.31 \text{ kN}$, is equal to $W_{tot} = 47.90 \text{ kN}$. Table 4.6 provides a comprehensive overview of the weight of each voussoir and the total weight of the middle arch.

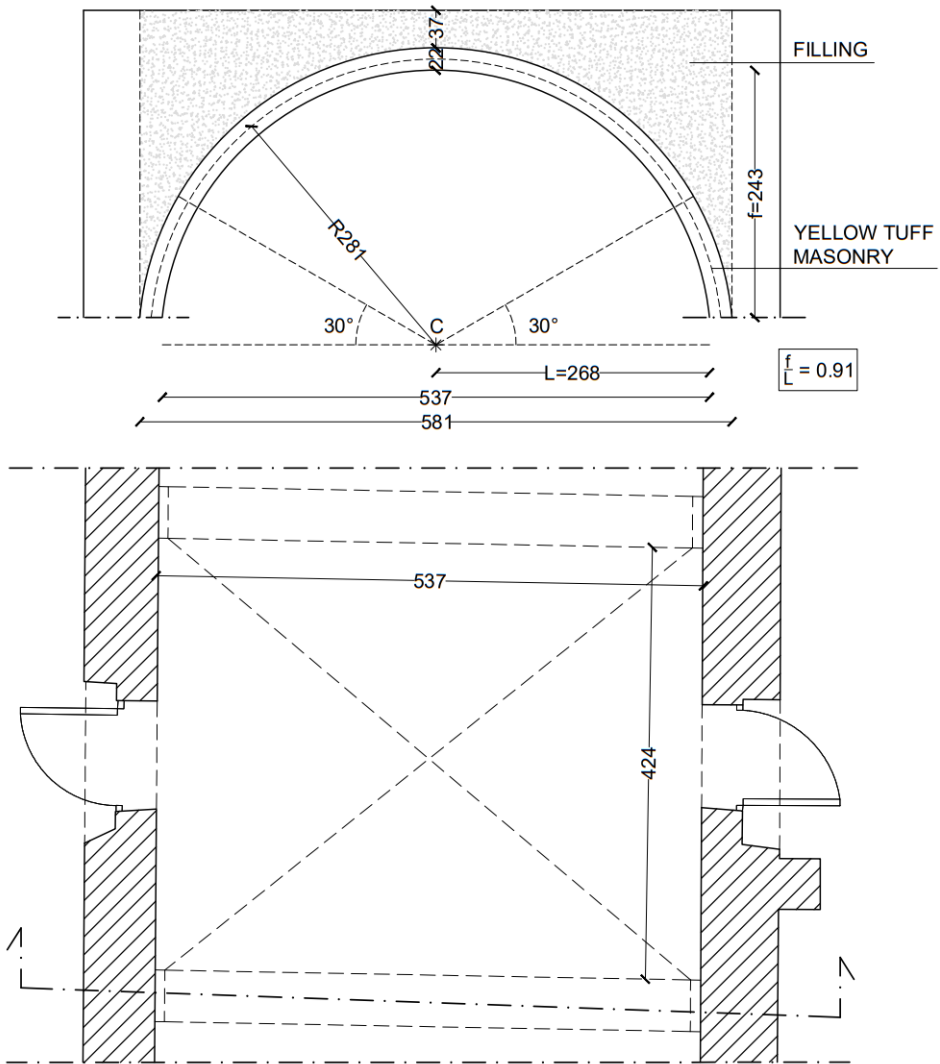


Figure 4.20. Cross vault $V^{0,2}_2$: Plan and Cross-Section.

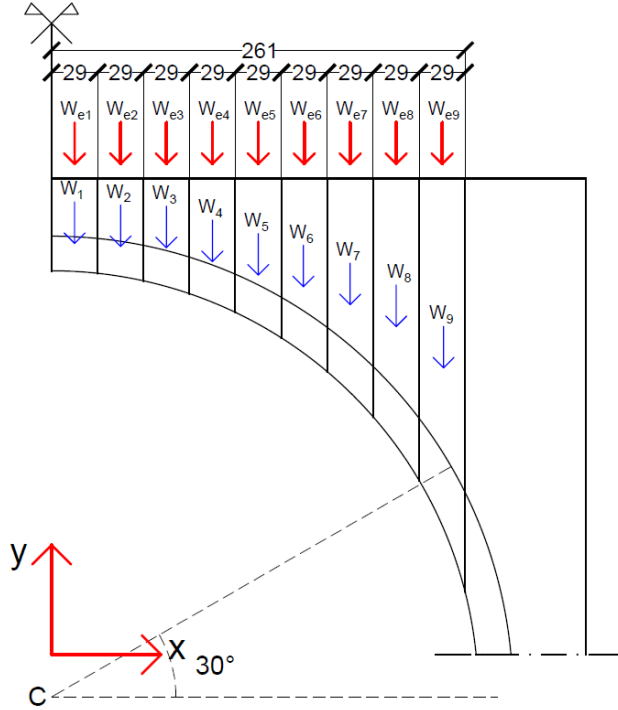

 Figure 4.21. Cross vault $V^{0,2}_2$: Discretization.

 Table 4.6. Cross vault $V^{0,2}_2$: Weights of voussoirs.

n.	x	x_G	A	s	Q_{es}	W_i	W_{es}	W_{tot}
(-)	(m)	(m)	(m ²)	(m)	(kN/m ²)	(kN)	(kN)	(kN)
1	0.00	0.15	0.17	1.00	0.50	2.76	0.15	2.90
2	0.29	0.44	0.18	1.00	0.50	2.90	0.15	3.05
3	0.58	0.73	0.20	1.00	0.50	3.20	0.15	3.35
4	0.87	1.02	0.23	1.00	0.50	3.67	0.15	3.81
5	1.16	1.31	0.27	1.00	0.50	4.31	0.15	4.46
6	1.45	1.60	0.32	1.00	0.50	5.18	0.15	5.33
7	1.74	1.89	0.40	1.00	0.50	6.33	0.15	6.48
8	2.03	2.18	0.49	1.00	0.50	7.91	0.15	8.05
9	2.32	2.48	0.65	1.00	0.50	10.32	0.15	10.47
TOT						46.59	1.31	47.90

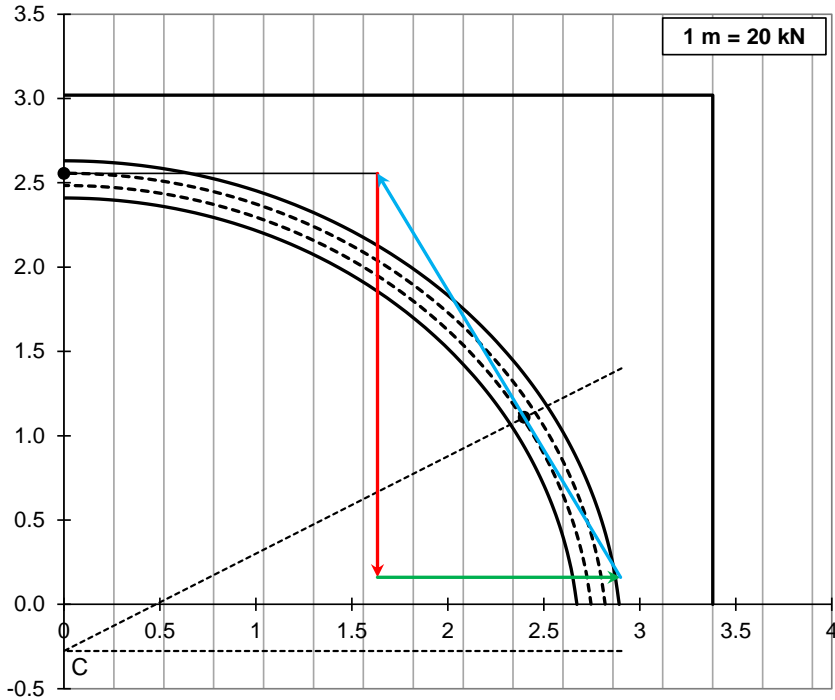
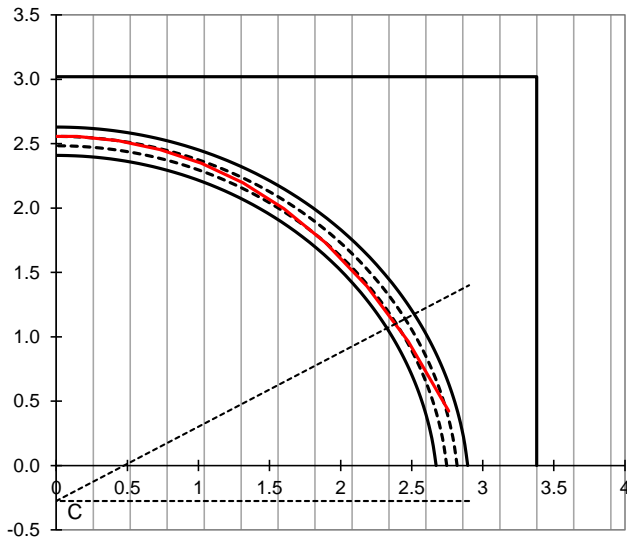


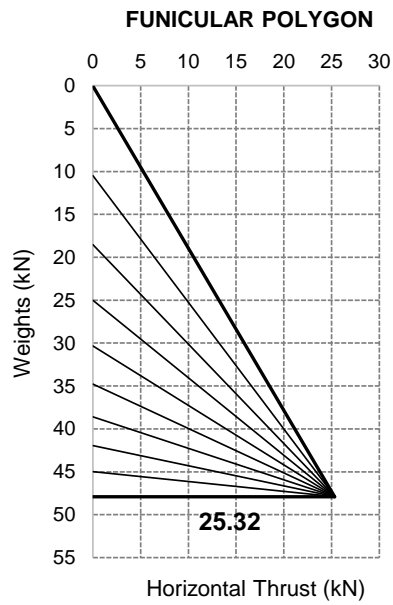
Figure 4.22. Cross vault $V^{0,2}$: Definition of Horizontal Thrust.

Considering the weights of the voussoirs, the position of the resultant of the weight (in red), the value obtained for the horizontal thrust with Méry's construction is $H=25.32$ kN (in green) (Figure 4.22).

The analysis carried out graphically in Figure 4.23 shows that the thrust line lies within the middle third, confirming the stability of the vault.



(a)



(b)

Figure 4.23. Cross vault $V^{0.2}$: thrustline (a) and funicular polygon (b).

4.4.3 Construction 0: lowered cloister vault V^{0,T_2} (ground floor)

The lowered cloister vault V^{0,T_2} of the Construction 0 (Figure 4.24) sets on a trapezoidal plan, whose main dimensions are 4.50 and 5.65 m. The cross-section of the vault reveals an intrados characterized by a horizontal part of 176 cm, a rise (f) of 166 cm and a span ($2L$) of 450 cm, resulting in a f/L ratio of 0.74. The arch has a distinctive radius of 242 cm and a thickness of 24 cm, assumed to be constant along the cross-section.

For the structural analysis, a portion of 1 m has been considered. Due to the arch's symmetry, the study has focused on one half of the structure. The arch has been subdivided into 9 ideal voussoirs to discretise the calculation of the load due to self-weight and the additional loads (Figure 4.25). A specific weight of the masonry and filling equal to 16 kN/m^3 and an additional load of 3 kN/m^3 (Cat. C of the NTC18) have been considered. The total weight of the vault, estimated summing the self-weight $W_i = 29.57 \text{ kN}$ and the additional loads $W_{es} = 6.74 \text{ kN}$, is equal to $W_{tot} = 36.31 \text{ kN}$. Table 4.7 provides a comprehensive overview of the weight of each voussoir and the total weight of the middle arch.

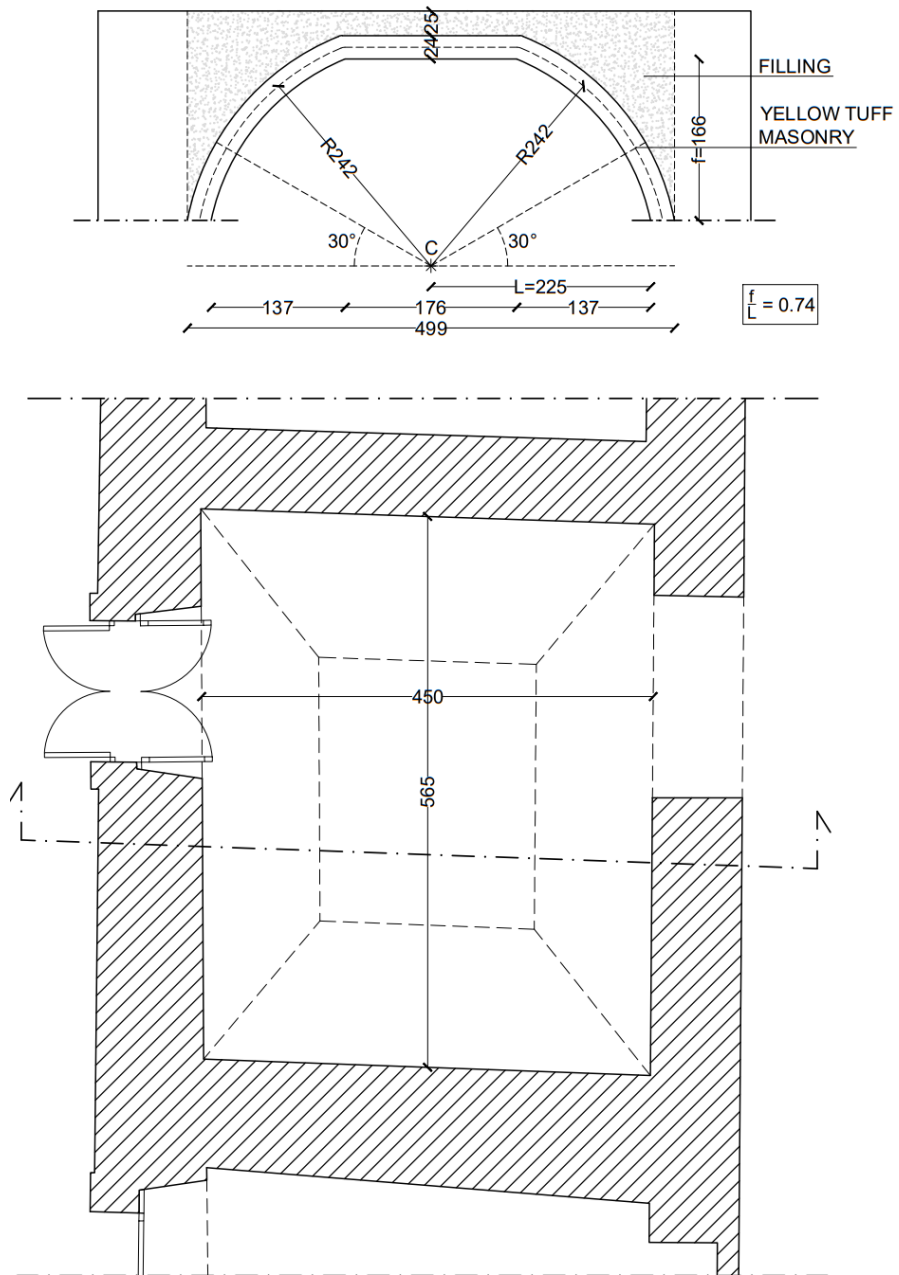


Figure 4.24. Lowered cloister vault V^0T_2 : Plan and Cross-Section.

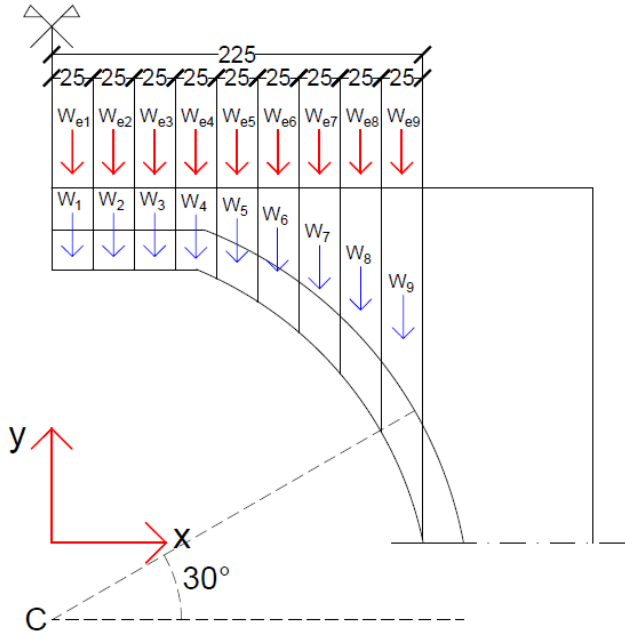


Figure 4.25. Lowered cloister vault V^{0,T_2} : Discretization.

Table 4.7. Weights of voussoirs.

n.	x	x_G	A	s	Q_{es}	W_i	W_{es}	W_{tot}
(-)	(m)	(m)	(m ²)	(m)	(kN/m ²)	(kN)	(kN)	(kN)
1	0.00	0.12	0.12	1.00	3.00	1.97	0.75	2.72
2	0.25	0.37	0.12	1.00	3.00	1.97	0.75	2.72
3	0.50	0.62	0.12	1.00	3.00	1.97	0.75	2.72
4	0.75	0.88	0.13	1.00	3.00	2.02	0.75	2.77
5	1.00	1.13	0.15	1.00	3.00	2.45	0.75	3.20
6	1.25	1.38	0.19	1.00	3.00	3.10	0.75	3.84
7	1.50	1.63	0.25	1.00	3.00	3.96	0.75	4.71
8	1.75	1.88	0.32	1.00	3.00	5.14	0.75	5.89
9	2.00	2.13	0.44	1.00	3.00	7.00	0.75	7.75
TOT						29.57	6.74	36.31

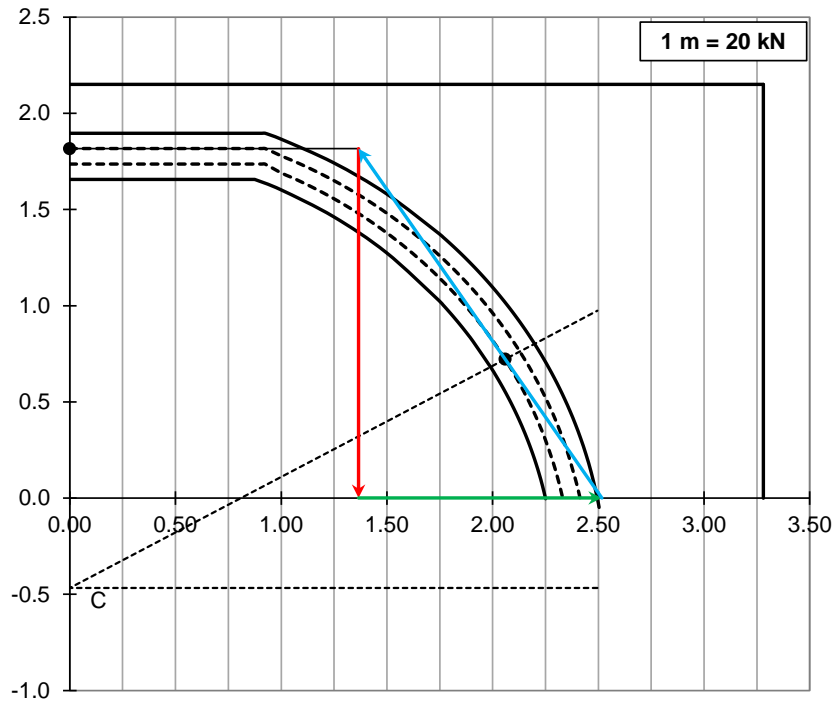
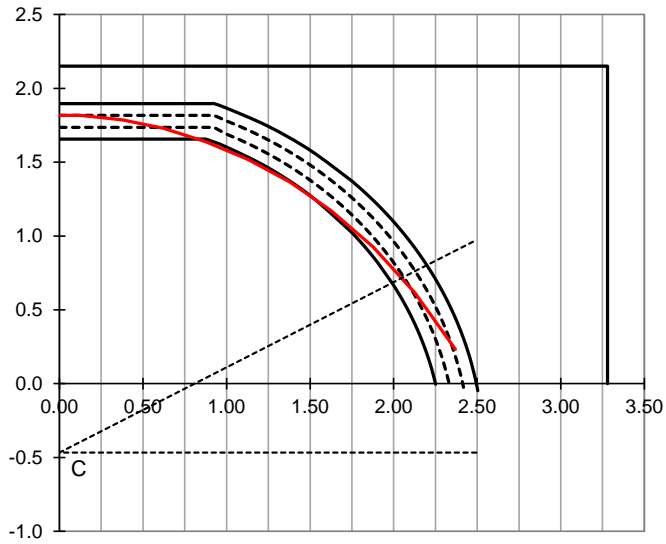


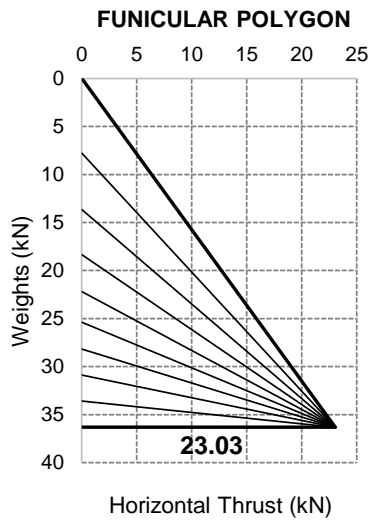
Figure 4.26. Lowered cloister vault V^0T_2 : Definition of Horizontal Thrust.

Considering the weights of the voussoirs, the position of the resultant of the weight (in red), the value obtained for the horizontal thrust with Méry's construction is $H=23.03$ kN (in green) (Figure 4.26).

The analysis carried out graphically in Figure 4.27 shows that the thrust line extends beyond the middle third. This implies that the voussoirs experience not only compression but also tension. It is crucial to note that the Méry's method is not suitable for assessing the stability of this vault typology under vertical load. Consequently, the analysis has been expanded by eliminating the assumption that the thrust line must be contained within the middle third but can extend throughout the entire thickness of the arch. Following this adjustment, infinite equilibrated solutions can be identified.

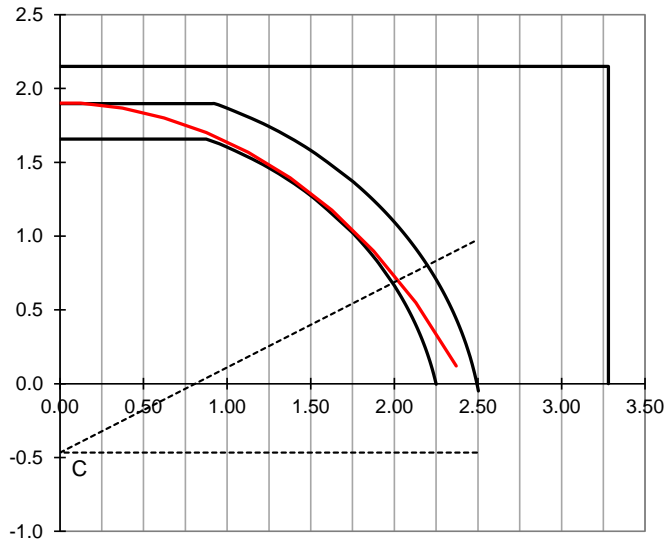


(a)

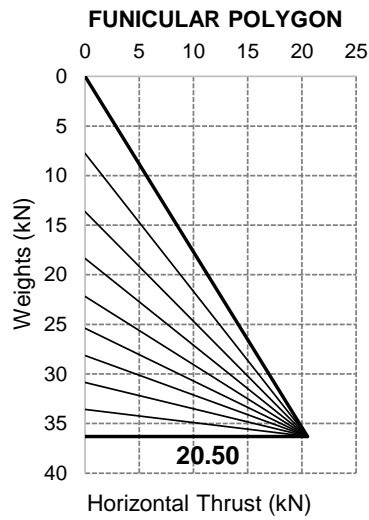


(b)

Figure 4.27. Lowered cloister vault V^{0,T_2} : thrustline (a) and funicular polygon (b).

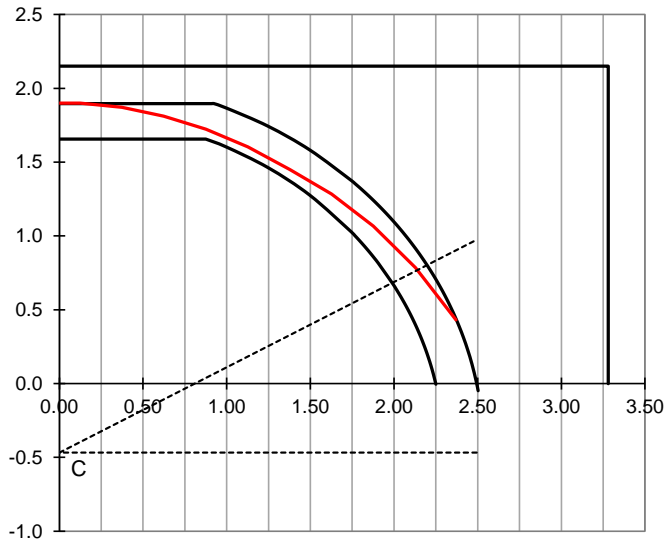


(a)

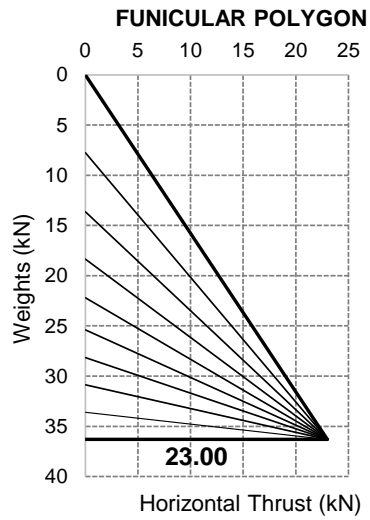


(b)

Figure 4.28. Lowered cloister vault V^{0,T_2} - minimum thrust: thrustline (a) and funicular polygon (b).

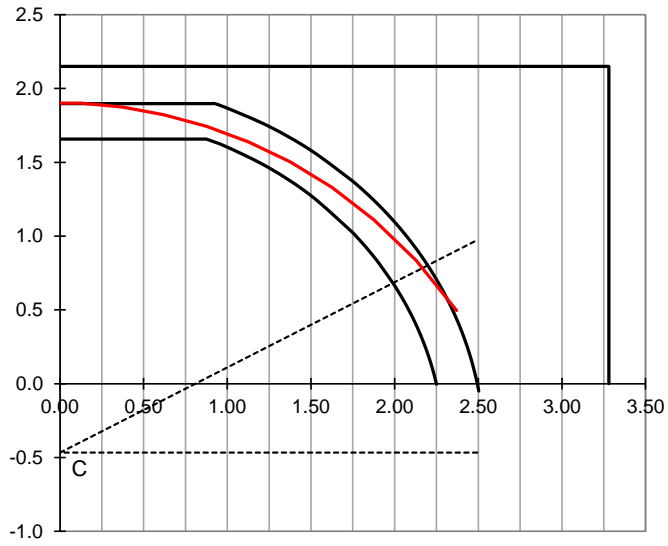


(a)

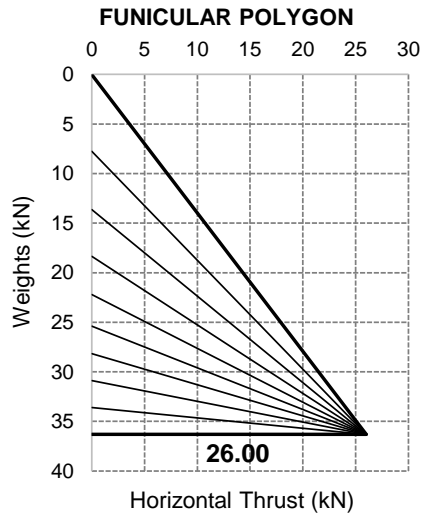


(b)

Figure 4.29. Lowered cloister vault $V^{0,T_2} - H = 23 \text{ kN}$: thrustline (a) and funicular polygon (b).

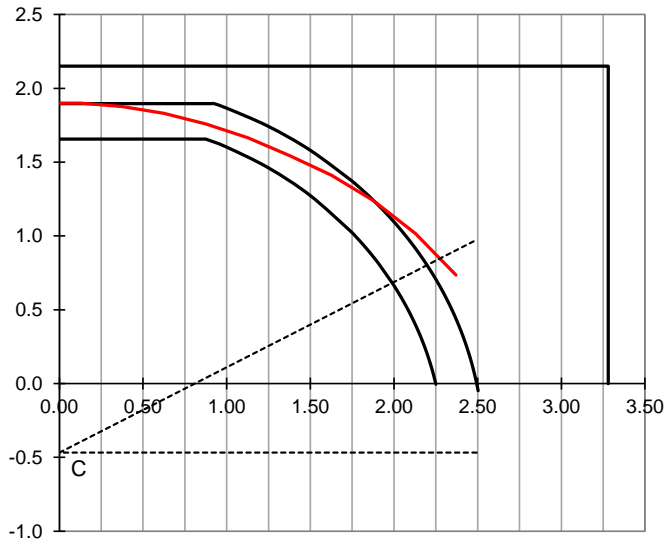


(a)

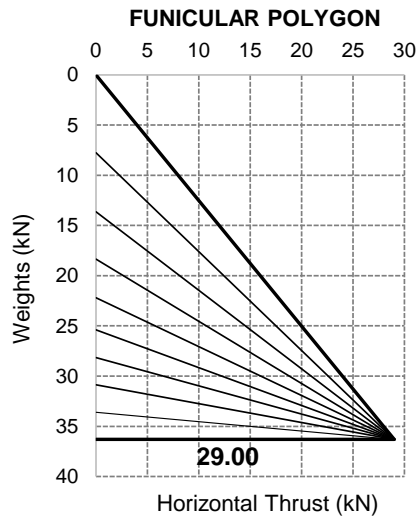


(b)

Figure 4.30. Lowered cloister vault $V^{0,T_2} - H = 26$ kN: thrustline (a) and funicular polygon (b).



(a)



(b)

Figure 4.31. Lowered cloister vault $V^{0,T_2} - H = 29 \text{ kN}$: thrustline (a) and funicular polygon (b).

The analyses depicted in Figures from 4.28 to 4.31, conducted with the assumption that the thrust line passes from the extrados of the arch at the crown, reveal the presence of various thrust lines situated within the thickness of the arch. In particular, an arch with sufficient thickness can show two limit conditions, known as maximum thrust and minimum thrust states. All thrust lines, representing equilibrated solutions, show a horizontal thrust within this range. The analyses have been carried out with different values of horizontal thrust: 20.50 kN, corresponding to the limit condition of minimum thrust, 23 kN, 26 kN and 29 kN. All these thrust lines remain within the thickness of the arch, except for the 29 kN horizontal thrust value, where the thrust line extends beyond the arch's thickness, as depicted in Figure 4.31.

According to the safe theorem of the limit analysis as formulated by Heyman (1982) [17]:

“If a thrust line can be found, for the complete arch, which is in equilibrium with the external loading (including self-weight), and which lies everywhere within the masonry of the arch ring, then the arch is safe.”

(Heyman, 1982. The masonry arch)

the vault is safe.

Table 4.8 presents a comprehensive summary of the results obtained for the three analysed vaults. The table includes information on the total weight, span dimension (B), rise (f), f/L ratio, and horizontal thrust values. Additionally, it provides a comparison between the horizontal thrust obtained using Méry's method ($H_{\text{Méry}}$) and the value derived considering the arch with three hinges, supporting a distributed load $H_0 = qB_1^2 / (8f_1)$, where B_1 is the horizontal distance between the two hinges in the 30° position, and f_1 is the rise. The comparison highlights significant differences, with the formula-based values being notably higher than those obtained with Méry's method. This contrast stems from the fact that the load is not distributed in the Méry's method.

Table 4.8. Summary of results.

Vault [-]	W_{tot} [kN]	L [m]	B [m]	f [m]	f/L [-]	H₀ [kN]	H_{Méry} [kN]
Barrel Vault	96.04	2.36	4.73	1.64	0.70	41.47	29.94
Cross Vault	95.79	2.68	5.37	2.41	0.91	41.57	25.32
Cloister Vault	72.62	2.25	4.50	1.66	0.74	36.93	23.03

Chapter 5

Structural modelling of complex masonry buildings

In this Chapter, a brief description of the main strategies for modelling of masonry structures is presented, with a specific focus on the macro-modelling procedure. Subsequently, the attention is focused on the SAM method, which is implemented into the CDS-Win software used for non-linear static analyses of the Convent. A more detailed explanation of this method is provided. In particular, for each element included in the equivalent frame model, relevant considerations are delineated, and possible failure mechanisms and deformation limits are highlighted. Following a theoretical examination of the approaches accepted by the European Technical Codes, an overview of the simplified method proposed by the research group in the framework of limit analysis is outlined. In particular, the simplified formulas proposed to predict the horizontal capacity of the single portal frame (Giordano et al., 2007), multi-bay masonry portal (Giordano et al., 2006) and multistorey unreinforced masonry frames (Lucibello, 2013 and Mazziotti, 2015) are briefly described. It's worth noting that the straightforward expression for predicting the horizontal capacity of multistorey unreinforced masonry frames is formulated as an extension of the two previous cases. Within this dissertation, the external loads are taken into account, by introducing in the formula a coefficient α . This coefficient accounts for the height of application of the resultant of the horizontal distribution of forces proportional to the masses is applied.

5.1 Strategies for modelling of masonry structures

Masonry is one of the oldest building materials and characterizes a significant part of the Italian architectural heritage. It is composed of masonry units with or without mortar. The masonry units are individual building blocks that make up the wall. Common masonry units include bricks and stones. The mortar is the binding material that bonds the masonry units together. This mortar, typically consisting of cement, sand and water, is applied between the masonry units in both horizontal and vertical joints.

Due to the great number of influencing factors, including dimension and anisotropy of the bricks, joint width and arrangement of the joints, material properties of brick and mortar and quality of workmanship, the numerical modelling of the masonry is a complex task (Asteris et al., 2015 [18]). According to Lourenco (2002) [19] and Asteris (2015) the different analytical procedures are listed below (Figure 5.1):

- *Detailed Micro-modelling.* Units and mortar in the joints are represented by continuum elements whereas the unit–mortar interface is represented by discontinuum elements. In this strategy, elastic and inelastic properties of both units and mortar are taken into account. The interface represents a potential crack plane. While this approach proves valuable for investigating the combined behaviour of units, mortar, and their interface, it is worth noting that it demands a substantial computational effort for analysis.
- *Simplified Micro-modelling.* Units are modelled as continuum elements, having the same size of the original bricks dimensions plus the joint thickness, and the interaction between the mortar joints and the masonry units are represented by means of interface elements with zero thickness and stiffness deduced from the stiffness of the real joints. Masonry is considered as a set of elastic blocks bonded by potential fracture lines at the joints. This approach encompasses various models, including: Discontinuum Finite Element Models (D-FEMs), Discrete Element (DE) Models, Boundary Element Models, Discrete Limit Analysis Models (D-LAM).
- *Macro-modelling.* Units, mortar and unit–mortar interface are smeared out in a homogeneous continuum. The masonry is considered as a homogeneous anisotropic continuum. This

approach is not suitable for the detailed stress analysis of a small masonry panel, due to the difficulty of capturing all its expected failure modes. This approach includes the following models: Continuum finite element macromodels and Discontinuum finite element macromodels.

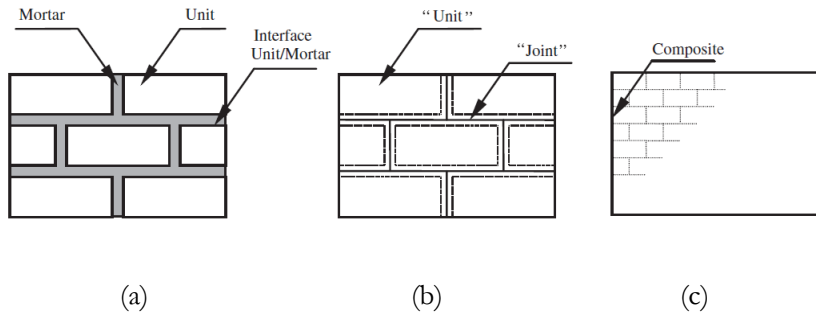


Figure 5.1. Modelling strategies for masonry structures: (a) detailed micro-modelling; (b) simplified micro-modelling; and (c) macro-modelling [19].

In this Section, the attention will be focused on the Macro-modelling approach, which proves highly effective for analysing large-scale masonry structures. This method is particularly practical due to its efficiency, significantly reducing the time required for analysis.

Since the complexity and the variety of the aspects involved, different macro-modelling strategies have been developed to carry out structural analysis of masonry buildings. In this articulated panorama of models, it is possible to classify them with different classification criteria.

A first distinction identifies the models based on **limit analysis** (Como and Grimaldi, 1985, [21], Abruzzese et al., 1992, [22]), which represent a particularly effective tool for estimating the collapse load and relative mechanism of structural systems. As defined by Heyman (1966 [23], 1982 [17], 1995 [24]), the hypothesis on the material behaviour are: (1) no tensile strength; (2) infinite compression strength; (3) absence of sliding at failure. With these hypotheses, the structures are considered as composed by blocks. It must be remarked, however, that it can hardly be used to describe the response and predict damage for moderate or service load levels not leading to a limit condition. Strictly speaking, limit analysis can only be used to assess the stability or safety of structures (Roca et al., 2010 [25]).

In order to overcome the above mentioned limitations of this approach, many authors have developed alternative methodologies, which should be

able to consider elastic deformations, possibly followed by inelastic deformations.

The most commonly used practical approach for the analysis of unreinforced masonry structure is the so called “**equivalent frame model**”. The earthquake damage observation has highlighted that as usually cracks and failure modes are concentrated in specific structural elements. Based on this observation, the walls are considered as an idealized frame, in which deformable elements, where the non-linear response is concentrated, connect rigid nodes, which are parts of the wall that are not usually subjected to damage (Lagomarsino et al., 2013 [20]). In this context, three primary macro-elements are considered:

- Piers, that are the main vertical elements of the wall;
- Spandrels, which are the parts of the walls between two vertical openings;
- Rigid portions, that are parts of the wall between the piers and spandrels.

Three classes of spandrel, having different behaviour, can be defined (Calderoni et al., 2011 [26]):

- “Weak spandrel”, characterised by lack of any tensile resistant element, so that the spandrel itself has not the capacity to connect two adjoining piers.
- “Truss-spandrel”, having at least one effectively anchored horizontal tensile-resistant element. In this case the effect of the tie is to avoid the separation between spandrel and piers.
- “Beam-spandrel”, reinforced with both lower and upper reinforcement elements.

The spandrel behaviour affects the response of the adjacent piers that can be considered as (Bucchi et al., 2013 [27]):

- Cantilever;
- Partially coupled;
- Shear type.

In case of walls featuring a regular arrangement of the openings, the definition of the correct dimensions for these three elements is a straightforward process. Complexity arises when dealing with walls characterized by irregularly positioned openings. In such instances, it is advisable to explore alternative modelling approaches outlined in the existing literature.

Within this category of models, it can be distinguished models that maintain a two-dimensional modelling of the wall panels (two-dimensional macro-models), and one-dimensional modelling (one-dimensional macro-models).

5.1.1 One-dimensional macro-models

The one-dimensional macro-models schematize the structure as an equivalent frame, in which the three parts of the wall (piers, spandrel and rigid offset) are modelled as one-dimensional elements. A brief summary of the different models existing in literature is provided by Bucchi et al. [27] and is briefly described below.

The first frame model, known as POR method, was proposed by Tomazevic (1978) [28] and was introduced in Italy in response to the 1976 Friuli Earthquake. Its primary goal was to enable incremental collapse analyses, even with manual calculation procedures. According to this method, masonry walls are schematized by piers connected by a rigid spandrels. Piers having a shear-type behaviour are considered. However, there are significant limitations to this approach:

- It assumes that in-plane damage for horizontally loaded masonry façades is only caused by shear forces in the piers, while both spandrels and nodal regions are supposed rigid and infinitely resistant.
- It considers an independent storey mechanism, which necessitates the consideration of the overall response of masonry structures.

The POR method was improved through two notable improvements. First, the PORFLEX method, presented by Braga and Dolce (1982) [29], extended the original approach by accounting for the limited strength of masonry spandrels and for the flexibility of the piers. Secondly, Dolce introduced the POR 90 method (1991) [30], which introduced a different approach to assessing pier stiffness. This method considered an equivalent height that depended on the dimensional characteristics of the spandrels. Another model, proposed by Calderoni et al. (1987) [31], schematizes the wall as a set of panels. In this model, the resistant part for each panel is schematized as a strut, where the inclination and stiffness are evaluated to replicate the global behaviour of the panel. The panel collapses when it reaches a limit equilibrium configuration or when the strut reaches its maximum compression strength.

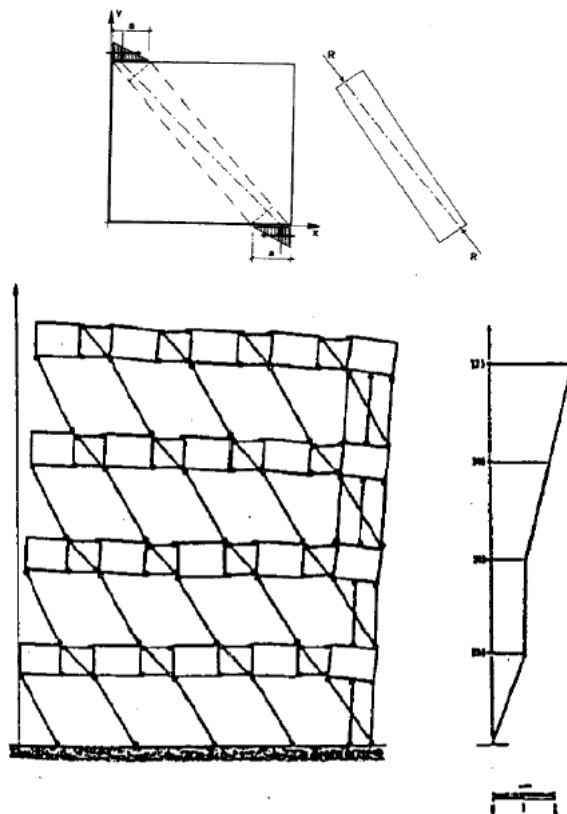


Figure 5.2. Model proposed by Calderoni, 1987.

A more detailed approach, also considered in the Italian Building Codes, is the Simplified Analysis Method (SAM), developed since 1996 by Magenes and Calvi [32], and then modified by Magenes and Della Fontana [33]. In contrast to the POR approach, the SAM considers the spandrel as deformable, allowing both horizontal movement (similar to POR) and rotation, not allowed in POR. In SAM, the wall is schematized using an equivalent frame, comprising the following components:

- Column elements, which represent the piers.
- Beam elements, symbolizing the spandrels.
- Rigid offsets, describing the joint panel. This joint is assumed to be infinitely rigid, as it typically remains uncracked (though exceptions may exist).

Both the pier and the spandrel exhibit an elastic-plastic behaviour with defined deformation limits. Specifically, these elements are considered elastic until they reach the threshold of a failure criterion, such as rocking, diagonal shear, or sliding shear for piers, and rocking and shear for spandrels. Once this threshold is surpassed, a plastic hinge is activated.

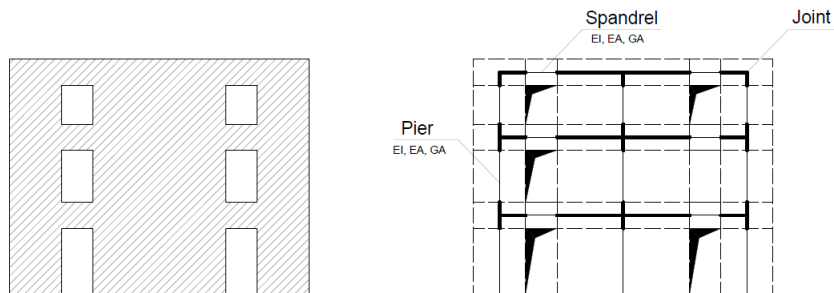


Figure 5.3. SAM model.

5.1.2 Two-dimensional macro-models

Two-dimensional macro-element models, unlike one-dimensional models, schematise the spandrels and rigid offset using two-dimensional macro-elements, having the real dimensions of the masonry elements. In this methodology, the wall is schematised by a set of macroscopic no tensile elements. The advantage this approach lies in the reduction of degrees of freedom, leading to a notable decrease in computational effort. Various authors proposed these type of models, including Braga & Liberatore (1990) [34], D’Asdia and Viskovic (1995) [35], Gambarotta and Lagomarsino (1996) [36], Calìo et al. (2012) [39].

Braga and Liberatore (1990) [34] proposed a model with two-dimensional macro-elements, known as “multi-fan panel element”, in which each macro-element consists of a series of elementary triangular blocks. The material behaviour is assumed linear elastic in compression and non-reacting in tension. The macro-element kinematics can be described by means of six degrees of freedom, the six nodal displacement components ($u_i, w_i, \varphi_i, u_j, w_j, \varphi_j$) of the end sections of the panel. A limitation of this model is that it does not take into account shear and sliding failure mechanisms.

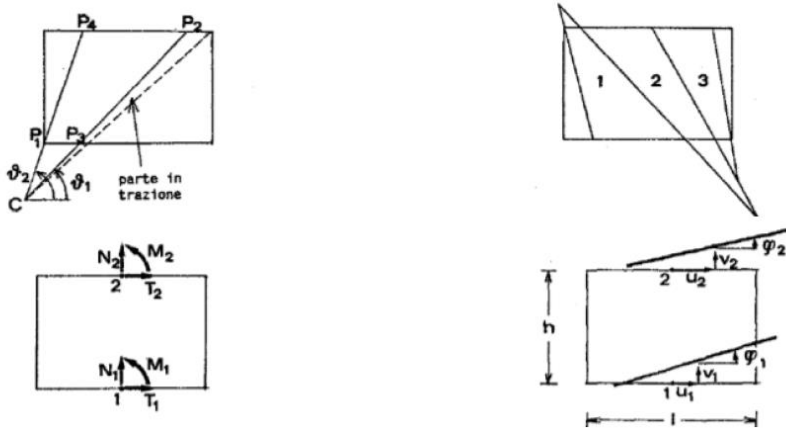


Figure 5.4. Braga and Liberatore model (1990).

D'Asdia and Viskovic (1995) [35] introduced an approach that based on linear finite elements with variable shape, known as PEFV (an Italian acronym). In this method, both the pier and the spandrel are modelled with a mesh of triangular finite elements that can change their dimensions according to the stress state.

Gambarotta and Lagomarsino (1996) [36] proposed a macro-element that works in plane. The macro-element is divided into three parts (Figure 5.6): two layers, inferior (1) and superior (3), in which the bending and axial effects are concentrated, and a central part (2), that suffers shear-deformations and presents no evidence of axial or bending deformations. Each end joint (i and j in Figure 5.6) and the interface joint (1 and 2 in Figure 5.6) have a total of three degrees of freedom (DOFs): two horizontal translations (u and w) and one rotation (φ). Consequently, the macro-element comprises 12 DOFs. Through the application of some simplifying assumptions, compatibility conditions can be defined, reducing the DOFs to eight for each macro-element: six components at the end joints i and j ($u_i, w_i, \varphi_i, u_j, w_j, \varphi_j$) and two components that characterize the entire macro-element (δ and φ). This model is implemented in the code 3Muri and more details are given in the manual of the software.

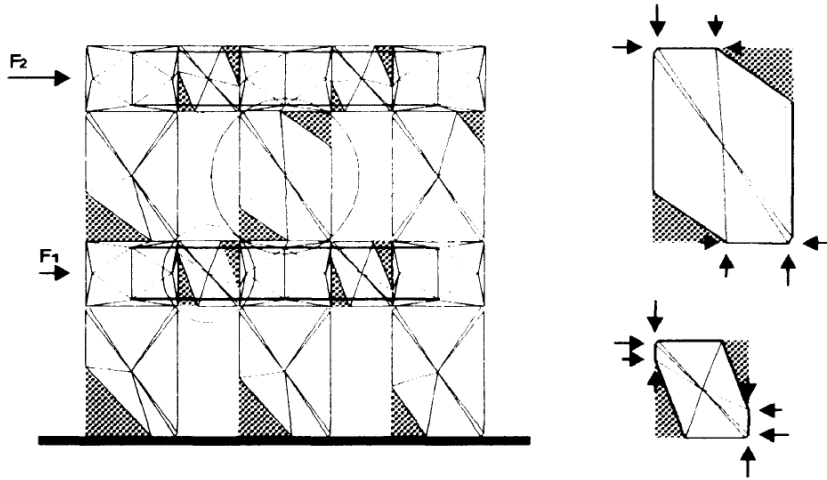


Figure 5.5. D'Asdia and Viskovic method (1995).

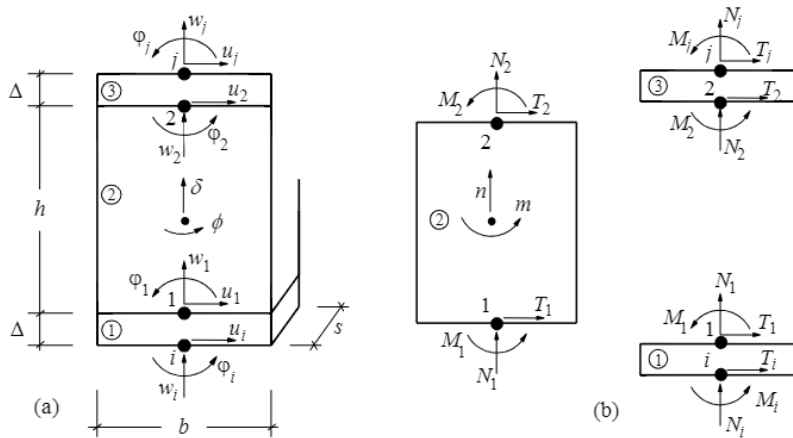


Figure 5.6. Kinematic model for the macro-element (Gambarotta and Lagomarsino, 1996).

Another type of macro-element was proposed by Calìo et al. (2012) [39]. This macro-element has the shape of an articulated quadrilateral frame with four rigid edges linked by four hinges and by two diagonal nonlinear springs (Figure 5.7). Each side of the panel can interact with other elements, or external supports, through nonlinear interface springs oriented orthogonally and longitudinally. The internal and external springs are able to replicate the in-plane failures. Each macro-element has three DOFs to

describe the displacements in the plane and an additional DOF to account for shear deformation.

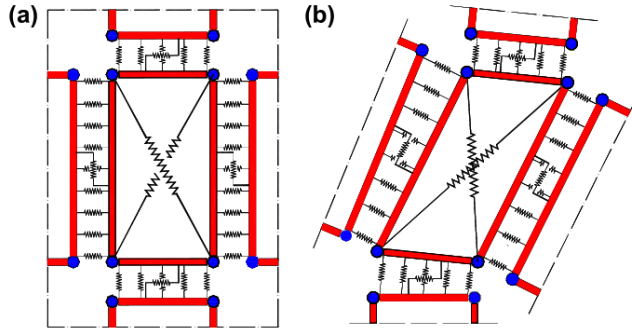


Figure 5.7. The basic macro-element proposed by Calio et al. (2012): (a) undeformed configuration; and (b) deformed configuration.

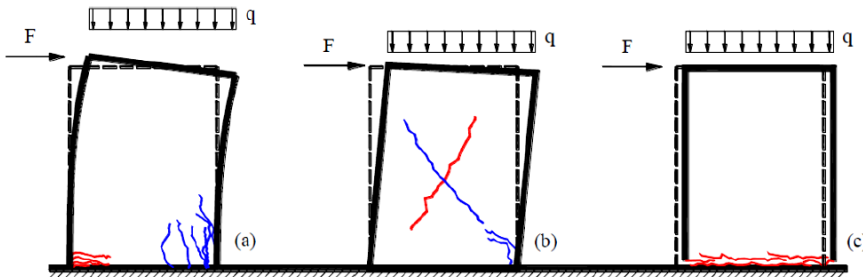


Figure 5.8. Main in-plane failure mechanisms of a masonry portion: (a) flexural failure; (b) shear-diagonal failure; and (c) shear-sliding failure.

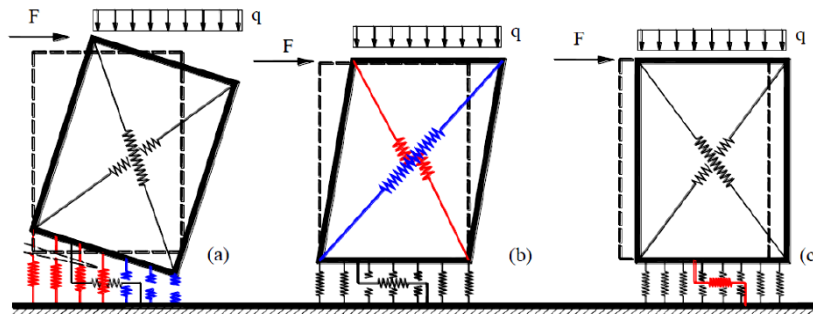


Figure 5.9. Simulation of the main in-plane failure mechanisms of a macro-element proposed by Calio et al. (2012): (a) flexural failure; (b) shear-diagonal failure; and (c) shear sliding failure.

In this work, after a brief description of the approaches accepted by the European technical codes, the equivalent frame approach known with the acronym SAM has been chosen. It is implemented in the software CDSwin used for the analysis of the convent case study.

5.2 The SAM method

After a brief description of the approaches accepted by the European technical codes, in this Section the attention is focused on the SAM method, implemented in the software CDS-WIN (Computer Design of Structure s, S.T.S. S.r.l., 2022) [40] used for the non-linear static analyses of the convent. At first glance, the utilization of the equivalent frame approach may be considered inadequate, for unreinforced masonry buildings. However it can prove highly effective for specific objectives, which include:

- Providing a good prediction of the strength of a building when subjected to a pattern of increasing horizontal forces;
- Offering a good prediction of the failure mechanisms in the single sub-elements, which lead to global collapse;
- Accurately estimating the overall deformation of the building (interstorey displacements), particularly at the ultimate limit state.

The method was developed based on the consideration that the distribution of internal forces at collapse is basically governed by strength of members and by equilibrium.

5.2.1 The pier element

In the SAM method, pier elements are modelled as elastic-plastic beam-column elements with flexural and shear deformability. An effective height is used for the definition of the stiffness matrix within a specific range, and to identify the end sections of the pier for strength checks. The definition of effective height follows a proposal made by Dolce (1989) [41], aimed to provide an adequate estimate of the piers stiffness in the elastic range (Figure 5.10).

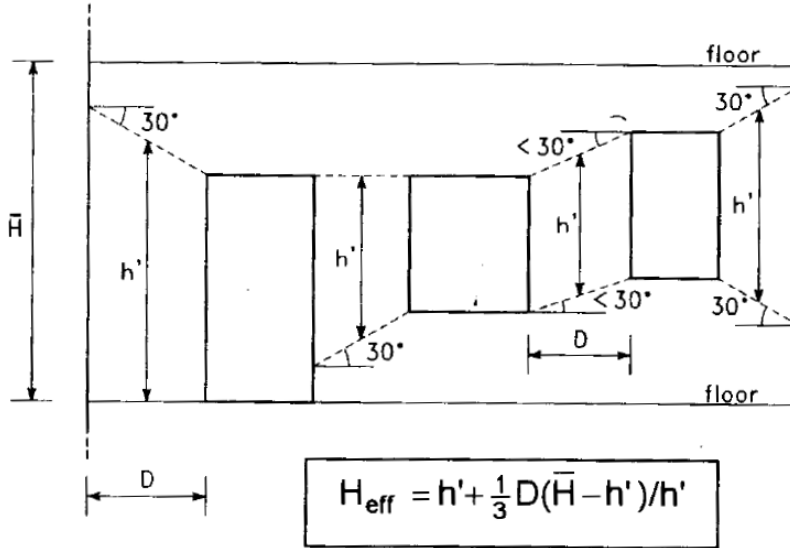


Figure 5.10. Definition of effective height proposed by Dolce (1989).

Piers can exhibit two possible failure mechanisms: flexural or “rocking” failure, and shear failure. The behaviour of the beam-column element is linear elastic until any of the failure criteria is met. The flexural or “rocking” strength of a pier can be easily calculated by assuming an equivalent rectangular stress-block for masonry in compression and determining the ultimate moment using:

$$M_u = \frac{t l^2 \sigma_0}{2} \left(1 - \frac{\sigma_0}{0.85 f_d} \right) \quad (1)$$

where l is the pier length, t is the thickness, $\sigma_0 = N/(lt)$ is the mean vertical stress on the pier due to N the axial load, f_d is the compressive strength of masonry. When the moment in any of the pier section reaches the limit value given by Equation (1), a plastic hinge is introduced in the section, allowing plastic rotation at constant moment.

Shear failure can occur in two possible failure modes, sliding failure and diagonal cracking. The shear strength V_u of the pier is defined by the lowest among the strength associated with each mode, given in the Equation (2) and Equation (3) for sliding failure and diagonal cracking, respectively:

$$V_s = l' t f_{vd} \quad (2)$$

$$V_t = l t \frac{1.5 \tau_{0d}}{b} \sqrt{1 + \frac{\sigma_0}{1.5 \tau_{0d}}} = l t \frac{f_{td}}{b} \sqrt{1 + \frac{\sigma_0}{f_{td}}} \quad (3)$$

$$f_{vd} = f_{vm0} + 0.4 \sigma_n \quad (4)$$

$$b = \begin{cases} 1 & \frac{h}{l} \leq 1 \\ \frac{h}{l} & 1 \leq \frac{h}{l} \leq 1.5 \\ 1.5 & \frac{h}{l} \geq 1 \end{cases} \quad (5)$$

where l is the length of the part of the pier in compression, f_{vd} is the shear strength defined by the Equation (4), $\sigma_0 = N/(lt)$ is the mean vertical stress on the pier due to N the axial load, f_{td} is the tensile strength, b is a coefficient depending on slenderness of the wall (defined in the Equation (5)), f_{vm0} is average masonry shear strength.

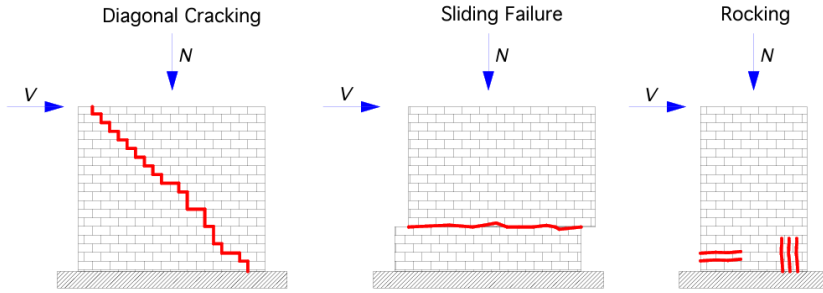


Figure 5.11. Piers failure mechanisms: diagonal cracking, sliding and bending failure/rocking.

A limit to the deformation of the pier is imposed in terms of maximum chord rotation θ . This limit depends on the failure mechanism observed in the pier. Beyond this limit, the load-carrying capacity is reduced to zero. According to Italian Building Code, for shear failure, the maximum chord rotation is set at 0.5% while for flexural failure, it is 1%. These limits are derived from drift values proposed in [32], obtained from shear tests conducted on doubly fixed piers.

5.2.2 The spandrel element

The formulation of spandrel beam elements follows a similar approach to that of piers. Nevertheless, the response of spandrels under seismic forces differs significantly because they are subjected to both shear and bending, with a negligible stress normal to the bedjoints. Spandrel typically exhibits two possible failure mechanisms, rocking and diagonal cracking. Sliding failure is not possible due to the interlocking phenomena originated at the interface between the end-sections of the spandrels and the adjacent piers. In the current implementation of the model, an elastic-plastic relation is proposed for the behaviour of the spandrels. For the definition of the ultimate bending moment M_u the current Italian Building Code (NTC 18), distinguishes two cases: spandrel with axial force known and unknown. If the axial force acting on the spandrel is known, the spandrel can be considered as a 90° rotated piers and the ultimate bending moment is equal to:

$$M_u = N \frac{h}{2} \left[1 - \frac{N}{(0.85 f_{hd} h t)} \right] \quad (6)$$

where h is the height of the spandrel, t is the thickness, 0.85 is a coefficient that takes into account the rectangular stress block distribution, f_{hd} is the compressive strength of masonry in horizontal direction.

If the axial force acting on the spandrel is unknown, the ultimate bending moment is defined as follow:

$$M_u = H_p \frac{h}{2} \left[1 - \frac{H_p}{(0.85 f_{hd} h t)} \right] \quad (7)$$

where H_p is the minimum between the tensile strength of the resistant element (such as tie rod) and the value given by the relation $0.4 f_{hd} h t$.

The ultimate shear strength is expressed as the minim between the ultimate shear strength associated to flexural behaviour (Equation (8)) and the ultimate shear strength in presence of ties (Equation (9)):

$$V_p = \frac{2 M_u}{l} \quad (8)$$

$$V_t = h t f_{vd,0} \quad (9)$$

5.3 Simplified method in the framework of limit analysis

The pioneering studies related to the application of limit analysis to understand the in-plane behaviour of masonry walls can be traced back to Como and Grimaldi (1983) [42]. Subsequently, over a decade later, further investigations were conducted by Giordano et al. (2007) [43], and Brandonisio et al. (2009) [44]. In this Section, an overview of the formulas proposed by the research group in the framework of limit analysis is provided.

5.3.1 The simple portal

In Giordano et al. (2007) [43] a simple formula for predicting the horizontal capacity of masonry portals was proposed and discussed.

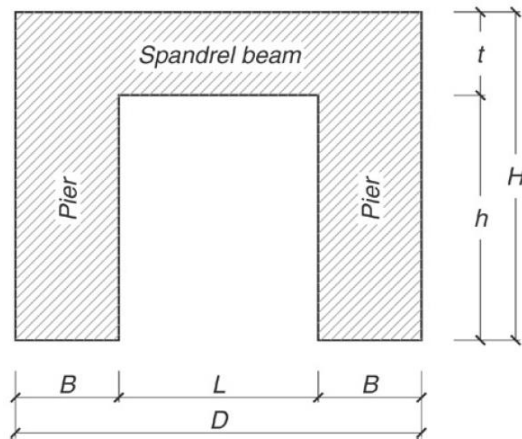


Figure 5.12. Simple portal.

Based on the following assumptions about material properties (Heyman, 1995 [24]):

- (i) Masonry has no tensile strength;
- (ii) Stresses are so low that masonry has effectively an unlimited compressive strength;
- (iii) Sliding failure does not occur,

in Figure 5.13 the possible crack hinges is shown.

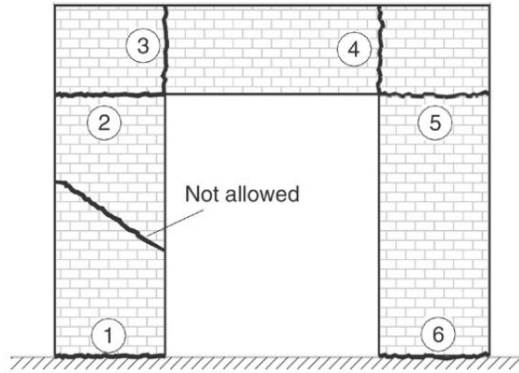


Figure 5.13. Possible crack pattern.

As depicted in Figure 5.13, they can only occur at the piers-to-spandrel connections. Among the 15 possible collapse mechanisms, four were chosen based on mechanical and engineering considerations (Figure 5.14), and exact expression for the kinematic multipliers were developed.

$$\frac{F}{W_{tot}} = \frac{B}{2h} \left(1 + \frac{W_{beam}}{W_{tot}} \right) \left(0.50 + \frac{B}{D} \right) \quad (10)$$

where:

$\frac{F}{W_{tot}}$ is the collapse multiplier;

B is the pier width;

h is the pier height;

W_{beam} is the weight of the beam;

W_{tot} is the total weight;

D is the length of two piers with the central opening.

This formula defines the collapse multiplier as a function of three key factors that primarily influence the failure modes: the first term represents the pier's overturning load, the second accounts for the stabilizing effect of the beam's weight, and the third term incorporates the opening percentage effect.

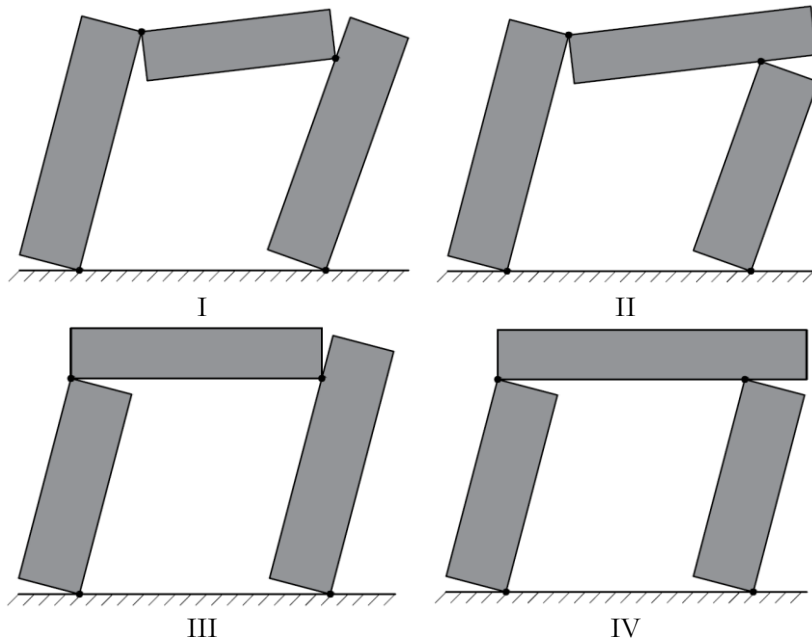


Figure 5.14. Collapse Mechanisms.

5.3.2 The multispan masonry portal frames

In a successive study carried out by the author (Giordano et al.. 2006 [45]), the case of the single portal frame was extended to a multi-bay masonry portal.

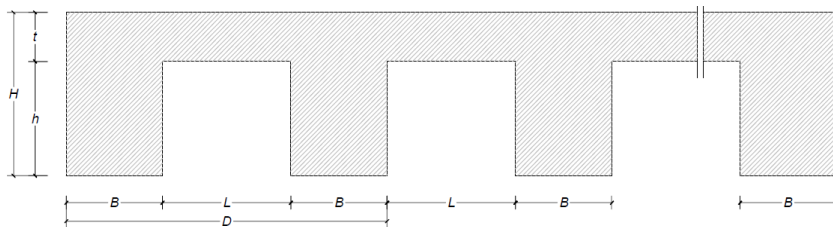


Figure 5.15. Multispan Masonry portal frame.

Exact expressions of the multiplier for the chosen mechanisms, as frame mechanism, mixed mechanism and storey mechanism, were derived.

For the **frame mechanism** the expression of the kinematic multipliers were defined as follows, for force applied at the left end (11), force applied

at the right end (12) and for force distributed along the piers (13), respectively:

$$\frac{F}{W_{tot}} = \frac{B}{2h} \left(1 + \frac{W_{beam}}{W_{tot}} \right) \left(0.50 + \frac{B}{D} \right) \quad (11)$$

$$\frac{F}{W_{tot}} = \frac{B}{2H} \left(\frac{W_p \sum_{i=0}^n \frac{1}{\psi^i}}{W_{tot}} + \frac{W_b \sum_{j=1}^{n-1} \frac{1}{\psi^j}}{W_{tot}} \right) \quad (12)$$

$$\frac{F}{W_{tot}} = \frac{B}{2H} \frac{n+1}{\sum_{r=0}^n \psi^r} \left(\frac{W_p \sum_{i=0}^n \psi^i}{W_{tot}} + \frac{W_b \sum_{j=1}^n \psi^j}{W_{tot}} \right) \quad (13)$$

where:

W_p is the weight of the single pier;

W_b is the weight of the single beam;

n is the number of bays;

ψ is a parameter defined in Equation (14):

$$\psi = \frac{HL}{HL - Bt - Lt} \quad (14)$$

L is the beam width;

t is the beam thickness.

For the **mixed mechanism**, the expression for the kinematic multiplier generalized for n bays is:

$$\frac{F}{W_{tot}} = \frac{B}{2h} \left(\frac{(n+1)W_p + 2W_b - W_c}{W_{tot}} \right) \quad (15)$$

where:

W_c is the weight of the cross node.

For **storey mechanism** the expression of the kinematic multiplier is formally the same as the one derived for the single portal frame and is defined as follows:

$$\frac{F}{W_{tot}} = \frac{B}{2h} \left(1 + \frac{W_b}{W_{tot}} \right) \quad (16)$$

5.3.3 The multi-bay multi-storey wall

In Lucibello (2013) [46], the application of Limit Analysis to single span portals and multiple span portals was extended to multi-bay multi-storey wall.

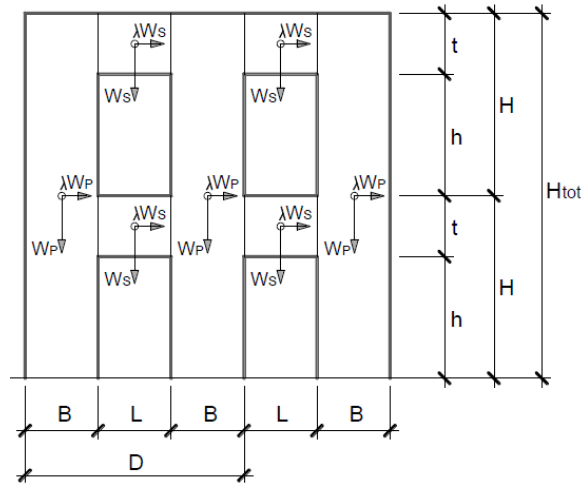


Figure 5.16. Multi-bay multi-storey wall .

The global collapse mechanism was hypothesized as generally it provides the smaller value of load multiplier. By drawing the kinematic chain, it can be noted that the centers of rotation are not aligned; consequently to trace the mechanism is necessary to allow the separation of parts (Figure 5.17) and the principle of virtual power cannot be applied.

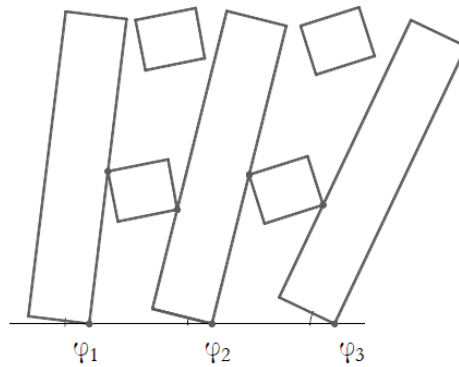


Figure 5.17. Frame mechanism: impossible collapse mechanism.

For this reason, the same hypothesis on the basis of the methodology adopted by Como and Grimaldi (1983) [42] was taken into account, i.e. the piers have the same angle of rotation with respect to the hinges at the base. Because of this assumption, there is a geometrical compenetration in the zone that mutually rotate in the deformed shape (Figure 5.18).

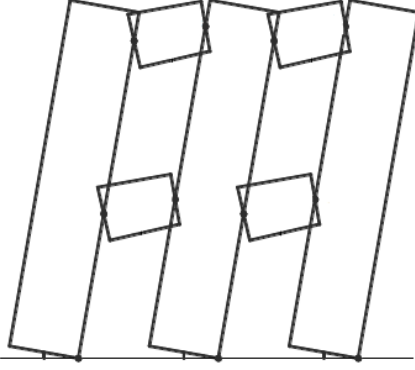


Figure 5.18. Global collapse mechanism: hypothesis of Como and Grimaldi.

The corresponding load multiplier was evaluated by means of the following closed form expression:

$$\lambda = \frac{B}{2H} \frac{\sum_{i=1}^{n_c+1} W_{p,i} + \sum_{j=1}^{n_c n_p} W_{s,j}}{n_p \sum_{i=1}^{n_c+1} W_{p,i} + \left(n_p + 1 - \frac{t}{H}\right) \sum_{j=1}^{n_c n_p} W_{s,j}} \quad (17)$$

$$= \frac{B}{2H} \frac{1}{n_p + \left(1 - \frac{t}{H}\right) \frac{\sum_{j=1}^{n_c n_p} W_{s,j}}{W_{tot}}}$$

Where W_s is the weight of the spandrel. Generally, the contribution of the spandrel to horizontal capacity is negligible, being the façade characterized by low values of the ratio between the area of spandrel and the total area of the façade $A_{spandrel}/A_{tot}$, variable in the range 10%-16%. If the contribution of spandrel is negligible, i.e. $\frac{\sum_{j=1}^{n_c n_p} W_{s,j}}{W_{tot}} = 0$, the formula becomes:

$$\lambda = \frac{B}{2H} \frac{1}{n_p} = \frac{B}{2H_{tot}} \quad (18)$$

In Mazziotti (2015) [47], in the case of piers with varying width, in order to provide a more accurate measure of the relative importance of the single

piers, the average value of the pier width was considered. Consequently, Equation (18) was revised as follows:

$$\lambda = \frac{\sum_{j=1}^n B_j^2}{\sum_{j=1}^n B_j} \frac{1}{H_{tot}} = \frac{B_{pes}}{H_{tot}} \quad (19)$$

Within this dissertation, the external loads are taken into account, by introducing a coefficient α . This coefficient accounts for the height of application of the resultant of the horizontal distribution of forces proportional to the masses is applied (Figure 5.19).

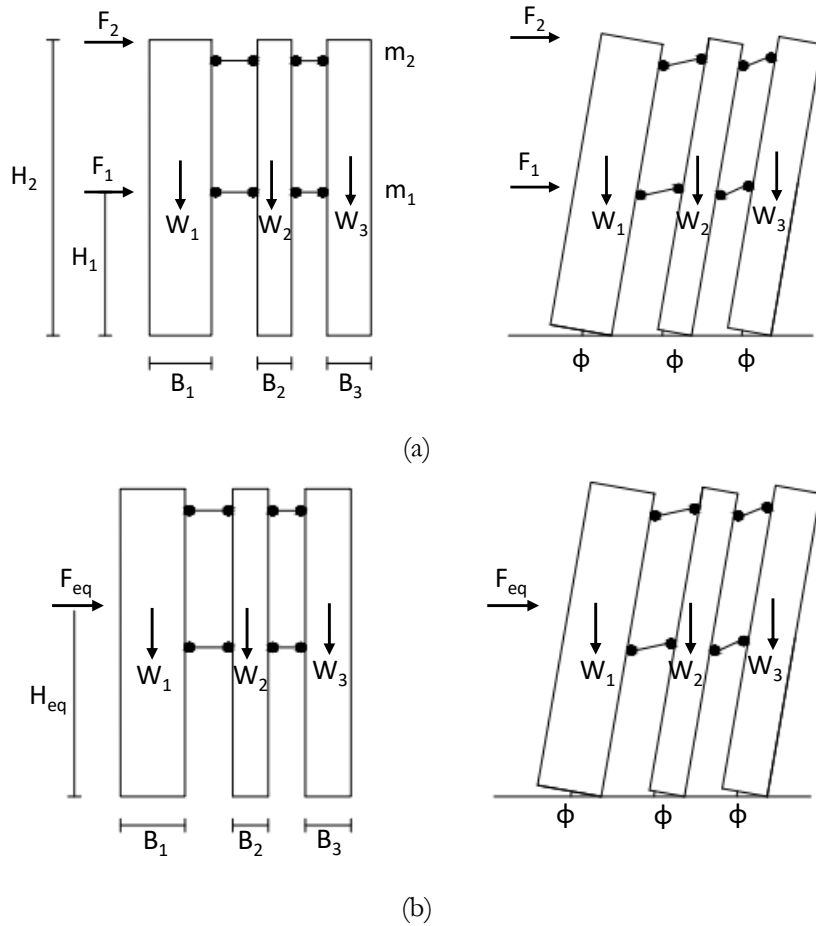


Figure 5.19. Generic masonry wall: Condition loads.

The (19) becomes:

$$\lambda_{eq} = \frac{B_{pes}}{\alpha H_{tot}} \quad (20)$$

The coefficient α can be expressed as:

$$\alpha = 2 \frac{\sum_{i=1}^m F_i H_i}{F_{tot}} \frac{1}{H_{tot}} = 2 \frac{H_{eq}}{H_{tot}} \quad (21)$$

in which:

F_i is the horizontal force proportional to the mass of the i th-floor;

H_i is the height of application of the horizontal force F_i .

H_{eq} is the equivalent height expressed as:

$$H_{eq} = \frac{\sum_{i=1}^m F_i H_i}{F_{tot}} \quad (22)$$

To better understand, a single block with three different condition loads can be considered (Figure 5.20). When the force is applied at the top of the block, the coefficient is equal to 2. If the force is applied in the middle, the coefficient becomes 1. In cases where the force is applied at a height between the middle and the top of the block, the coefficient varies between 1 and 2.

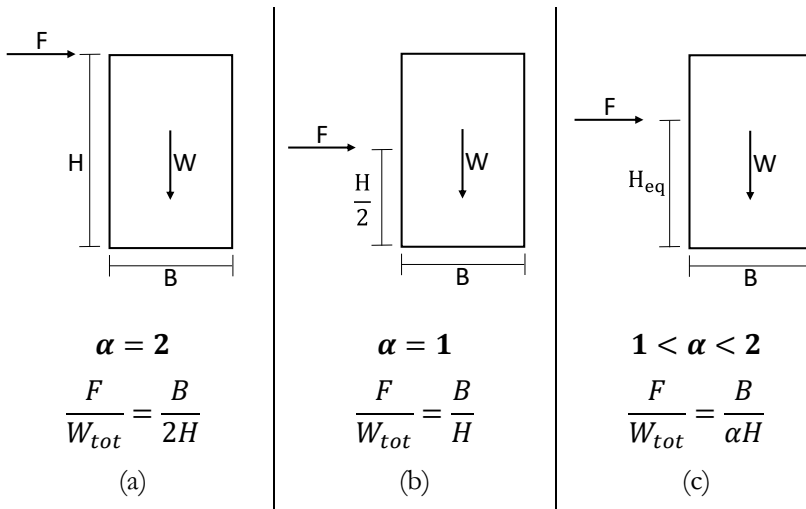


Figure 5.20. Values of coefficient α for different condition loads.

Chapter 6

Structural modelling of St. Domenico Convent in Naples

This Chapter deals with description of the structural model of the Saint Domenico Convent in Naples. The Convent case study consists of eight constructions, built over different periods, ranging from the 8th to the 17th century, and having different features in terms of structural typology. Given the complexity of the Convent, it will be analysed via non-linear static analysis by assuming two limit hypotheses. The first hypothesis involves the analysis of the single construction, by neglecting the interaction with the others; the second hypothesis assumes perfect interaction among all the constructions, considering them as a single structure. In addition, 2D nonlinear static analysis will be conducted to gain a deeper understanding of the structural behaviour. To this aim, 2D models for the walls, 3D models for each individual construction, as well as a model for the entire convent have been developed by using the CDS-WIN analysis program. At first some considerations about the adopted strategy of modelling are presented. Subsequently, an overview of the simplifications introduced in the structural models of each construction and in the entire Convent model, the mechanical properties of the material and indications about the reference systems of each structural model are provided.

6.1 The strategy of modelling adopted for the St. Domenico Convent

The equivalent frame approach has been adopted, in compliance with the current Italian Building Code (NTC 18), by assuming a weak spandrel (pendulum), because of the lack of any tensile resistant element. The assumption of weak spandrel model comports that the spandrel will not be considered as resistant element. However, the software CDS provided a control of the deformation by evaluating the rotation of the plastic hinges of the spandrels.

At first glance, the utilization of the equivalent frame approach may be considered inadequate, for unreinforced masonry buildings. However it can prove highly effective for specific objectives, which include:

- Offering a good individuation of possible local crisis that can lead to the collapse of the structure.
- Accurately estimating the overall deformation of the building (interstorey displacements), particularly at the ultimate limit state.
- Allowing the adoption of a lumped plasticity model, in which nonlinear behaviour is concentrated in flexural and shear plastic hinges, at the end of sections of piers.

The rigid diaphragm constraint has been assumed and the foundations has been neglected, according to §8.3 of NTC 18.

6.2 Simplifications introduced in the structural models

In this Section, an overview of the simplifications introduced in the structural models of each construction and in the entire Convent model is outlined.

About the structural model of *Construction 0*, the following simplifications have been applied:

- The underground floor has been neglected;
- The contribution of the wall supported by vaults at first, mezzanine and second floors, in transverse direction, has been considered only in terms of vertical loads, through the application of vertical

forces. However, their contributions in terms of stiffness and strength have been neglected.

Construction 1 and Construction 2

- The underground floor has been neglected.

Construction 6

- The underground floor has been neglected;
- Due to the impossibility to perform survey, it has been assumed that the walls between elevation 0 and elevation 2.8 meters have the same thicknesses and openings as the walls located on the upper floor.

Construction 7

- For the wall facing Via San Pietro a Majella, in the absence of more detailed investigations, the wall thickness has been assumed to be the same as that of the walls above.
- In the absence of more detailed investigations, a foundation depth of 50 cm was considered.
- The contribution of the wall supported by vaults at first, mezzanine and second floors, in transverse direction, has been considered only in terms of vertical loads, through the application of vertical forces. However, their contributions in terms of stiffness and strength have been neglected.

Regarding the structural model of the *entire Convent*, the floors are positioned at uniform heights, eliminating any staggered floor arrangements. The heights considered for the structural models of each Construction and for the entire Convent model (referred to as C0-1-2-6-7) are listed in Table 6.1.

Table 6.1. Height of the floors considered for the structural models.

Level	Height of floors					
	C0	C1	C2	C6	C7	C0-1-2-6-7
<i>[-]</i>	<i>[m.a.s.l.]</i>					
Foundations	37.93	38.00	37.35	37.05	35.90	37.93
Ground Floor	38.43	38.50	38.75	39.85	36.45	38.43
First Floor	44.00	44.00	44.00	44.05	44.00	44.00
Mezzanine Floor	48.85	50.15		48.20	48.77	48.85
Second Floor	52.95	54.65		52.50	52.95	52.95
Roof (1)	58.10				58.90	58.10
Roof (2)	60.90					60.90

CDS models of each constructions and of the entire Convent are depicted in Figures 6.1 and 6.2.

6.3 Mechanical properties of material

The mechanical properties of tuff have been determined with reference to Table C8.5.I of the current Italian Building Code NTC18, taking into account an intermediate knowledge level LC2. Specifically, the median values within the Table's range have been adopted, except for the specific weight, where the maximum value has been considered. The adopted values for the mechanical properties are given in Table 6.2. It is important to note that a FC value of 1.20 has been selected in alignment with the LC2 knowledge level.

Table 6.2. Mechanical properties of the tuff.

Elastic Modulus	Shear Modulus	Specific Weight	Compressive Strength	Shear Strength
<i>[kg/cm²]</i>	<i>[kg/cm²]</i>	<i>[kg/cm³]</i>	<i>[kg/cm²]</i>	<i>[kg/cm²]</i>
10,800	3,600	1,600	15	0.28

6.4 Reference system

To understand the location of the reference systems adopted in each construction, please consult **Appendix 2**. Additionally, note that the reference system for the entire convent aligns with that of Construction 0. It's important to note that the results of the analyses presented in the following Chapter are expressed with respect to the reference system of each individual construction. However, when comparing the results between the individual constructions and the entire convent, they are rewritten using the reference system of the entire convent, which coincides with that of Construction 0, as previously mentioned.

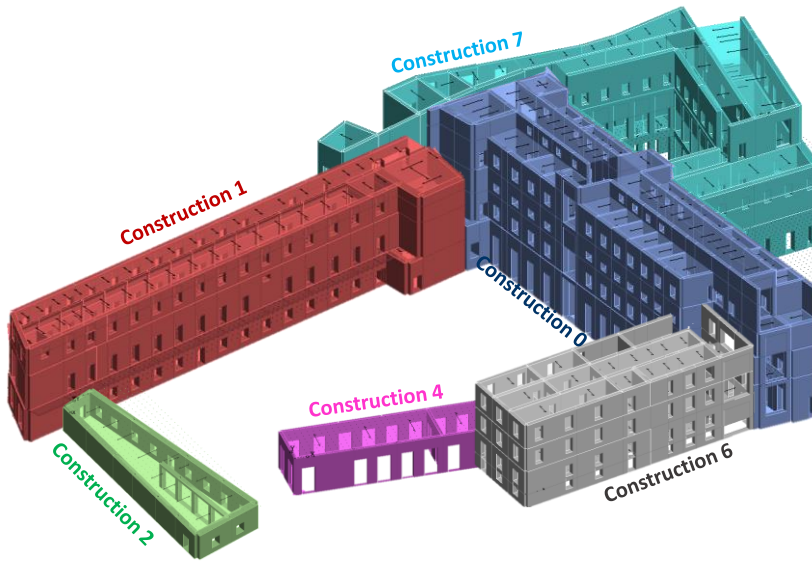


Figure 6.1. Structural models of each Construction.

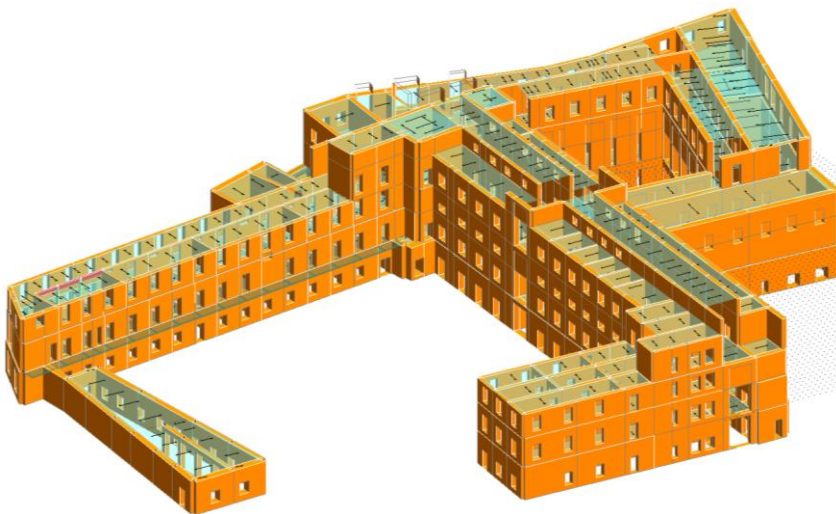


Figure 6.2. Structural model of the Convent.

Chapter 7

Non-linear behavior under horizontal loads

This Chapter deals with nonlinear static analysis of the Saint Domenico Convent in Naples. As discussed in previous Chapters, the Convent case study consists of eight constructions, built over different periods, ranging from the 8th to the 17th century, and having different features in terms of structural typology. Due to the complexity of the Convent and to gain a deeper understanding of the structural behaviour, it has been analysed by assuming two limit hypotheses. The first hypothesis involves the analysis of the single construction, by neglecting the interaction with the others; the second hypothesis assumes perfect interaction among all the constructions, considering them as a single structure. In addition, 2D walls analyses within each construction have been performed, with the aim to identify the weakest wall alignment that lead to the collapse of the structure and the local crises. In this Chapter, the results of the non-linear static analyses for each structural model are given. In particular, the results are provided in terms of capacity curves and failure mechanisms. Furthermore, a comparative analysis between the capacity curve of the 3D structure and the 2D walls is provided. To validate the results obtained with nonlinear static analysis through the SAM method, the analysis of 2D walls has been compared with the results obtained with the simplified formula proposed by the research group in the framework of limit analysis. The Chapter concludes with a comparison between the results obtained from analysing each individual construction and those from analysing the entire Convent as a single structure.

7.1 Non-linear Static Analysis of single Construction

In this Section, the results of the nonlinear static analysis carried out for each construction are presented.

Construction 0

- *Nonlinear static analysis of 3D structure*

The pushover analysis has been performed for the 3D structures adopting two load patterns of forces: one proportional to the first vibration mode of the structure and the other proportional to the masses. Note that the analyses has been carried out with a multi-collapse assumption. Figures 7.1 and 7.2 provide the capacity curves of 3D structure defined in terms of (1) base shear vs displacement of the control point, and (2) base shear divided by the weight (F/w) vs displacement divided by the total height of the structure (d/H). The capacity curves exhibit different values in terms of base shear in the two orthogonal direction but comparable values in terms of displacement.

The failure mechanisms depicted in Figure 7.3 reveal flexural failure of the piers and spandrels, with occasional instances of shear failure of the piers.

- *Nonlinear static analysis of 2D walls*

To gain deeper understanding of the structural behaviour, nonlinear static analysis of 2D walls have been conducted. These analyses allow the identification of the weakest alignment that lead to the collapse of the structure and of the local crises. For visual representations of the various alignments, please refer to **Appendix 2**. Without losing of generality, the distribution of forces proportional to the masses has been adopted.

The results are expressed in terms of capacity curves, also offering a comparative analysis with the capacity curve of the 3D structure (Figures 7.4 and 7.5). In x direction, the walls 1x and 5x are the weakest alignments, with maximum base shears of 53 t and 81t, respectively. In terms of ratio d/H , wall 5x exhibits the collapse of the first element at lower value (0.43%) compared to other walls. The comparison between the 3D model curve and the 2D model curves shows that collapse of the first element in the 3D model occurs at the same d/H value as wall 5x. In the y direction, the walls exhibit comparable maximum base shear, with a peak value of 80 t observed for wall 1y.

- *Comparison between 2D walls analyses and the simplified formula*

To check the results of the nonlinear static analysis, the straightforward formula to predict the horizontal capacity of masonry unreinforced walls presented in previous Chapters has been applied. The results have been compared with the capacity curve of the 2D wall (Figure 7.6). The outcomes reveal a close approximation between the formula's predictions and the ultimate load of the wall.

It is important to note that, being the formula based on Heyman's hypotheses, which assumes infinite compressive strength of the masonry, a compressive strength of 100 kg/cm² has been employed to simulate the infinite compressive strength of the material. This assumption allows for a meaningful comparison with the simplified formula.

For the comparison between the simplified formula and the capacity curves of others 2D walls please refer to **Appendix 5**.

This procedure has been also adopted for the other constructions. The results are synthesized in the follow.

Construction 1

- *3D capacity curves*

The capacity curves exhibit different values in terms of base shear in the two orthogonal directions but comparable values in terms of displacement.

- *Failure mechanisms of 3D structure*

The Figures reveal flexural failure of the piers and spandrels, with occasional instances of shear failure of the piers.

- *2D capacity curves*

In the x direction, wall 1x emerges as the most vulnerable alignment, exhibiting a maximum base shear of 143 t. Concerning the d/H ratio, wall 3x experiences the collapse of the first element at a lower value (0.37%) compared to other walls. In the y direction, walls show comparable maximum base shear, peaking at 32 t (wall 7y).

Construction 2

- *3D capacity curves*

The capacity curves exhibit different values in terms of base shear in the two orthogonal directions but comparable values in terms of displacement.

- *Failure mechanisms of 3D structure*

The Figures reveal flexural failure of the piers and spandrels, with occasional instances of shear failure of the piers.

- *2D capacity curves*

In x direction, wall 2x is the weakest alignment, with a maximum base shear equal to 82 t. The comparison between the 3D model curve and the 2D model curves reveals that the 3D model curve shares the same ultimate displacement of the wall 1x, which is equal to 3 cm, the smallest among the ultimate displacements. In y direction, the base shears of the two walls are similar.

Construction 4

- *3D capacity curves*

The capacity curves exhibit different values in terms of base shear and ultimate displacement in the two orthogonal directions.

- *Failure mechanisms of 3D structure*

The Figures reveal flexural failure of the piers and spandrels, with occasional instances of shear failure of the piers.

- *2D capacity curves*

In x direction, wall 2x is the weakest alignment, with a maximum base shear of 28 t. In y direction, the pushover curve of the walls coincide.

Construction 6

- *3D capacity curves*

The capacity curves exhibit different values in terms of base shear in the two orthogonal directions but comparable values in terms of displacement.

- *Failure mechanisms of 3D structure*

The Figures reveal flexural failure of the piers and spandrels, with occasional instances of shear failure of the piers in y direction. In x direction, it can be observed shear failure of the piers in many cases, and in few instances, both flexural failure of piers and spandrels.

- *2D capacity curves*

In x direction, wall 1x is the weakest alignment, with a maximum base shear of 166 t. In y direction, walls exhibit comparable maximum base shear, with a maximum value of 54 t (wall 5y). The comparison between the 3D model curve and the 2D model curves shows that the 3D model curve shares the same ultimate displacement as walls 6y and 7y, which is 7 cm, the smallest ultimate displacement.

Construction 7

- *3D capacity curves*

The capacity curves exhibit comparable values in terms of base shear and ultimate displacement in the two orthogonal directions.

- *Failure mechanisms of 3D structure*

The Figures reveal flexural failure of the piers and spandrels, with occasional instances of shear failure of the piers.

- *2D capacity curves*

In x direction, walls 1x, 2x, 3x and 10x are the weakest alignments, each with a maximum base shear of 5 t. The comparison between the 3D model curve and the 2D model curves reveals that the 3D model curve shares the same ultimate displacement as walls 4x, 7x and 12x, which is 15 cm. In y direction, walls 4y, 5y, 6y and 9y are the weakest alignments, with a maximum base shear of 7 t.

To provide a comprehensive summary of the results, the maximum values of force and displacement and of base shear expressed as percentage of weight (F/W) and displacement expressed as a percentage of the height of the structure (d/H) in x and y direction for the two considered load patterns and for each construction are summarized in Table 7.1 and Table 7.2.

Table 7.1. *Distribution of forces proportional to the masses*: Maximum values of forces and displacement and of F/W and d/H ratios in x and y direction.

Construction	Direction	F_{\max}	d_{\max}	$(F/W)_{\max}$	$(d/H)_{\max}$
$[-]$	$[-]$	$[t]$	$[cm]$	$[\%]$	$[\%]$
C0	x direction	1324.41	18.84	7.5%	0.8%
	y direction	816.33	16.59	4.6%	0.7%
C1	x direction	1809.59	10.80	19.6%	0.7%
	y direction	881.01	7.33	9.6%	0.5%
C2	x direction	361.91	7.05	53.7%	1.3%
	y direction	133.85	4.34	19.8%	0.8%
C4	x direction	132.92	1.73	23.7%	0.3%
	y direction	31.76	6.39	5.7%	1.0%
C6	x direction	1477.41	7.28	28.0%	0.5%
	y direction	632.51	10.51	12.0%	0.7%
C7	x direction	1990.65	19.37	9.7%	0.8%
	y direction	1911.50	18.26	9.3%	0.8%

Table 7.2. *Distribution of forces proportional to the first vibration mode*: Maximum values of forces and displacement and of F/W and d/H ratios in x and y direction.

Construction	Direction	F_{\max}	d_{\max}	$(F/W)_{\max}$	$(d/H)_{\max}$
$[-]$	$[-]$	$[t]$	$[cm]$	$[\%]$	$[\%]$
C0	x direction	925.17	18.23	5.2%	0.8%
	y direction	451.29	16.47	2.6%	0.8%
C1	x direction	1514.40	8.52	16.4%	0.5%
	y direction	579.44	7.20	6.3%	0.5%
C2	x direction	361.91	7.05	53.7%	1.3%
	y direction	133.85	4.34	19.8%	0.8%
C4	x direction	132.92	1.73	23.7%	0.3%
	y direction	31.76	6.39	5.7%	1.0%
C6	x direction	1038.89	5.67	19.7%	0.4%
	y direction	415.64	9.76	7.9%	0.6%
C7	x direction	1563.90	16.74	7.6%	0.7%
	y direction	1442.96	13.45	7.0%	0.8%

CONSTRUCTION 0
Distribution of forces proportional to the masses

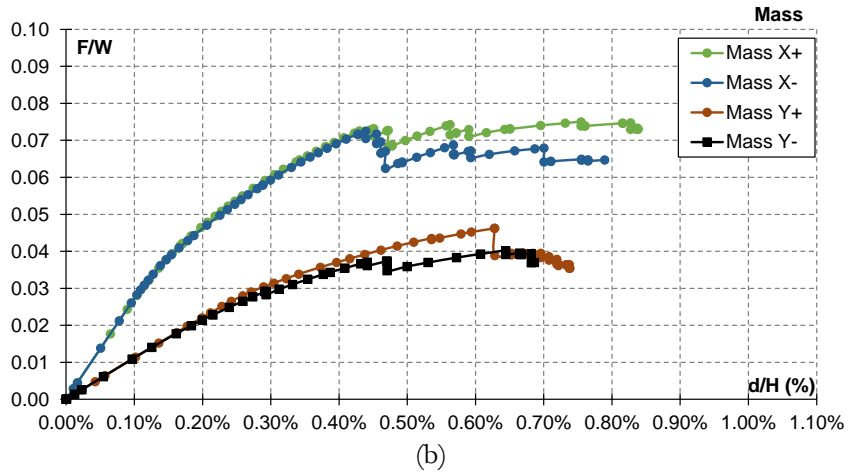
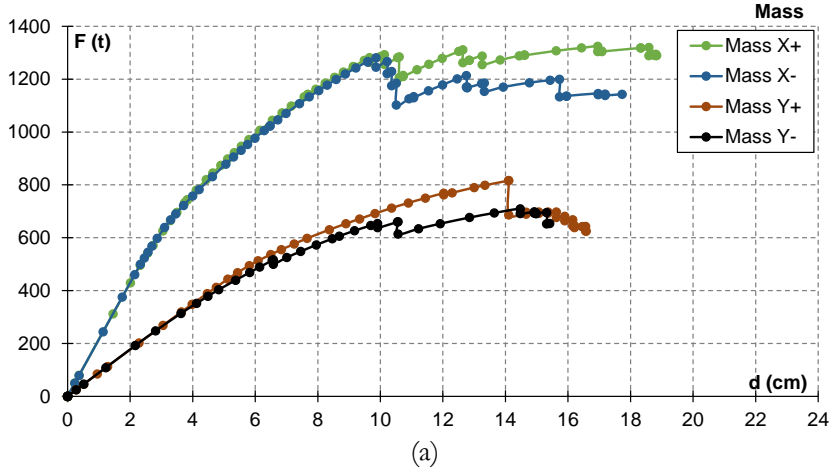


Figure 7.1. *Construction 0* – Distribution of forces proportional to masses: capacity curves in terms of (a) forces vs displacements; (b) Forces divided by weight vs displacements divided by total height of the structure.

Distribution of forces proportional to the first vibration mode of the structure

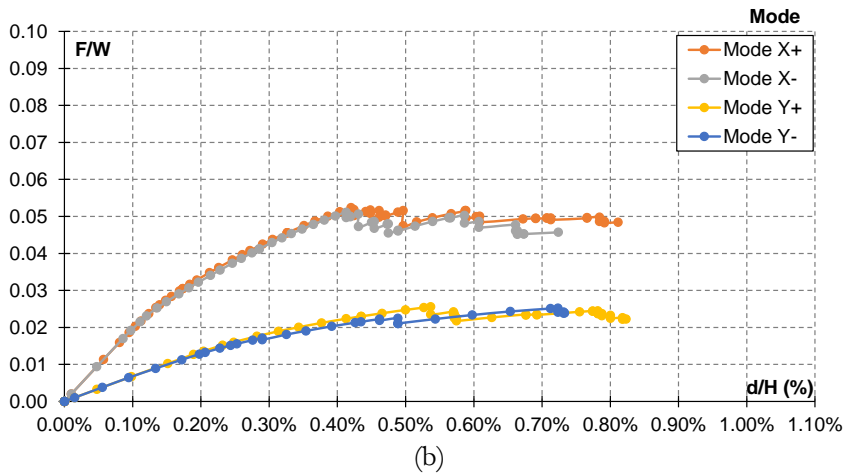
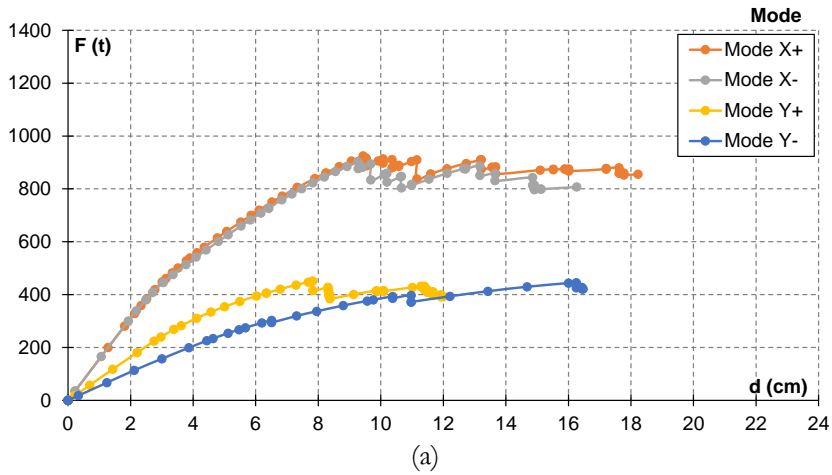
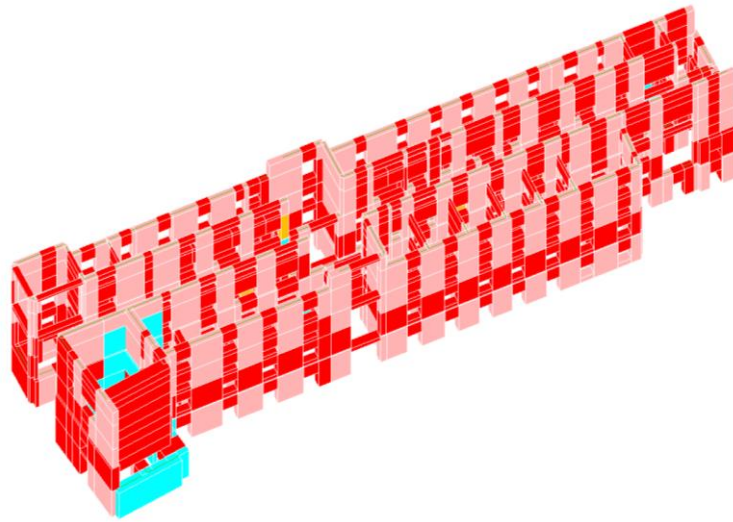


Figure 7.2. *Construction 0* – Distribution of forces proportional to the first vibration mode: capacity curves in terms of (a) forces vs displacements; (b) Forces divided by weight vs displacements divided by total height of the structure.

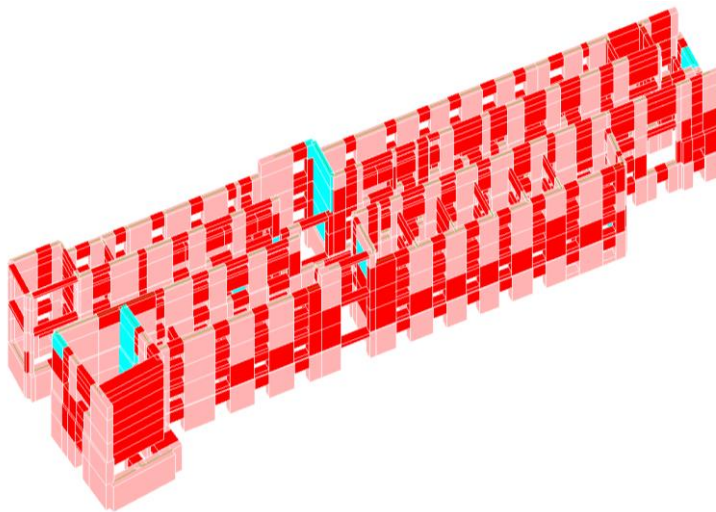
Failure mechanisms
Mass X+



■ Elastic ■ M ■ V ■ N

(a)

Mass Y+

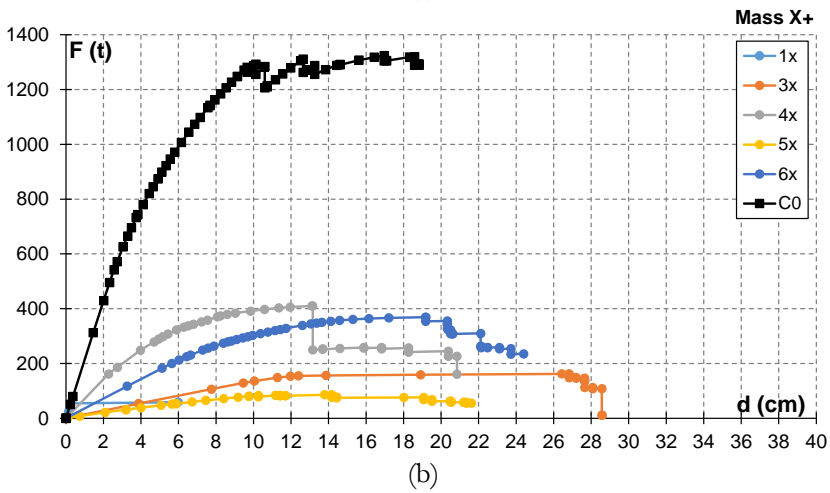
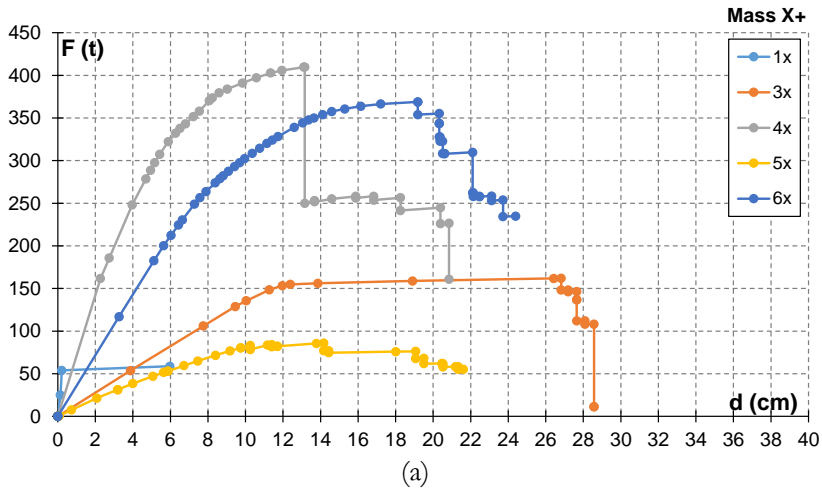


■ Elastic ■ M ■ V ■ N

(b)

Figure 7.3. *Construction 0* – Failure Mechanism in (a) x and (b) y direction.

2D walls analysis



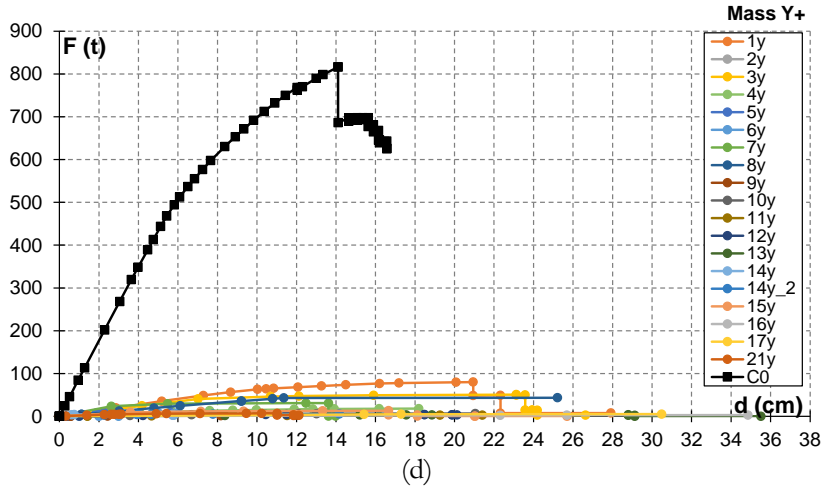
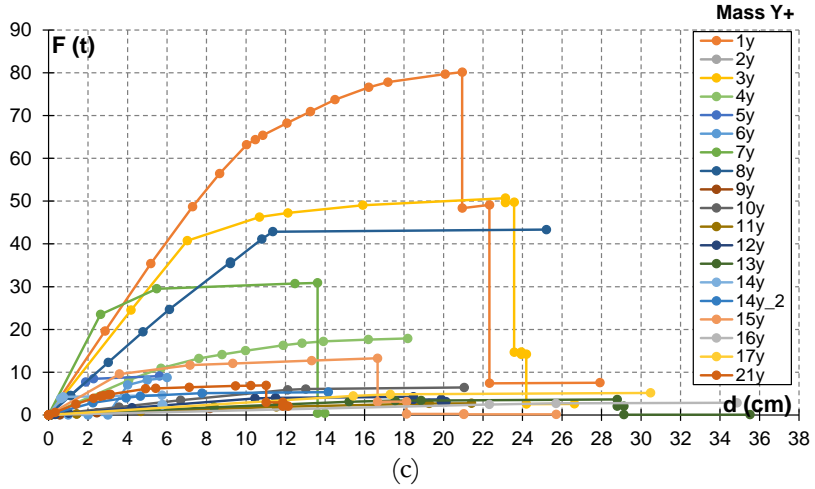
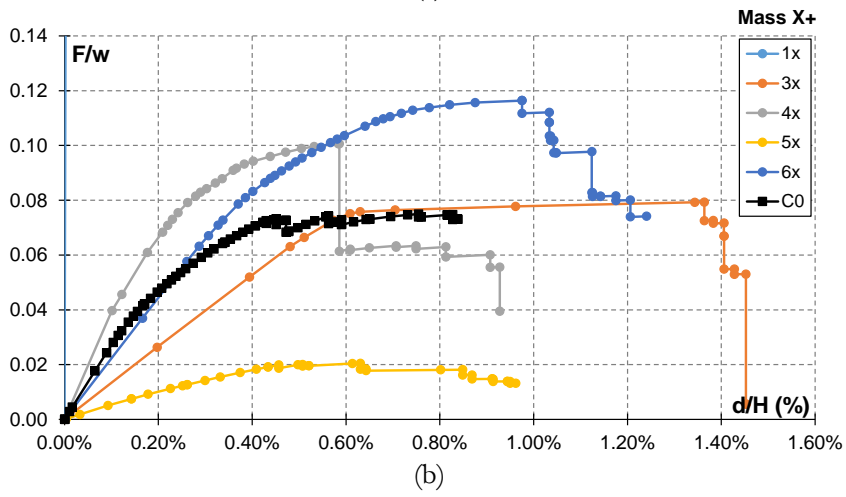
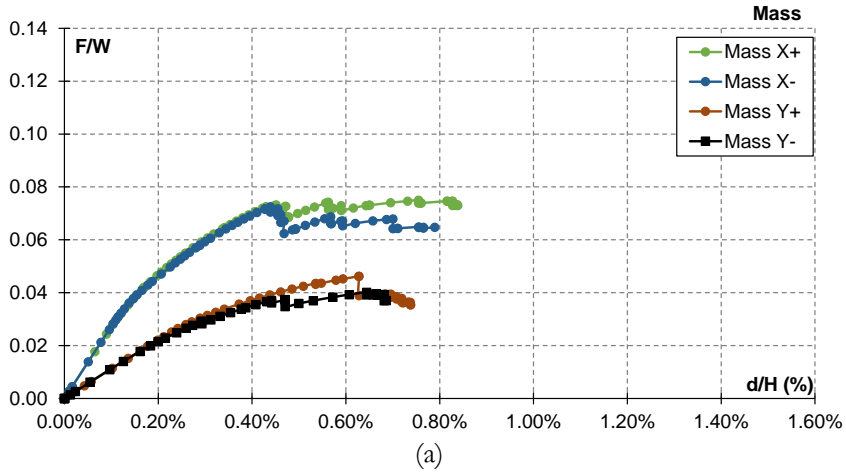


Figure 7.4. *Construction 0* – Capacity curves in terms of forces vs displacements of (a) 2D walls in x direction; (b) comparison between capacity curve of 2D walls and 3D structure in x direction. Capacity curves in terms of forces vs displacements of (c) 2D walls in y direction; (d) comparison between capacity curve of 2D walls and 3D structure in y direction.



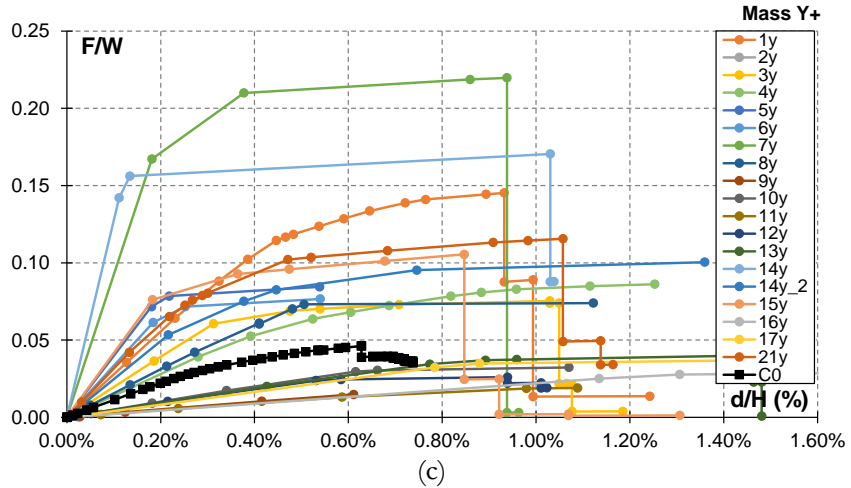


Figure 7.5. *Construction 0* – Capacity curves in terms of Forces divided by weight vs displacements divided by total height of the structure of (a) 3D structure; (b) 2D walls; (c) comparison between capacity curve of 2D walls and 3D structure.

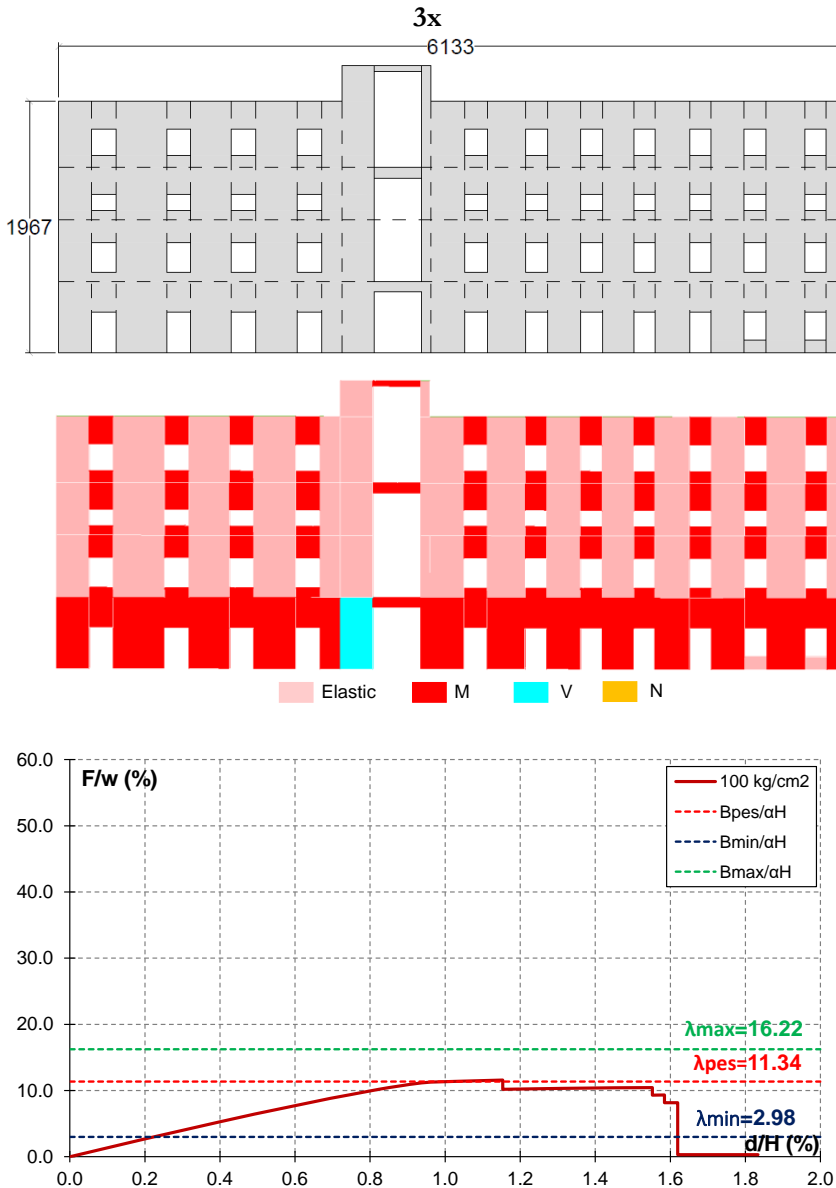


Figure 7.6. Construction 0 (wall 3x) – Failure mechanisms and comparison between the simplified formula and the pushover curve in term of Forces divided by weight vs displacements divided by total height of the structure.

CONSTRUCTION 1
Distribution of forces proportional to the masses

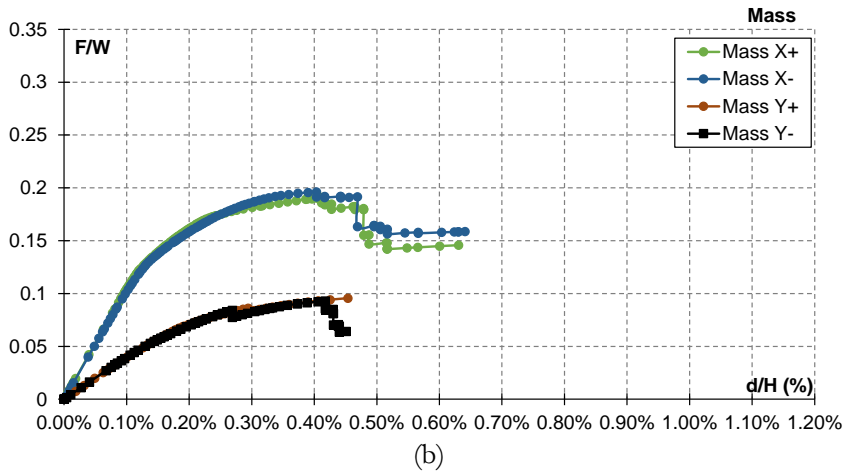
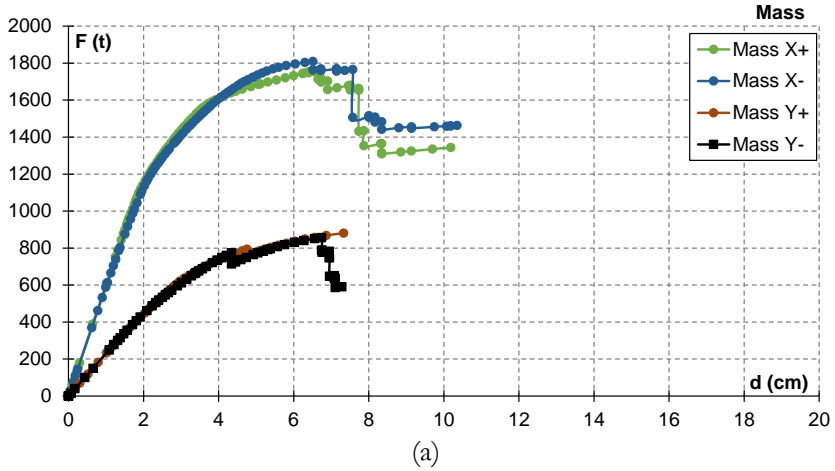


Figure 7.7. *Construction 1* – Distribution of forces proportional to masses: capacity curves in terms of (a) forces vs displacements; (b) Forces divided by weight vs displacements divided by total height of the structure.

Distribution of forces proportional to the first vibration mode of the structure

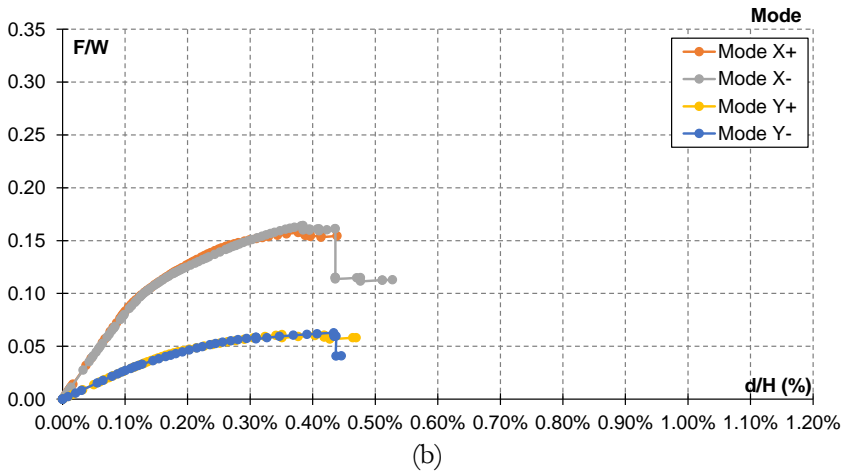
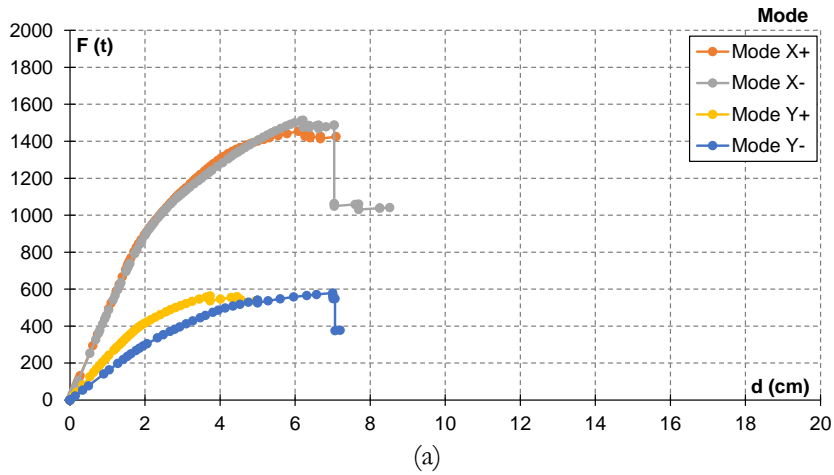
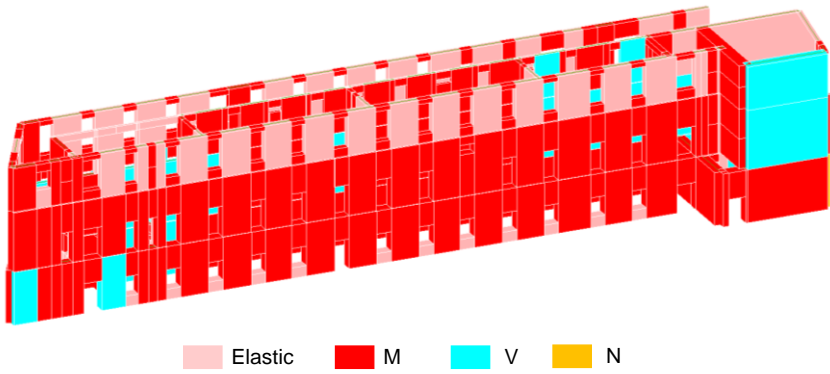


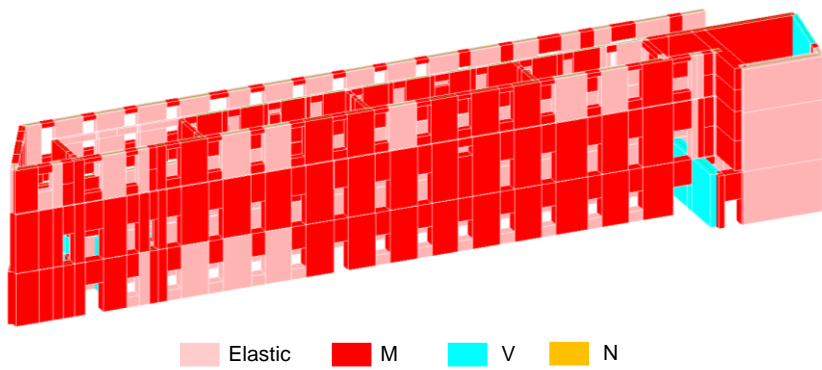
Figure 7.8. *Construction 1* – Distribution of forces proportional to the first vibration mode: capacity curves in terms of (a) forces vs displacements; (b) Forces divided by weight vs displacements divided by total height of the structure.

Failure mechanisms
Mass X+



(a)

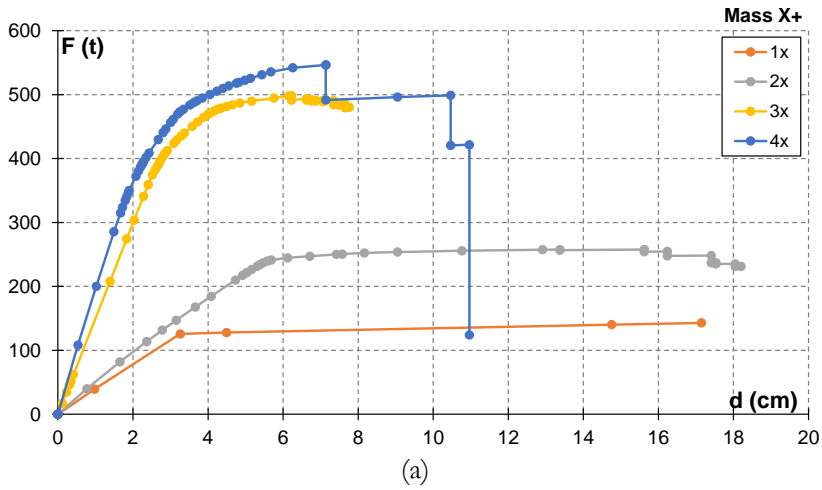
Mass Y+



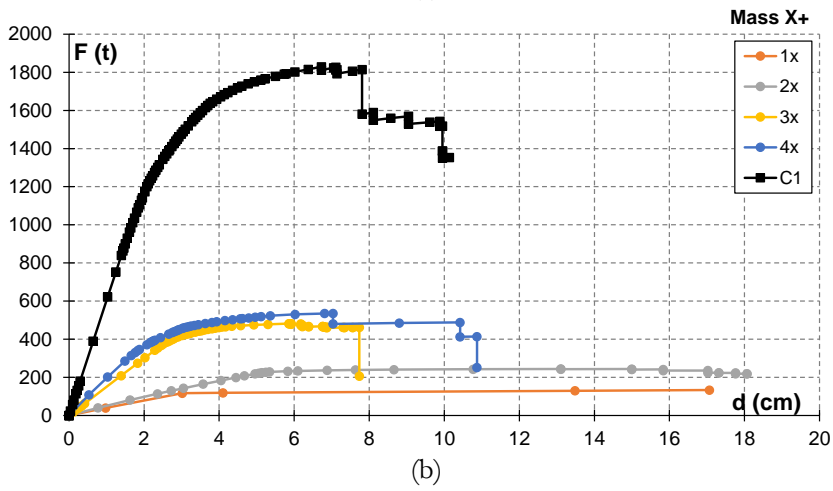
(b)

Figure 7.9. *Construction 1* – Failure Mechanism in (a) x and (b) y direction.

2D walls analysis



(a)



(b)

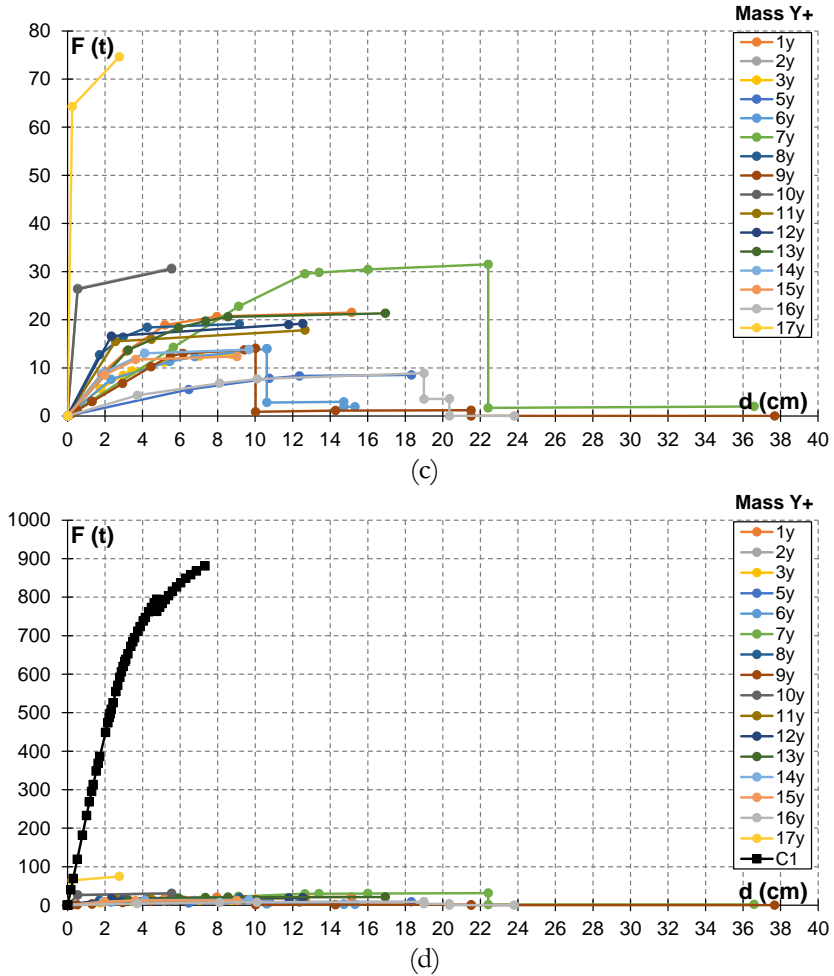
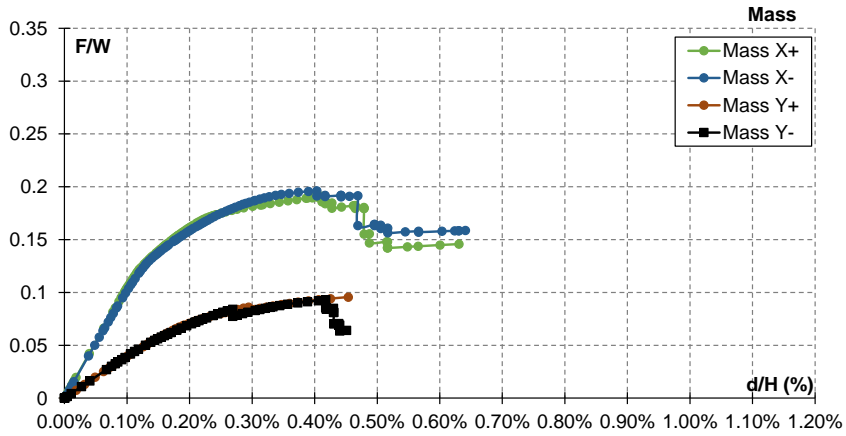
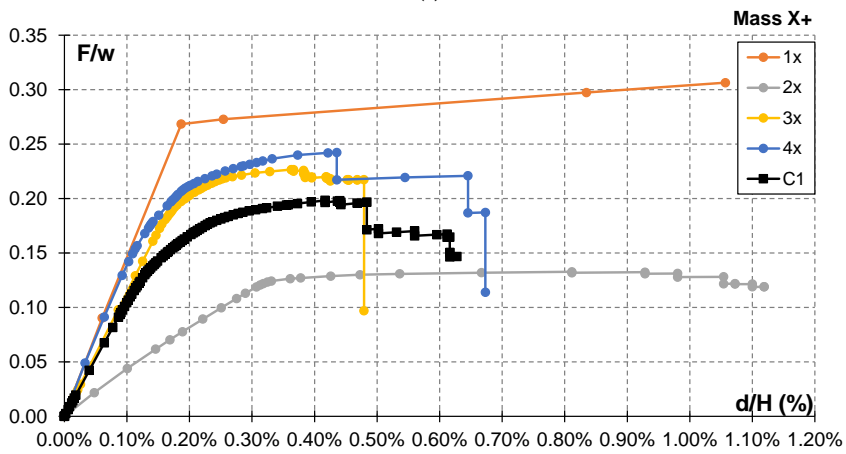


Figure 7.10. *Construction 1* – Capacity curves in terms of forces vs displacements of (a) 2D walls in x direction; (b) comparison between capacity curve of 2D walls and 3D structure in x direction. Capacity curves in terms of forces vs displacements of (c) 2D walls in y direction; (d) comparison between capacity curve of 2D walls and 3D structure in y direction.



(a)



(b)

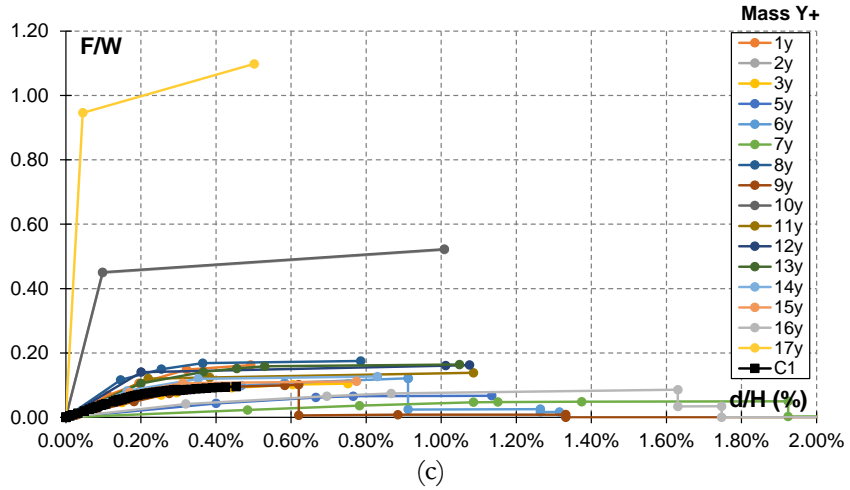
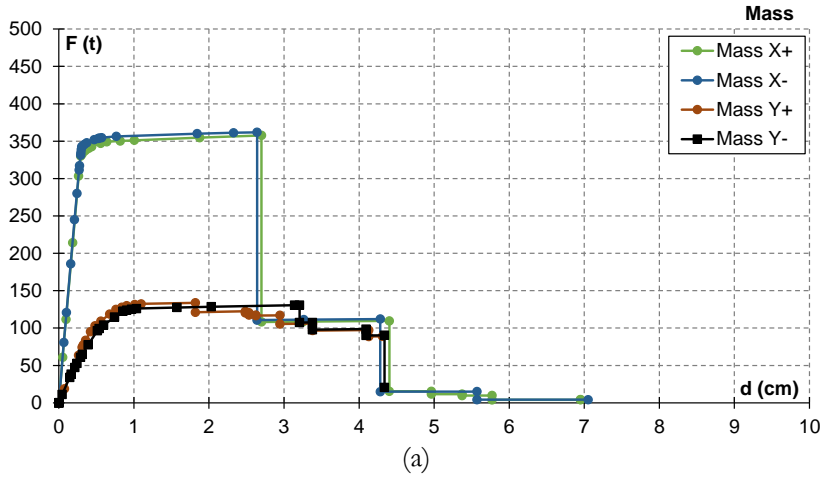
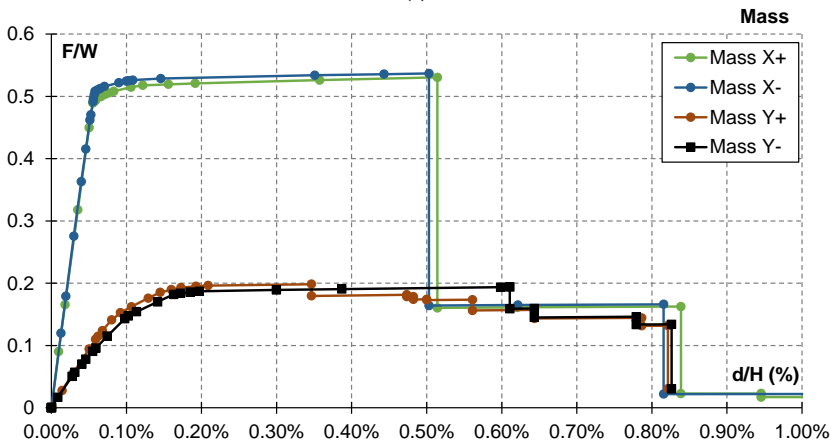


Figure 7.11. *Construction 1* – Capacity curves in terms of Forces divided by weight vs displacements divided by total height of the structure of (a) 3D structure; (b) 2D walls; (c) comparison between capacity curve of 2D walls and 3D structure.

CONSTRUCTION 2 Distribution of forces proportional to the masses



(a)



(b)

Figure 7.12. *Construction 2* – Distribution of forces proportional to masses: capacity curves in terms of (a) forces vs displacements; (b) Forces divided by weight vs displacements divided by total height of the structure.

Distribution of forces proportional to the first vibration mode of the structure

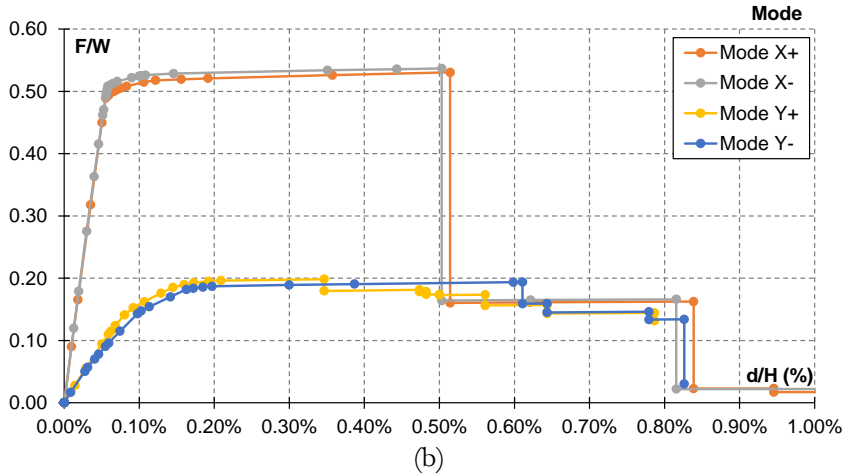
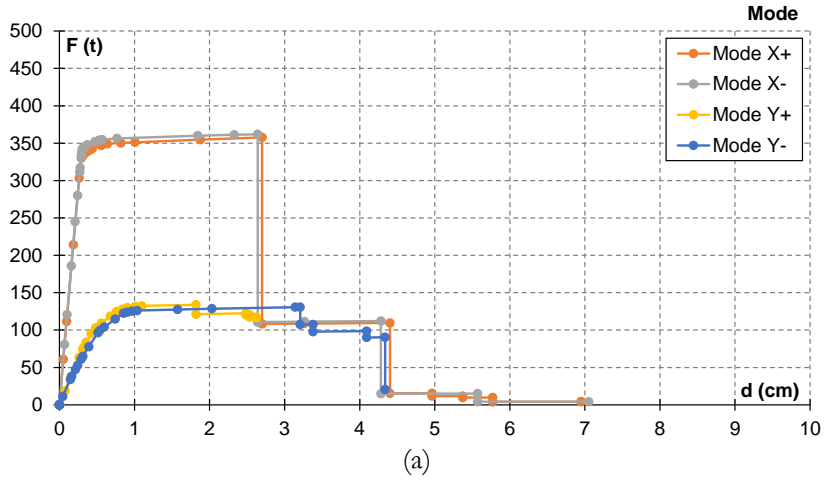
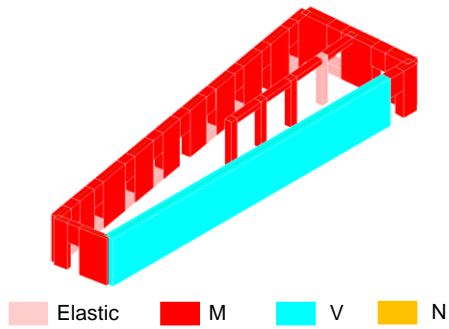


Figure 7.13. *Construction 2* – Distribution of forces proportional to the first vibration mode: capacity curves in terms of (a) forces vs displacements; (b) Forces divided by weight vs displacements divided by total height of the structure.

**Failure mechanisms
Mass X+**



(a)

Mass Y+

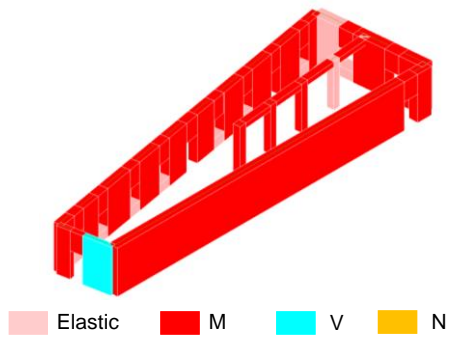
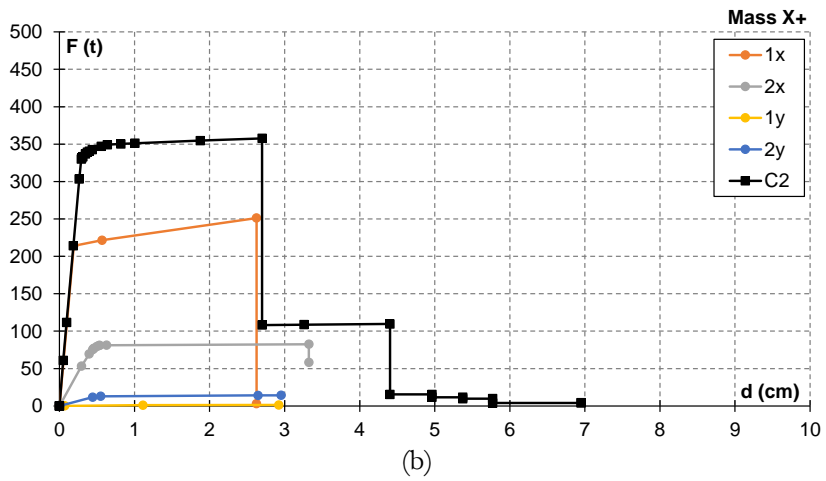
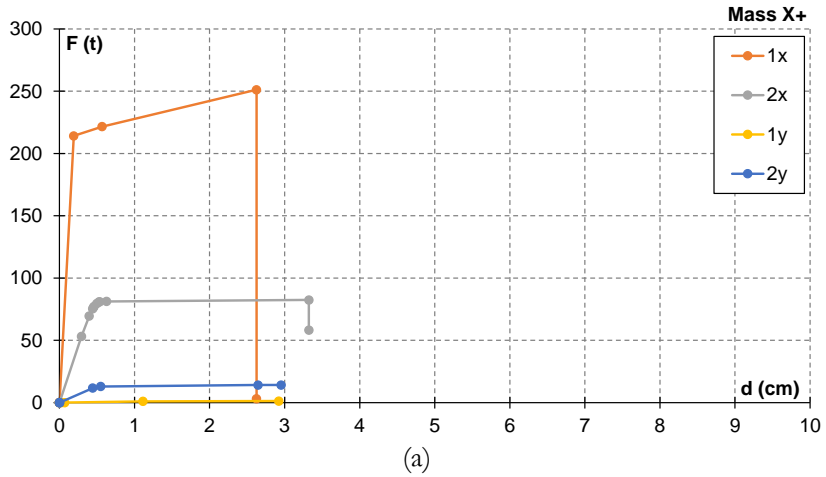


Figure 7.14. *Construction 2* – Failure Mechanism in (a) x and (b) y direction.

2D walls analysis



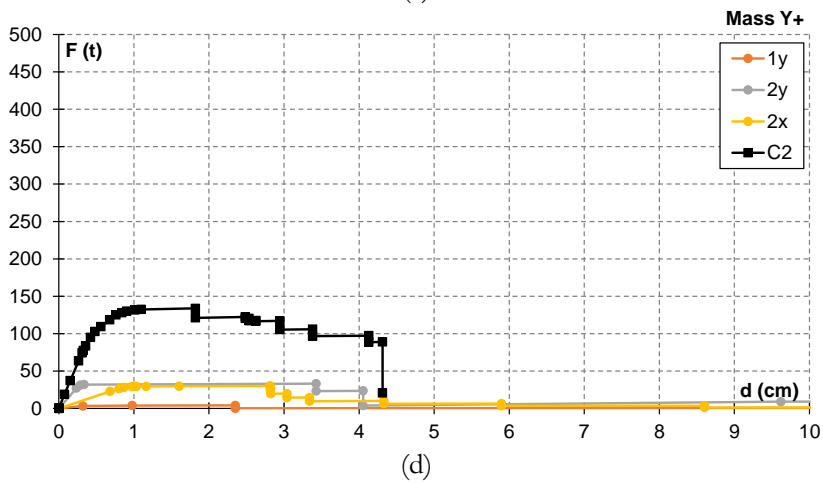
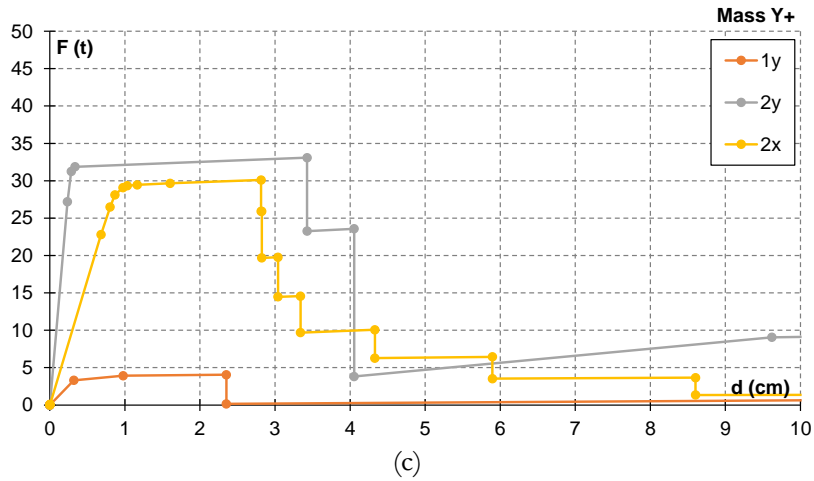
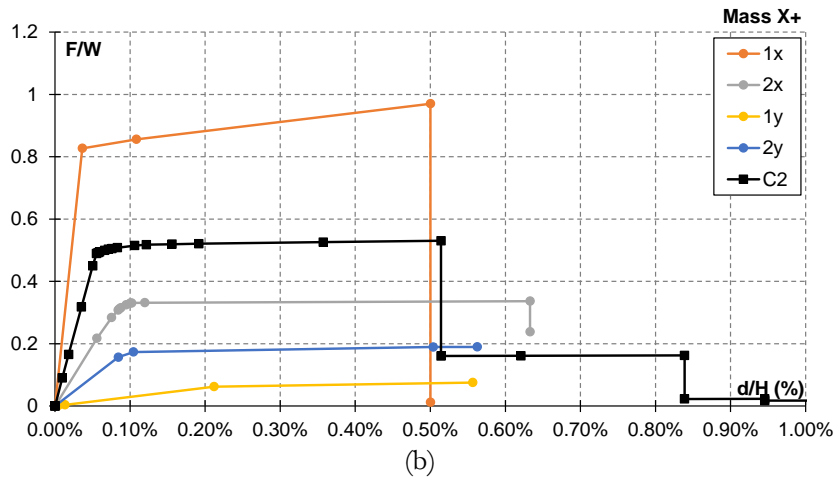
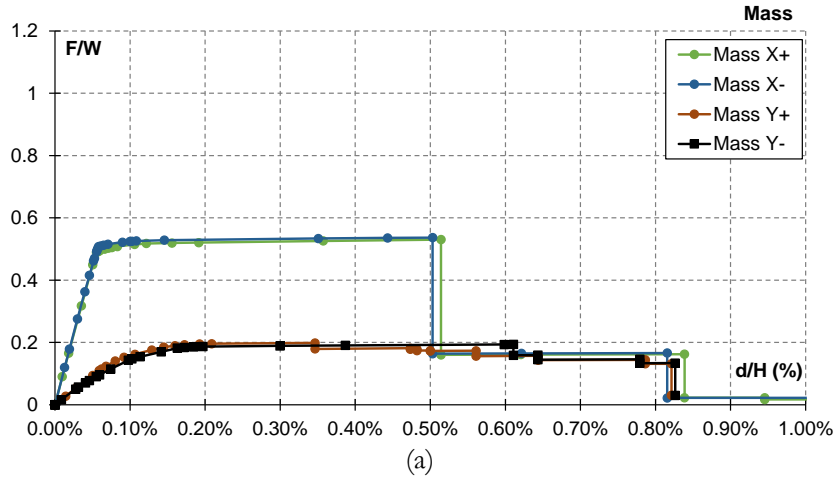


Figure 7.15. *Construction 2* – Capacity curves in terms of forces vs displacements of (a) 2D walls in x direction; (b) comparison between capacity curve of 2D walls and 3D structure in x direction. Capacity curves in terms of forces vs displacements of (c) 2D walls in y direction; (d) comparison between capacity curve of 2D walls and 3D structure in y direction.



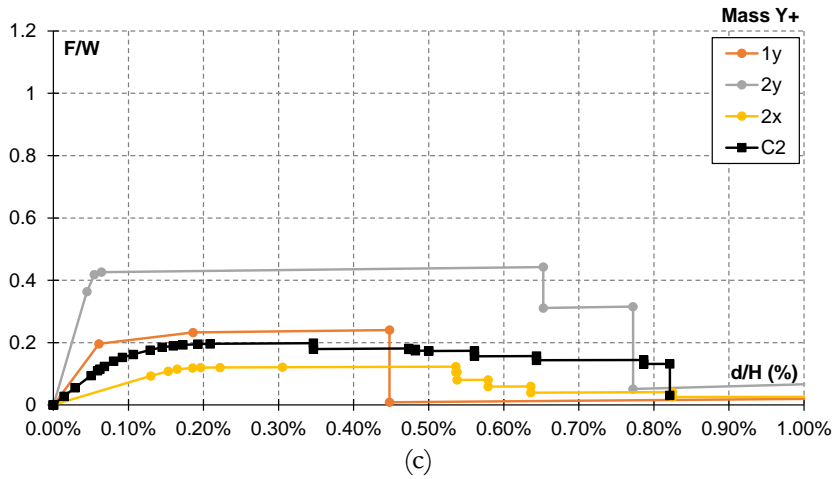


Figure 7.16. *Construction 2* – Capacity curves in terms of Forces divided by weight vs displacements divided by total height of the structure of (a) 3D structure; (b) 2D walls; (c) comparison between capacity curve of 2D walls and 3D structure.

CONSTRUCTION 4
Distribution of forces proportional to the masses

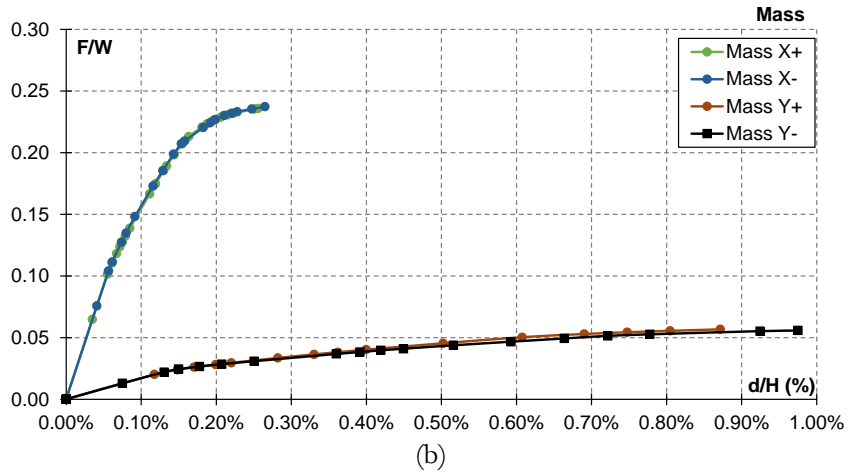
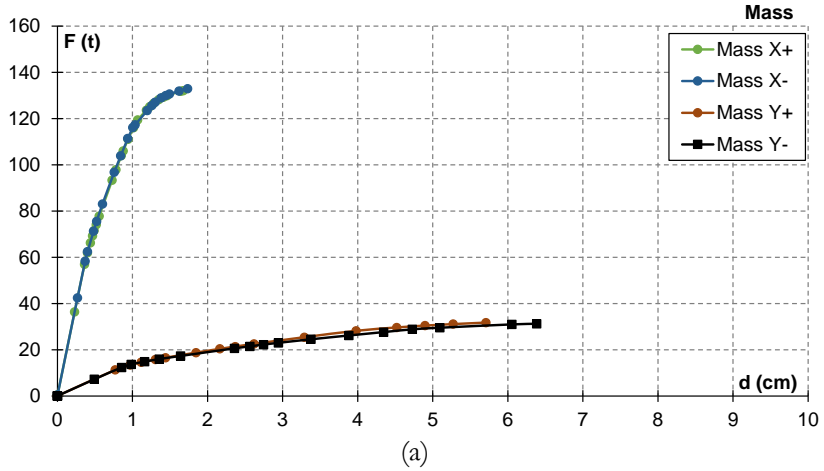


Figure 7.17. *Construction 4* – Distribution of forces proportional to masses: capacity curves in terms of (a) forces vs displacements; (b) Forces divided by weight vs displacements divided by total height of the structure.

Distribution of forces proportional to the first vibration mode of the structure

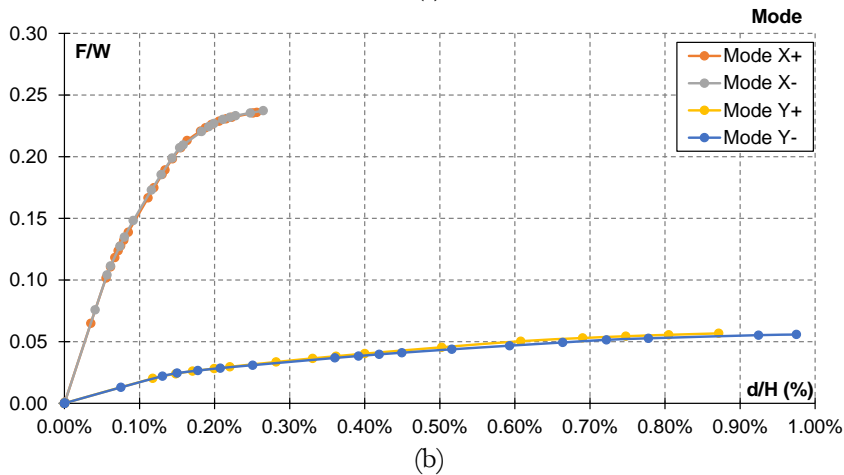
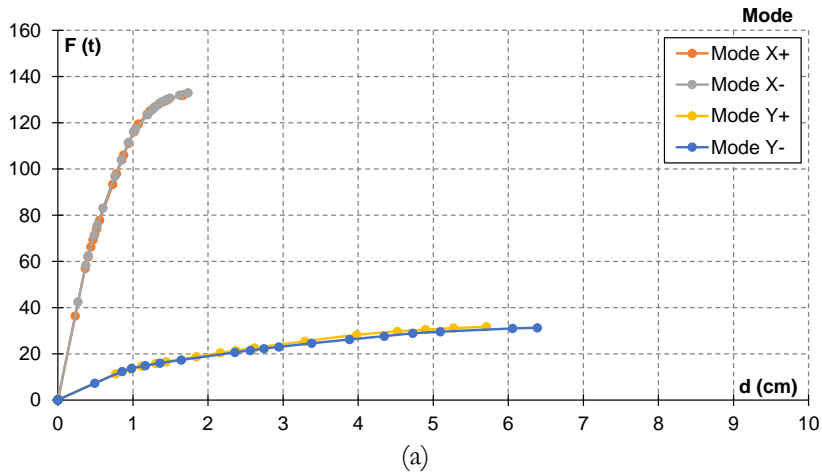
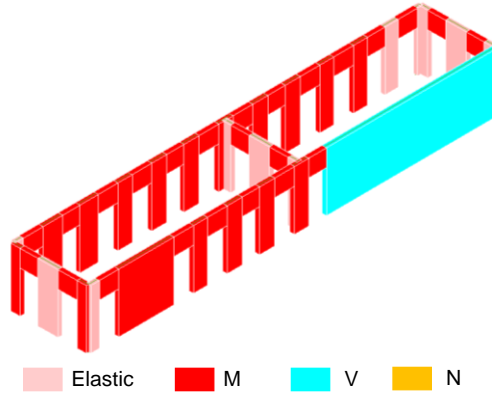


Figure 7.18. *Construction 4* – Distribution of forces proportional to the first vibration mode: capacity curves in terms of (a) forces vs displacements; (b) Forces divided by weight vs displacements divided by total height of the structure.

Failure mechanisms
Mass X+



(a)

Mass Y+

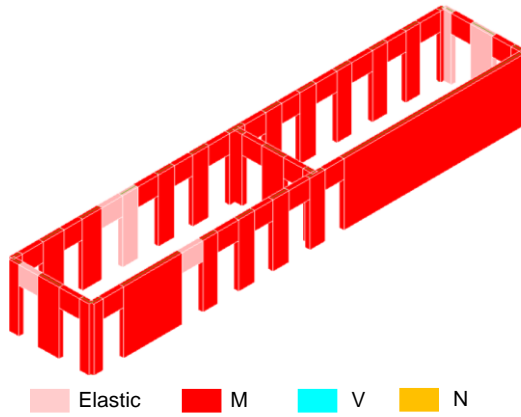
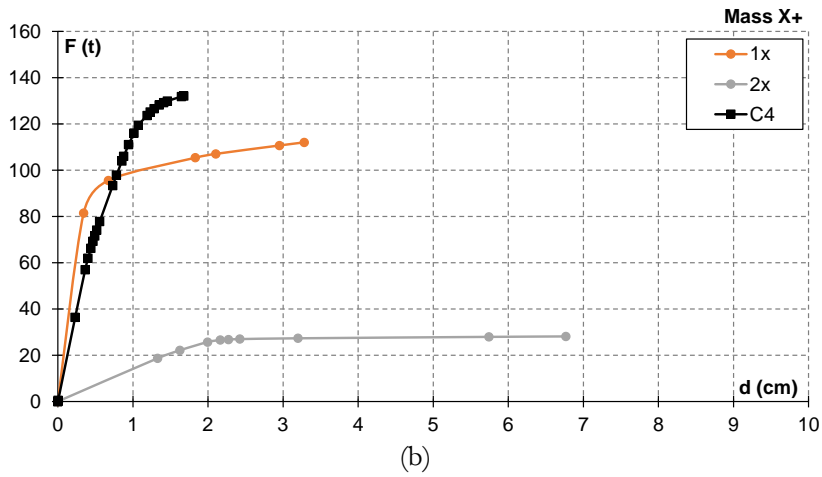
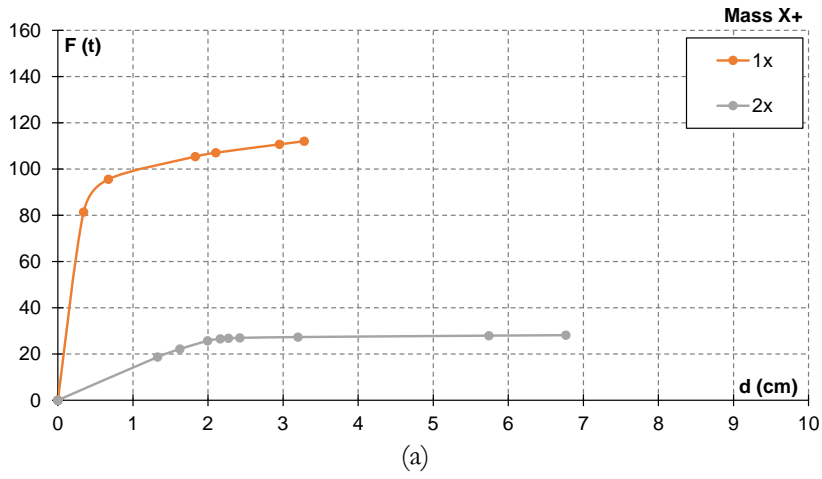


Figure 7.19. *Construction 4* – Failure Mechanism in (a) x and (b) y direction.

2D walls analysis



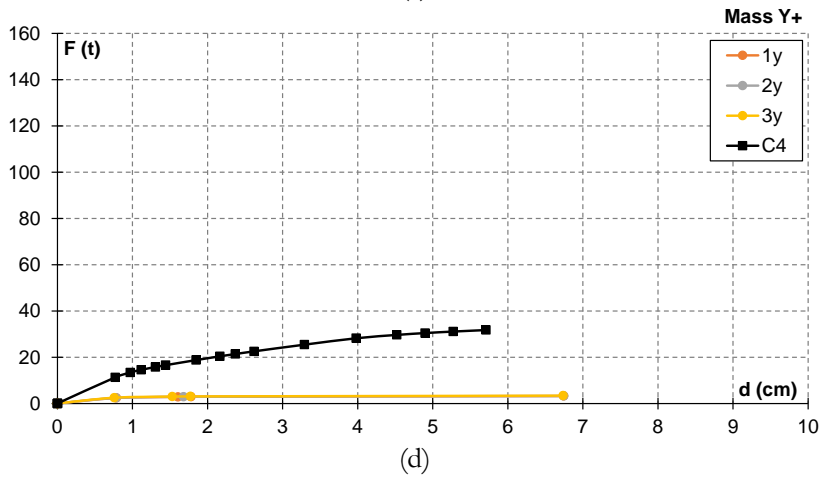
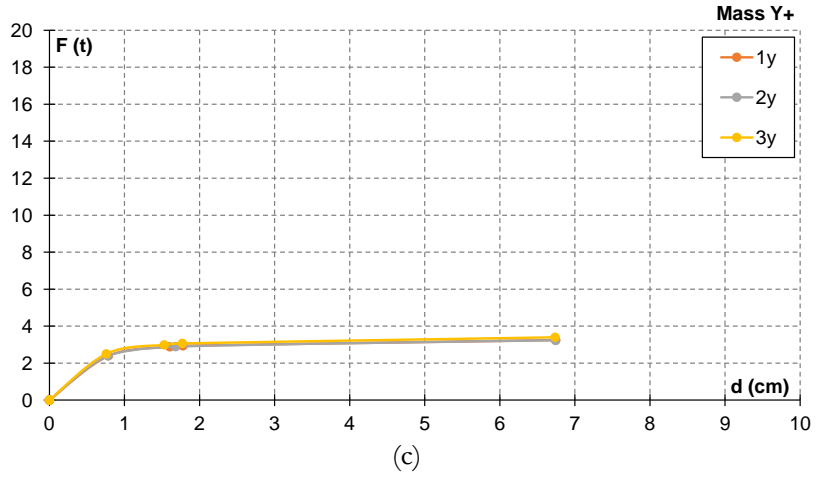
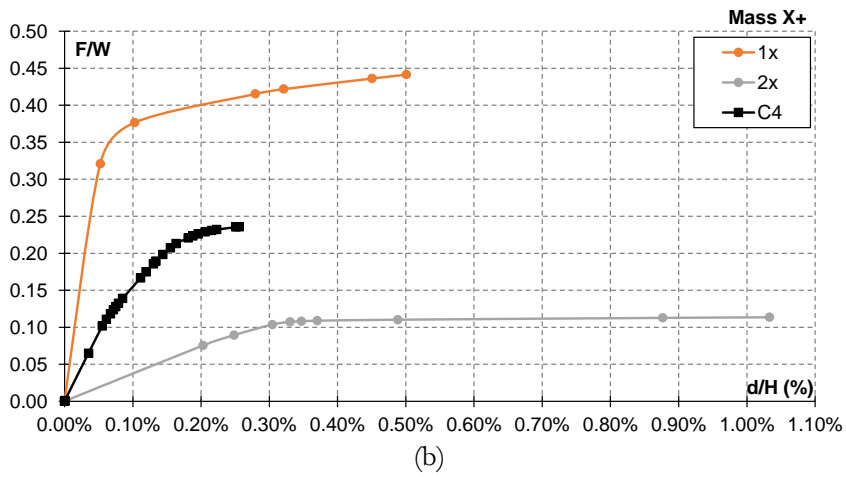
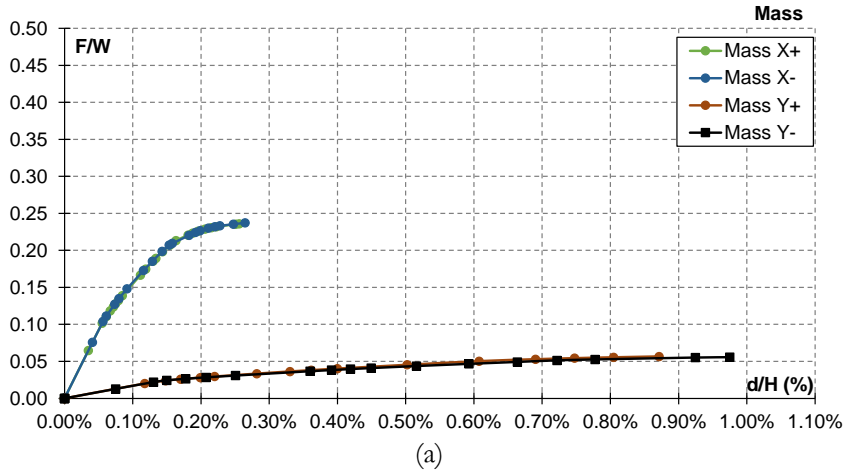
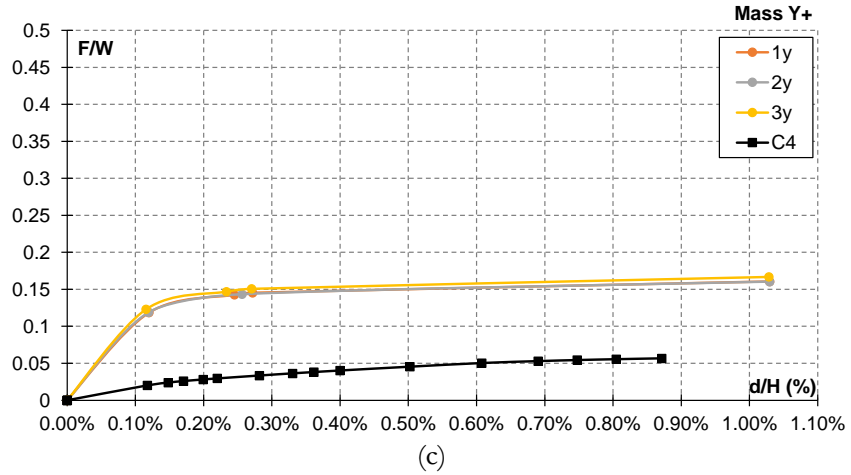


Figure 7.20. *Construction 4* – Capacity curves in terms of forces vs displacements of (a) 2D walls in x direction; (b) comparison between capacity curve of 2D walls and 3D structure in x direction. Capacity curves in terms of forces vs displacements of (c) 2D walls in y direction; (d) comparison between capacity curve of 2D walls and 3D structure in y direction.





(c)
 Figure 7.21. *Construction 4* – Capacity curves in terms of Forces divided by weight vs displacements divided by total height of the structure of (a) 3D structure; (b) 2D walls; (c) comparison between capacity curve of 2D walls and 3D structure.

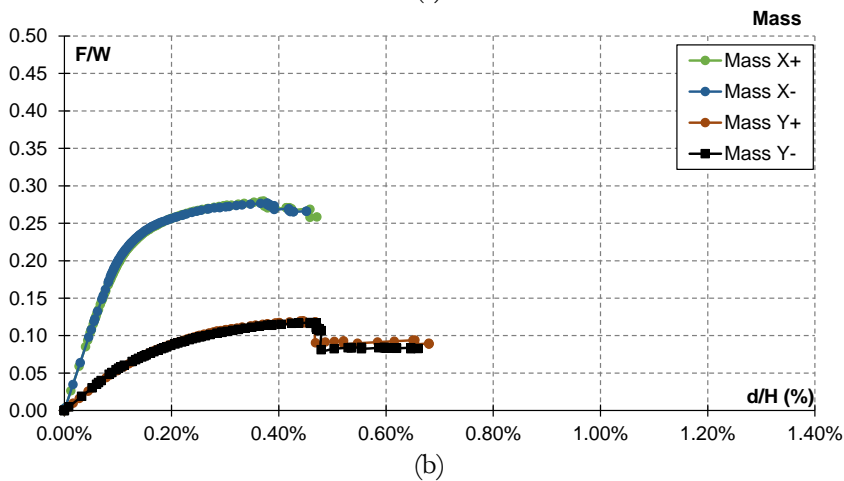
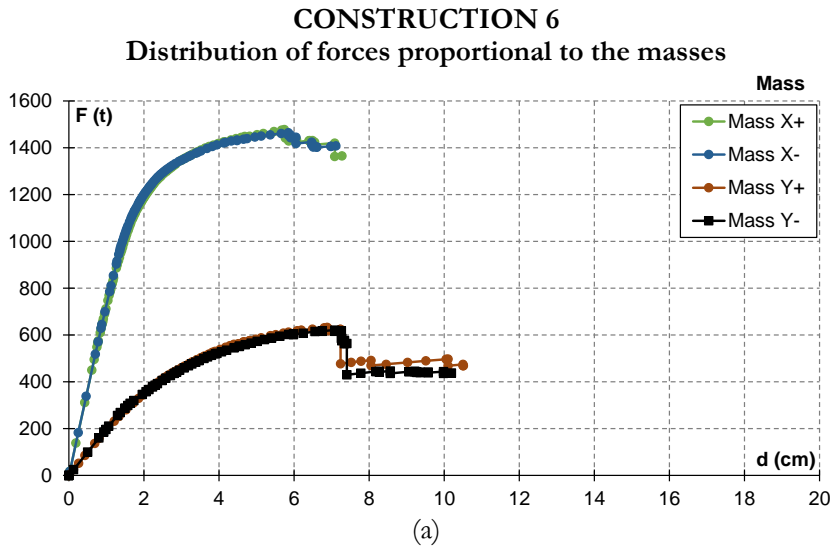
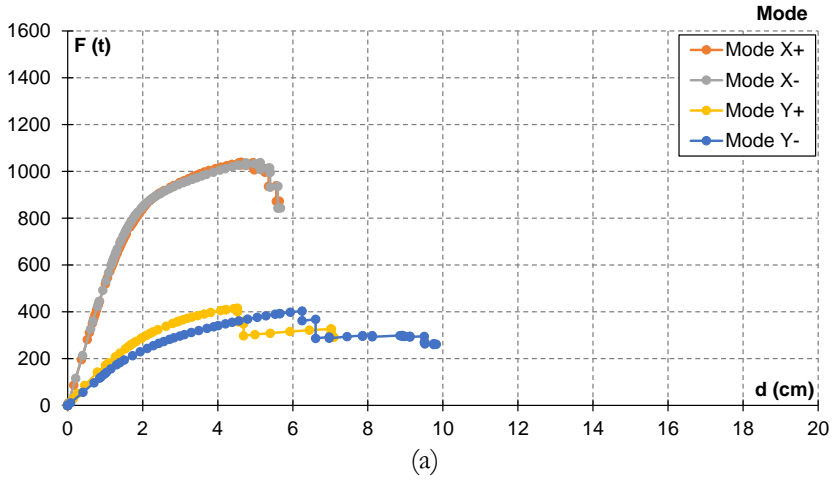
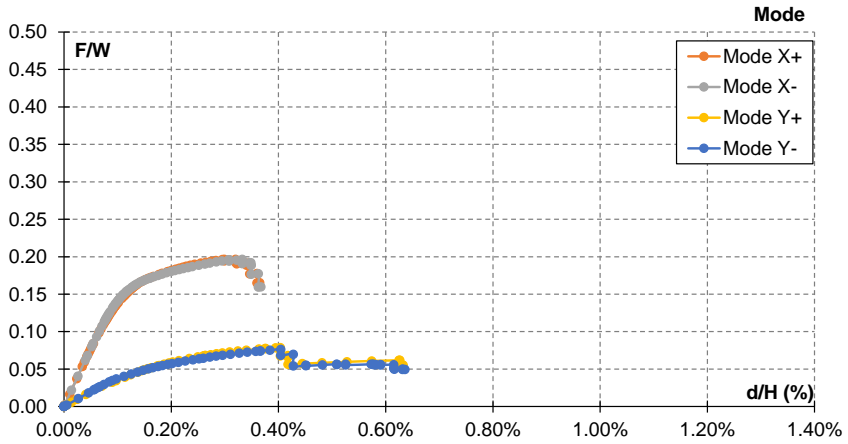


Figure 7.22. *Construction 6* – Distribution of forces proportional to masses: capacity curves in terms of (a) forces vs displacements; (b) Forces divided by weight vs displacements divided by total height of the structure.

Distribution of forces proportional to the first vibration mode of the structure



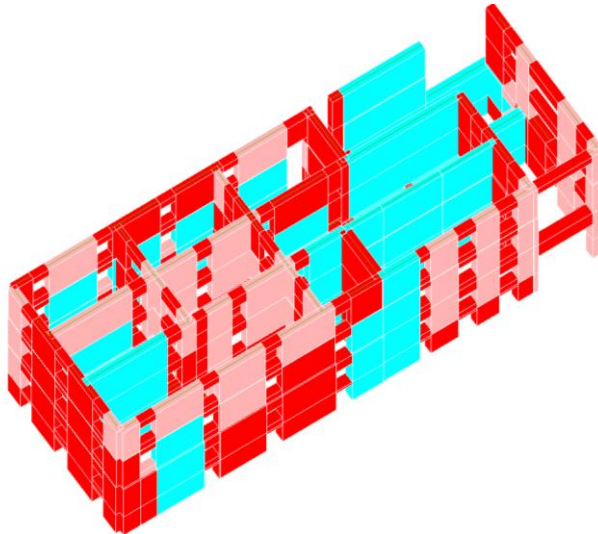
(a)



(b)

Figure 7.23. *Construction 6* – Distribution of forces proportional to the first vibration mode: capacity curves in terms of (a) forces vs displacements; (b) Forces divided by weight vs displacements divided by total height of the structure.

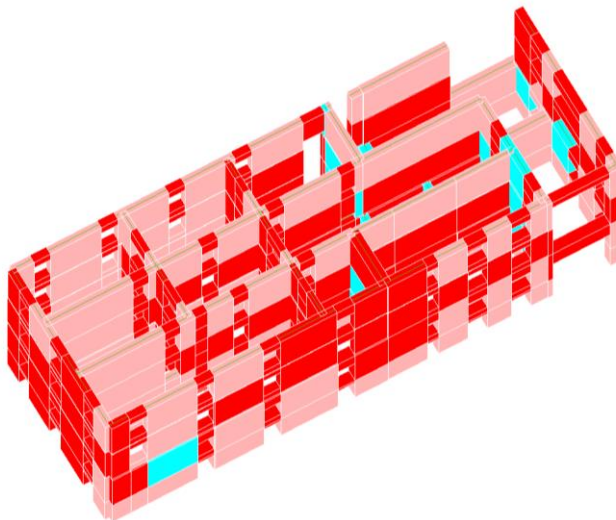
**Failure mechanisms
Mass X+**



■ Elastic ■ M ■ V ■ N

(a)

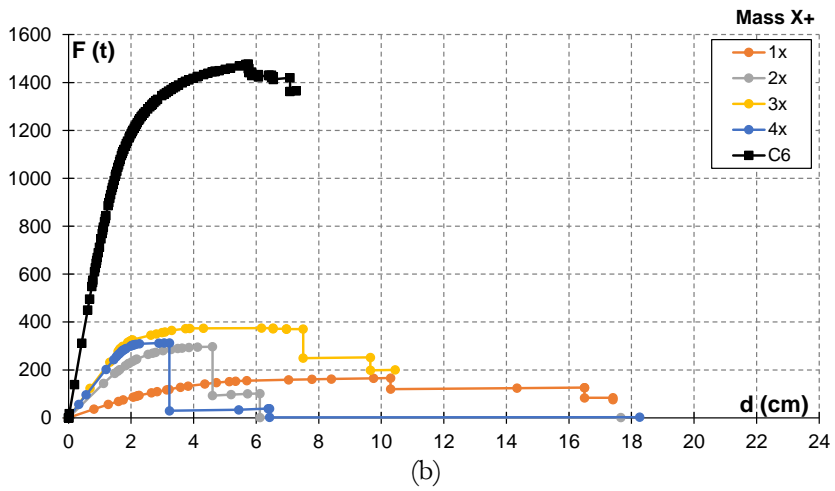
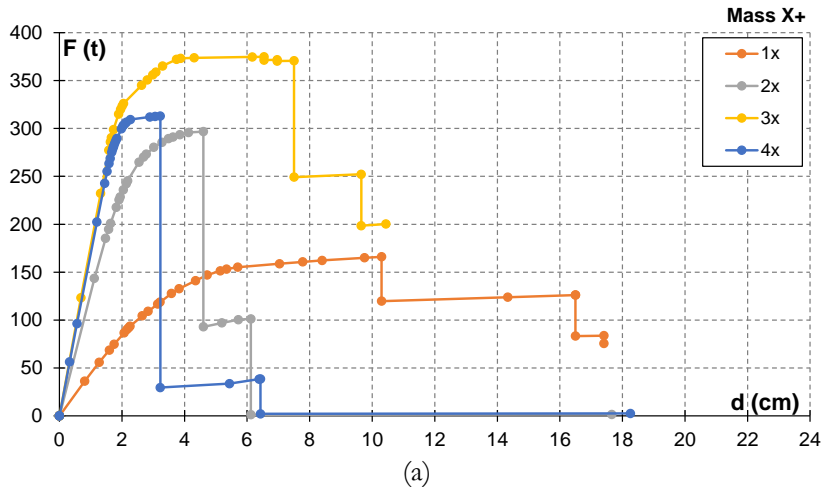
Mass Y+



■ Elastic ■ M ■ V ■ N

Figure 7.24. *Construction 6* – Failure Mechanism in (a) x and (b) y direction.

2D walls analysis



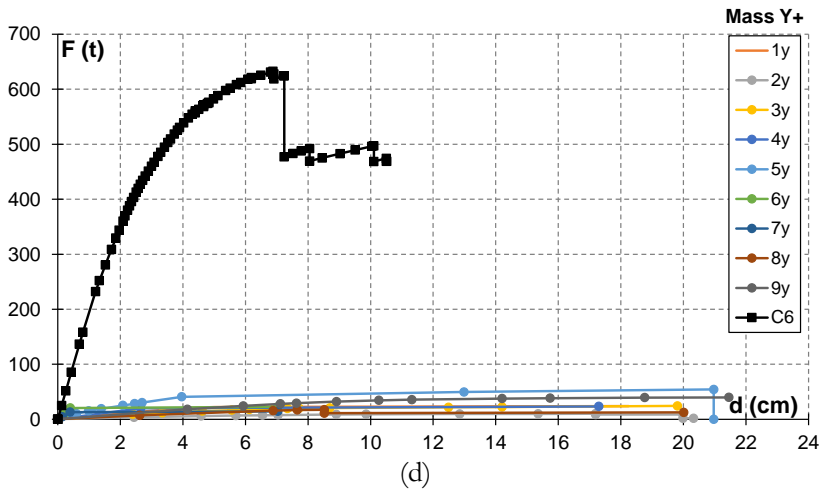
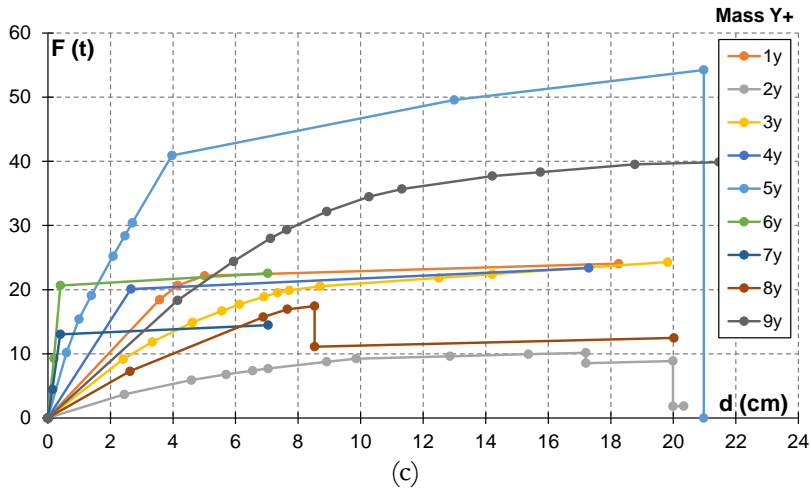
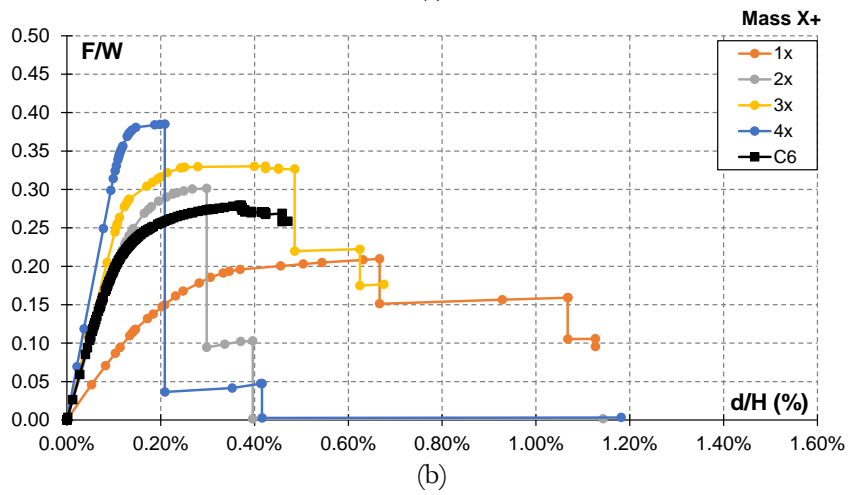
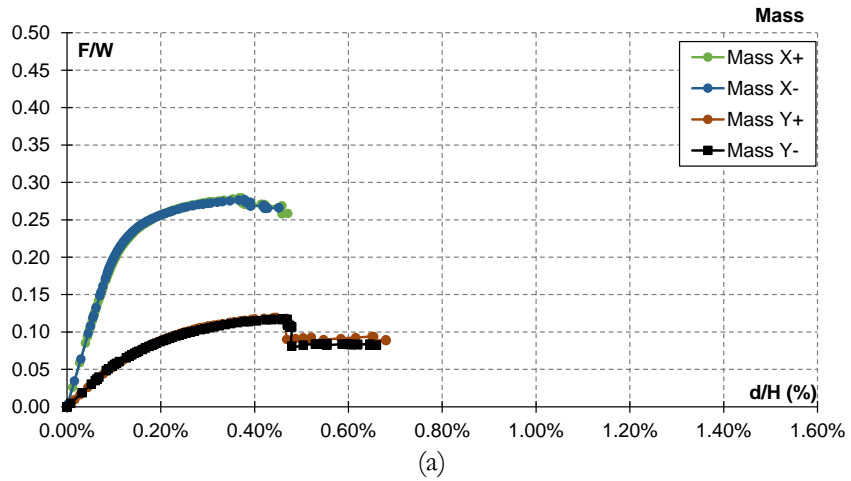


Figure 7.25. *Construction 6* – Capacity curves in terms of forces vs displacements of (a) 2D walls in x direction; (b) comparison between capacity curve of 2D walls and 3D structure in x direction. Capacity curves in terms of forces vs displacements of (c) 2D walls in y direction; (d) comparison between capacity curve of 2D walls and 3D structure in y direction.

Non-linear behavior under horizontal loads



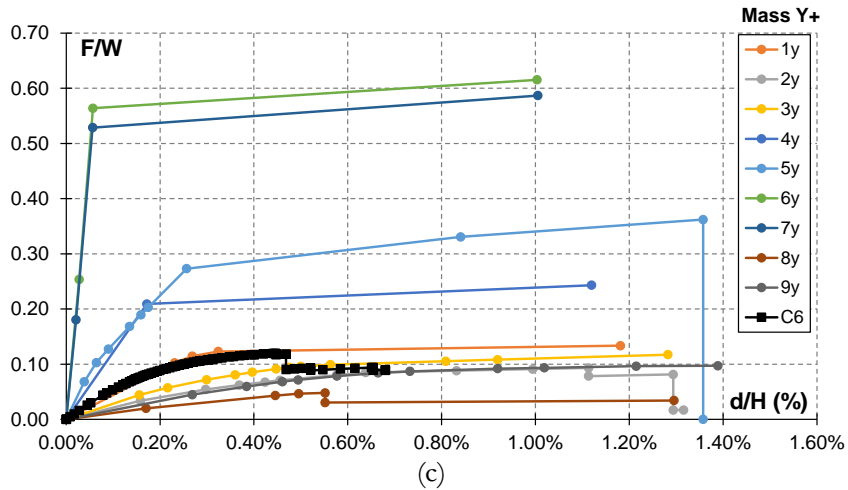
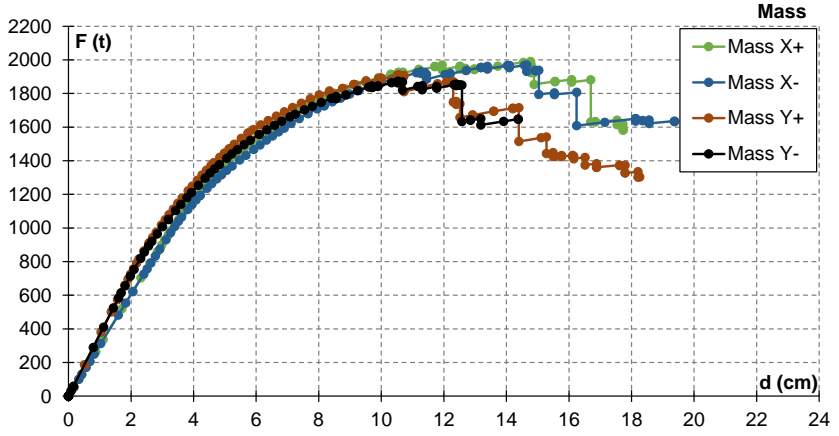
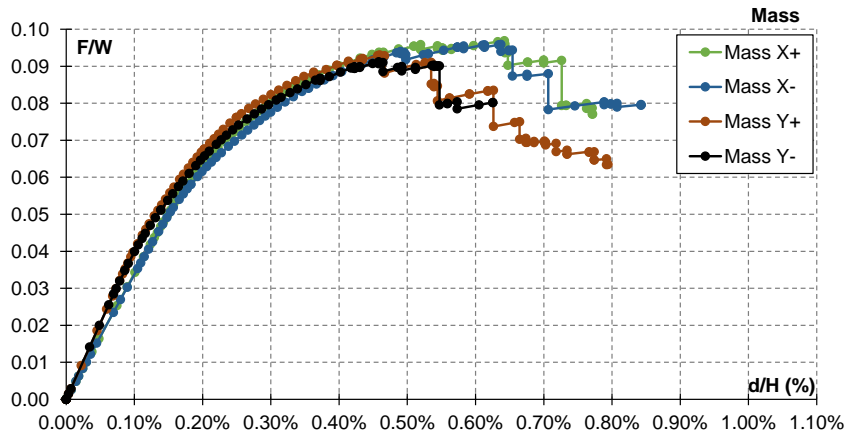


Figure 7.26. *Construction 6* – Capacity curves in terms of Forces divided by weight vs displacements divided by total height of the structure of (a) 3D structure; (b) 2D walls; (c) comparison between capacity curve of 2D walls and 3D structure.

CONSTRUCTION 7
Distribution of forces proportional to the masses



(a)



(b)

Figure 7.27. *Construction 7* – Distribution of forces proportional to masses: capacity curves in terms of (a) forces vs displacements; (b) Forces divided by weight vs displacements divided by total height of the structure.

Distribution of forces proportional to the first vibration mode of the structure

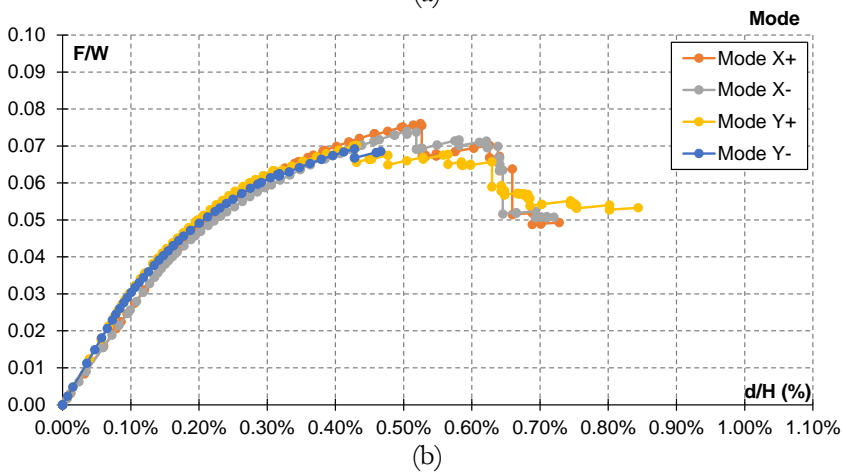
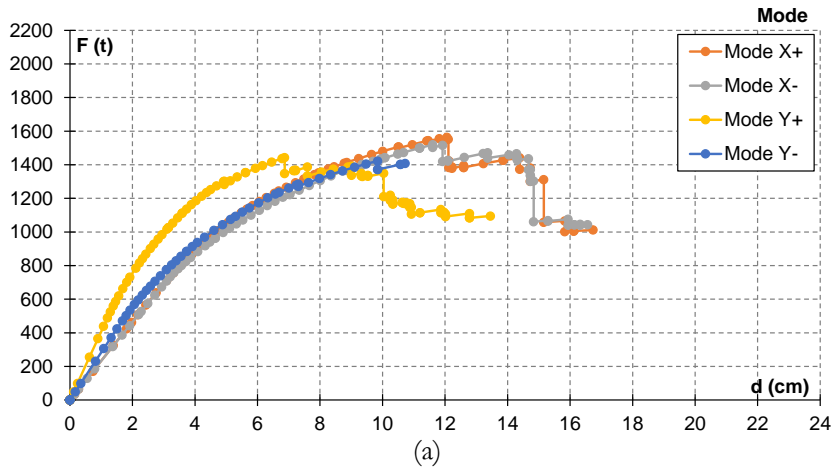
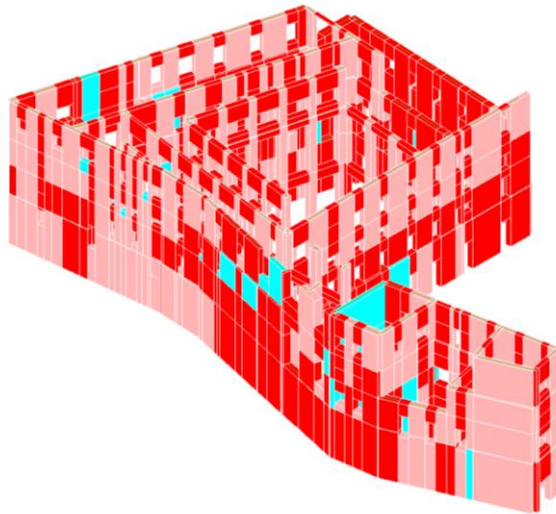


Figure 7.28. *Construction 7* – Distribution of forces proportional to the first vibration mode: capacity curves in terms of (a) forces vs displacements; (b) Forces divided by weight vs displacements divided by total height of the structure.

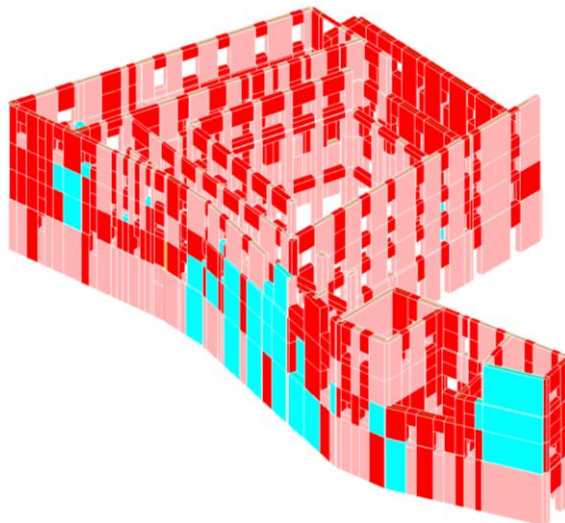
Failure mechanisms
Mass X+



█ Elastic █ M █ V █ N

(a)

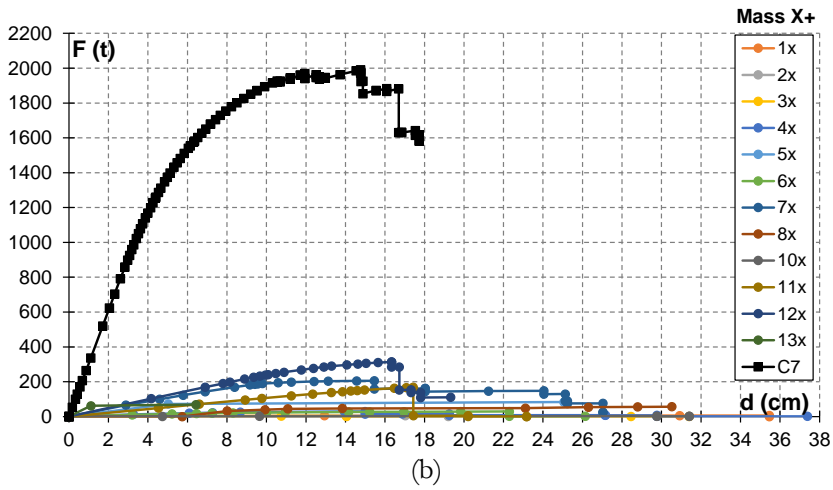
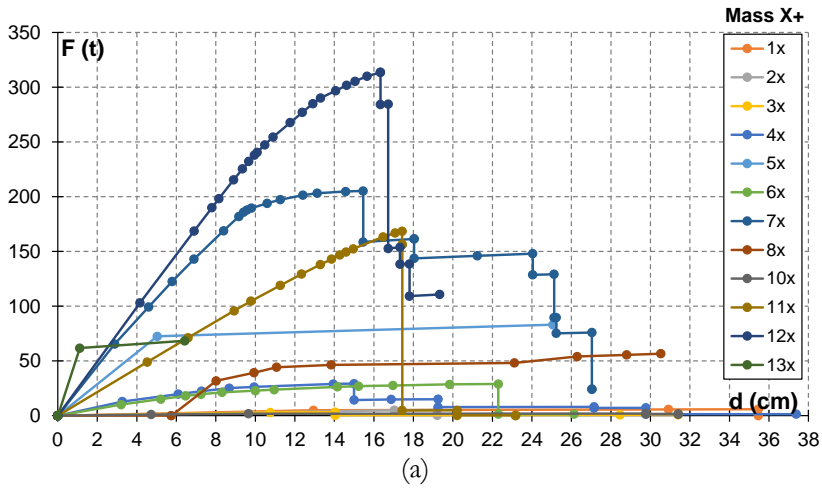
Mass Y+



█ Elastic █ M █ V █ N

Figure 7.29. *Construction 7* – Failure Mechanism in (a) x and (b) y direction.

2D walls analysis



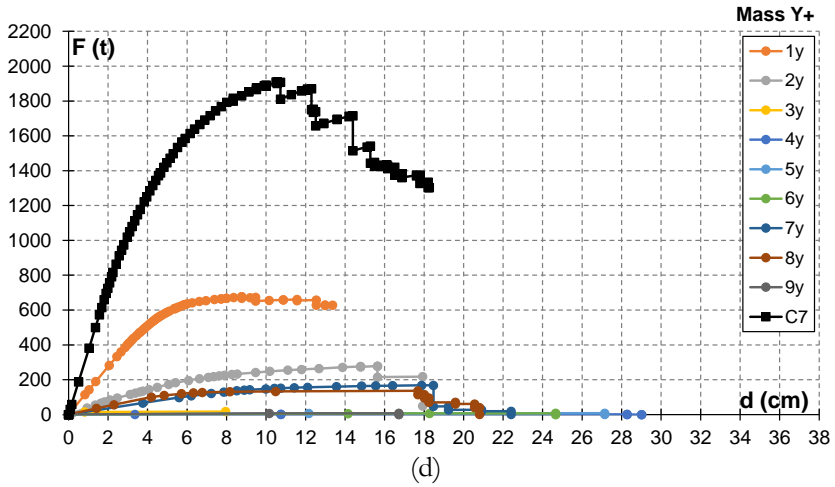
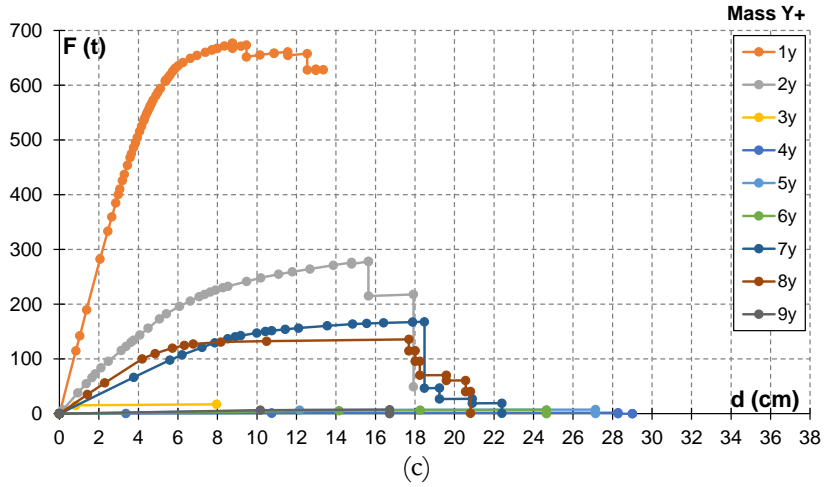
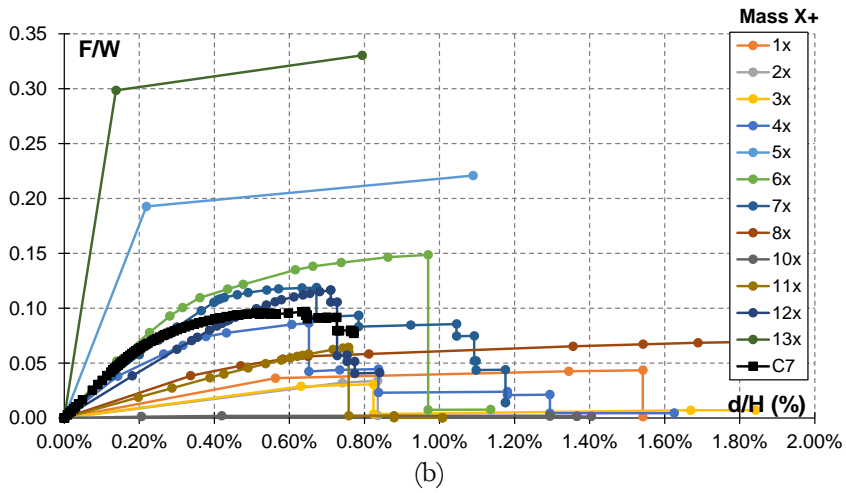
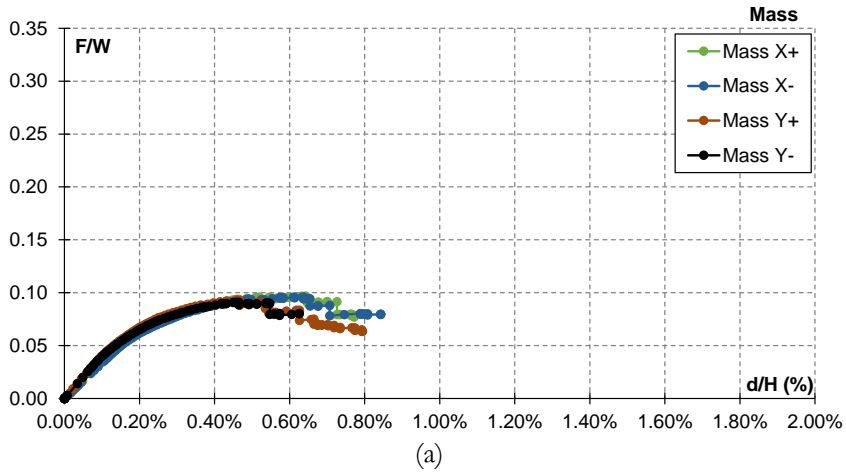


Figure 7.30. *Construction 7* – Capacity curves in terms of forces vs displacements of (a) 2D walls in x direction; (b) comparison between capacity curve of 2D walls and 3D structure in x direction. Capacity curves in terms of forces vs displacements of (c) 2D walls in y direction; (d) comparison between capacity curve of 2D walls and 3D structure in y direction.



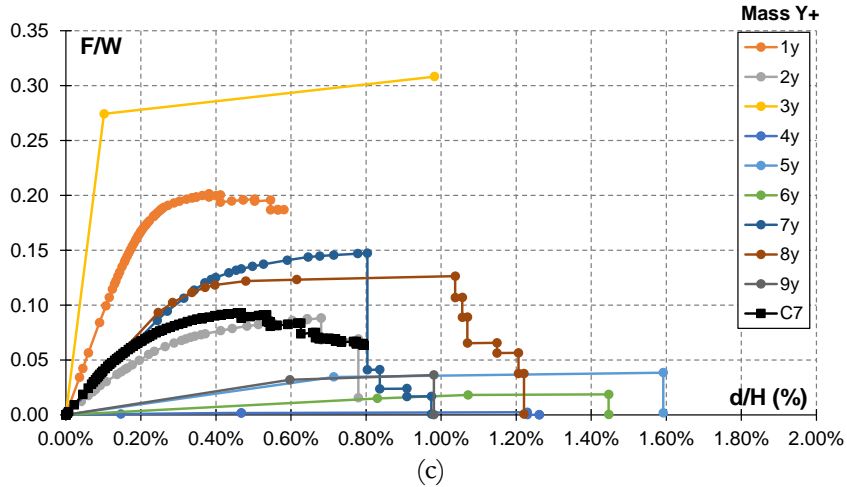


Figure 7.31. *Construction 7* – Capacity curves in terms of Forces divided by weight vs displacements divided by total height of the structure of (a) 3D structure; (b) 2D walls; (c) comparison between capacity curve of 2D walls and 3D structure.

7.2 Non-linear Static Analysis of entire Convent

According to the hypothesis of perfect interaction between the constructions, the analyses have been carried out considering all the constructions as a single structure.

In Figures 7.33-34, the capacity curves of the convent are given.

For the load pattern of forces proportional to the masses of the structure, the pushover curves exhibit maximum base shears of 3506 t and 3324 t and ultimate displacements of 15 cm and 11.79 cm, respectively in x and y direction (Figure 7.33a); in terms of percentage of weight, they show maximum values of 7.6% and 7.2% and in terms of displacement expressed as a percentage of height of the structure 0.7%H and 0.5%H, in x and y direction respectively (Figure 7.33b).

For the load pattern of forces proportional to the first vibration mode of the structure, the pushover curves exhibit maximum base shears of 2189 t and 1236 t and ultimate displacements of 14.90 cm and 5.85 cm, respectively in x and y direction (Figure 7.34a); in terms of percentage of weight, they show maximum values of 4.7% and 2.7% and in terms of

displacement expressed as a percentage of height of the structure $0.7\%H$ and $0.33\%H$, in x and y direction respectively (Figure 7.34b).

Table 7.3 and Table 7.4 provide the maximum values of force and displacement and of the ratio F/W and the ratio d/H in x and y direction for the two considered load patterns.

Table 7.3. *Distribution of forces proportional to the masses*: Maximum values of forces and displacement and of F/W and d/H ratios in x and y direction.

Construction	Direction	F_{\max}	d_{\max}	$(F/W)_{\max}$	$(d/H)_{\max}$
[-]	[-]	[t]	[cm]	[%]	[%]
C0-1-2-6-7	x direction	3506.34	15.00	7.6%	0.7%
	y direction	3324.16	11.79	7.2%	0.5%

Table 7.4. *Distribution of forces proportional to the masses*: Maximum values of forces and displacement and of F/W and d/H ratios in x and y direction.

Construction	Direction	F_{\max}	d_{\max}	$(F/W)_{\max}$	$(d/H)_{\max}$
[-]	[-]	[t]	[cm]	[%]	[%]
C0-1-2-6-7	x direction	2189.55	14.90	4.7%	0.7%
	y direction	1235.73	5.85	2.7%	0.3%

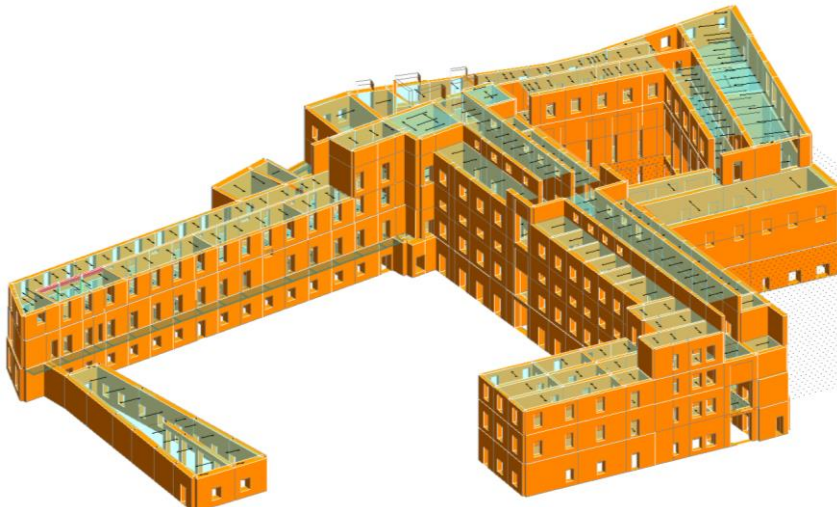


Figure 7.32. Structural model of the Constructions C0-1-2-6-7.

CONSTRUCTIONS 0-1-2-6-7

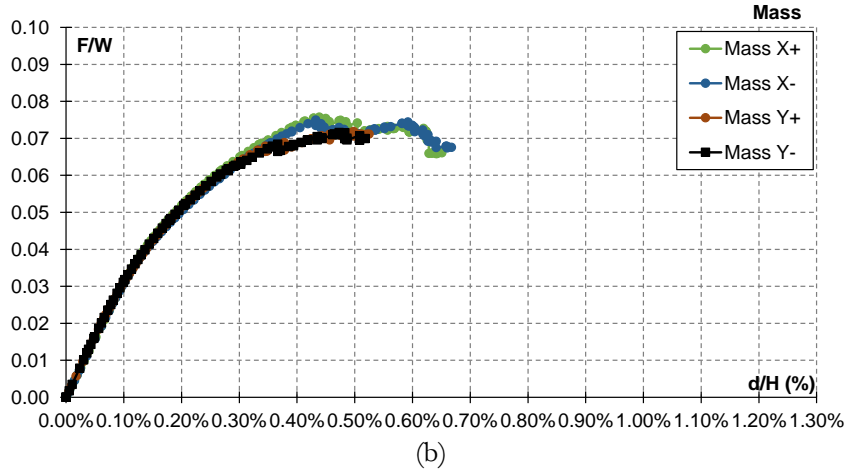
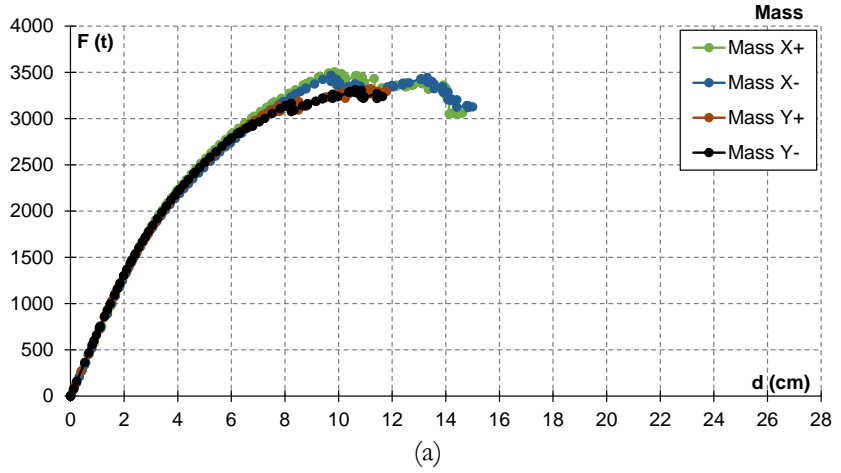


Figure 7.33. *Constructions 0-1-2-6-7* – Distribution of forces proportional to masses: capacity curves in terms of (a) forces vs displacements; (b) Forces divided by weight vs displacements divided by total height of the structure.

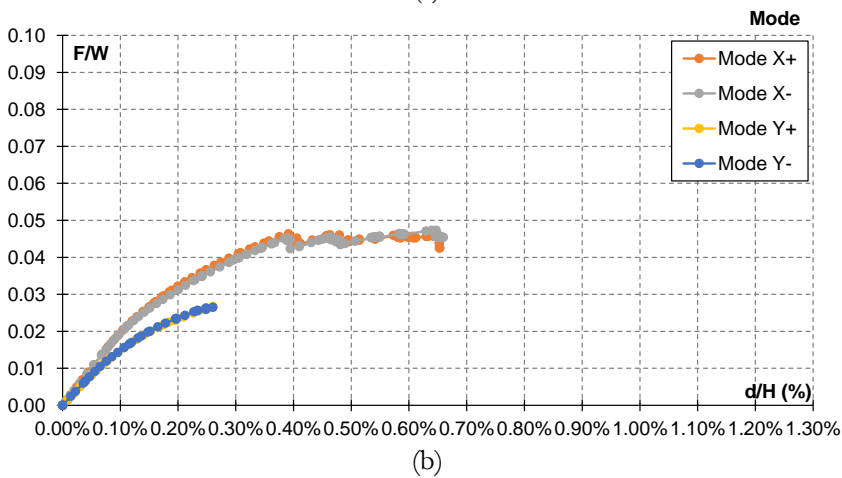
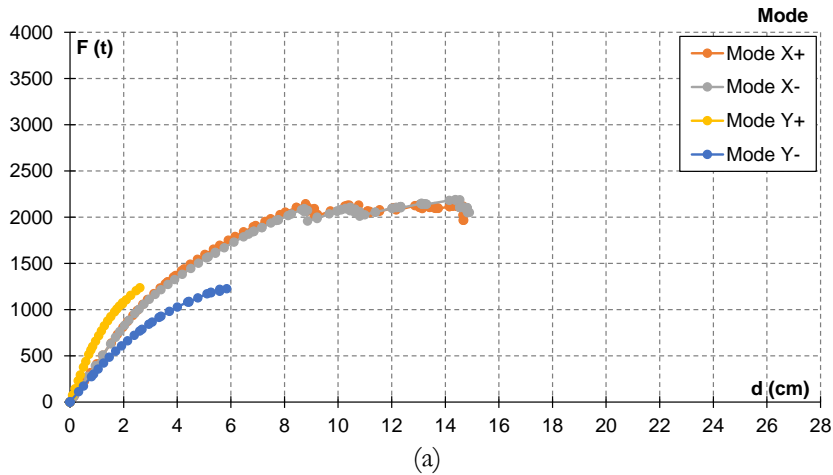
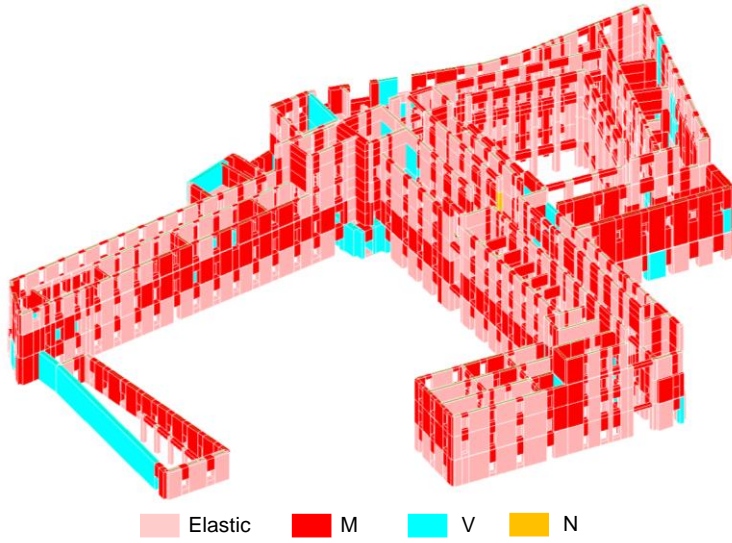


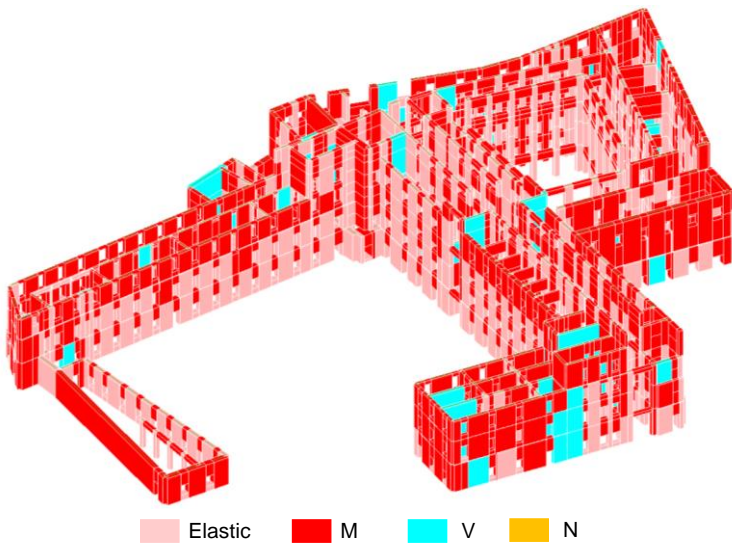
Figure 7.34. *Constructions 0-1-2-6-7* – Distribution of forces proportional to the first vibration mode: capacity curves in terms of (a) forces vs displacements; (b) Forces divided by weight vs displacements divided by total height of the structure.

Figure 7.35 illustrates the failure mechanisms which led the collapse of the structure in the two orthogonal directions. The results are shown for the distribution of forces proportional to the masses. The Figures reveal flexural failure of the piers and spandrels, with occasional instances of shear failure of the piers.

CONSTRUCTIONS 0-1-2-6-7
Mass X+



(a)
Mass Y+



(b)

Figure 7.35. *Construction 0-1-2-6-7*: Failure Mechanism in (a) x and (b) y direction.

7.3 Comparison between the single Construction and the entire Convent

This Section provides a comparison between the capacity curves of each construction and of the entire convent. To make the comparison between the constructions more clear, the capacity curves are shown considering the reference system of the C0-1-2-6-7, coinciding with the reference system of the Construction 0. For the location of the reference systems of each construction refer to **Appendix 2**.

The following considerations can be made.

When considering the *distribution of forces proportional to the masses* (Figure 7.36-37):

- In x direction, construction C0-1-2-6-7 displays an ultimate displacement that falls between the ultimate displacements of each construction. Moreover, its maximum F/w ratio is quite coincident with the maximum F/w ratio of C0.
- In y direction, construction C0-1-2-6-7 shows an ultimate displacement that is intermediate among the ultimate displacements of each construction, with a maximum F/w ratio falling between the maximum F/w ratios of C0 and C7.

When considering the *distribution of force proportional to the first vibration mode of the structure* (Figure 7.38-39):

- In x direction, C0-1-2-6-7 exhibits an ultimate displacement similar to the ultimate displacement of C7. Additionally, its maximum F/w ratio aligns closely with the maximum value of C0.
- In y direction, C0-1-2-6-7 is characterized by an ultimate displacement and a maximum base shear value that are notably lower than those of the other constructions. Regarding the F/w ratio, it reaches a maximum value similar to that of C0.

Distribution of forces proportional to the masses
x direction

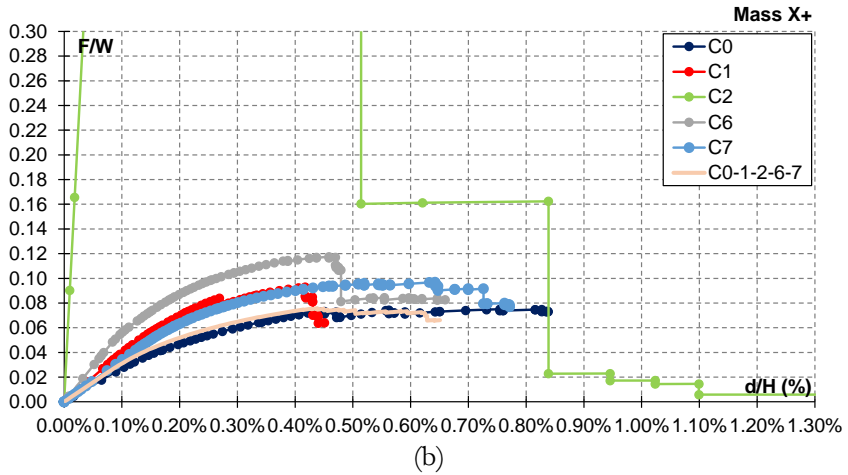
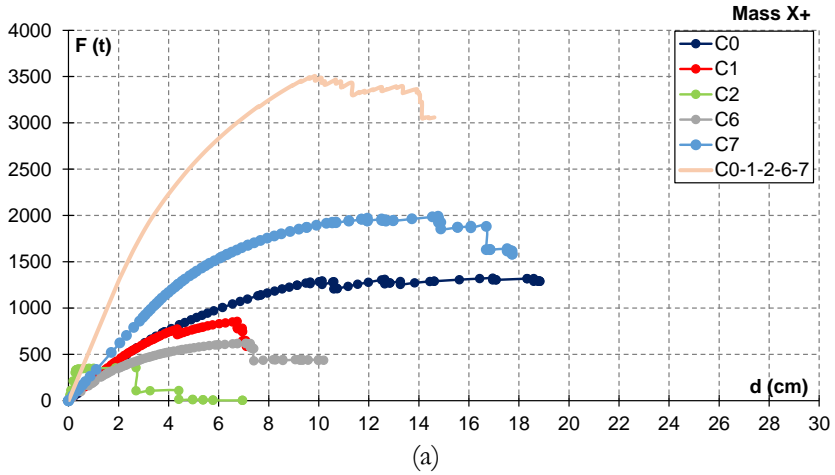


Figure 7.36. *Mass (x direction)*. Comparison between capacity curve of single construction and the entire convent in terms of (a) forces vs displacements; (b) Forces divided by weight vs displacements divided by total height of the structure.

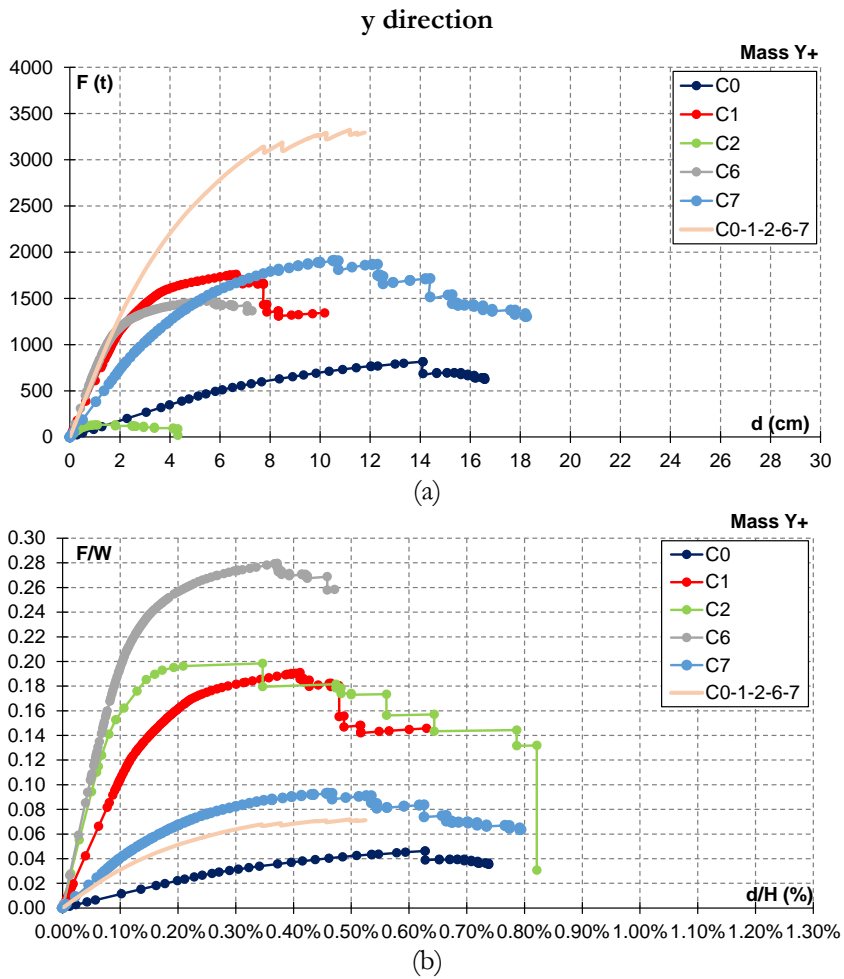


Figure 7.37. *Mass (y direction)*. Comparison between capacity curve of single construction and the entire convent in terms of (a) forces vs displacements; (b) Forces divided by weight vs displacements divided by total height of the structure.

Distribution of forces proportional to the first vibration mode
x direction

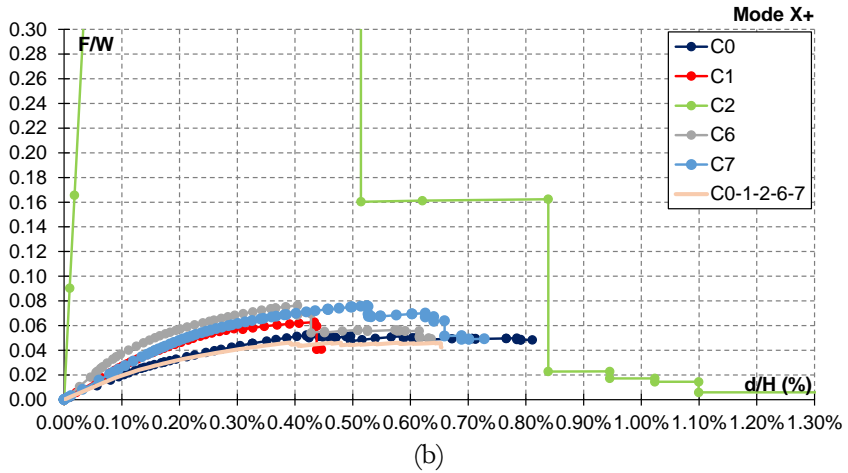
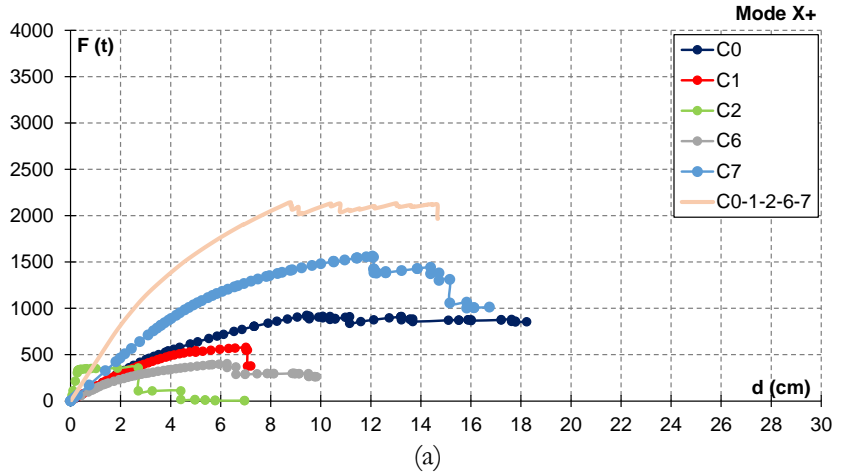


Figure 7.38. Mode (x direction). Comparison between capacity curve of single construction and the entire convent in terms of (a) forces vs displacements; (b) Forces divided by weight vs displacements divided by total height of the structure.

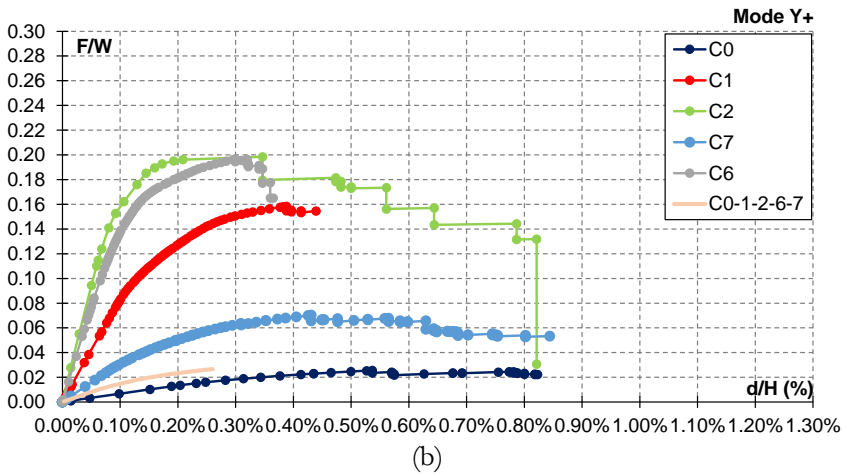
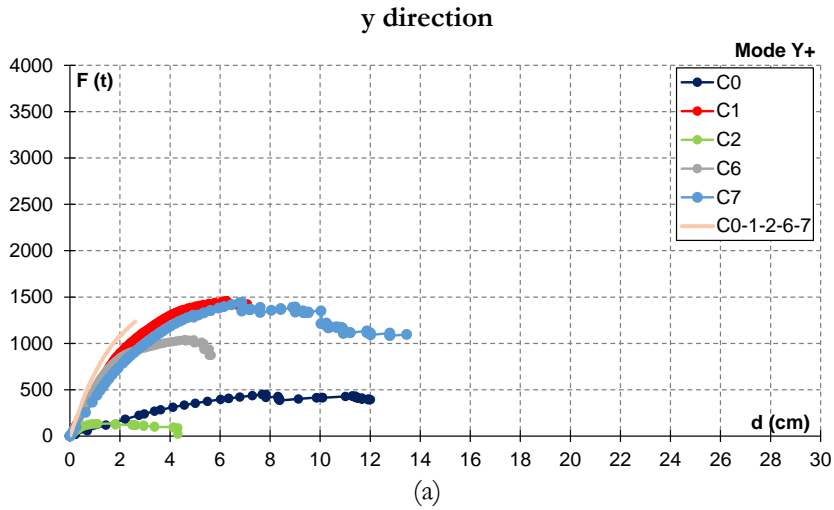


Figure 7.39. *Mode (y direction)*. Comparison between capacity curve of single construction and the entire convent in terms of (a) forces vs displacements; (b) Forces divided by weight vs displacements divided by total height of the structure.

Chapter 8

Seismic vulnerability assessment of St. Domenico Convent

This Chapter deals with the seismic vulnerability assessment of the Saint Domenico Convent in Naples. As outlined in previous Chapters, given the complexity of the Convent and to gain a deeper understanding of the structural behaviour, nonlinear static analysis was carried out for the single constructions, by neglecting the interaction with the others, and for the entire convent, assuming a perfect interaction among them. The assessment of seismic vulnerability employed the N2 method by Fajfar (1999), in accordance with the current Italian Building Code NTC 18. In this Chapter, the results in terms of Seismic Vulnerability Indexes for the analysed constructions are provided. Following a historical overview of the N2 method and a brief theoretical description of the method, the application of the method is shown graphically and the seismic vulnerability indexes for the two limit hypotheses, i.e. individual construction and the entire convent, are provided. The Chapter concludes with a comparative analysis of the seismic vulnerability indexes for both the single constructions and the entire convent.

8.1 The N2 method: historical overview and procedure

The N2 method is a nonlinear pushover-based procedure, implemented in the current Italian Building Code NTC 18. The letter **N** came from

Nonlinear, while the number **2** signifies the utilization of two mathematical models. The origin and development of the N2 method has been comprehensively documented in a recent book by Fajfar (2021) [48]. Its roots can be traced back to the mid-1980s with publications by Fajfar and Fischinger in 1987 [49] and 1989 [50]. The idea came from the Q model proposed by Saïidi and Sozen (1981) [51], in which two types of simplification were involved: “(1) reduction of a MDOF model of a structure to a SDOF oscillator, and (2) approximation of the varying incremental stiffness properties of the entire structure by a single nonlinear spring.” Over time, the method evolved into a more mature version, as presented in the paper by Fajfar and Gaspersic (1996) [52]. In this version, the method was still limited to planar building models, although a simplified pushover analysis of the spatial model had already been developed (Kilar and Fajfar 1997 [53]). In Fajfar et al. 1997 [54] and Fajfar and Gaspersic (1998) [55] the method was extended to bridges. In Fajfar 1999 [56], the N2 method was formulated in the Acceleration – Displacement format (AD). The utilization of this AD format, in which the acceleration is on the vertical axis and the displacement is on the horizontal axis, allows the graphical comparison between the capacity of an SDOF system and the demands of earthquake ground motion on the structure. The spectrum plotted in the AD format was originally called ADRS (Acceleration-Displacement Response Spectrum). In Fajfar 1999, a detailed explanation of the N2 method in the new format and its application to some illustrative examples were provided. This paper, along with a subsequent publication by Fajfar in 2000 [57], stands as key paper of the N2 method when formulated in the AD format. The differences between the two paper are clarified in Fajfar 2021. In this publication, a response to a comment of the reviewers, inquiring about the disparities between the two papers, is provided:

“The basic objective of the paper published in EESD (Fajfar, 1999) was to demonstrate that it is feasible to replace equivalent elastic demand spectra in capacity spectrum method with inelastic demand spectra. In the paper under review, the basic objective is to present the simplest version of the proposed method together with the basic derivations to a broader, more practically oriented audience. Necessarily, there are many similarities between the two papers, but also many differences. In the paper under review, the simplest version of the inelastic demand spectra is used, which does not require any interaction. Each step of the procedure is explained with more details and a summary of the method is presented in a transparent form. The derivations of basic equations are presented.”

In 2001, the N2 method as developed and described in Fajfar 2000 was implemented in the main body of Part 1 of EC8 (EC8-1) [13]. However, the basic version of the N2 method had two important limitations:

1. It was still limited to planar structural models;
2. Due to its basic assumption of vibration in a single mode, a simple pushover-based analysis, like N2 method, cannot properly account for higher mode effects and torsional vibration.

The extension of the applicability of the N2 method to the spatial structural models was introduced in a keynote paper at the 12th ECEE by Fajfar (Fajfar 2002 [58]). This involved replacing the planar model with a spatial one, where two separate analyses with lateral loads applied in only one direction were performed. The results obtained from these two independent analyses, including displacements, storey drifts, joint rotations, and forces, were combined using the SRSS rule.

An extended N2 method, which also considered dynamic torsional effects, was developed in 2005 (Fajfar et al., 2005 [59]). In Kreslin and Fajfar 2011 [60], the N2 method was extended to the structures with a non-negligible influence of higher modes along the height of the building. In particular, this extension was combined with the previously developed extension for torsion in a single procedure (see also Kreslin and Fajfar 2012 [61]).

After providing a historical overview of the N2 method and its evolution over time, a description of the basic N2 method procedure is presented below, according to the comprehensive explanation of the method provided in Fajfar 1999 and Fajfar 2000 and the current Italian Building Code NTC 18.

Step 1. Base shear – displacements relationship by a pushover analysis.

At first, a planar MDOF structural model is considered. According to the Italian Building Code, nonlinear force-displacement relation of the MDOF system is obtained by subjecting the structure to a monotonically increasing pattern of lateral forces, representing the inertial forces proportional to mass and proportional to the first vibration mode, as suggested in NTC 18.

Step 2. Transformation of the force-displacement relationship of the MDOF into that of an equivalent SDOF system.

To compare the capacity of the structure with the seismic demand, determined by using the Response Spectra, an equivalent SDOF system is considered, whose mass, displacement and force are defined as defined in Equations (1), (2) and (3):

$$m^* = \sum m_i \Phi_i \quad (1)$$

$$D^* = \frac{D_t}{\Gamma} \quad (2)$$

$$F^* = \frac{V}{\Gamma} \quad (3)$$

where m_i is the story mass, Φ is the displacement shape, D_t is the time-dependent top displacement, V is the base shear of the MDOF model and Γ is the modal participation factor.

Step 3. Idealization of the force-displacement relationship of the equivalent SDOF system into an elasto-plastic form.

The force-displacement relation of the equivalent SDOF system is idealized into an elasto-plastic form. It is determined with graphical procedure: nonlinear force-displacement curve of the equivalent SDOF system and elasto-plastic curve cross at a force equal to 60 per cent of the yield strength and the areas of the original and idealized curve are approximately equal. The elastic period of the idealized bilinear system T^* can be determined as:

$$T^* = 2\pi \sqrt{\frac{m^* D_y^*}{F_y^*}} \quad (4)$$

where F_y^* and D_y^* are the yield strength and displacement, respectively. Dividing the forces in the force-displacement curve for the equivalent SDOF system, the acceleration-displacement relation is obtained.

Step 4. Definition of the seismic demand.

If the elastic period T^* is greater than T_c , the inelastic displacement demand is equal to the elastic one (refer to § 3.2.3.2.3 of NTC 18).

$$d_{max}^* = d_{e,max}^* = S_{De}(T^*) \quad (5)$$

If T^* is smaller than T_c , it is determined as expressed in the Equation (6).

$$d_{max}^* = \frac{d_{e,max}^*}{q^*} \left[1 + (q^* - 1) \frac{T_c}{T^*} \right] \geq d_{e,max}^* \quad (6)$$

where q^* is the ratio between the elastic inertial force and the yield force of the inelastic system.

$$q^* = \frac{S_e(T^*) m^*}{F_y^*} \quad (7)$$

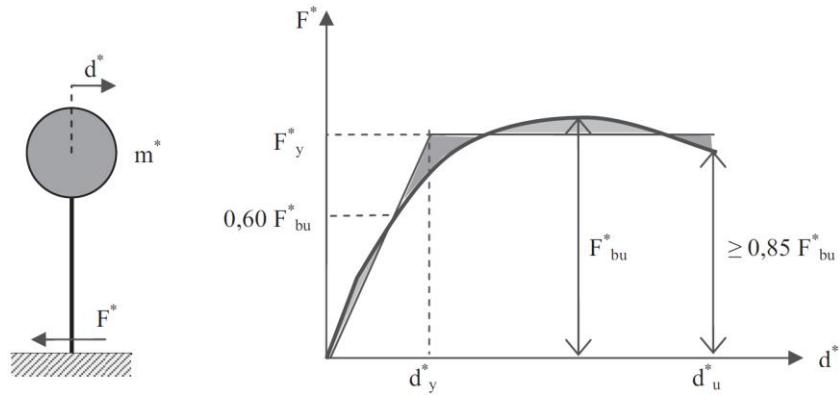


Figure 8.1. Idealization of the force-displacement relationship of the equivalent SDOF system into an elasto – plastic form.

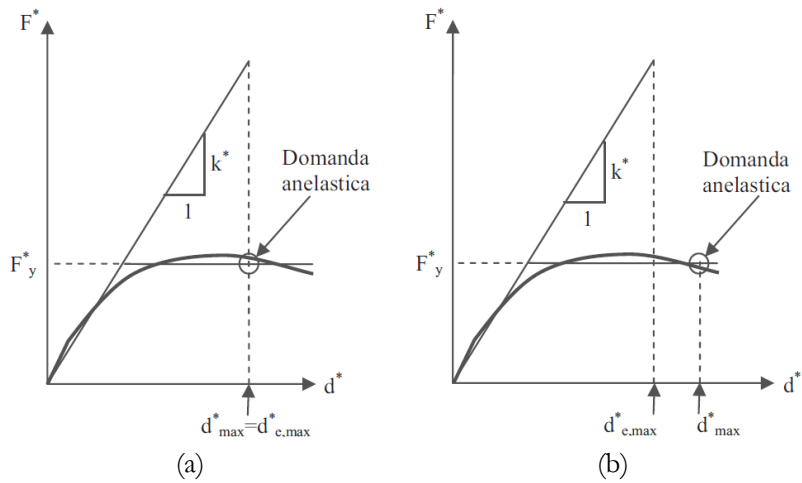


Figure 8.2. Seismic demand for (a) $T^* > T_c$ (a) and (b) $T^* < T_c$.

8.2 Seismic Vulnerability Assessment of the Convent

In this Section, the application of N2 method is shown graphically and the seismic vulnerability indexes ζ_E are provided for the two limit hypotheses: for each construction individually and for the entire convent.

8.2.1 Seismic vulnerability assessment of the single constructions

Figures from 8.3 to 8.8 depict the assessment of demand and capacity in both x and y directions using the Acceleration-Displacement Response Spectrum (ADRS), for cases with the lowest vulnerability indexes. It is worth noting that:

- in the case of *Construction 0* and *Construction 7*, the capacity curves of the equivalent SDOF system in the two orthogonal directions are similar, having similar values in terms of maximum strength and ultimate displacement.
- For *Construction 1*, the capacity curves of the equivalent SDOF system in the two orthogonal directions are characterized by markedly different maximum strength values.
- In the case of *Construction 2*, the ζ_E index defined in terms of accelerations significantly differs from the ζ_E index expressed in terms of displacements. This divergence arises from the fact that the capacity in terms of acceleration can be as high as 0.28g, corresponding to a return period of 2500 years, according to the current Italian Building Code.
- For the *Construction 4*, the capacity curves of the equivalent SDOF system in the two orthogonal directions are significantly different in terms of both maximum strength and ultimate displacement.
- For the *Construction 6*, the capacity curves of the equivalent SDOF system in the two orthogonal directions exhibit notable differences in maximum strength and ultimate displacement.

CONSTRUCTION 0

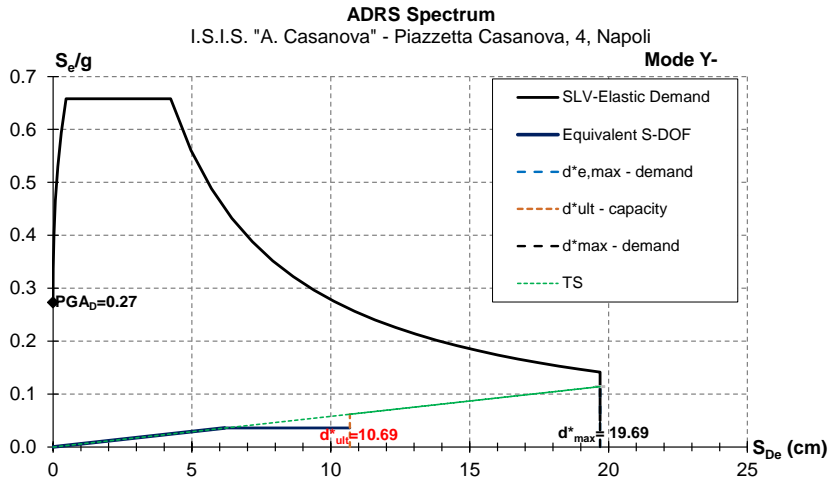
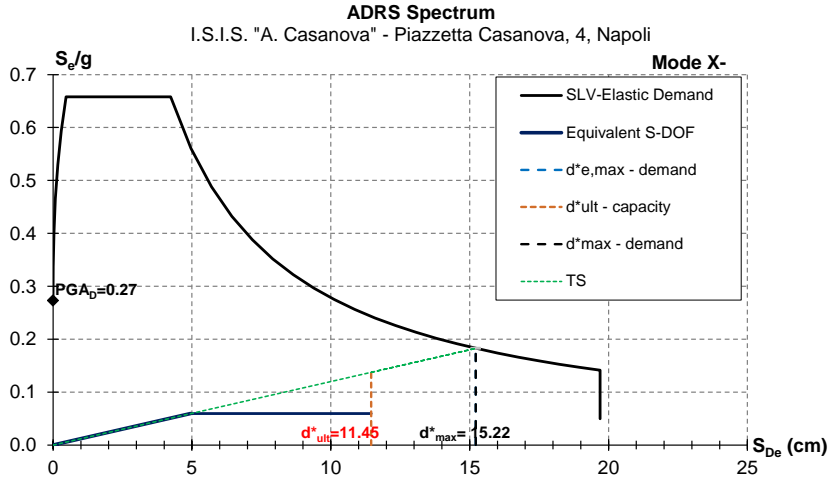


Figure 8.3. *Construction 0*: ADRS Spectrum in (a) x and (b) y direction.

$$\zeta_{E,x} = \frac{11.45}{15.22} = 0.75$$

$$\zeta_{E,y} = \frac{10.69}{19.69} = 0.54$$

CONSTRUCTION 1

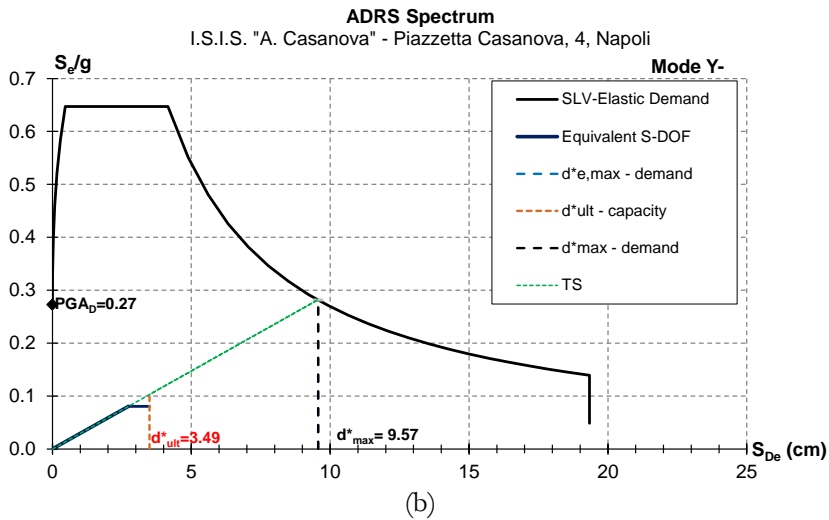
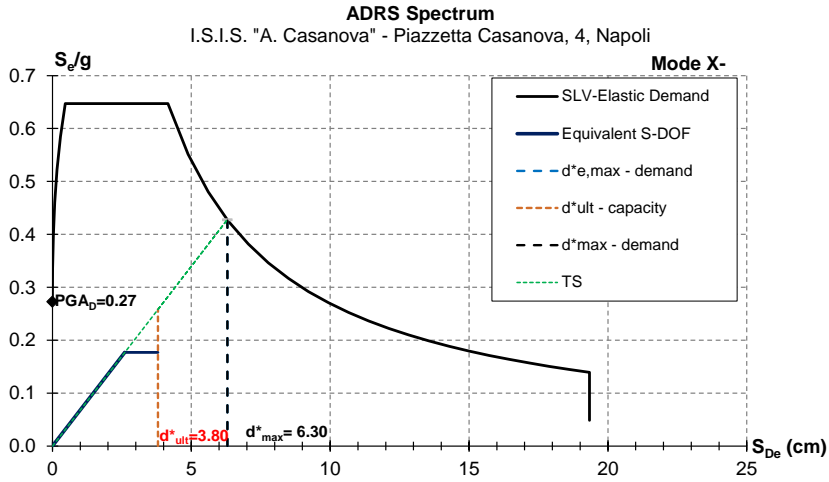


Figure 8.4. *Construction 1*: ADRS Spectrum in (a) x and (b) y direction.

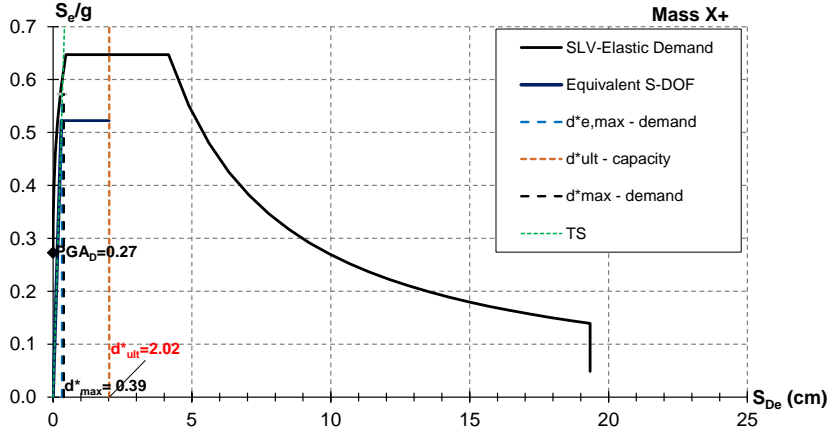
$$\zeta_{E,x} = \frac{3.80}{6.30} = 0.60$$

$$\zeta_{E,y} = \frac{3.49}{9.57} = 0.36$$

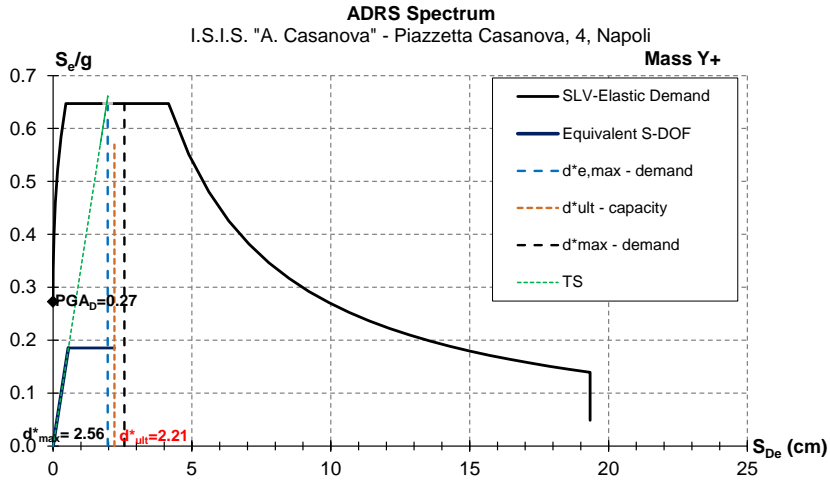
CONSTRUCTION 2

ADRS Spectrum

I.S.I.S. "A. Casanova" - Piazzetta Casanova, 4, Napoli



(a)



(b)

Figure 8.5. Construction 2: ADRS Spectrum in (a) x and (b) y direction.

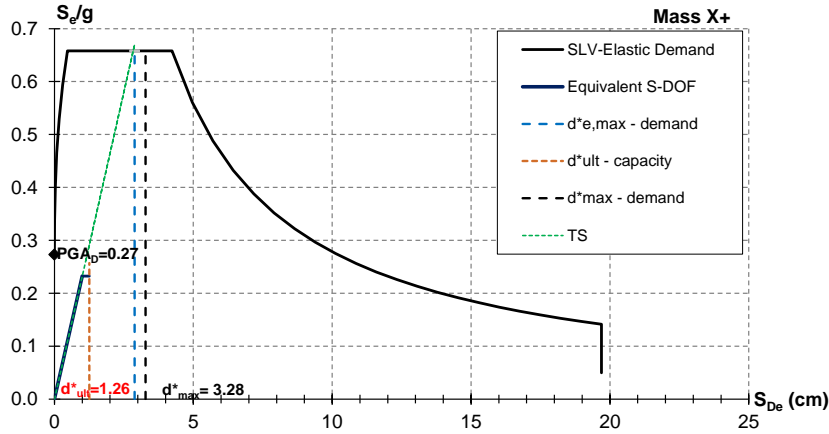
$$\zeta_{E,x} = \frac{2.02}{0.39} = 5.23$$

$$\zeta_{E,y} = \frac{2.21}{2.56} = 0.86$$

CONSTRUCTION 4

ADRS Spectrum

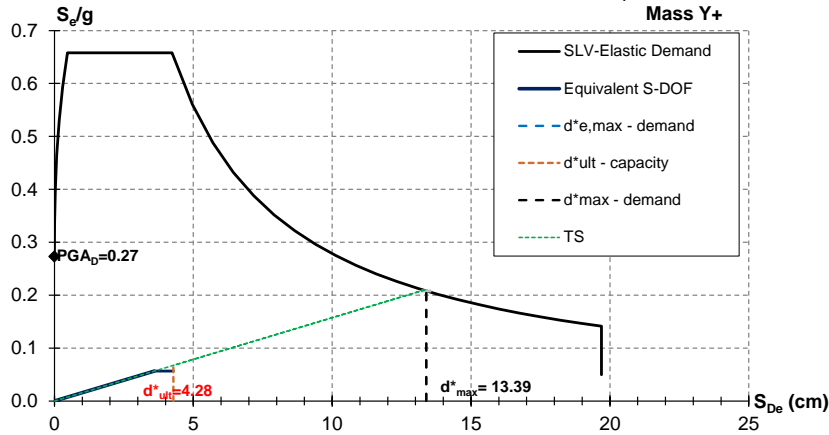
I.S.I.S. "A. Casanova" - Piazzetta Casanova, 4, Napoli



(a)

ADRS Spectrum

I.S.I.S. "A. Casanova" - Piazzetta Casanova, 4, Napoli



(b)

Figure 8.6. Construction 4: ADRS Spectrum in (a) x and (b) y direction.

$$\zeta_{E,x} = \frac{1.26}{3.28} = 0.38$$

$$\zeta_{E,y} = \frac{4.28}{13.39} = 0.32$$

CONSTRUCTION 6

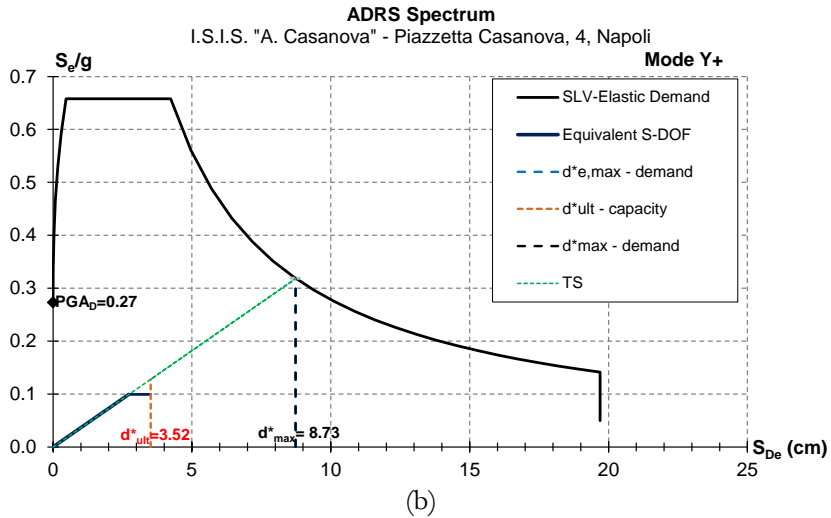
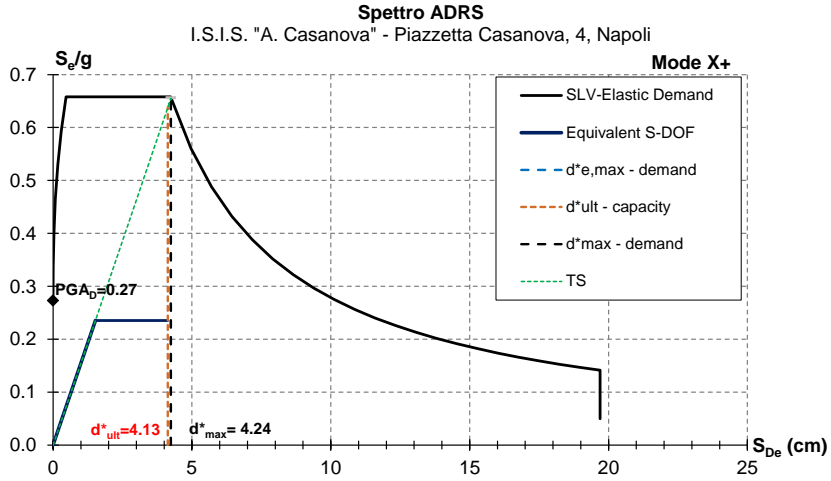


Figure 8.7. *Construction 6*: ADRS Spectrum in (a) x and (b) y direction.

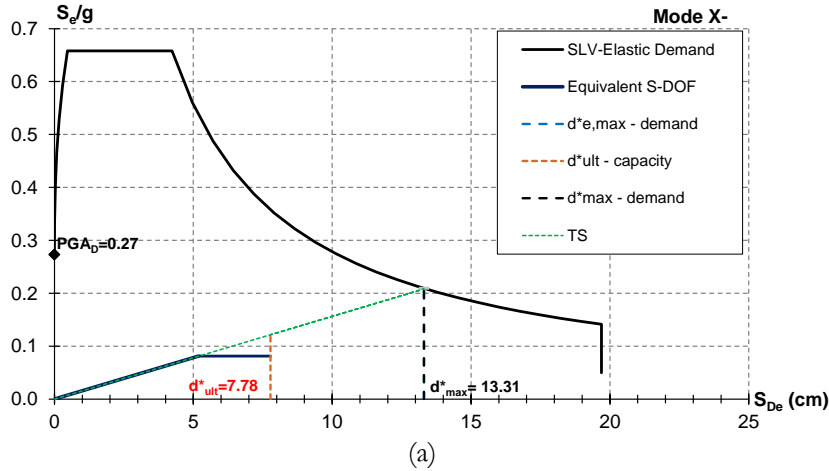
$$\zeta_{E,x} = \frac{4.13}{4.24} = 0.97$$

$$\zeta_{E,y} = \frac{3.52}{8.73} = 0.40$$

CONSTRUCTION 7

ADRS Spectrum

I.S.I.S. "A. Casanova" - Piazzetta Casanova, 4, Napoli



ADRS Spectrum

I.S.I.S. "A. Casanova" - Piazzetta Casanova, 4, Napoli

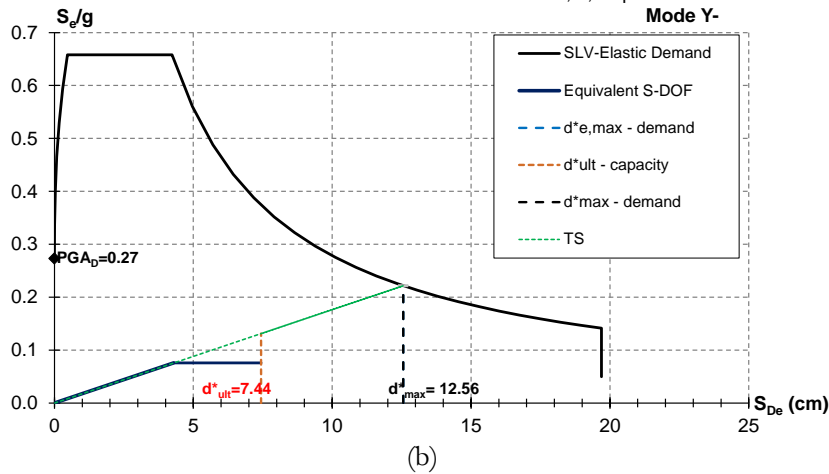


Figure 8.8. Construction 7: ADRS Spectrum in (a) x and (b) y direction.

$$\zeta_{E,x} = \frac{7.78}{13.31} = 0.58$$

$$\zeta_{E,y} = \frac{7.44}{12.56} = 0.59$$

Seismic vulnerability indexes for each construction are visually presented in Figures from 8.9 to 8.14 and summarized in Table 8.1. The results reveal that all constructions exhibit seismic vulnerability values ranging from a minimum lower than 1 to a maximum exceeding 1. The only exception is Construction 4, which shows a maximum value of 0.435. Specifically:

- *Construction 0* displays a minimum value of 0.622 for the distribution of forces proportional to the first vibration mode of the structure in y direction (Mode Y-) and a maximum of 1.135 for the distribution of forces proportional to the masse in x direction (Mass X+).
- *Construction 1* reveals a minimum value of 0.369 for the distribution of forces proportional to the first vibration mode of the structure in y direction (Mode Y-) and a maximum of 1.465 for the distribution of forces proportional to the masse in x direction (Mass X-).
- *Construction 2* exhibits a minimum value of 0.855 in y direction (Mode Y+ and Mass Y+) and a maximum of 1.465 in x direction (Mode X+, Mode X+ and Mass X+ and Mass X-).
- *Construction 4* demonstrates a minimum value of 0.333 in y direction (Mode Y+ and Mass Y+) and a maximum of 0.435 in x direction (Mode X- and Mass X-).
- *Construction 6* displays a minimum value of 0.409 for the distribution of forces proportional to the first vibration mode of the structure in y direction (Mode Y+) and a maximum of 1.465 for the distribution of forces proportional to the masse in x direction (Mass X+ and Mass X-).
- *Construction 7* reveals a minimum value of 0.585 for the distribution of forces proportional to the first vibration mode of the structure in x direction (Mode X-) and a maximum of 1.360 for the distribution of forces proportional to the masse in x direction (Mass X-).

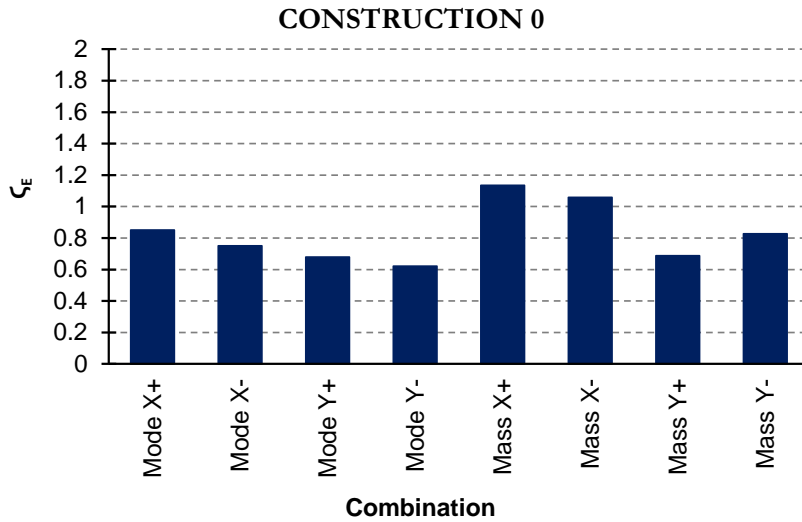


Figure 8.9. *Construction 0*: Seismic Vulnerability Indexes.

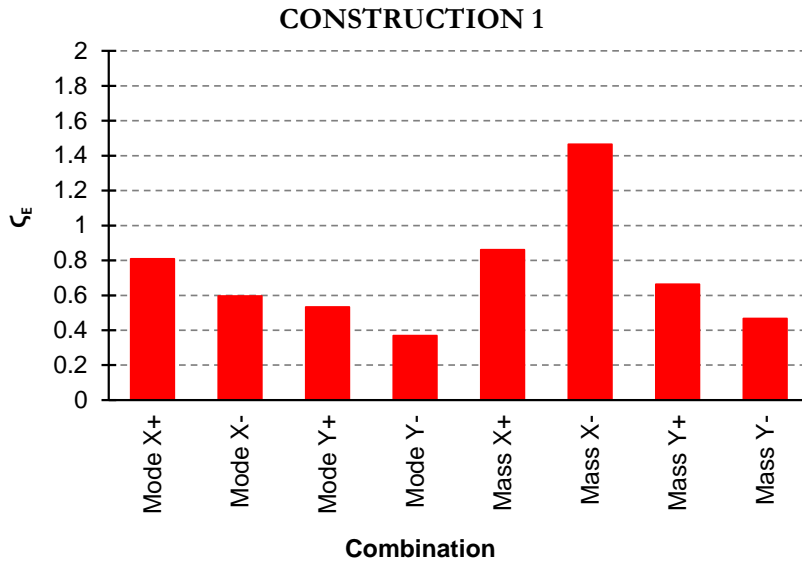


Figure 8.10. *Construction 1*: Seismic Vulnerability Indexes.

CONSTRUCTION 2

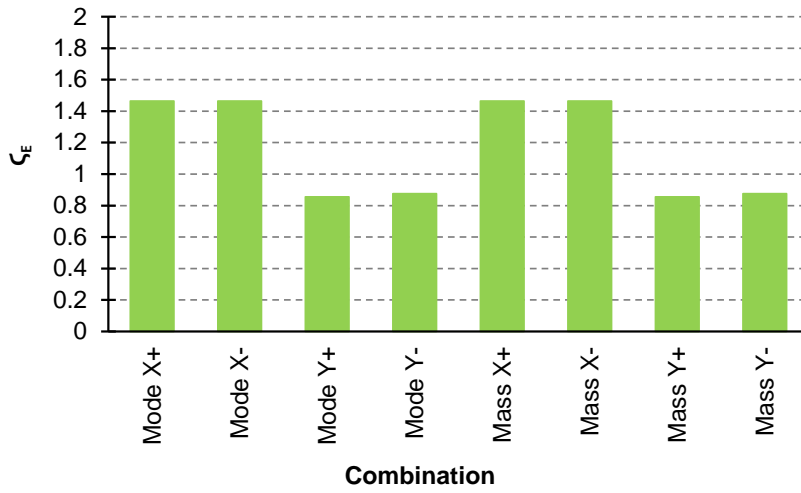


Figure 8.11. *Construction 2*: Seismic Vulnerability Indexes.

CONSTRUCTION 4

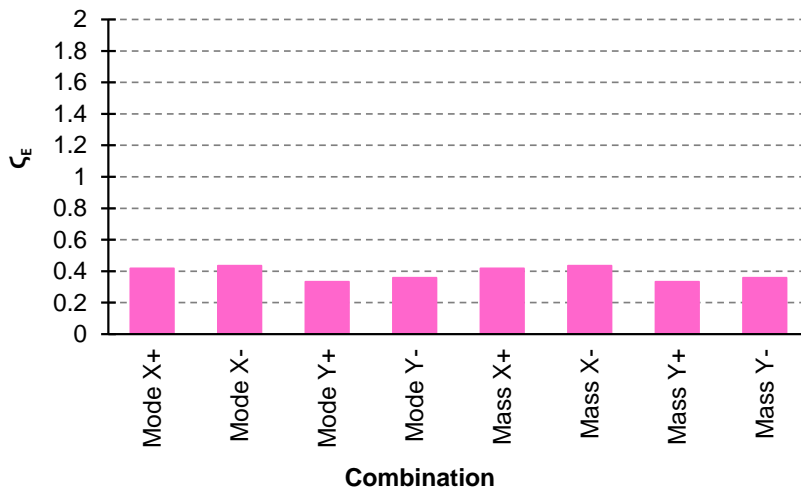


Figure 8.12. *Construction 4*: Seismic Vulnerability Indexes.

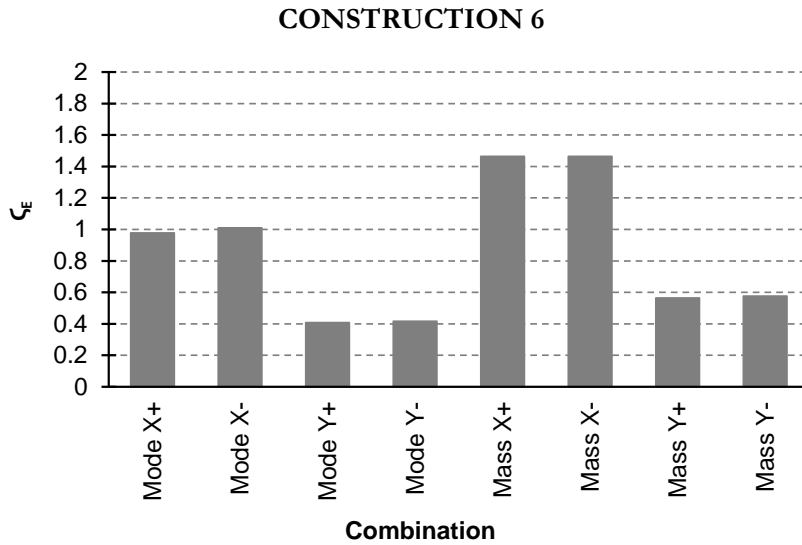


Figure 8.13. *Construction 6*: Seismic Vulnerability Indexes.

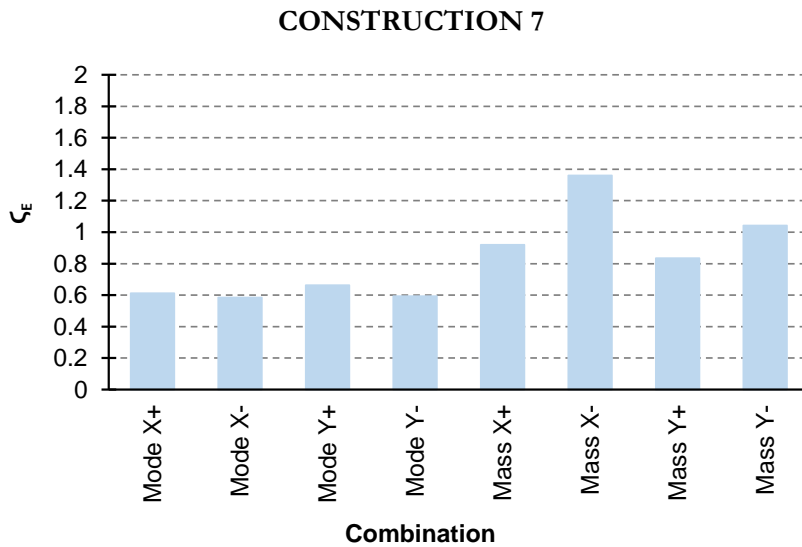


Figure 8.14. *Construction 7*: Seismic Vulnerability Indexes.

Table 8.1. Seismic Vulnerability Indexes of single constructions.

Combination	ζ_E					
	C0	C1	C2	C4	C6	C7
1 Mode X+	0.851	0.81	1.465	0.419	0.978	0.613
2 Mode X-	0.751	0.596	1.465	0.435	1.01	0.585
3 Mode Y+	0.68	0.534	0.855	0.333	0.409	0.664
4 Mode Y-	0.622	0.369	0.876	0.358	0.416	0.594
5 Mass X+	1.135	0.861	1.465	0.419	1.465	0.92
6 Mass X-	1.059	1.465	1.465	0.435	1.465	1.36
7 Mass Y+	0.687	0.664	0.855	0.333	0.565	0.836
8 Mass Y-	0.828	0.468	0.876	0.358	0.576	1.043
Max	1.135	1.465	1.465	0.435	1.465	1.360
Min	0.622	0.369	0.855	0.333	0.409	0.585

8.2.2 Seismic vulnerability assessment of the entire convent

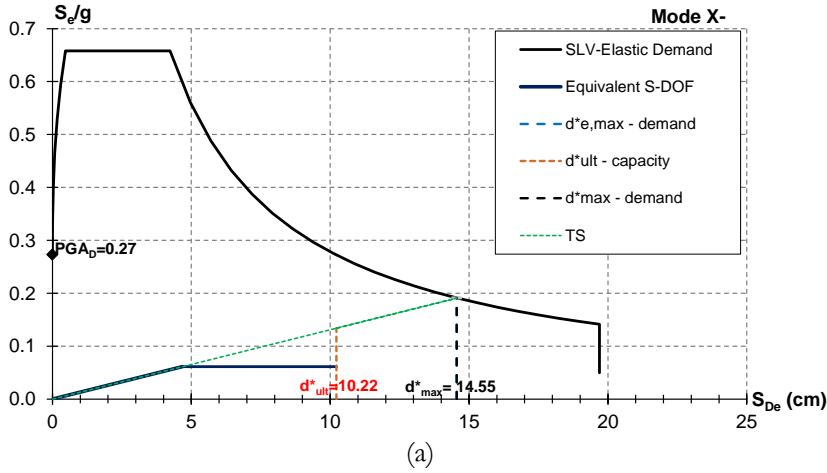
Figure 8.15 depicts the assessment of demand and capacity in both x and y directions using the Acceleration-Displacement Response Spectrum (ADRS), for cases with the lowest vulnerability indexes. It is worth noting that for *Constructions 0-1-2-6-7*, the capacity curves of the equivalent SDOF system in the two orthogonal directions display significant disparities, particularly in terms of ultimate displacement.

Seismic vulnerability indexes for each construction are visually presented in Figure 8.16 and summarized in Table 8.2. The results reveal that for the entire convent (referred to as C0-1-2-6-7), the seismic vulnerability indexes range from a minimum value of 0.254 obtained with a distribution of forces proportional to the first vibration mode of the structure in y direction (Mode Y+ and Mode Y-) to a maximum value of 0.938 obtained with a distribution of forces proportional to the masses in x direction (Mass X-). It should be noted that vulnerability indexes in the y direction, with a force distribution proportional to the first vibration mode (Mode Y+ and Mode Y-) are significantly lower than the values in the orthogonal direction and the values obtained with a force distribution proportional to the masses.

CONSTRUCTIONS 0-1-2-6-7

ADRS Spectrum

I.S.I.S. "A. Casanova" - Piazzetta Casanova, 4, Napoli



ADRS Spectrum

I.S.I.S. "A. Casanova" - Piazzetta Casanova, 4, Napoli

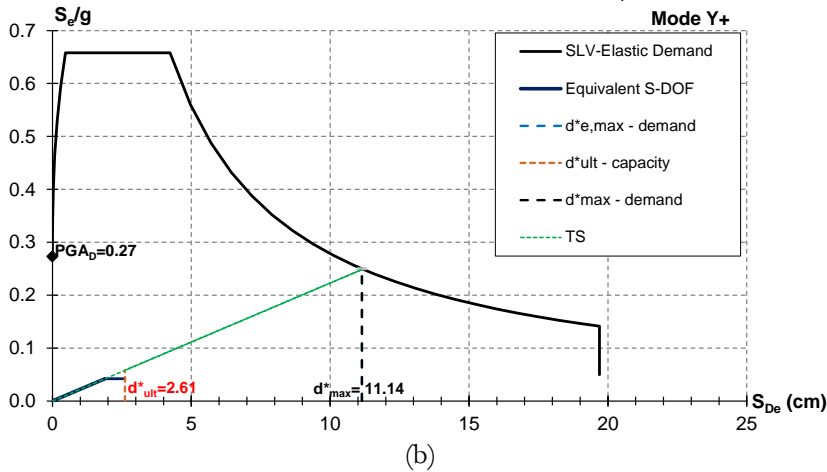


Figure 8.15. *Construction 7*: ADRS Spectrum in (a) x and (b) y direction.

$$\zeta_{E,x} = \frac{10.22}{14.55} = 0.70$$

$$\zeta_{E,y} = \frac{2.61}{11.14} = 0.24$$

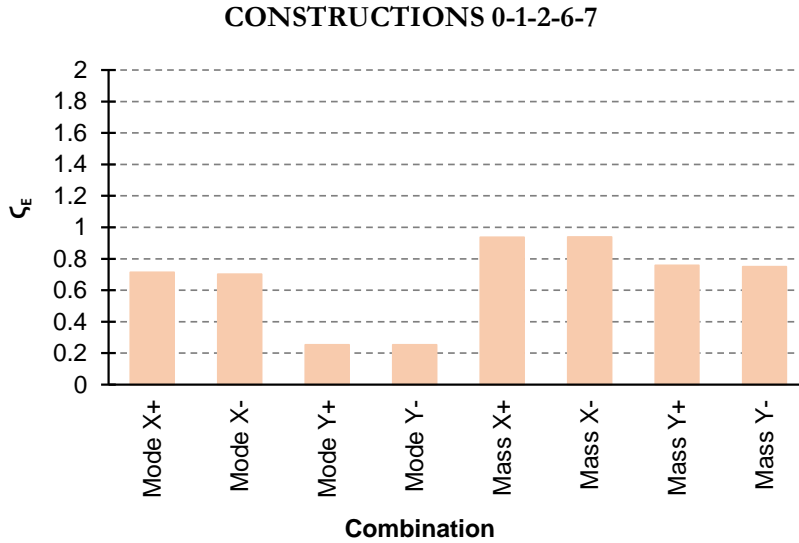


Figure 8.16. *Constructions 0-1-2-6-7*: Seismic Vulnerability Indexes.

Table 8.2. Seismic Vulnerability Indexes of Construction C0-1-2-6-7.

Combination		S_E
		C0-1-2-6-7
1	Mode X+	0.715
2	Mode X-	0.702
3	Mode Y+	0.254
4	Mode Y-	0.254
5	Mass X+	0.937
6	Mass X-	0.938
7	Mass Y+	0.759
8	Mass Y-	0.75
Max		0.938
Min		0.254

8.3 Comparison of the results

In this Section, a comparative analysis of the results in terms of seismic vulnerability indexes is presented. To make the comparison between the constructions more clear, the seismic vulnerability indexes are rewritten considering the reference system of the C0-1-2-6-7, coinciding with the reference system of the Construction 0. For the location of the reference systems of each construction refer to **Appendix 2**. Figure 8.17 illustrates the seismic vulnerability indexes of the single constructions and of the entire convent (C0-1-2-6-7) in the two orthogonal directions, considering both the distribution of forces proportional to the masses and the distribution of forces proportional to the first vibration mode of the structure. This comparison is summarized in Table 8.3. The results reveal that all the single constructions exhibit seismic vulnerability values ranging from a minimum lower than 1 to a maximum exceeding 1. The only exception is Construction 4, which shows a maximum value of 0.435. For C0-1-2-6-7 they range from a minimum of 0.254 to a maximum of 0.938.

It is noteworthy that in the x direction (Figure 8.18), the seismic vulnerability indexes of C0-1-2-6-7 fall within the range defined by the minimum and maximum values of the seismic vulnerability indexes of the individual constructions. This observation holds true for both the distribution of forces proportional to the masses and the distribution proportional to the first vibration mode of the structure. In contrast, in the y direction (Figure 8.19), the seismic vulnerability indexes of C0-1-2-6-7 are significantly lower compared to the seismic vulnerability indexes of the single constructions, particularly when considering the distribution of forces proportional to the first vibration mode of the structure. A detailed explanation of this outcome will be provided in the subsequent Chapter.

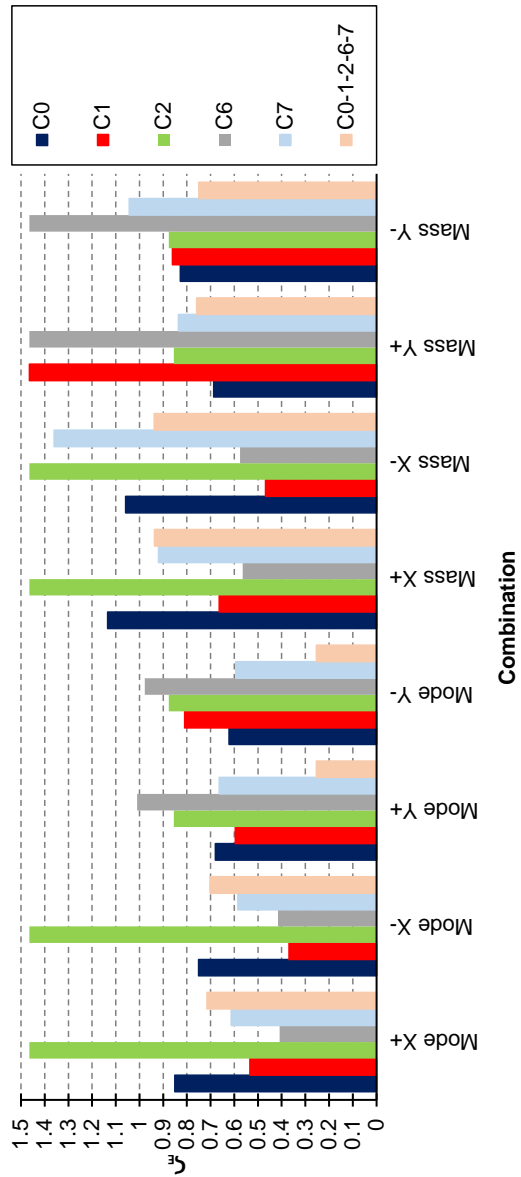


Figure 8.17. Comparison between Seismic Vulnerability Indexes of the single construction and the entire convent.

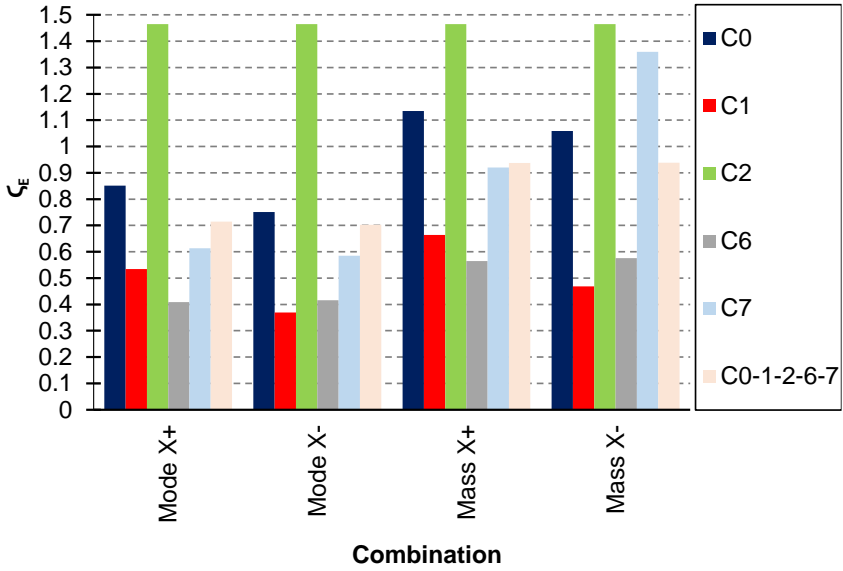


Figure 8.18. Comparison between Seismic Vulnerability Indexes of the single construction and the entire convent: x direction.

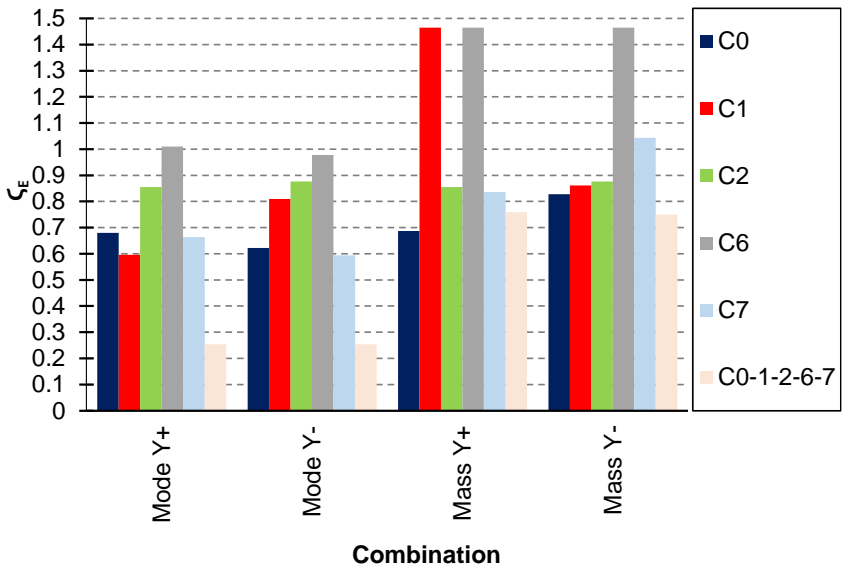


Figure 8.19. Comparison between Seismic Vulnerability Indexes of the single construction and the entire convent: y direction.

Table 8.3. Comparison between Seismic Vulnerability Indexes of the single construction and the entire convent.

Combination	ζ_E						
	C0	C1	C2	C4	C6	C7	C0-1-2-6-7
1 Mode X+	0.851	0.534	1.465	0.613	0.409	0.851	0.715
2 Mode X-	0.751	0.369	1.465	0.585	0.416	0.751	0.702
3 Mode Y+	0.68	0.596	0.855	0.664	1.01	0.68	0.254
4 Mode Y-	0.622	0.81	0.876	0.594	0.978	0.622	0.254
5 Mass X+	1.135	0.664	1.465	0.92	0.565	1.135	0.937
6 Mass X-	1.059	0.468	1.465	1.36	0.576	1.059	0.938
7 Mass Y+	0.687	1.465	0.855	0.836	1.465	0.687	0.759
8 Mass Y-	0.828	0.861	0.876	1.043	1.465	0.828	0.75
Max	1.135	1.465	1.465	0.435	1.465	1.360	0.938
Min	0.622	0.369	0.855	0.333	0.409	0.585	0.254

Chapter 9

Discussion

In this dissertation the structural analysis of complex monumental buildings has been carried out, through the case study of the Saint Domenico Convent in Naples. The Convent Case Study consists of eight constructions, built in different periods, ranging from the 8th to the 17th century, each characterized by different features in terms of structural typology. This Chapter aims to discuss the results presented in this dissertation. First and foremost, the adopted procedure for the structural analysis of the Convent is outlined. Given the complexity of the construction, this procedure includes the nonlinear static analysis of the single Construction, by neglecting the interaction with the others, the nonlinear static analysis of the entire Convent, assuming a perfect interaction among them, and nonlinear static analysis of 2D walls to gain a deeper understanding of the structural behaviour. To check the results obtained with nonlinear static analysis through the SAM method, a comparison with the outcomes obtained from a simplified formula proposed by the research group in the framework of limit analysis is also conducted and explored.

To validate the proposed procedure it has been applied to the Case Study of Saint Carlo all'Arena Convent, as presented in **Appendix 3**.

Subsequently, the impact of adding structural portions to existing ones is assessed in terms of capacity curves and seismic vulnerability indexes. The results reveal that for irregular buildings, both in terms of plan and height, the structural analysis of single Constructions and the entire building is crucial, as irregularities significantly influence the outcomes of the seismic vulnerability assessment.

Finally, a proposal of definition of complex monumental buildings and their typical complexities is formulated. This proposal derives from the analysis of the Saint Domenico Convent and Saint Carlo all'Arena Convent.

9.1 The procedure adopted for the seismic vulnerability assessment

In this dissertation, the Saint Domenico Maggiore Convent in Naples has been analysed, as seminal case of complex monumental building, defined in Sorrentino et al. (2022) [62]. The convent case study consists of eight constructions, built in different periods, from the 8th to the 17th century, and having different features in terms of structural typology. Due to the complexity of the Convent and to gain a deeper understanding of the structural behaviour, nonlinear static analyses have been carried out by assuming two limit hypotheses. The first hypothesis involves the analysis of the single construction, by neglecting the interaction with the others; the second hypothesis assumes perfect interaction among all the constructions, considering them as a single structure. In addition, 2D walls analyses within each construction have been performed, with the aim to identify the weakest wall alignment that lead to the collapse of the structure and the local crisis.

To check the results obtained with nonlinear static analysis through the SAM method, the analysis of 2D walls has been compared with the results obtained with the simplified formula proposed by the research group in the framework of limit analysis. Being the formula based on Heyman's hypotheses, including the assumption of infinite compressive strength of the material, the analysis has been conducted considering a value of 100 kg/cm².

9.2 The extension of the procedure on the Saint Carlo all'Arena Convent in Naples

To validate and discuss the proposed analysis procedure for complex monumental buildings, which often involve the addition of different constructions over the years, it has been applied to the Saint Carlo all'Arena Convent in Naples. **Appendix 3** provides an in-depth analysis of this convent, including a historical account of its evolution, preliminary considerations regarding its compliance with architectural principles, and the seismic vulnerability assessment.

Figure 9.1 and Figure 9.2 illustrate this second case study, offering an panoramic view and a plan of the convent. Situated in the historical center of Naples, within the San Carlo all’Arena neighbourhood, this masonry building has a rectangular floor plan with maximum dimensions of 68 x 65 m, including a courtyard spanning 27 x 36 m, as depicted in Figure 9.2. The overall height varies due to its proximity to a hill, ranging from a maximum of 28.20 m to a minimum of 24 m.

The walls are made in tuff masonry, except for the walls facing the courtyard at the highest level, which are made of airbrick masonry. Wall thickness varies, starting from 155 cm at the first level and reducing to 30 cm at the highest level. The building’s floors feature a variety of vault types, including cloister, barrel and cross vaults, and the slabs are composed of steel beams.



Figure 9.1. San Carlo all’Arena Convent in Naples.

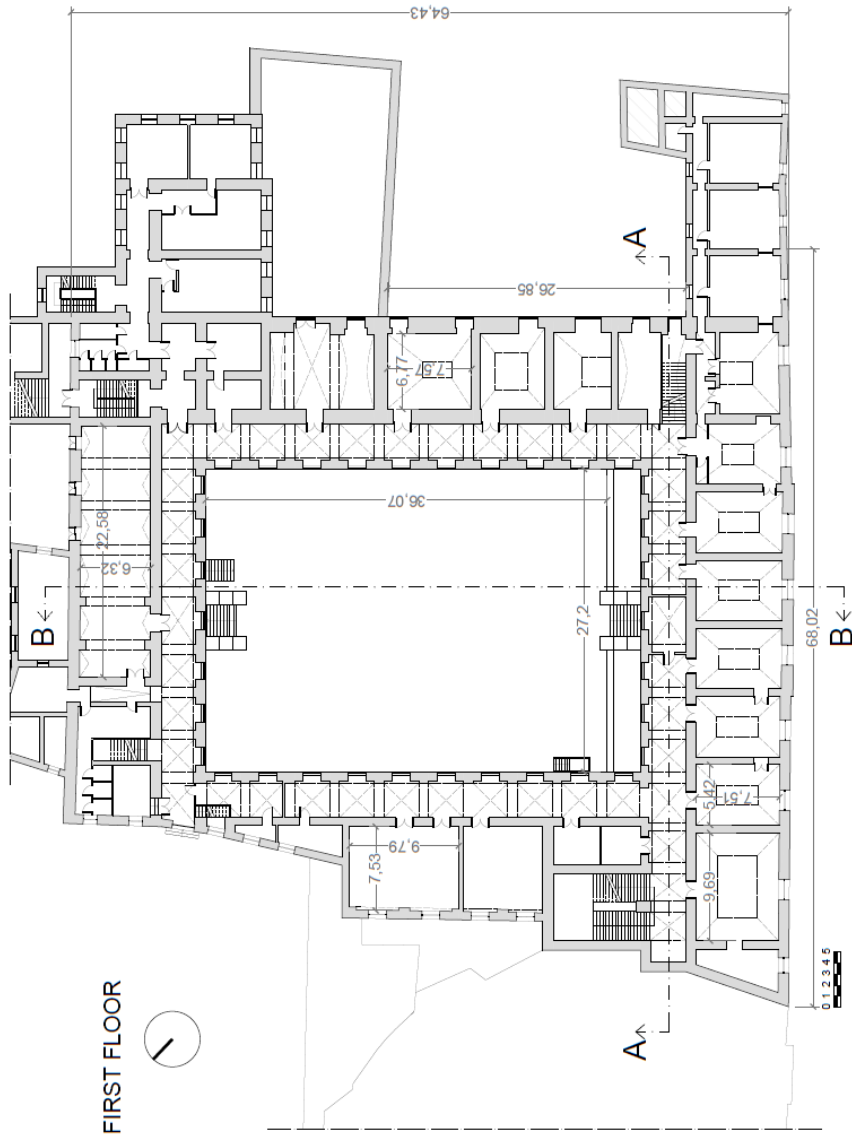


Figure 9.2. Plan of the first floor.

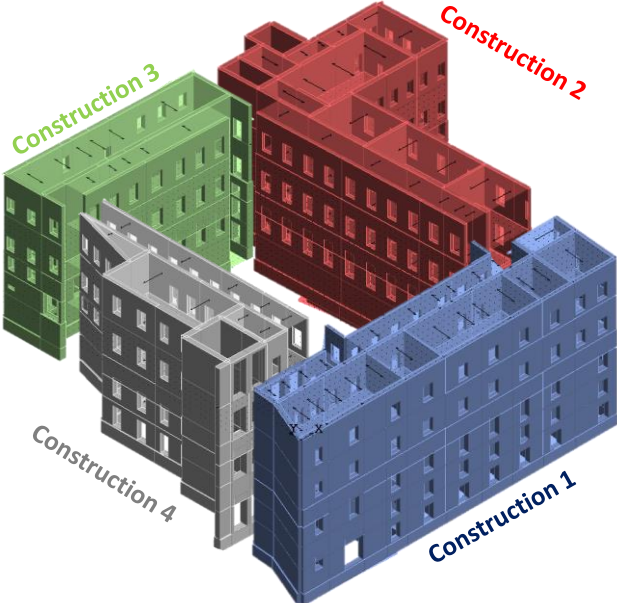


Figure 9.3. Structural models of each construction.

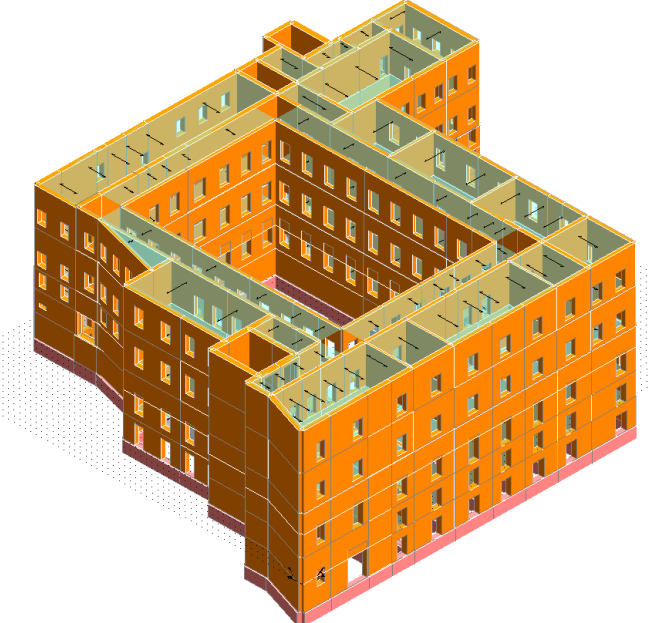


Figure 9.4. Structural model of the Convent.

Similar to St. Domenico Maggiore Covent, the St. Carlo all'Arena Convent stands as a significant example of complex building, resulting from the addition of various constructions in different periods, ranging from the 17th, when the initial section was constructed, to the 20th century. Just as outlined for the Saint Domenico Convent, nonlinear static analysis was employed to assess the Saint Carlo all'Arena Convent, considering both individual constructions and the convent as a whole. Figures 9.3 and 9.4 illustrate the structural models of the individual construction and of the Convent.

In the follow, some results of the pushover analysis are presented, including capacity curves for each construction. In particular, Figures from 9.5 to 9.8 illustrate the capacity curves for each construction, comparing them with the capacity curve of the entire convent. The analysis considers two force distributions: one proportional to the masses and the other proportional to the first vibration mode of the structure. The curves are graphed in terms of (1) base shear vs displacement of the control point and (2) base shear divided by the weight (F/w) vs displacement divided by the total height of the structure (d/H). Observations from the graphs reveal that, for both force distribution scenarios in the x direction, the capacity curve of the convent exhibits a similar ultimate displacement as the curves for Constructions 2 and 3. In terms of F/w , the curves display similar maximum values, except for the capacity curve of Construction 3, which features significantly higher values, nearly double that of the others.

In the y direction, the capacity curve of the complex has an ultimate displacement lower than the ultimate displacements of the individual Constructions. Specifically, for a force distribution proportional to the masses, the convent's curve reaches an ultimate displacement of 12 cm, while the curves for other constructions range between 14 cm and 16 cm. With a force distribution proportional to the first vibration mode of the structure, the convent's curve reaches an ultimate displacement of 10 cm, while other constructions curves vary between 13 cm and 16 cm. In terms of F/w , the capacity curve of the complex exhibit a maximum value falling between the values of the other constructions curves.

Distribution of forces proportional to the masses
x direction

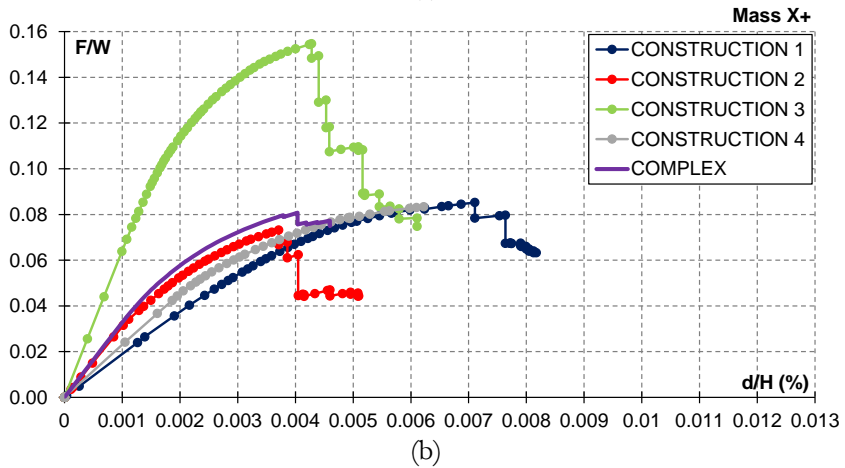
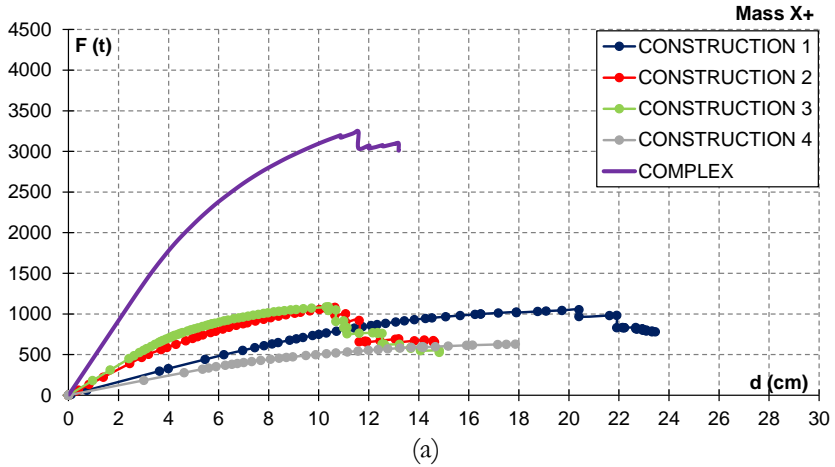


Figure 9.5. *Mass (x direction)*. Comparison between capacity curve of single construction and the entire convent in terms of (a) forces vs displacements; (b) Forces divided by weight vs displacements divided by total height of the structure.

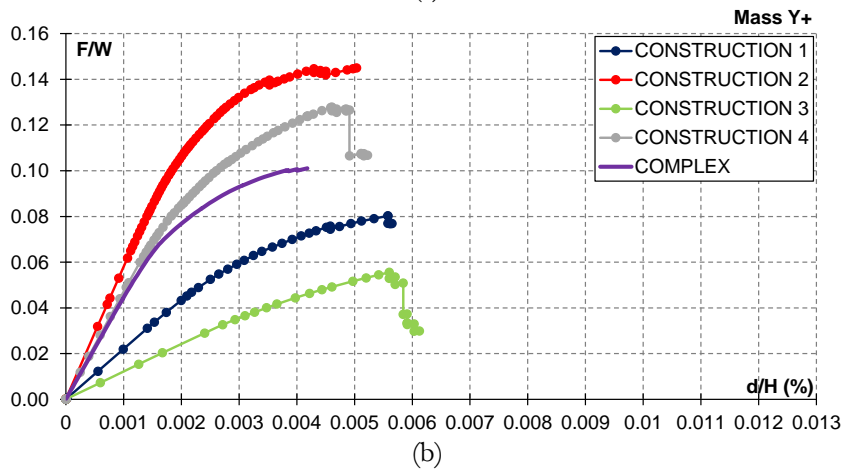
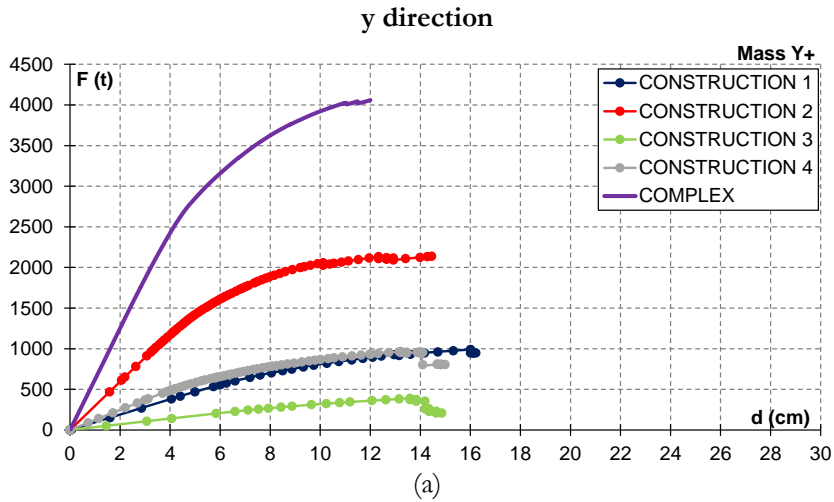


Figure 9.6. *Mass (y direction)*. Comparison between capacity curve of single construction and the entire convent in terms of (a) forces vs displacements; (b) Forces divided by weight vs displacements divided by total height of the structure.

Distribution of forces proportional to the first vibration mode
x direction

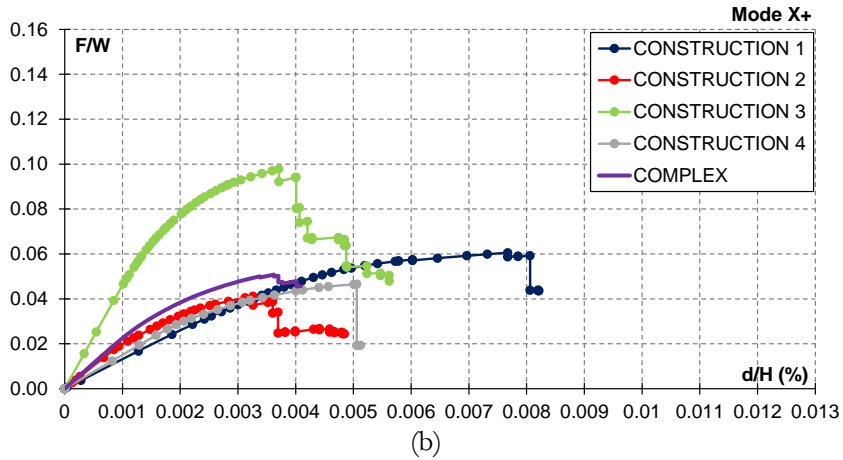
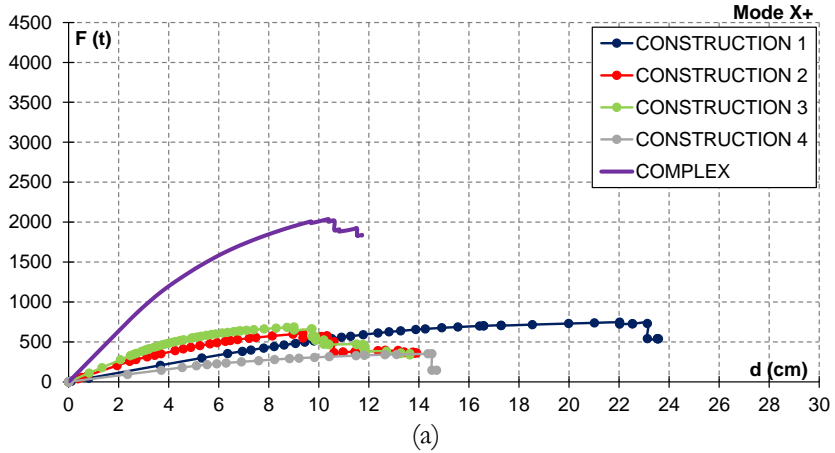


Figure 9.7. *Mode (x direction)*. Comparison between capacity curve of single construction and the entire convent in terms of (a) forces vs displacements; (b) Forces divided by weight vs displacements divided by total height of the structure.

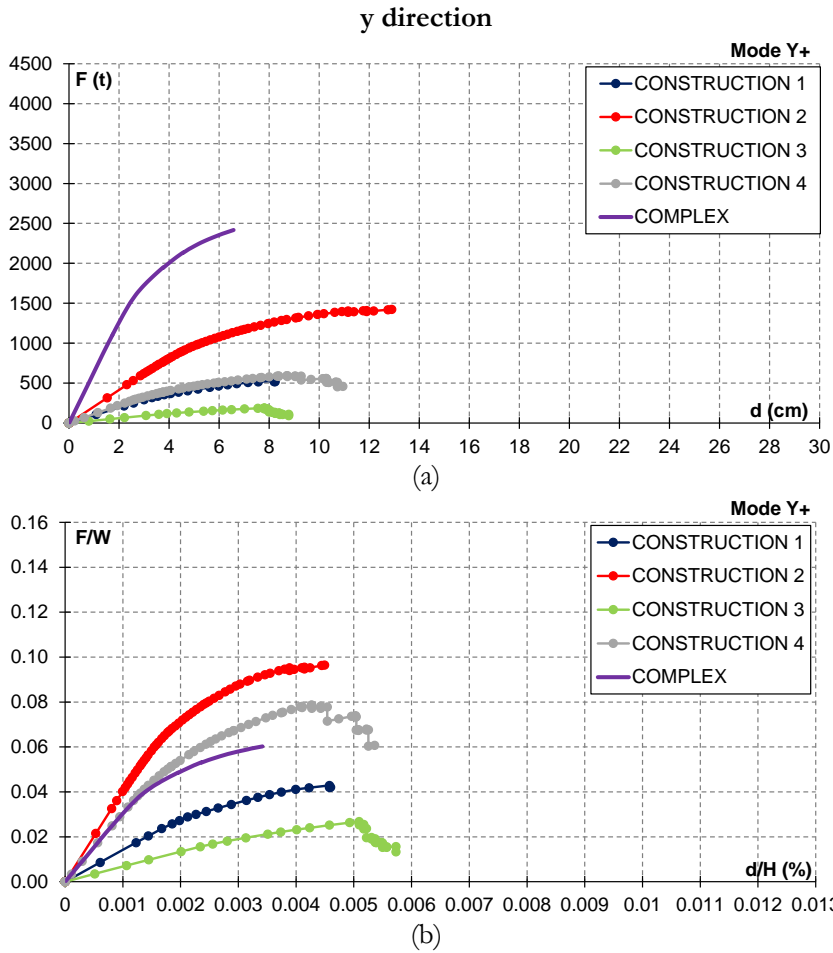


Figure 9.8. *Mode (y direction)*. Comparison between capacity curve of single construction and the entire convent in terms of (a) forces vs displacements; (b) Forces divided by weight vs displacements divided by total height of the structure.

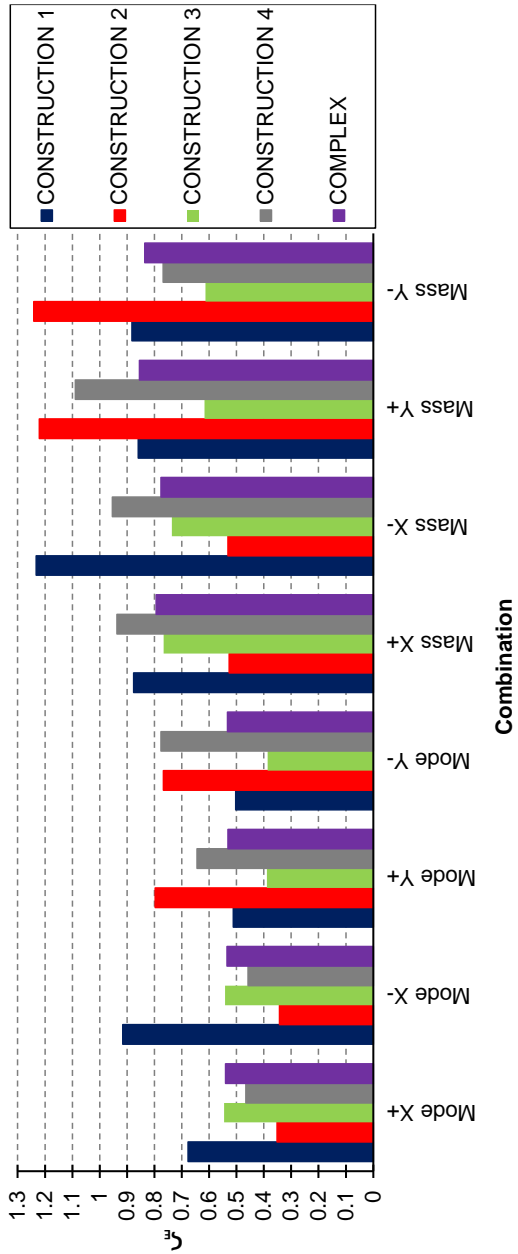


Figure 9.9. Comparison between Seismic Vulnerability Indexes of the single construction and the entire convent.

Figure 9.9 graphically presents seismic vulnerability indexes for each construction and for the complex. The results reveal that:

- *Construction 1* displays seismic vulnerability indexes ranging from a minimum value of 0.503, achieved with a distribution of forces proportional to the first vibration mode of the structure in the y direction (Mode Y+), to a maximum value of 1.232, obtained with a distribution of forces proportional to the masses in the x direction (Mass X-);
- For *Construction 2*, the seismic vulnerability indexes range from a minimum value of 0.343 obtained with a distribution of forces proportional to the first vibration mode of the structure in the x direction (Mode X-) to a maximum value of 1.241 obtained with a distribution of forces proportional to the masses in the y direction (Mass Y-);
- *Construction 3* exhibits seismic vulnerability indexes ranging from a minimum value of 0.386, achieved with a distribution of forces proportional to the first vibration mode of the structure in the y direction (Mode Y-), to a maximum value of 0.766, obtained with a distribution of forces proportional to the masses in the x direction (Mass X+);
- *Construction 4* exhibits seismic vulnerability indexes ranging from a minimum value of 0.458, obtained with a distribution of forces proportional to the first vibration mode of the structure in the x direction (Mode X-), to a maximum value of 1.089, achieved with a distribution of forces proportional to the masses in the y direction (Mass Y+);
- The *Complex* showcases seismic vulnerability indexes spanning from a minimum value of 0.531, achieved with a force distribution proportional to the first vibration mode of the structure in the y-direction (Mode Y+), to a maximum value of 0.855, obtained with a force distribution proportional to the masses in the y-direction (Mass Y+).

It is worthy to note that Constructions 1 and 3 exhibit higher values in the x direction, while Constructions 2 and 4 demonstrate higher values in the y direction. Interestingly, the complex displays comparable values of seismic vulnerability indexes in both orthogonal directions.

9.3 Non-linear behavior of the constructions of St. Domenico Maggiore Convent

This Section focuses on the impact of adding new structures to the existing ones on the capacity curves. For this purpose, three additional structural models have been analysed: Construction 0-1 (C0-1), Construction 0-1-7 (C0-1-7) and Construction 0-1-6-7 (C0-1-6-7). Figures from 9.10 to 9.13 illustrate the comparison between the capacity curves of the Constructions C0, C0-1, C0-1-7, C0-1-6-7 and C0-1-2-6-7 in the two orthogonal directions, considering both the distribution of forces proportional to the masses and the distribution of forces proportional to the first vibration mode of the structure. In particular, the capacity curves are given in terms of (1) base shear vs displacement of the control point, and (2) base shear divided by the weight (F/w) vs displacement divided by the total height of the structure (d/H).

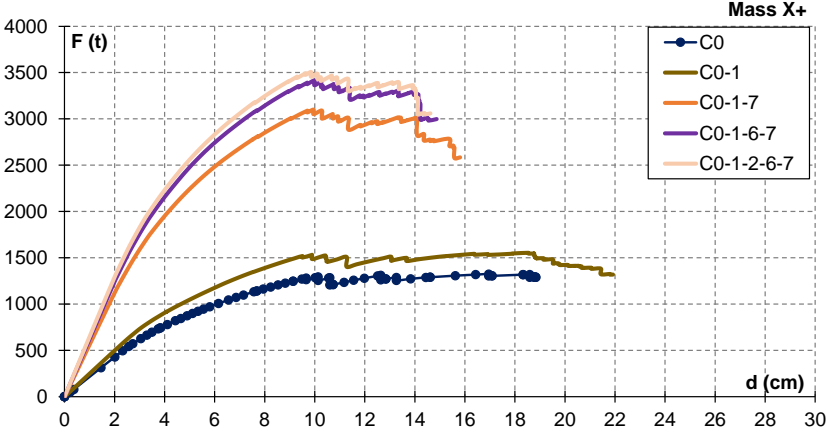
In the case of *distribution of forces proportional to the masses* it can be observed that:

- The capacity curve of C0-1 is similar to the capacity curve of the C0, in both orthogonal directions. However, the capacity curve of C0-1 in the x direction exhibits a higher maximum base shear of 1500 t, while the capacity curve in the y direction shows a maximum base shear of 1000 t.
- When considering the presence of the C7 (C0-1-7), a significant increase in maximum base shear is observed in both orthogonal direction, with values rising from 1500 t to 3100 t in the x direction and from 1100 t to 2900 t in the y direction. Moreover, there is a notable increase in stiffness. In terms of ultimate displacement, the x direction experiences a reduction from 22 cm to 16 cm, while the ultimate displacement in the y direction for C0-1-7 remains the same as that of C0-1.
- The addition of C6 results in a slight increment in stiffness and maximum base shear in the x direction, with no significant reduction in ultimate displacement. In the y direction, there is a greater increase in stiffness and a reduction in ultimate displacement, decreasing from 20 cm to 16 cm.
- The addition of C2 doesn't cause notable variations.

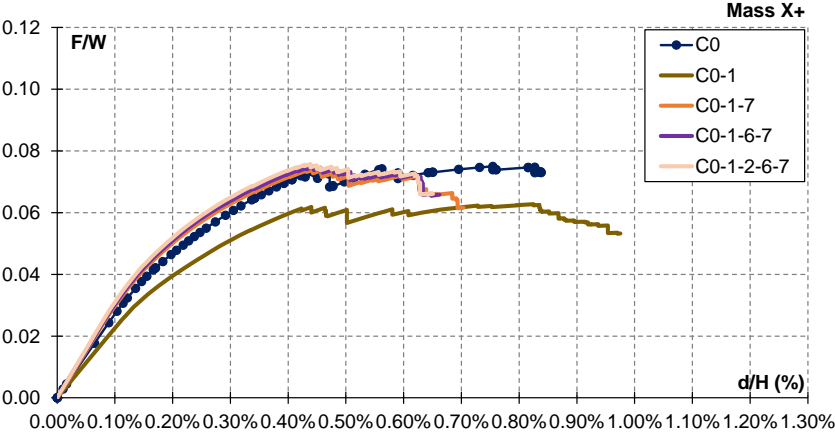
In the case of *distribution of forces proportional to the first vibration mode of the structure* the following considerations can be made:

- The capacity curve of C0-1 is similar to the capacity curve of the C0, in both orthogonal directions. Notably, the capacity curve of C0-1 in the x direction features a higher maximum base shear of 1000 t, while the capacity curve in the y direction shows a maximum base shear of 500 t.
- When introducing the C7 (C0-1-7), there is an increase in maximum base shear in both orthogonal directions. The values rise from 1500 t to 2000 t in the x direction and from 500 t to 1000 t in the y direction. Furthermore, there is a significant increase in stiffness in the y direction. Regarding ultimate displacement, the x direction experiences a reduction from 22 cm to 16 cm, while the y direction sees a reduction from 7 cm to 4 cm.
- The addition of C6 leads to a slight increase in stiffness and maximum base shear in the x direction, with no significant reduction in ultimate displacement. In the y direction, there is a more substantial increase in stiffness and a reduction in ultimate displacement, decreasing from 4 cm to 2.5 cm.
- The addition of C2 doesn't cause notable variations.

Distribution of forces proportional to the masses
x direction



(a)



(b)

Figure 9.10. Mass (x direction). The impact of adding new structures to the existing ones on the capacity curves in terms of (a) forces vs displacements; (b) Forces divided by weight vs displacements divided by total height of the structure.

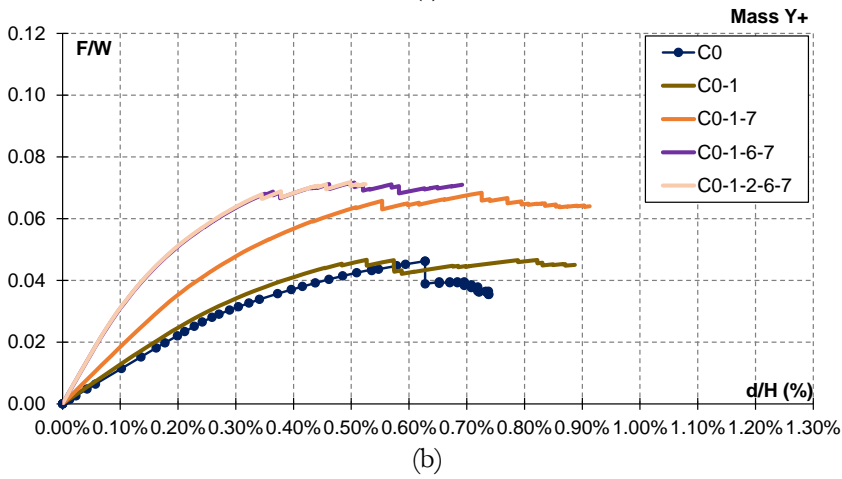
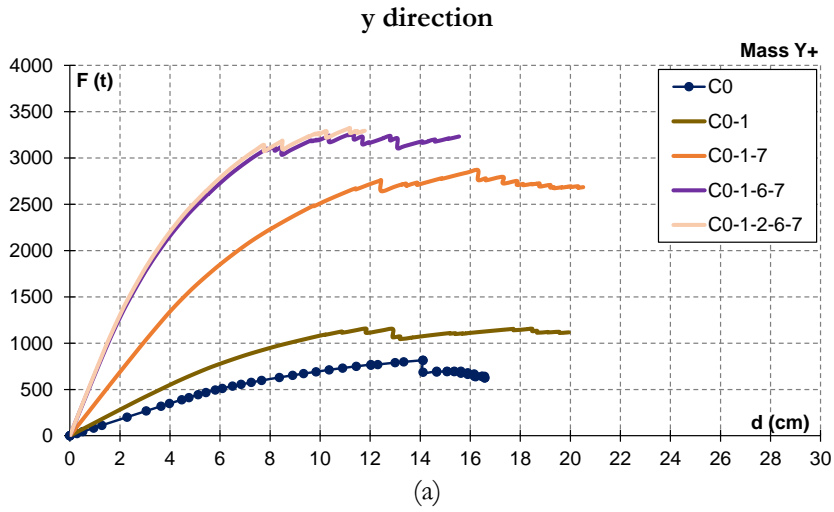
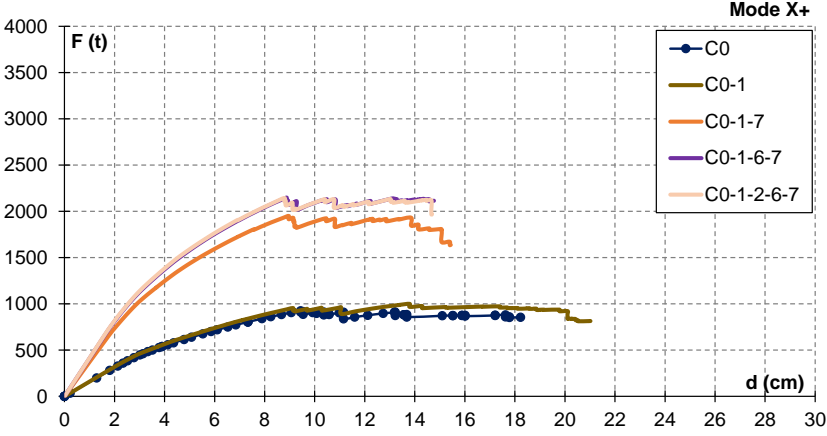
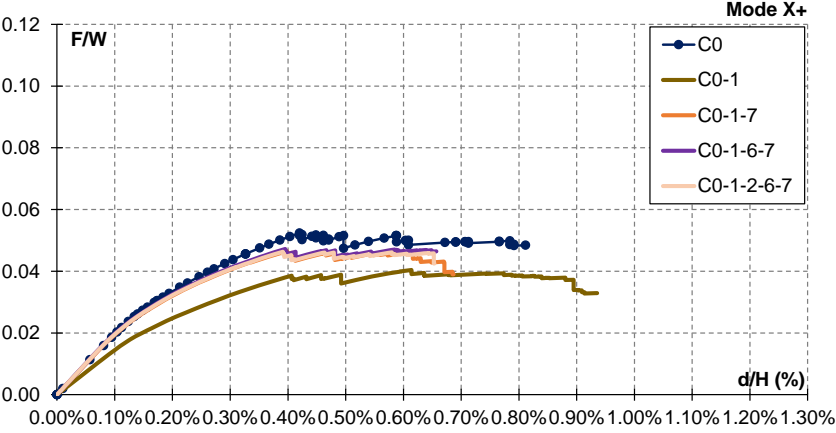


Figure 9.11. *Mass (y direction)*. impact of adding new structures to the existing ones on the capacity curves in terms of (a) forces vs displacements; (b) Forces divided by weight vs displacements divided by total height of the structure.

Distribution of forces proportional to the first vibration mode
x direction



(a)



(b)

Figure 9.12. Mode (x direction). The impact of the addition of Constructions on the capacity curve in terms of (a) forces vs displacements; (b) Forces divided by weight vs displacements divided by total height of the structure.

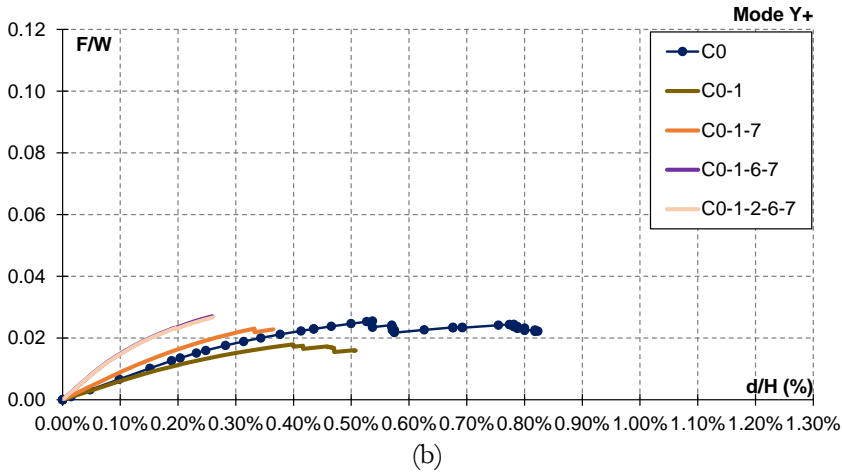
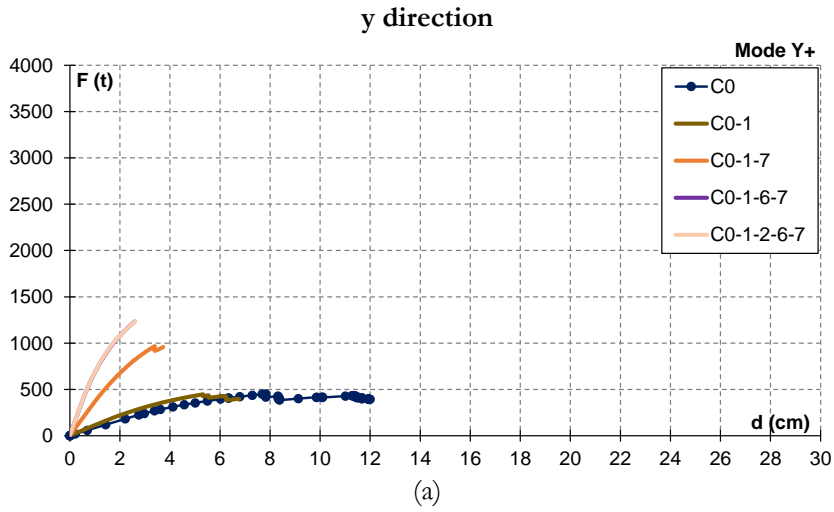


Figure 9.13. *Mode (y direction)*. The impact of adding new structures to the existing ones on the capacity curves in terms of (a) forces vs displacements; (b) Forces divided by weight vs displacements divided by total height of the structure.

9.4 Seismic vulnerability assessment of St. Domenico Convent

This Section focuses on the impact of adding new structures to the existing ones on the seismic vulnerability indexes. Figure 9.14 illustrates the comparison between the seismic vulnerability indexes of the Constructions C0, C0-1, C0-1-7, C0-1-6-7 and C0-1-2-6-7 in the two orthogonal directions, considering both the distribution of forces proportional to the masses and the distribution of forces proportional to the first vibration mode of the structure.

When considering the *distribution of forces proportional to the masses*, the following observations can be made:

- Adding C1 to C0 results in an increase in the seismic vulnerability indexes in y direction.
- The introduction of C2, C6 and C7 (C0-1-2-6-7) doesn't notably increase the indexes in both directions compared to C0-1.

For the *distribution of forces proportional to the first vibration mode of the structure*:

- The addition of the C1 to C0 (C0-1) leads to a decrease in the seismic vulnerability indexes in y direction. The indexes range from 0.68 and 0.62 for Mode Y+ and Mode Y- of C0 to 0.40 and 0.45.
- Introducing C2, C6, and C7 (C0-1-2-6-7) results in a further decrease, particularly in the y direction. In this case, the indexes range from values of 0.43 and 0.45 for Mode Y+ and Mode Y- to values equal to 0.25.

It is important to note that in x direction (Figure 9.15) there isn't a substantial variation in the seismic vulnerability indexes between the two forces distributions. However, in the y direction (Figure 9.16), the seismic vulnerability indexes obtained using the force distribution proportional to the first vibration mode of the structure are noticeably lower than those obtained using the force distribution proportional to the masses. This discrepancy is attributed to the presence of height irregularities that impact the pushover curves and, consequently, the seismic vulnerability indexes. Specifically, the height irregularities result in an increase in the value of the top floor and a concentration of shear forces at certain walls, leading to the formation of a mechanism and the subsequent cessation of the capacity curves. For a more comprehensive explanation, please refer to the following Section.

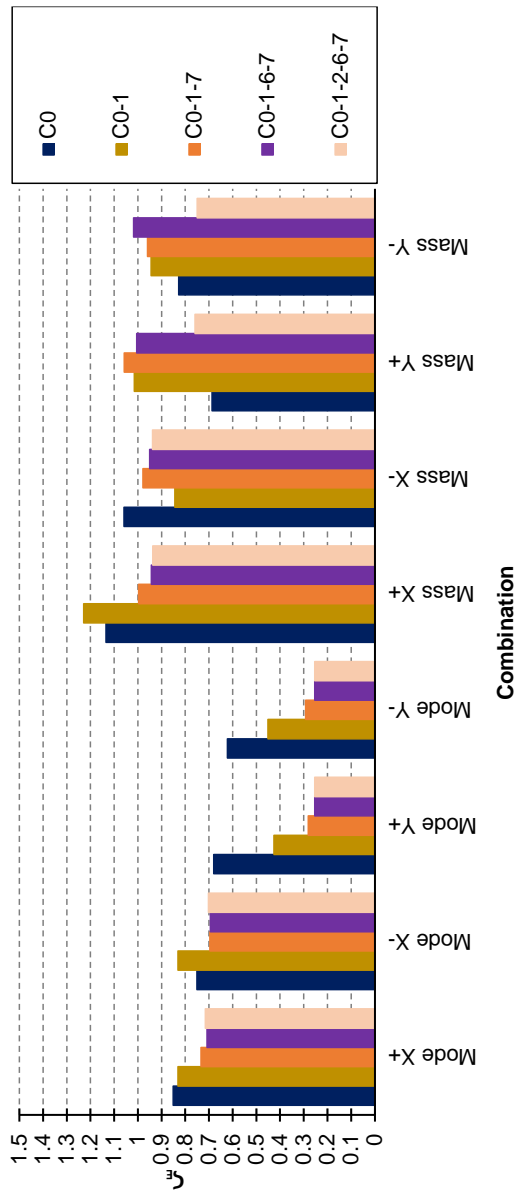


Figure 9.14. The effect of the addition of Constructions on the seismic vulnerability indexes.

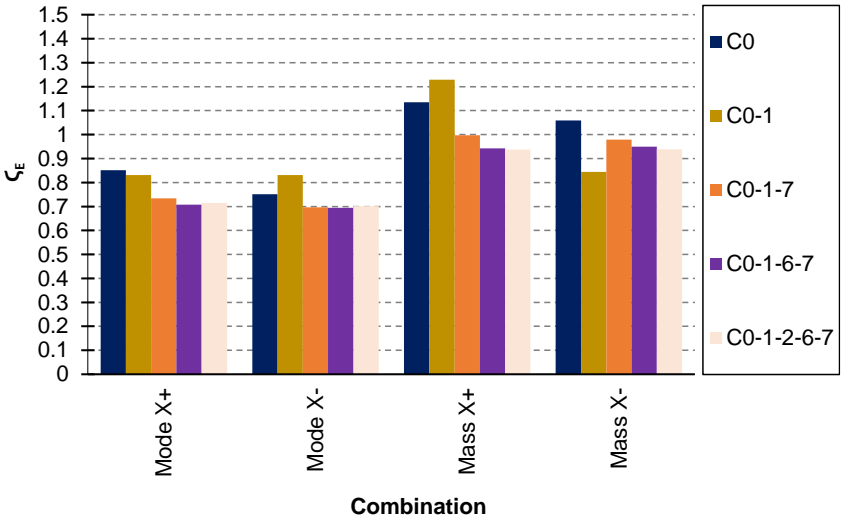


Figure 9.15. Comparison between Seismic Vulnerability Indexes in x direction.

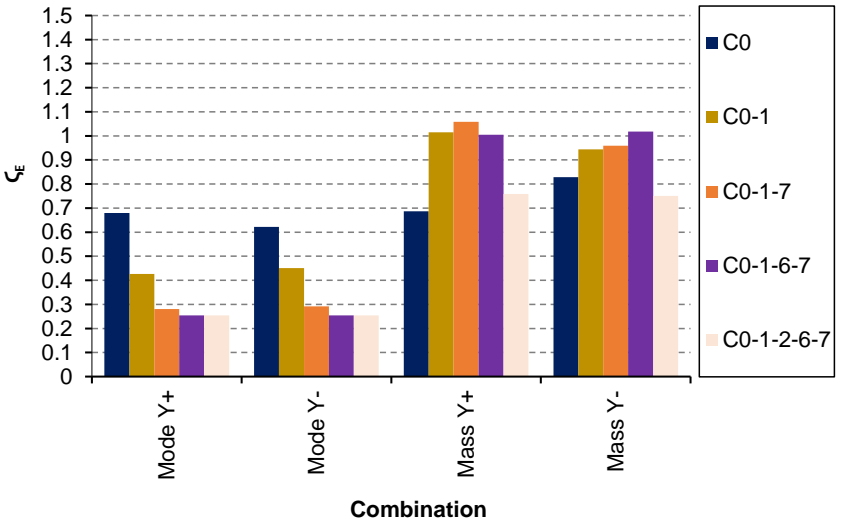


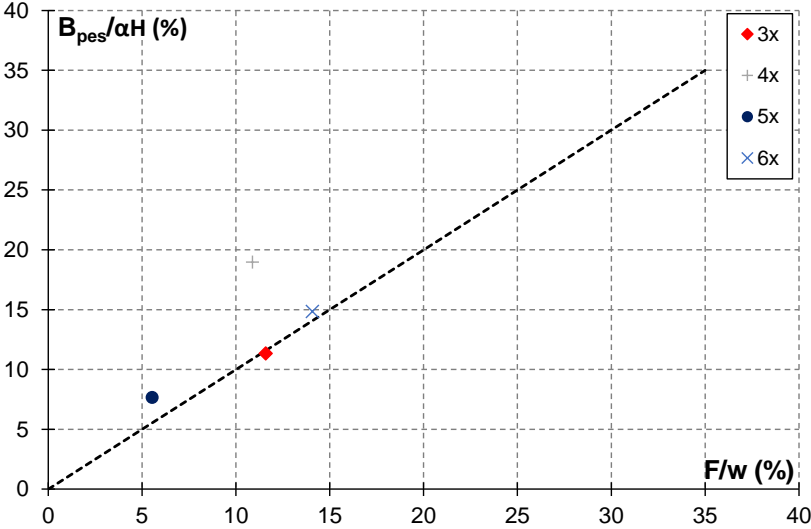
Figure 9.16. Comparison between Seismic Vulnerability Indexes in y direction.

9.5 Simplified method to check the non-linear static analysis through the Limit Analysis

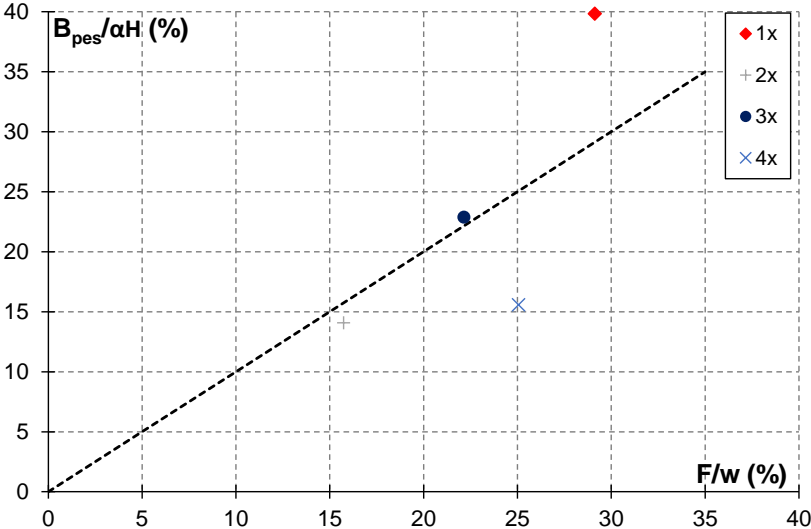
To check the results obtained with nonlinear static analysis through the Limit Analysis, the nonlinear analyses of 2D walls have been compared with the results obtained with the simplified formula proposed by the research group in the framework of limit analysis. Since the proposed formula is based on Heyman hypothesis of infinite compressive strength of the masonry, a compressive strength of 100 kg/cm² has been assumed to approximate the infinite strength of the masonry. The application of the formula and the pushover analysis curves are provided in **Appendix 5**. The overall results of these comparisons are summarized in Figure 8.17. The points representing the load multiplier for each wall generally fall close to the bisector line. However, there are some exceptions, mainly associated with the following considerations:

- For Construction 0, walls 4x and 5x exhibit a shear failure mechanism.
- In Construction 1, walls 1x and 4x display shear failure mechanisms, with wall 4x additionally showing significant irregularities in the arrangement of openings.
- In the San Carlo all’Arena Convent, wall 4x lacks openings at the ground floor and has substantial variations in pier width.
- In the San Carlo all’Arena Convent, wall 15x lacks openings at the ground floor and features an irregular arrangement of openings.

The scatter between the values obtained with the simplified formula and those from the pushover analysis is depicted in Figure 9.18 and detailed in Table 9.1. Notably, the formula tends to underestimate the capacity of the walls (negative scatter) in only few cases and the scatter exceeds 20% in those instances. Consequently, the results suggest that the values obtained with the proposed formula provide a good approximation of those from the pushover analysis. The scatter tends to be larger when there is greater irregularity in the arrangement of openings in both the vertical and horizontal directions and when the failure mechanism differs from flexural failure.



(a)



(b)

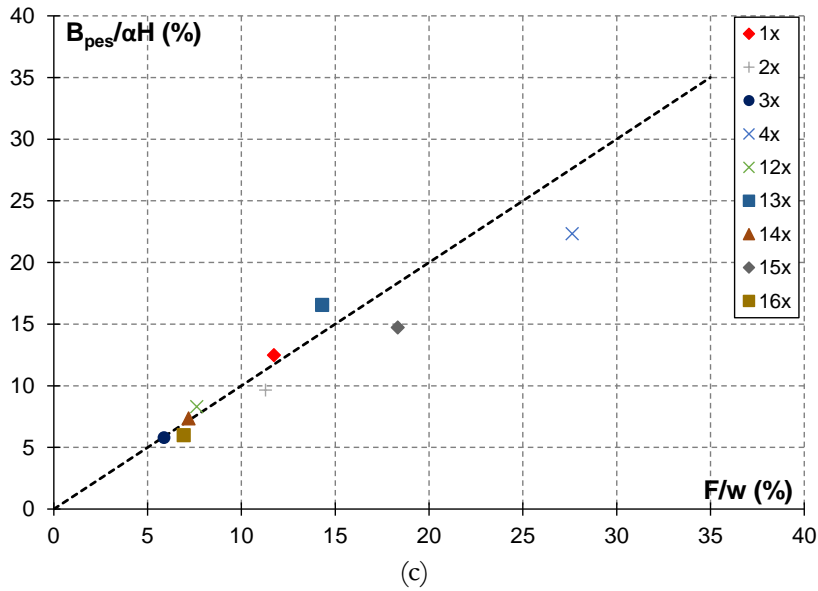


Figure 9.17. Horizontal collapse multipliers: (a) Construction 0; (b) Construction 1 and (c) San Carlo all’Arena.

Table 9.1. Scatter between the proposed formula and the pushover analysis.

	Wall	$B_{pes}/\alpha H$	F/w	Scatter
	[-]	[%]	[%]	[%]
C0	3x	11.34	11.59	2.21
	4x	18.96	10.88	-42.60
	5x	7.66	5.53	-27.77
	6x	14.85	14.07	-5.23
C1	1x	39.84	29.13	-26.89
	2x	14.08	15.73	11.74
	3x	22.89	22.15	-3.23
	4x	15.57	25.06	60.94
SCA	1x	12.48	11.73	-6.02
	2x	9.66	11.28	16.74
	3x	5.80	5.87	1.20
	4x	22.33	27.62	23.69
	12x	8.32	7.62	-8.43
	13x	16.56	14.29	-13.70
	14x	7.36	7.18	-2.41
	15x	14.73	18.32	24.39
	16x	6.00	6.92	15.34

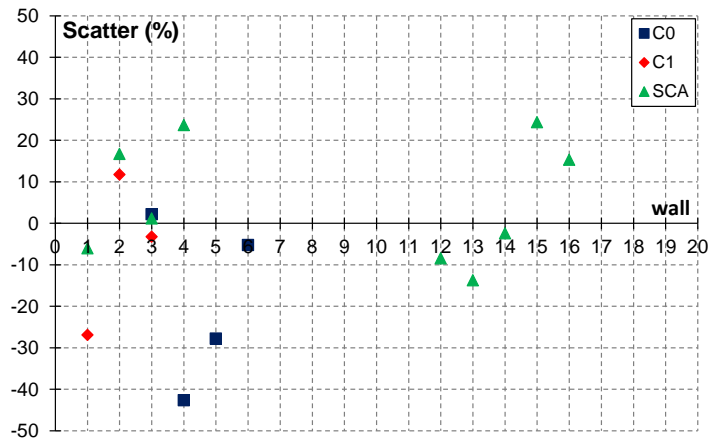


Figure 9.18. Scatter between the proposed formula and the pushover analysis.

9.6 The impact of irregularities on the seismic vulnerability assessment

As highlighted in the previous Sections, when considering the distribution of forces proportional to the first vibration mode in the y direction (Mode Y), the capacity curves for Constructions C0-1-6-7 and C0-1-2-6-7 show a significant reduction in terms of ultimate displacement. The Seismic Vulnerability Indexes in the y direction are notably lower than those obtained using force distribution proportional to the masses. This discrepancy is attributed to the presence of irregularities that affect the pushover curves and, consequently, the seismic vulnerability indexes. In this Section the impact of the irregularities on the seismic vulnerability assessment is analysed. To this end, Tables from 9.2 to 9.6 provide modal forces at various floors in the x and y directions for Constructions C0, C0-1, C0-1-7, C0-1-6-7, and C0-1-2-6-7. The following observations can be made:

- A significant increase in weights and forces in both orthogonal directions is noted with the addition of C7 (C0-1-7).
- With the inclusion of C6 (C0-1-6-7), the impact on weights is minimal, while the forces in the x-direction remain relatively consistent. However, the forces in the y direction double, primarily due to increasing irregularities in both plan and height of the construction.
- The addition of C2 does not result in significant variations.

Figure 9.19 illustrates the variations in forces in the y direction (red line) and in the x direction (blue line), as well as the changes in weight (green line) at the fifth floor, resulting from the addition of the other constructions to C0. Notably, the weight at the fifth floor experiences a minimal variation, specifically 3%, with the introduction of other constructions (C0-1-2-6-7). It is important to highlight that the inclusion of Constructions 6 and 2 does not contribute to any increase in weight, maintaining a consistent trend. Similarly, the force in the x direction at the fifth floor shows a negligible variation when additional constructions are introduced to C0, with the change relative to the initial value of C0 being -11% for Construction C0-1-2-6-7. Concerning the forces in the y direction at the fifth floor, the graph indicates a significant 160% increase compared to the initial value of Construction C0. Notably, the addition of Construction 1 has a marginal impact, with a variation of only 2%. The inclusion of C7 and C6 (C0-1-6-7

and C0-1-2-6-7) demonstrates a linear trend in force variation, progressing from 2% to 148%. The introduction of C2 further amplifies the variation from 148% to 160%.

The substantial increase in forces in the y direction due to the addition of Construction 6 and Construction 2 (C0-1-6-7 and C0-1-2-6-7) results in a concentration of high shear forces in the piers of the top floor, leading to the formation of a mechanism at the last floor that arrests the capacity curve.

Table 9.2. Modal forces at various floors: C0.

Level	z_i	W_i	$F_{i,x}$	$F_{i,x}/F_{TOT,x}$	$F_{i,y}$	$F_{i,y}/F_{TOT,y}$
$[-]$	$[m]$	$[t]$	$[t]$	$[\%]$	$[t]$	$[\%]$
1	5.57	5605	3921	32%	1568	29%
2	10.42	3349	3412	28%	1459	27%
3	14.52	4568	2759	23%	1253	23%
4	19.67	2644	1500	12%	768	14%
5	22.47	1495	577	5%	308	6%
TOT		17662	12168	100%	5356	100%

Table 9.3. Modal forces at various floors: C0-1.

Level	z_i	W_i	$F_{i,x}$	$F_{i,x}/F_{TOT,x}$	$F_{i,y}$	$F_{i,y}/F_{TOT,y}$
$[-]$	$[m]$	$[t]$	$[t]$	$[\%]$	$[t]$	$[\%]$
1	5.57	9185	5500	38%	1601	30%
2	10.42	5998	3909	27%	1474	27%
3	14.52	5340	2933	20%	1242	23%
4	19.67	2733	1529	11%	783	14%
5	22.47	1526	583	4%	314	6%
TOT		24782	14453	100%	5413	100%

Table 9.4. Modal forces at various floors: C0-1-7.

Level	z_i	W_i	$F_{i,x}$	$F_{i,x}/F_{TOT,x}$	$F_{i,y}$	$F_{i,y}/F_{TOT,y}$
$[-]$	$[m]$	$[t]$	$[t]$	$[\%]$	$[t]$	$[\%]$
1	5.57	16716	7779	35%	3424	31%
2	10.42	8546	6464	29%	3035	28%
3	14.52	10318	5067	23%	2529	23%
4	19.67	4831	2255	10%	1418	13%
5	22.47	1548	556	3%	490	4%
TOT		41959	22120	100%	10895	100%

Table 9.5. Modal forces at various floors: C0-1-6-7.

Level	z_i	W_i	$F_{i,x}$	$F_{i,x}/F_{TOT,x}$	$F_{i,y}$	$F_{i,y}/F_{TOT,y}$
$[-]$	$[m]$	$[t]$	$[t]$	$[\%]$	$[t]$	$[\%]$
1	5.57	18153	8012	36%	6169	33%
2	10.42	9715	6638	29%	5315	28%
3	14.52	11106	5117	23%	4258	23%
4	19.67	5019	2229	10%	2334	12%
5	22.47	1546	524	2%	764	4%
TOT		45539	22520	100%	18839	100%

Table 9.6. Modal forces at various floors: C0-1-2-6-7.

Level	z_i	W_i	$F_{i,x}$	$F_{i,x}/F_{TOT,x}$	$F_{i,y}$	$F_{i,y}/F_{TOT,y}$
$[-]$	$[m]$	$[t]$	$[t]$	$[\%]$	$[t]$	$[\%]$
1	5.57	18901	7834	35%	6543	33%
2	10.42	9716	6511	29%	5623	28%
3	14.52	11107	5060	23%	4510	23%
4	19.67	5019	2206	10%	2477	12%
5	22.47	1546	513	2%	805	4%
TOT		46288	22124	100%	19958	100%

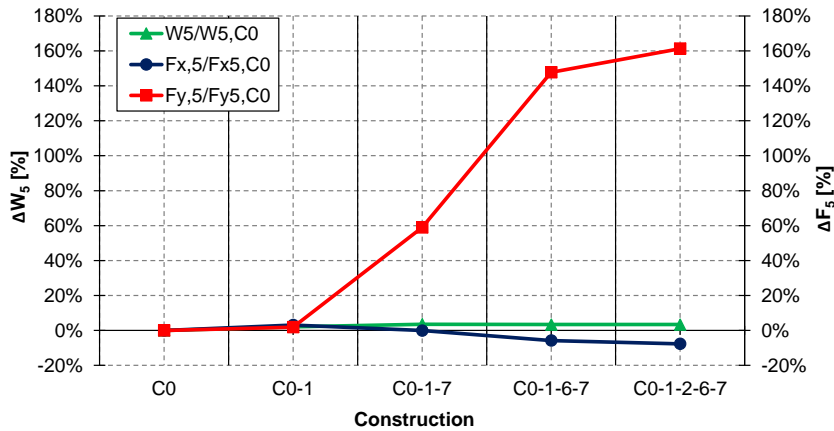


Figure 9.19. Variation of forces in the x direction (blue line) and y direction (red line), and weight variation (green line) at the fifth floor due to the addition of constructions.

The mechanism at the last floor that arrests the capacity curve is evident in the evolution of plastic hinges of the wall 8y of the Construction 0, depicted in Figure 9.21. In particular, it can be observed that plastic hinges form in correspondence to the piers of the two last floors, with a shear failure mechanism. A comparison between the evolution of plastic hinges in wall 8y of Construction 0 and Construction C0-1-2-6-7 (Figure 9.22) reveals a larger number of plastic hinges in the former, with the presence of plastic hinges in the last four floors. The collapse mechanism in wall 8y, as shown in Figure 9.23, unveils a shear failure mechanism in the piers in Construction C0-1-2-6-7 and shear and flexural failure mechanisms in the piers of Construction C0. These results highlight that irregularities significantly impact the entire structure, leading to the formation of a mechanism that arrests the capacity curve. However, on the single construction (C0), their impact is comparatively minor, resulting in a larger ultimate displacement and an increased number of plastic hinges.

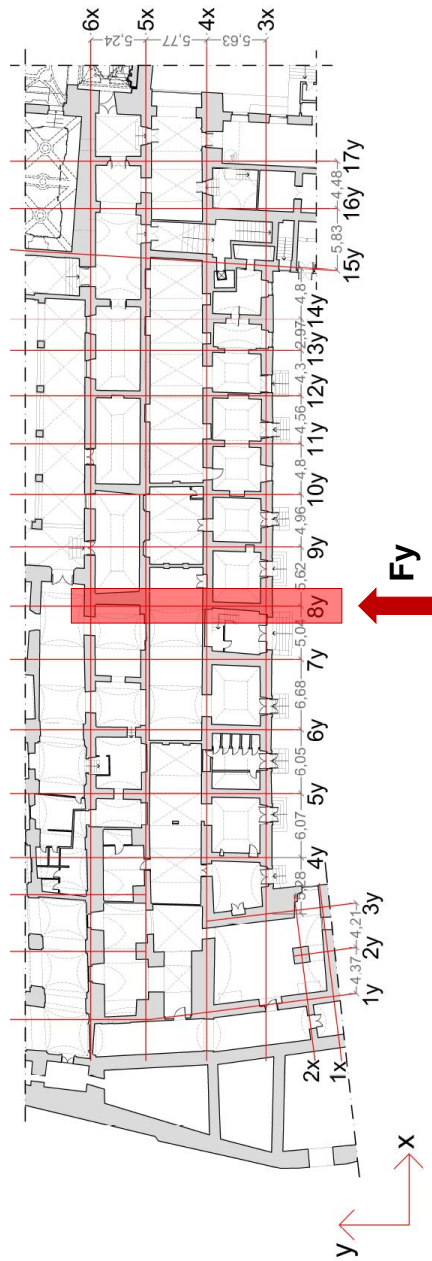
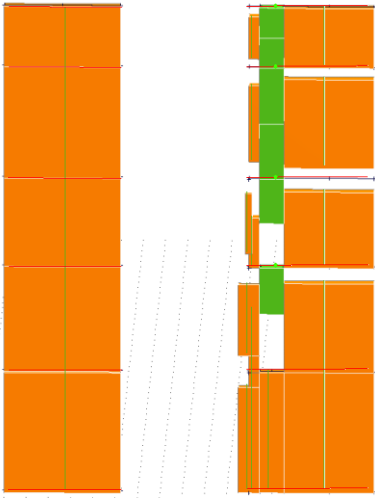
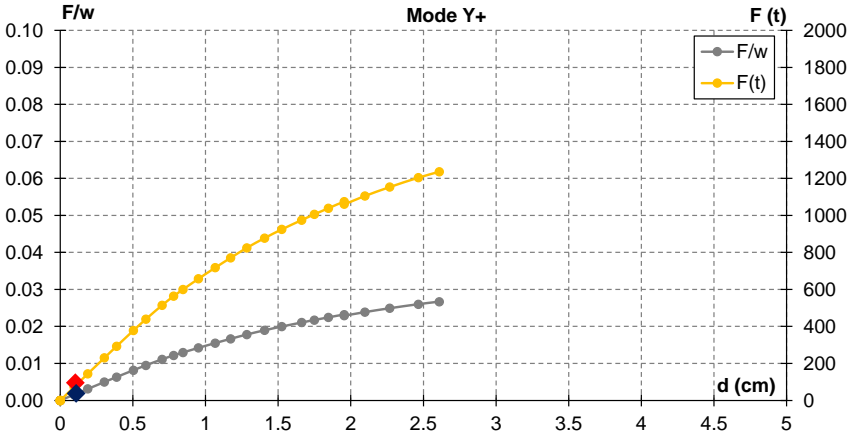


Figure 9.20. Analysed wall: 8y.

Evolution of plastic hinges of C0-1-2-6-7: Mode Y+
Construction 0 – Wall 8y

STEP 1



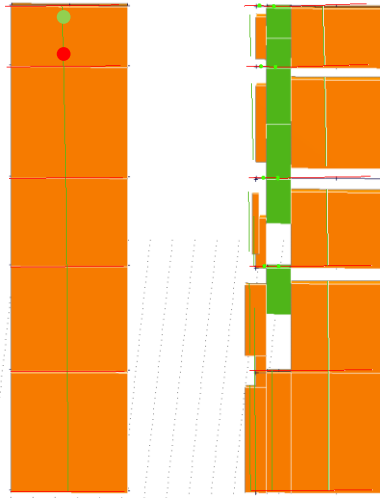
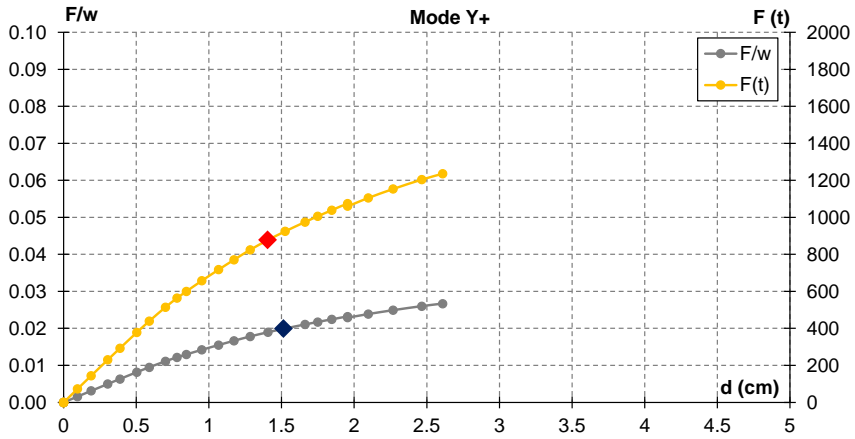
Low damage Severe damage Collapse

(a)

Evolution of plastic hinges of C0-1-2-6-7: Mode Y+

Construction 0 – Wall 8y

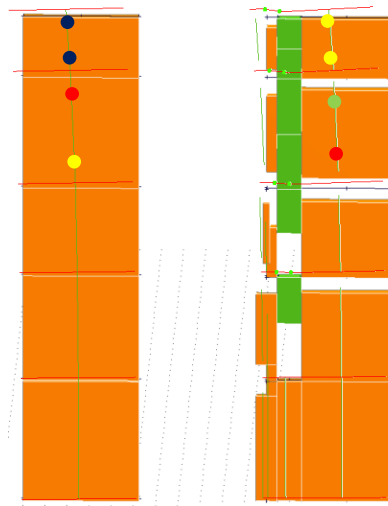
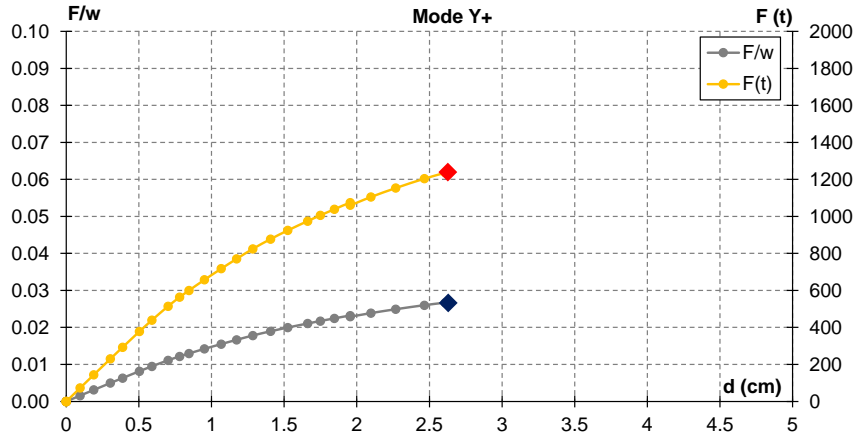
STEP 15



■ Low damage
 ■ Severe damage
 ■ Collapse

(b)

Evolution of plastic hinges of C0-1-2-6-7: Mode Y+
Construction 0 – Wall 8y
STEP 27



Low damage
 Severe damage
 Collapse

(c)

Figure 9.21. Evolution of plastic hinges of the wall 8y of the C0.

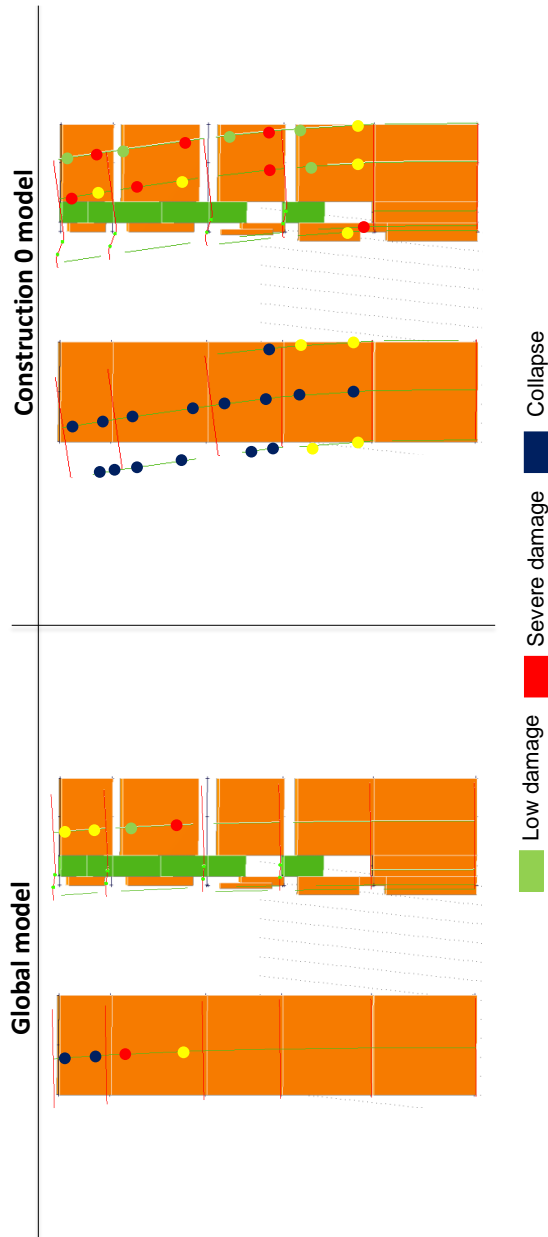


Figure 9.22. Evolution of plastic hinges of the wall 8y of the C0: comparison between the analysis of C0 and of C0-1-2-6-7.

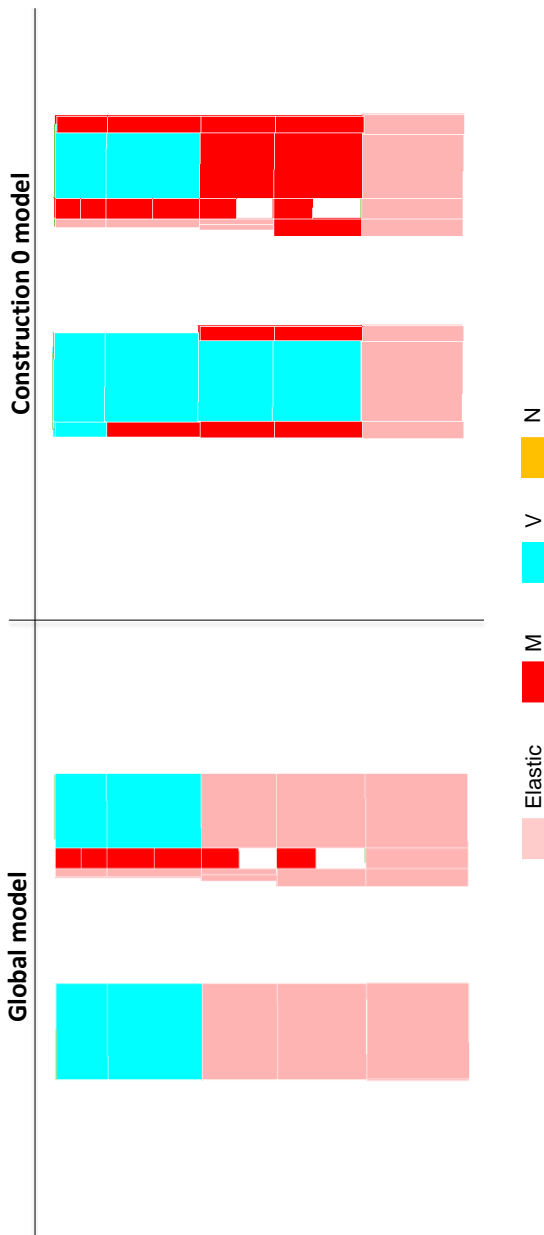


Figure 9.23. Collapse mechanism of the wall 8y of the C0: comparison between the analysis of C0 and of C0-1-2-6-7.

9.7 Proposal of definition of complex monumental building

From the analysis of the Saint Domenico Convent and Saint Carlo all’Arena Convent, a proposal of definition of complex monumental buildings and their typical complexities emerges and is formulated as follows.

A complex monumental building is a masonry construction characterized by the following typical complexities:

- *Historical modifications*, such as the addition of structures to the existing one over the years or the inclusion of additional floors in elevation. The addition of structural portions to existing ones necessitates a more meticulous analysis, especially in seismic areas. The nonlinear static analysis procedure presented in this dissertation includes the analysis of the single construction by neglecting the interaction with the others, as well as 2D walls analysis and nonlinear analysis of the entire Convent, assuming a perfect interaction among various constructions. This approach provides a comprehensive understanding of the structural behaviour, as detailed in previous Sections. The addition of floors can impact vertical stresses, underscoring the importance of their evaluation.
- *The presence of adjacent structures*, which may have varying floor heights or different structural typologies, including cases where adjacent structures are churches.
- *Foundations at different heights*, which can affect the selection of the seismic reference level.
- *Different occupancies*, even within the same floor. These differences can lead to the addition or closure of openings to accommodate various functions. Furthermore, changes in occupancy over the years result in variations in live loads.
- *The presence of alterations*, such as the addition or closure of openings.

It’s important to note that the issue of adding structural portions to existing ones over the years is a characteristic shared with aggregate structures. However, complex buildings cannot be assimilated to aggregate buildings; they are the result of adding structural portions to existing ones, but unlike aggregate buildings, which are more typical in cities, they exhibit an unity.

Conclusive Remarks

This dissertation deals with the structural analysis and behaviour of the Saint Domenico Convent in Naples, as a paradigmatic example of complex monumental buildings. Located in the historical centre of the city, it results from the addition of various constructions in different periods, similar to many masonry buildings of this type. Specifically, the convent comprises eight constructions, built between the 8th and 17th centuries, each characterized by distinct features in terms of structural typology.

In this thesis primarily devoted to the nonlinear behaviour of masonry structures, an analysis of the historical evolution, along with alterations and changes in use, focusing on the nonlinear behaviour of masonry structures, has been provided.

Additionally, preliminary considerations about the structural layout of the constructions have been offered, based on the analysis of geometrical data, such as the architectural plan and prospective view of the walls. These considerations are of great importance for the analysis of the construction quality of the convent, that is evaluated in terms of its adherence to “the rules of art”, delineated in significant ancient treatise, as the treatise by Rondelet (1802), Breyman (1885), Cavalieri San Bertolo (1839) and Leon Battista Alberti (1452).

Given the complexity of the Convent, nonlinear analyses have been performed using a methodology intended for all complex buildings. This procedure includes the analysis of the single construction, by neglecting the interaction with the others, the analysis of the entire convent as unified structure, assuming perfect interaction among all the constructions, and the analysis of the incremental addition of constructions. In addition, 2D walls analyses within each construction have been carried out, with the aim to identify the weakest wall alignment that lead to the collapse of the structure and the local crises.

The results of the nonlinear static analyses reveal that irregularities in height within a single construction, particularly when considering the distribution of forces proportional to the first vibration mode of the structure, lead to a substantial reduction in ultimate displacement and seismic vulnerability indexes in the analysis of the entire convent. In particular, when assessing the entire convent, these irregularities in the single construction result in a noteworthy amplification of forces and a concentration of high shear forces, culminating in a mechanism that arrests the capacity curve.

In the author's opinion, analysing individual constructions, the entire structure, and the gradual addition of constructions is essential in the analysis of complex monumental buildings. In fact, in such instances, the addition of other constructions might accentuate irregularities that could exist in just one of the many constructions. This fact has been demonstrated in the previous analyses, wherein, despite a minimal rise in mass, the forces on the top floor increased by 160% due to the addition of constructions on the lower floors.

To validate and discuss the proposed analysis procedure for complex monumental buildings, it has been applied to the St. Carlo all'Arena Convent in Naples.

In this thesis, simplified formulas for checking the ultimate load resulting from nonlinear analyses are also discussed. A comparison between the nonlinear analyses of 2D walls and the simplified formula proposed by the research group within the framework of limit analysis is presented. The results of this comparison indicate that the values obtained with the proposed formula offer a good approximation of those derived from the pushover analysis. However, the scatter tends to be larger when there is greater irregularity in the arrangement of openings in both the vertical and horizontal directions and when the failure mechanism differs from flexural failure.

Starting from the analysis of these Convents, a proposal of definition of complex monumental buildings can be formulated, accompanied by an identification of their typical complexities. Even if characterized by certain unity, these buildings differ from monumental buildings, such as the Reggia di Caserta, Palazzo Farnese, or ecclesiastical monuments, that has an unity even if their construction spans over the years. Moreover, they cannot be assimilated to aggregate buildings, as first proposed by A. Giuffrè (1993) and subsequently developed by various researchers, where the addition of structural portions over the years is necessary to provide unity to urban development.

Appendix 1

The earthquake experienced by the convent over the years

In this section, a comprehensive list of the earthquakes experienced by the convent from the 13th century up to the current year is provided. These data are sourced from the Database Macrosismico Italiano of the INGV. For each seismic event, the following information is included:

- Intensity in Naples (Int. at place);
- Date of the seismic event (year, month, day);
- Position of the epicenter (epicentral area, latitude and longitude);
- Intensity in the epicentral area (I_0);
- Moment magnitude (M_w).

This detailed compilation of seismic events offers valuable insights into the historical seismic activity affecting the area around the convent.

Table A1.1 – Earthquake experienced by the convent from 13th century.

Int. at place	Year	Mo	Da	EpicentralArea	Lat Def	Lon Def	Io Def	Mw Def
D	1280			Napoli				
7	1293	9	4	Sannio-Matese	41.304	14.548	8-9	5.8
7-8	1349	9	9	Lazio-Molise	41.554	13.942	10	6.8
7-8	1386	3	17	Napoli	40.849	14.25	7-8	3.75
5	1406	9	16	Napoli	40.849	14.25	5	3.12
8	1456	12	5	Appennino centro-meridionale	41.302	14.711	11	7.19
7	1456	12	30	Appennino centro-meridionale				
6	1457	1	8	Napoli	40.849	14.25	6	3.37
F	1457	2	10	Capua	41.106	14.214	5-6	4.4
5	1466	1	15	Irpinia-Basilicata	40.765	15.334	8-9	5.98
5	1498	10	7	Campi Flegrei (Pozzuoli)	40.835	14.186	5-6	3.25
F	1498	10	20	Campi Flegrei (Pozzuoli)	40.822	14.123	7	3.63
5	1499	3	18	Napoli	40.849	14.25	5	3.12
6	1505	5	18	Campi Flegrei (Agnano)	40.83	14.149	7-8	3.75
5	1508	7	19	Napoli	40.849	14.25	5	3.12
5	1517	3	29	Irpinia	41.011	15.21	7-8	5.33
5	1520	1	28	Campi Flegrei (Pozzuoli)	40.835	14.186	6-7	3.5
5	1536	8	7	Napoli	40.849	14.25	5	3.12
4	1537	2	14	Campi Flegrei (Pozzuoli)	40.822	14.123	6-7	3.5
6	1538	4	20	Campi Flegrei	40.849	14.25	5-6	3.25
4	1538	9	20	Campi Flegrei (Pozzuoli)	40.833	14.192	5-6	3.25
4	1538	9	22	Campi Flegrei (Pozzuoli)	40.833	14.192	5-6	3.25
4	1538	9	23	Campi Flegrei (Pozzuoli)	40.833	14.192	5-6	3.25
4	1538	9	24	Campi Flegrei (Pozzuoli)	40.833	14.192	5-6	3.25
4	1538	9	25	Campi Flegrei (Pozzuoli)	40.833	14.192	5-6	3.25
4	1538	9	26	Campi Flegrei (Pozzuoli)	40.833	14.192	5-6	3.25
4	1538	9	27	Campi Flegrei (Pozzuoli)	40.833	14.192	5-6	3.25
4	1538	9	28	Campi Flegrei (Pozzuoli)	40.835	14.186	5-6	3.25
4	1538	9	28	Campi Flegrei (Pozzuoli)	40.835	14.186	5-6	3.25
4	1538	9	29	Campi Flegrei (Pozzuoli)	40.835	14.186	5-6	3.25

The earthquake experienced by the convent over the years

5	1538	9	29	Campi Flegrei (Pozzuoli)	40.822	14.123	8	3.88
3	1560	5	11	Costa pugliese centrale	41.249	16.485	8	5.66
7	1561	7	31	Penisola sorrentina	40.685	14.717	8	5.56
4-5	1561	8	19	Vallo di Diano	40.563	15.505	10	6.72
5-6	1564	7		Campi Flegrei	40.835	14.186	5	3.12
5	1566	5	6	Campi Flegrei	40.835	14.186	5	3.12
4-5	1568	12	27	Campi Flegrei (Pozzuoli)	40.822	14.123	6	3.37
5	1570	4	30	Campi Flegrei (Pozzuoli)	40.835	14.186	6-7	3.5
6-7	1575	6	5	Napoli	40.849	14.25	5-6	3.25
5	1582	6	5	Campi Flegrei (Pozzuoli)	40.822	14.123	8	3.88
5	1601	8	10	Napoli	40.849	14.25	5	3.12
5	1627	7	30	Capitanata	41.737	15.342	10	6.66
5-6	1631	12		Area Vesuviana	40.817	14.309	5-6	3.25
3	1638	3	27	Calabria centrale	39.048	16.289	11	7.09
5	1646	5	31	Gargano	41.905	15.993	10	6.72
F	1654	7	24	Sorano	41.635	13.683	9-10	6.33
4-5	1657	1	29	Capitanata	41.726	15.393	8-9	5.96
5	1685	5		Penisola Sorrentina	40.722	14.731	5-6	4.73
5	1687	4	25	Penisola Sorrentina	40.628	14.485	6	4.63
8	1688	6	5	Sannio	41.283	14.561	11	7.06
3	1688	7	23	Capitanata	41.687	15.337	7-8	5.33
3	1688	8	14	Beneventano	41.208	14.669	6-7	4.86
5	1692	3	4	Irpinia	40.903	15.196	8	5.88
F	1693	1	8	Pollino	39.873	16.157	7	5.27
7	1694	9	8	Irpinia-Basilicata	40.862	15.406	10	6.73
F	1694	10	7	Penisola sorrentina	40.669	14.453	5-6	4.71
3	1694	10	9	Avellino	40.914	14.793	5-6	4.4
5	1702	3	14	Sannio-Irpinia	41.131	14.778	6-7	4.86
6	1702	3	14	Sannio-Irpinia	41.12	14.989	10	6.56
4-5	1702	4	2	Sannio-Irpinia	41.131	14.778	6-7	4.86
3-4	1703	1	14	Valnerina	42.708	13.071	11	6.92
3	1703	1	16	Appennino laziale-abruzzese				
3	1703	2	2	Aquilano	42.434	13.292	10	6.67
4-5	1706	11	3	Maiella	42.076	14.08	10-11	6.84

Appendix 1

5	1720	8	28	Cassinese	41.491	13.814	5-6	4.35
5	1731	3	20	Tavoliere delle Puglie	41.274	15.757	9	6.33
4-5	1731	10	17	Tavoliere delle Puglie	41.317	15.947	6-7	4.86
7	1732	11	29	Irpinia	41.064	15.059	10-11	6.75
3	1733	5	15	Puglia				
3-4	1735	1	26	Casertano	41.038	14.387	5	4.16
4	1737	3	31	Monti di Avella	40.92	14.661	7	5.1
3	1739	2	12	Tavoliere delle Puglie	41.462	15.545	5-6	4.4
4	1739	2	27	Benevento	41.131	14.778	5-6	4.4
4	1741	8	6	Irpinia	41.049	14.97	7-8	5.44
5-6	1742	8	17	Napoli	40.849	14.25	5-6	3.25
4-5	1743	2	20	Ionio settentrionale	39.847	18.774	9	6.68
6-7	1756	10	22	Napoletano	40.756	14.338	6-7	3.5
4-5	1760	12	23	Area vesuviana	40.801	14.404	6-7	3.5
4-5	1777	6	6	Tirreno meridionale				
4	1779	10	1	Napoletano	40.736	14.447	6	3.37
3	1779	12	12	Napoletano	40.814	14.343	6	3.37
F	1782	1	11	Benevento	41.131	14.778	5	4.16
NF	1783	2	5	Calabria meridionale	38.297	15.97	11	7.1
4	1783	3	28	Calabria centrale	38.785	16.464	11	7.03
5	1794	6	12	Irpinia	41.108	14.924	7	5.26
F	1794	6	15	Area vesuviana	40.786	14.367	4	2.87
7-8	1805	7	26	Molise	41.5	14.474	10	6.68
3	1805	10	13	Pianura Campana	41.002	14.393	7	5.1
F	1806	7	21	Cassinese	41.491	13.814	5-6	4.4
3-4	1806	8	26	Colli Albani	41.718	12.725	8	5.61
3	1814	11	25	Beneventano	41.131	14.778	5-6	4.4
3	1817	4	17	Potentino	40.576	15.763	4-5	3.97
F	1821	8	2	Calabria centrale	38.939	16.456	7	5.1
3	1821	11	22	Costa molisana	41.975	15.214	7-8	5.59
F	1826	2	1	Potentino	40.52	15.726	8	5.74
F	1826	10	26	Salento	40.502	17.433	6-7	5.22
NF	1828	2	2	Isola d'Ischia	40.745	13.899	8-9	4.01
3	1832	3	8	Crotonese	39.079	16.919	10	6.65

The earthquake experienced by the convent over the years

3-4	1836	4	25	Calabria settentrionale	39.567	16.737	9	6.18
5	1836	11	20	Appennino lucano	40.142	15.776	8	5.86
F	1841	2	21	Gargano	41.627	15.637	6-7	5.17
F	1846	8	8	Potentino	40.523	16.13	6-7	5.18
5	1851	8	14	Vulture	40.96	15.669	10	6.52
3-4	1851	8	14	Vulture	40.994	15.653	7-8	5.48
4	1853	4	9	Irpinia	40.818	15.215	8	5.6
2	1854	2	12	Cosentino	39.256	16.295	10	6.34
6	1857	12	16	Basilicata	40.352	15.842	11	7.12
F	1858	3	7	Campania meridionale	40.108	15.612	7-8	5.39
F	1858	3	7	Vibonati	40.111	15.674	4	3.7
3	1858	5	24	Tavoliere delle Puglie	41.092	16.192	4-5	4.35
F	1861	12	9	Torre del Greco	40.786	14.367	5-6	3.25
2	1867	8	15	Isola d'Ischia	40.746	13.909	4-5	2.99
3	1870	10	4	Cosentino	39.22	16.331	9-10	6.24
3	1872	10	8	Cosentino	39.412	16.309	5	4.72
2	1873	3	12	Appennino marchigiano	43.089	13.244	8	5.85
2-3	1873	7	12	Val Comino	41.686	13.778	7-8	5.38
4	1874	12	6	Val Comino	41.655	13.827	7-8	5.48
NF	1875	3	17	Costa romagnola	44.209	12.659	8	5.74
6-7	1875	12	6	Gargano	41.689	15.677	8	5.86
NF	1880	7	24	Isola di Ventotene	40.797	13.431	6	4.63
NF	1881	3	4	Isola d'Ischia	40.747	13.895	9	4.14
3	1881	9	10	Chietino	42.237	14.335	7-8	5.41
5	1882	6	6	Isernino	41.557	14.202	7	5.2
5	1883	7	28	Isola d'Ischia	40.744	13.885	9-10	4.26
2	1885	9	17	Benevento	41.147	14.861	5	4.26
2	1885	12	26	Molise	41.545	14.586	5-6	4.66
NF	1887	12	3	Calabria settentrionale	39.564	16.221	8	5.55
2	1889	12	8	Gargano	41.83	15.688	7	5.47
3-4	1893	1	25	Vallo di Diano	40.513	15.36	7	5.15
3-4	1895	2	1	Monti del Partenio	41.011	14.56	5	4.29
3	1895	8	9	Adriatico centrale	42.54	15.015	6	5.11
3-4	1901	7	31	Sorano	41.719	13.75	7	5.16

Appendix 1

F	1903	5	4	Valle Caudina	41.034	14.557	7	4.69
3	1903	12	7	Beneventano	41.04	14.527	4-5	4.14
4-5	1905	3	14	Avellinese	40.951	14.807	6-7	4.9
F	1905	8	25	Valle Peligna	42.019	14.026	6	5.15
3-4	1905	9	8	Calabria centrale	38.811	16	10-11	6.95
3-4	1905	11	26	Irpinia	41.134	15.028	7-8	5.18
3	1907	12	18	Monti Picentini	40.845	14.892	5-6	4.52
2	1908	12	28	Stretto di Messina	38.146	15.687	11	7.1
4	1910	6	7	Irpinia-Basilicata	40.898	15.421	8	5.76
4	1913	10	4	Molise	41.513	14.716	7-8	5.35
5	1915	1	13	Marsica	42.014	13.53	11	7.08
NF	1915	9	23	Marsica	42.415	13.076	6	5.07
F	1916	7	3	Isola di Stromboli	38.9	15.291	5-6	4.66
2-3	1919	10	22	Anzio	41.436	12.535	6-7	5.22
3	1922	12	29	Val Roveto	41.793	13.632	6-7	5.24
3	1923	11	8	Appennino campano-lucano	40.677	15.449	6	4.73
3	1924	3	26	Sannio	41.341	14.786	4	4.06
3-4	1924	5	9	Irpinia	40.893	14.772	4	4.71
2	1925	9	24	Molise occidentale	41.719	14.188	7	5.26
4	1927	5	25	Sannio	41.25	14.624	6	4.98
NF	1927	12	26	Colli Albani	41.7	12.701	7	4.89
4	1930	4	27	Salernitano	40.769	14.7	7	4.98
7	1930	7	23	Irpinia	41.068	15.318	10	6.67
3	1930	10	30	Senigallia	43.689	13.385	8	5.83
3	1936	4	3	Valle Caudina	41.041	14.585	5-6	4.25
3	1948	8	18	Gargano	41.575	15.748	7-8	5.55
2	1956	9	22	Gargano	41.584	15.721	6	4.64
6-7	1962	8	21	Irpinia	41.23	14.953	9	6.15
NF	1967	12	9	Adriatico centrale	42	16.41		4.36
4	1971	5	6	Irpinia	41.169	15.275	6	4.83
F	1971	11	29	Alta Val d'Agri	40.336	15.773	5	4.5
3	1973	8	8	Appennino campano-lucano	40.668	15.436	5-6	4.75
4	1975	6	19	Gargano	41.689	15.677	6	5.02
2	1977	7	24	Irpinia	41.097	15.02	5-6	4.37

The earthquake experienced by the convent over the years

2	1978	2	8	Irpinia	41.106	14.991	5-6	4.44
4	1979	9	19	Valnerina	42.73	12.956	8-9	5.83
3	1980	6	14	Marsica	41.905	13.696	5-6	4.96
7	1980	11	23	Irpinia-Basilicata	40.842	15.283	10	6.81
4	1980	12	3	Irpinia-Basilicata	40.729	15.476	6	4.83
3-4	1981	1	9	Irpinia-Basilicata	40.699	15.636	5-6	4.36
5-6	1981	2	14	Monti di Avella	40.992	14.62	7-8	4.88
4	1982	3	21	Golfo di Policastro	39.841	15.747	7-8	5.23
NF	1984	4	29	Umbria settentrionale	43.262	12.525	7	5.62
5-6	1984	5	7	Monti della Meta	41.667	14.057	8	5.86
3	1996	4	3	Irpinia	40.661	15.454	6	4.9
4	1999	10	9	Area vesuviana	40.789	14.377	5	3.24
3-4	2002	11	1	Molise	41.741	14.843	7	5.72
2	2003	6	1	Molise	41.661	14.821	5	4.44
F	2016	8	24	Monti della Laga	42.698	13.233	10	6.18
F	2016	10	26	Valnerina	42.904	13.09		6.07
4-5	2016	10	30	Valnerina	42.83	13.109		6.61

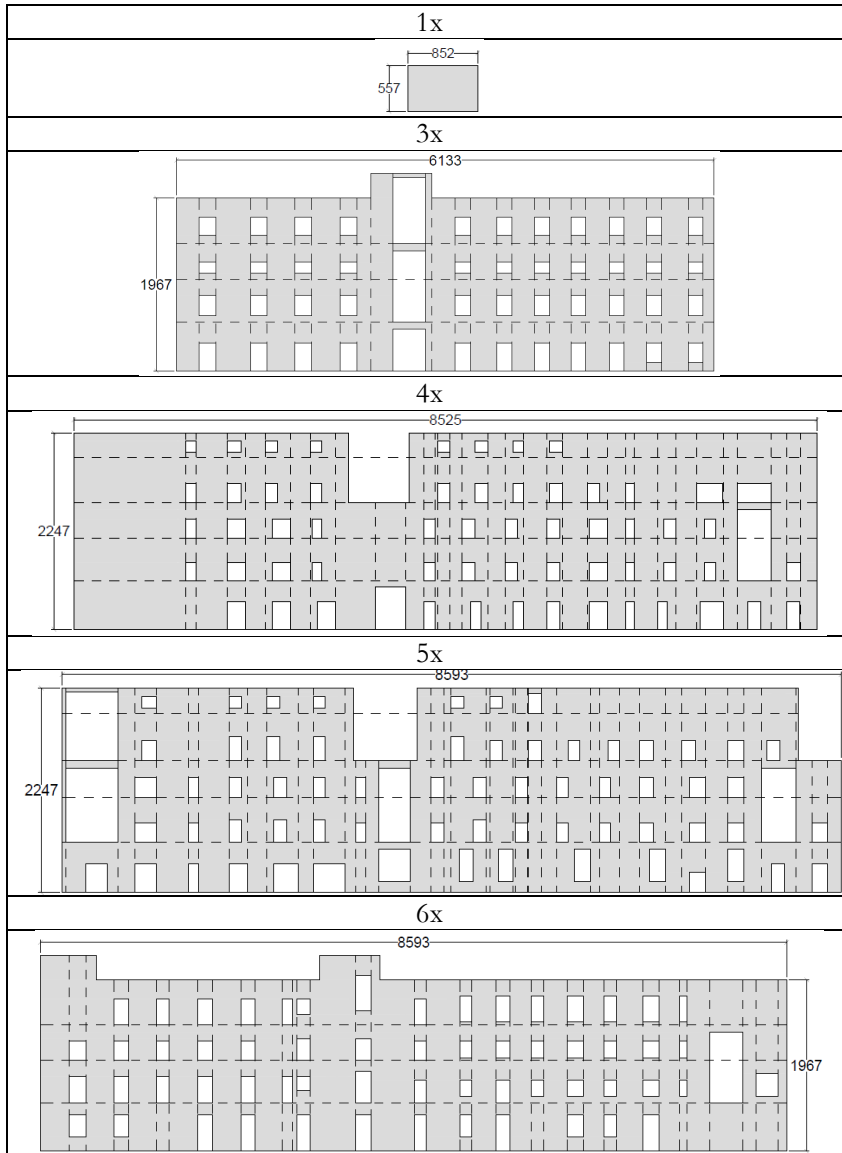
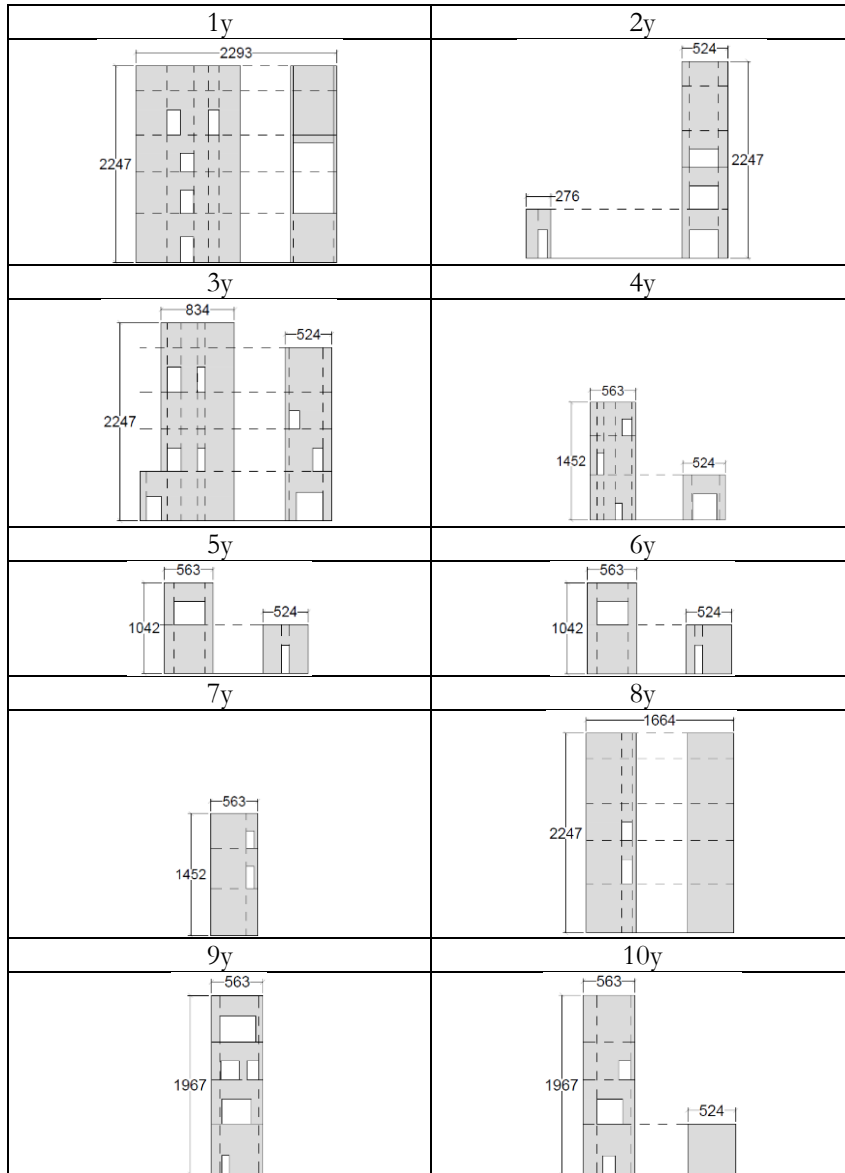


Figure A2.2. Construction 0: wall alignments – x direction.

Wall alignments



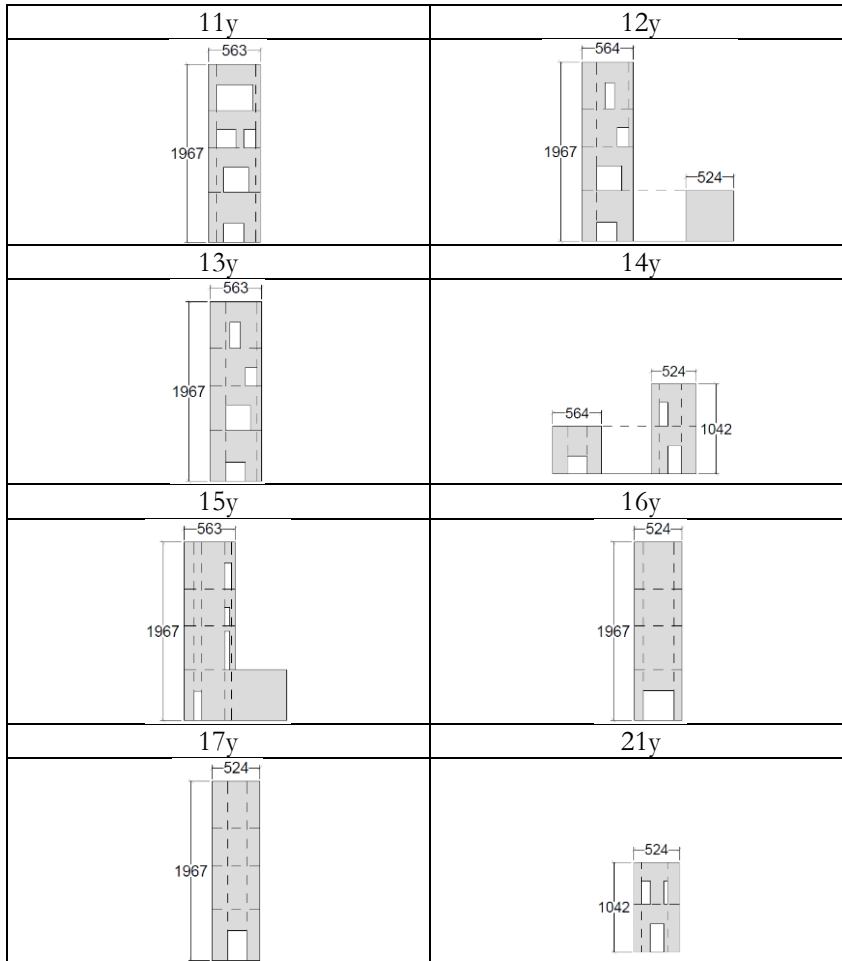


Figure A2.3. *Construction 0*: wall alignments – y direction.

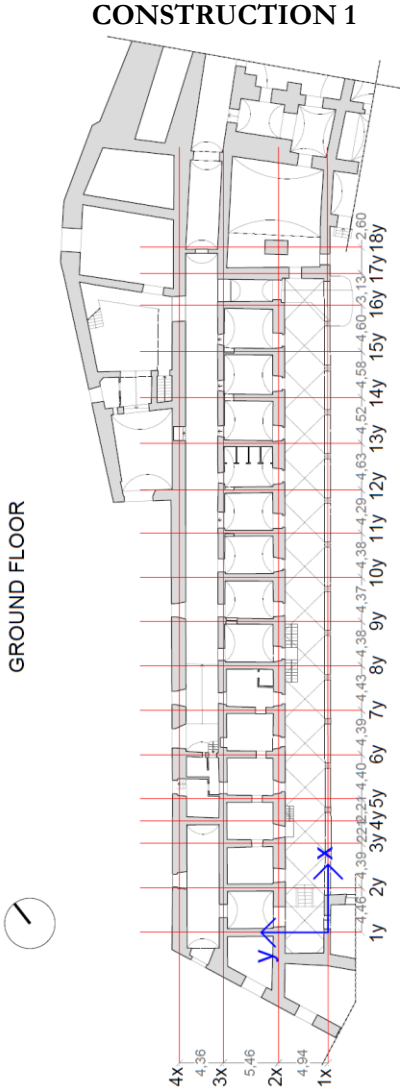
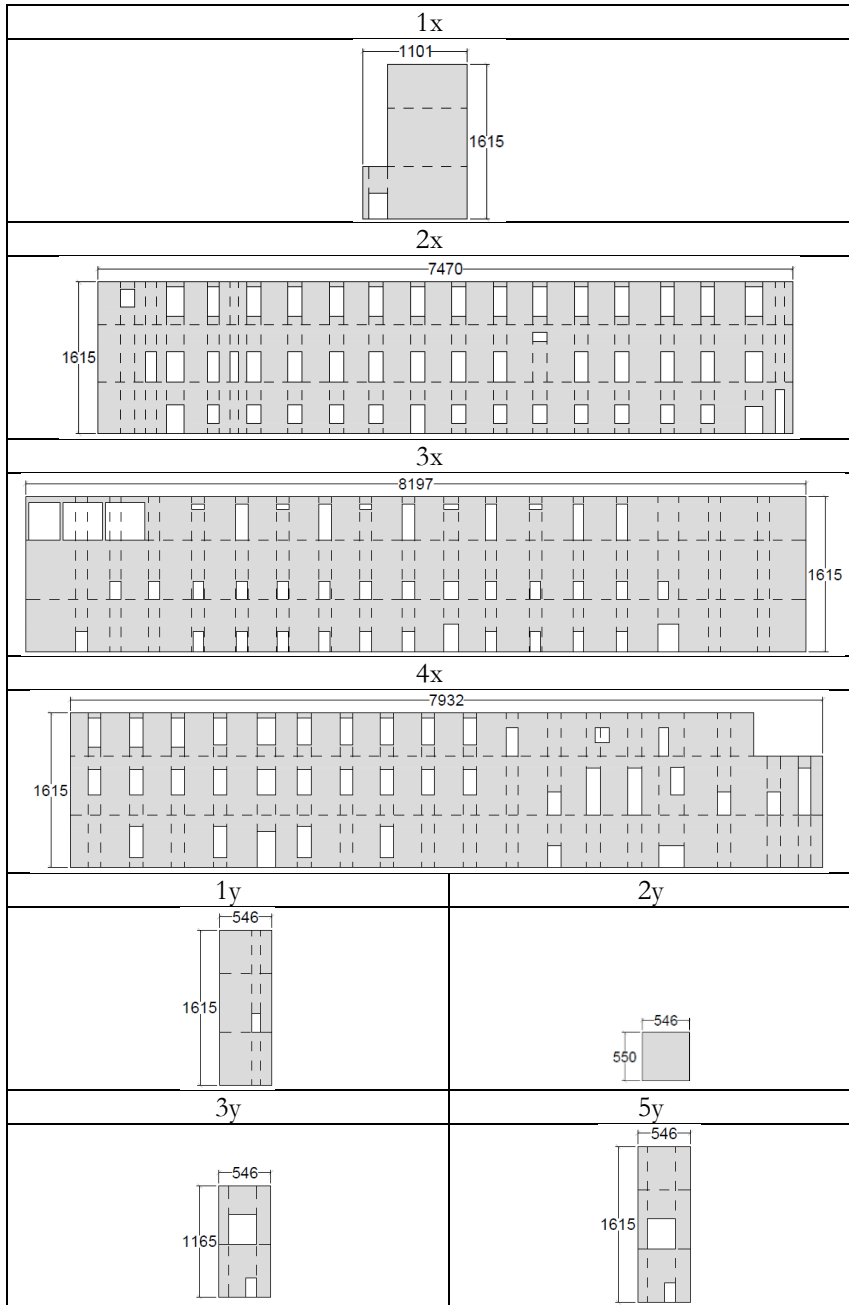


Figure A2.4. Construction 1: wall alignments – plan.

Appendix 2



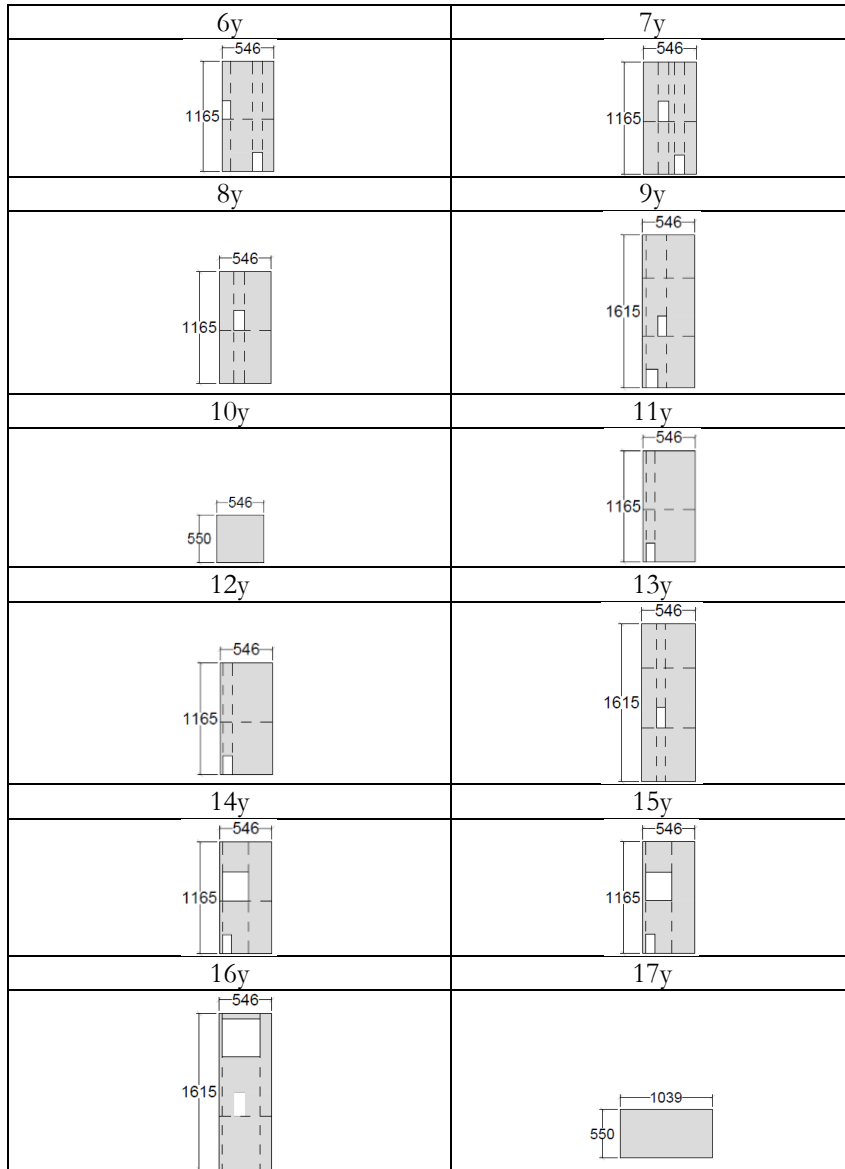


Figure A2.5. *Construction 1*: wall alignments.

CONSTRUCTION 2

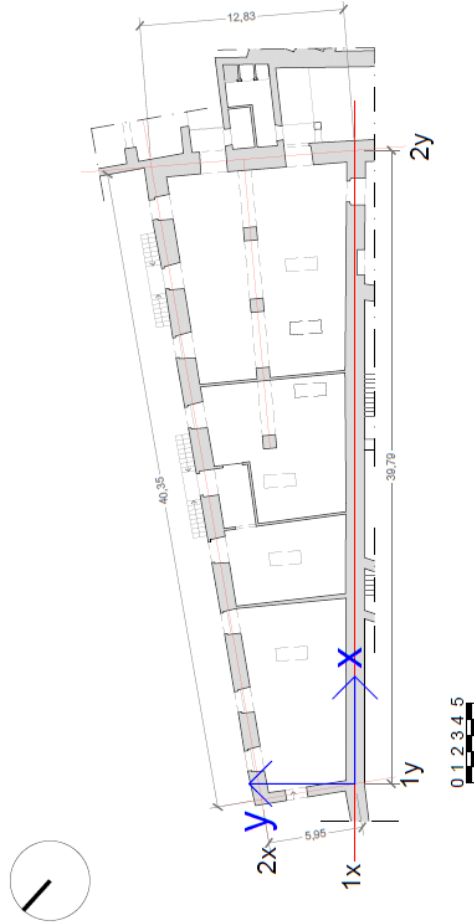


Figure A2.6. *Construction 2*: wall alignments – plan.

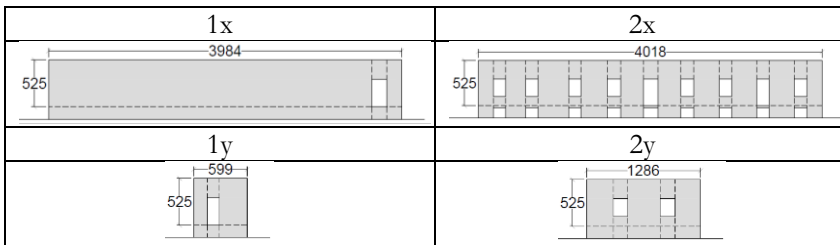


Figure A2.7. *Construction 2*: wall alignments.

CONSTRUCTION 4

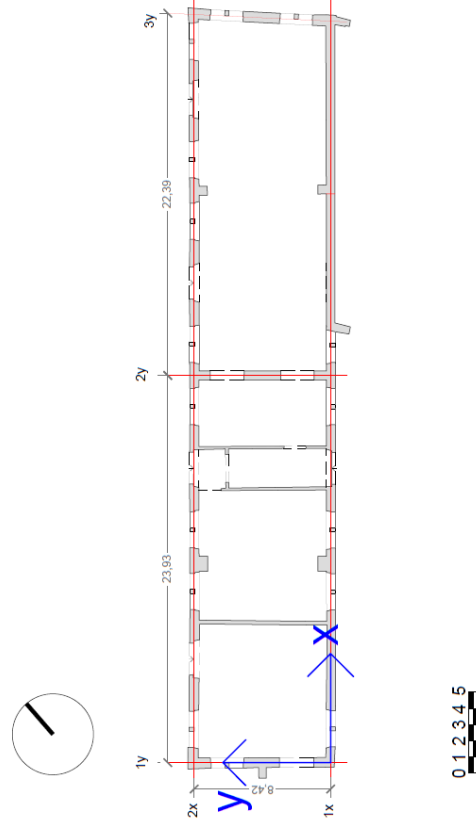


Figure A2.8. *Construction 4*: wall alignments – plan.



Figure A2.9. *Construction 4*: wall alignments.

CONSTRUCTION 6

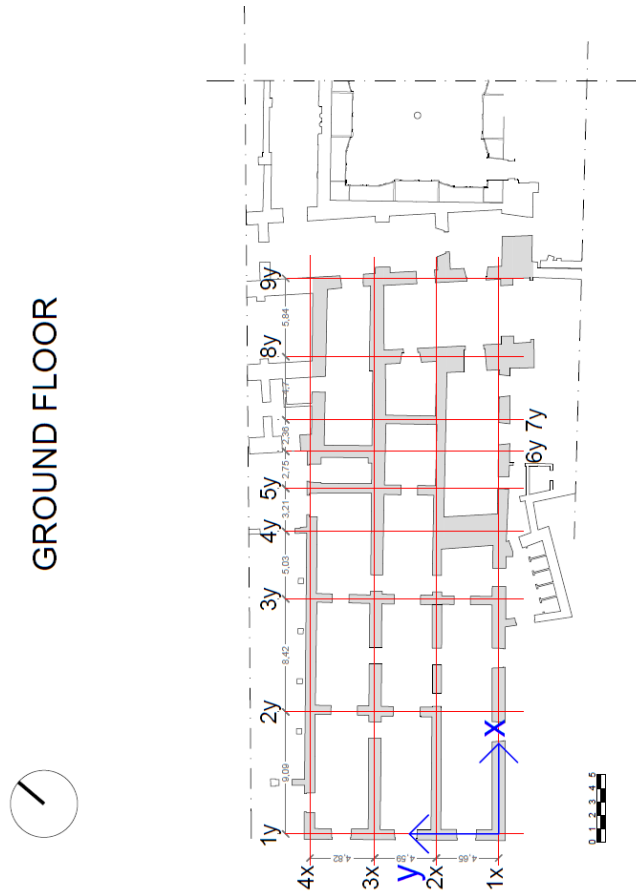


Figure A2.10. Construction 6: wall alignments – plan.

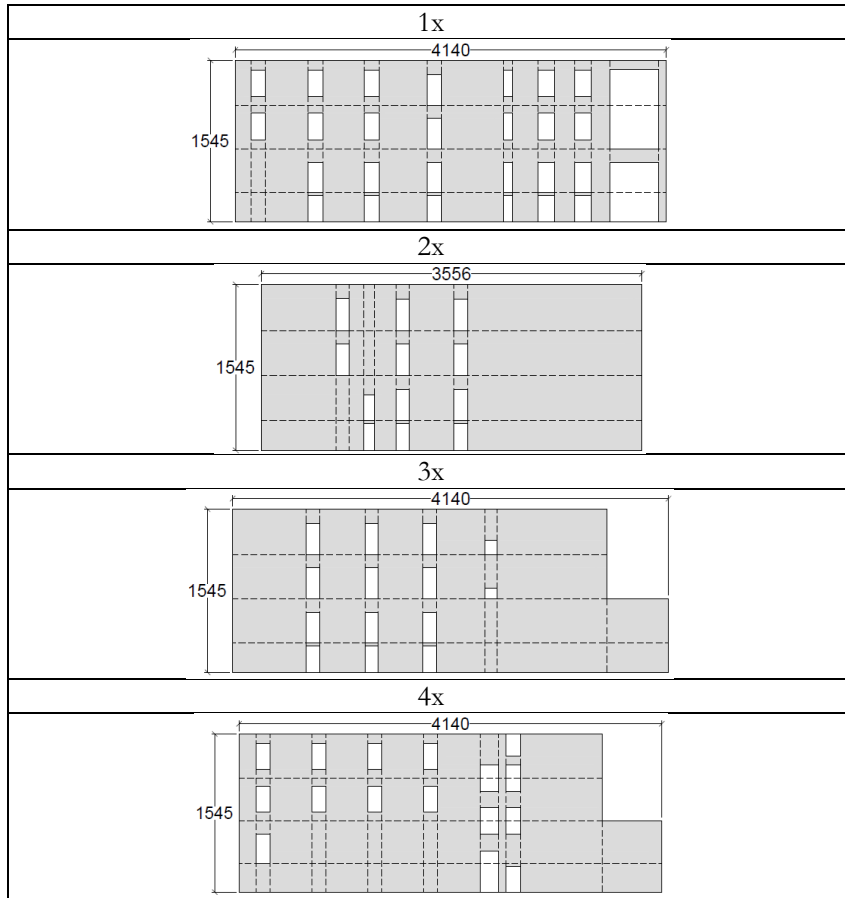


Figure A2.11. *Construction 6*: wall alignments – x direction.

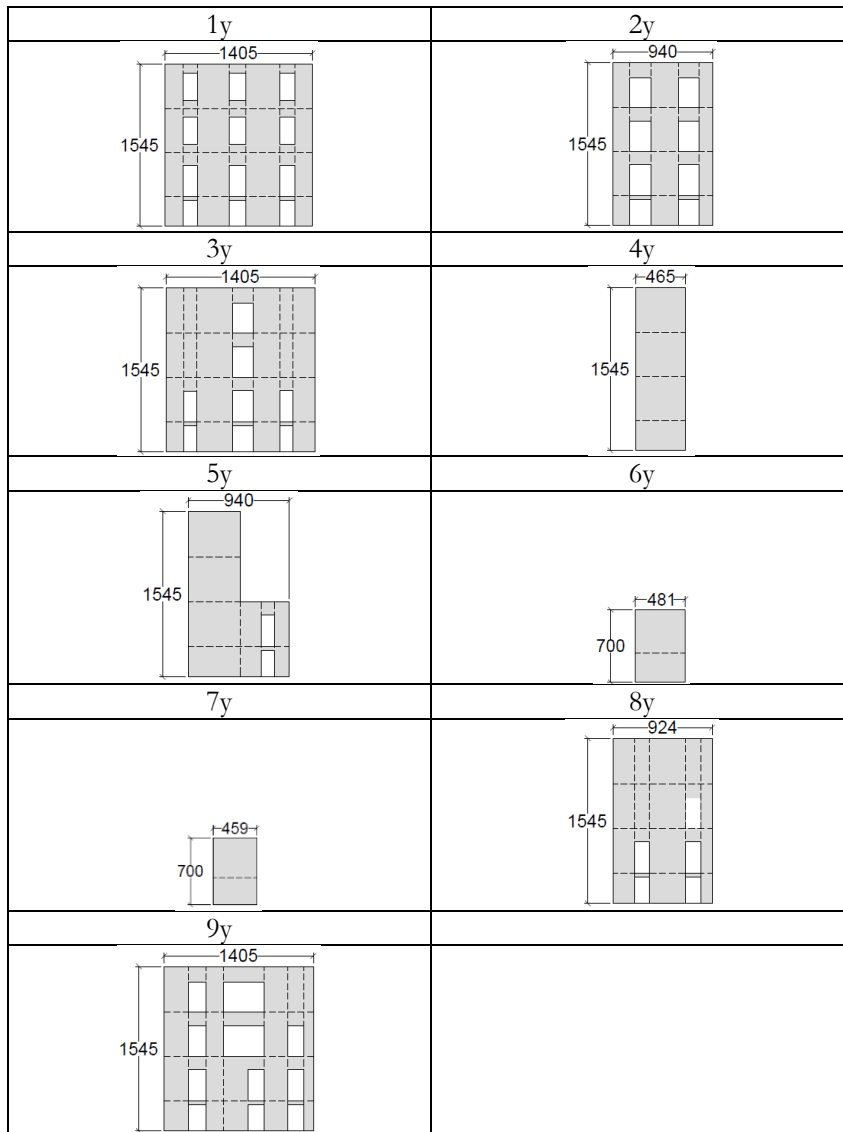


Figure A2.12. *Construction 6*: wall alignments – y direction.

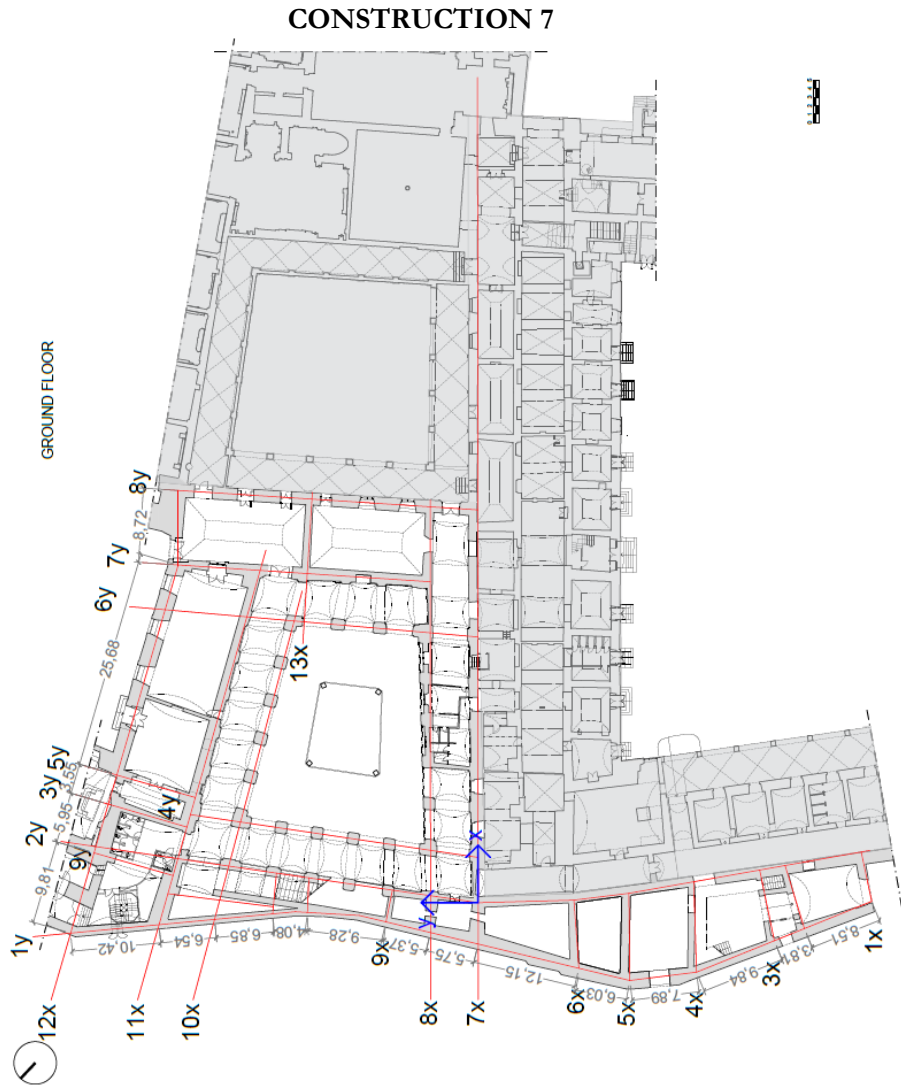
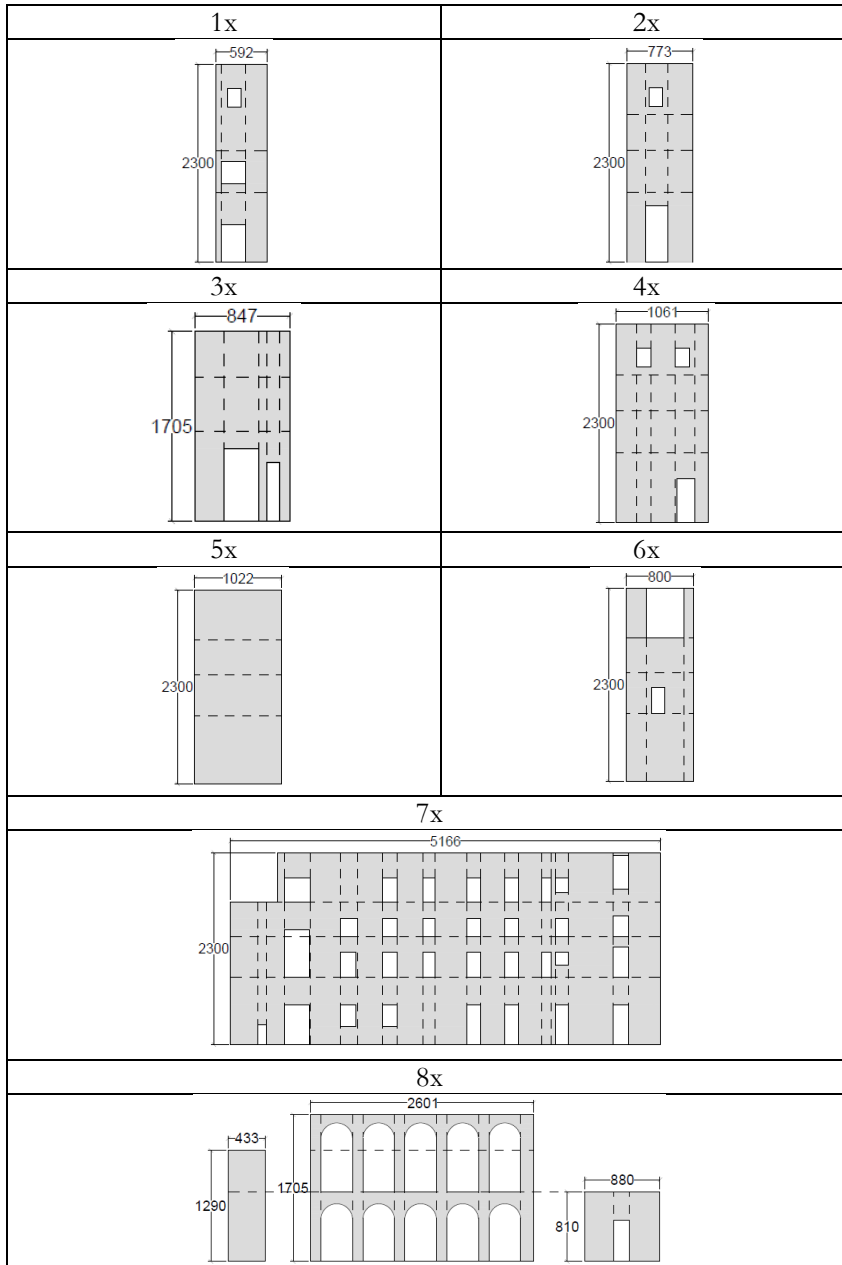
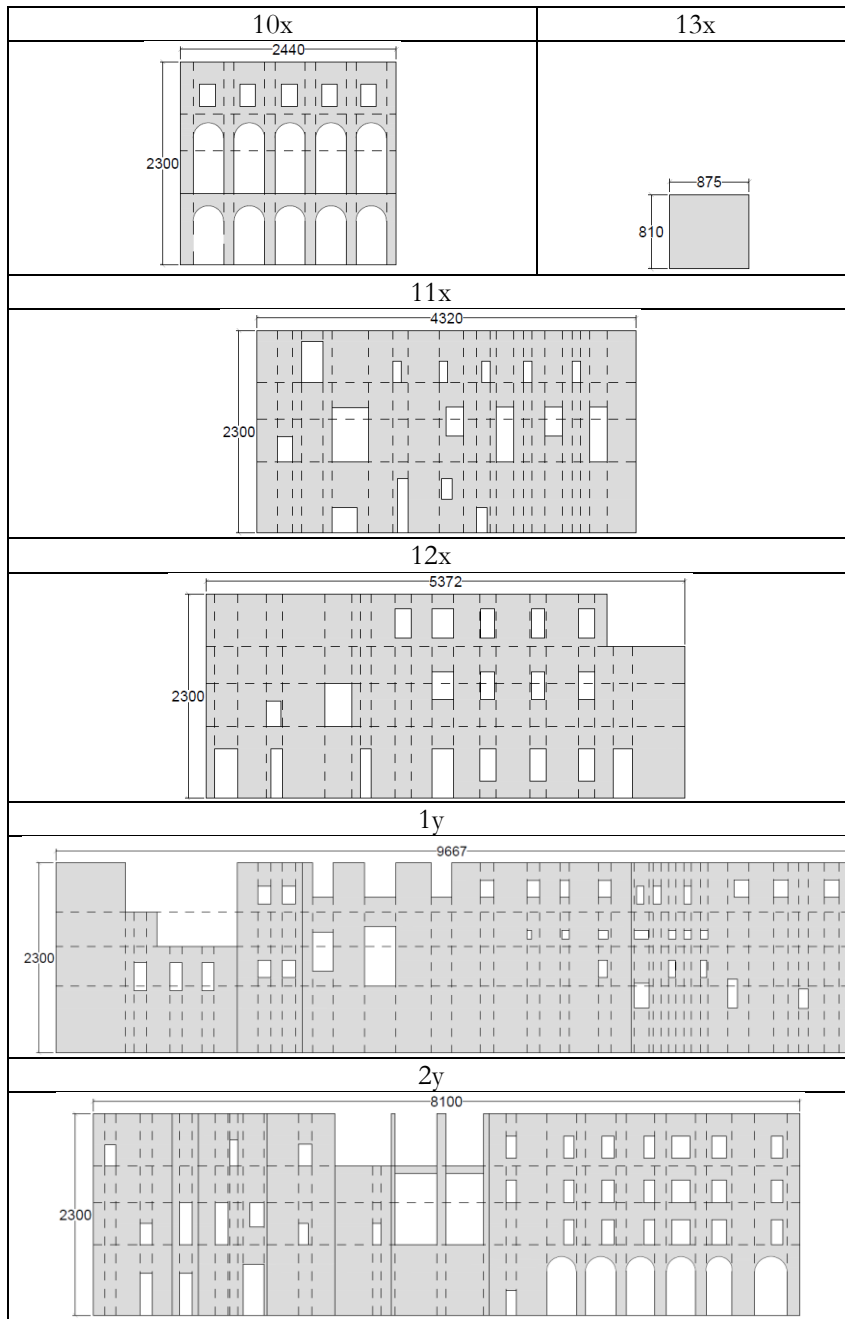


Figure A2.13. *Construction 7*: wall alignments – plan.

Appendix 2



Wall alignments



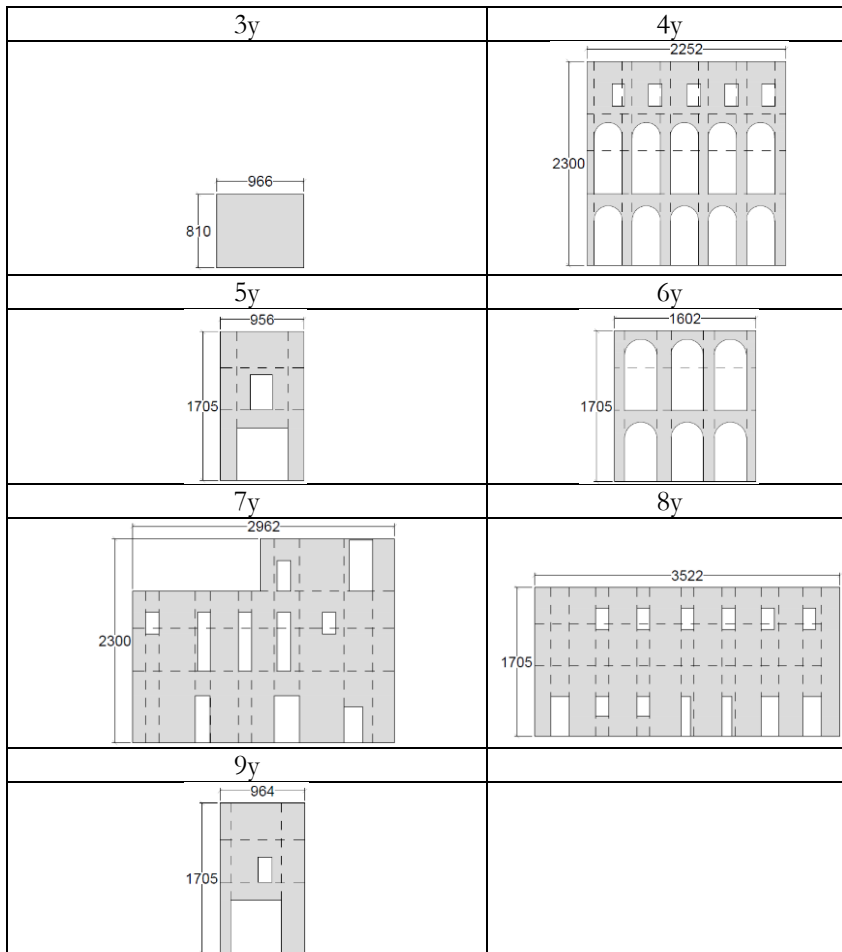


Figure A2.14. *Construction 7*: wall alignments.

Appendix 3

The Case Study of St. Carlo all'Arena Convent in Naples

This Chapter deals with the structural assessment of St. Carlo all'Arena Convent in Naples, a masonry building located in the historical centre of Naples, within San Carlo all'Arena neighbourhood. Like St. Domenico Maggiore Convent, St. Carlo all'Arena Convent stands as a significant example of complex building, resulting from the addition of various constructions in different periods, ranging from the 17th, when the initial section was constructed, to the 20th century. To analyse the structural behaviour of the structure and the seismic vulnerability of this complex, the procedure outlined in previous chapters and applied to the St. Domenico Convent Case study has been employed. The Chapter provides an in-depth historical account of the evolution of the complex, detailing construction phases, as documented in Polcari (2018) and addressing the structural challenges the convent encountered following the 2016 Norcia Earthquake, which led to the closure of the Third level. Following that, preliminary considerations about the alignment of the Convent to the rules of art are provided. For the seismic vulnerability assessment, two distinct assumptions has been considered: one that considers no interaction between the individual constructions, and another that assumes perfect interaction among them. The results of the non-linear static analyses conducted on each construction are presented and compared with the analyses of the entire convent. Additionally, to gain a deeper insight into the structural behaviour of the complex, 2D wall analyses have been performed using non-linear static analysis, with a distribution of forces proportional to the masses. These results, presented in terms of capacity curves, are further compared to the capacity curve of the 3D structure.

A3.1 Description of the Case Study

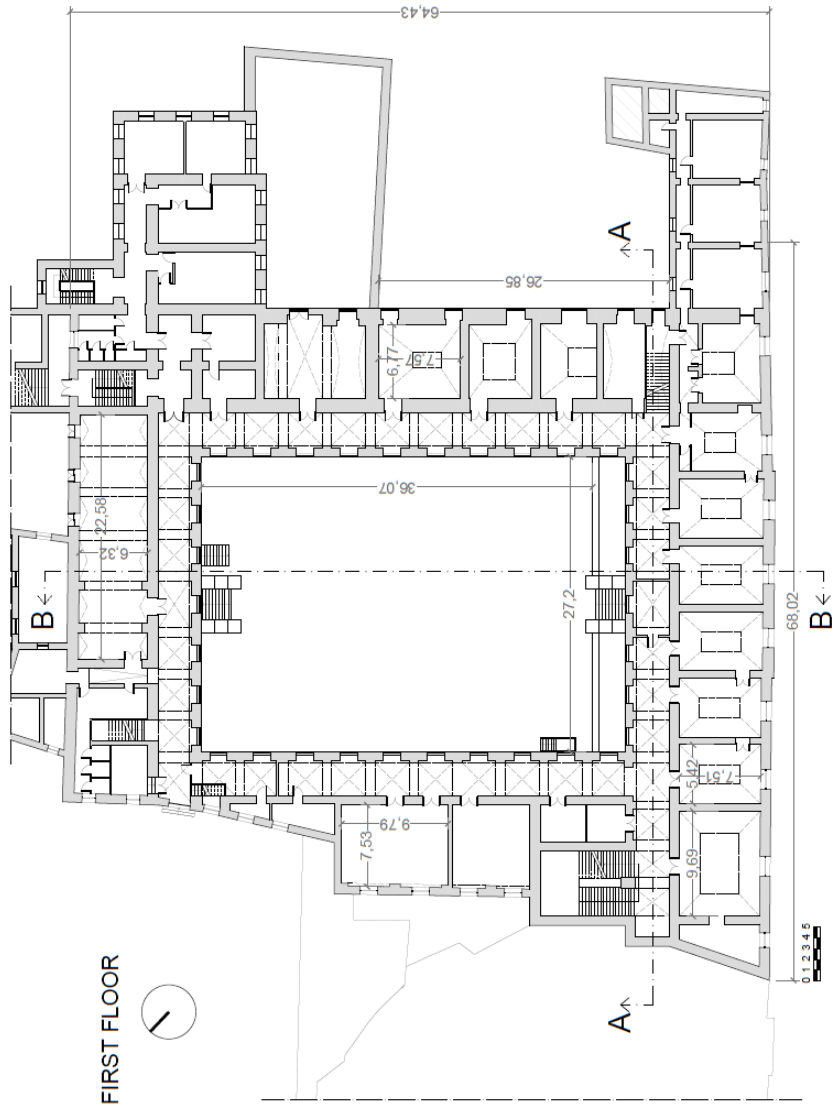
San Carlo all'Arena Convent (Figure A3.1) is a masonry building located in the historical centre of Naples, within San Carlo all'Arena neighbourhood. This Convent features a rectangular floor plan with maximum dimensions of 68 x 65 m, inclusive of a courtyard spanning 27 x 36 m, as depicted in Figure A3.2a. Its overall height varies due to its location near a hill, with the maximum height reaching 28.20 m and the minimum at 24 m. This variation in height is detailed in the cross-sections provided in Figures A3.2b and A3.2c:

- The Southern part facing via Foria and the Eastern part of the building are located at the lowest elevation. These two parts consist of four levels, one of which is a mezzanine level, resulting in an overall height of 28.20 m.
- The remaining parts, given the hilly terrain, have a lower height of 24.0 m, with three levels and a basement. The basement serves as a mezzanine for the Southern and Eastern parts.

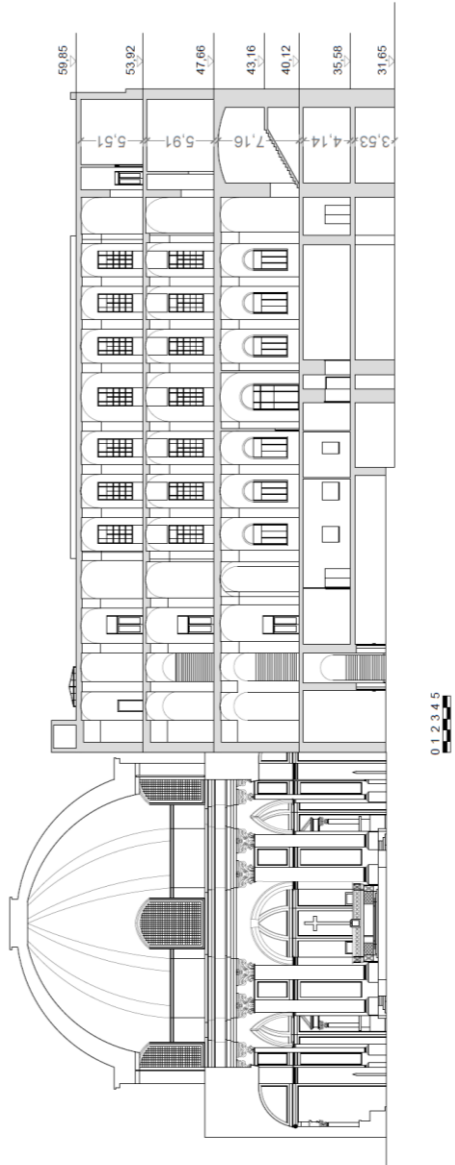
The walls are made in tuff masonry, except for the walls facing the courtyard at the highest level, which are made of airbrick masonry. The thickness of the walls varies, ranging from 155 cm at the first level to 30 cm at the highest level. The building's floors feature a variety of vault types, including cloister, barrel and cross vaults, and the slabs are composed of steel beams.



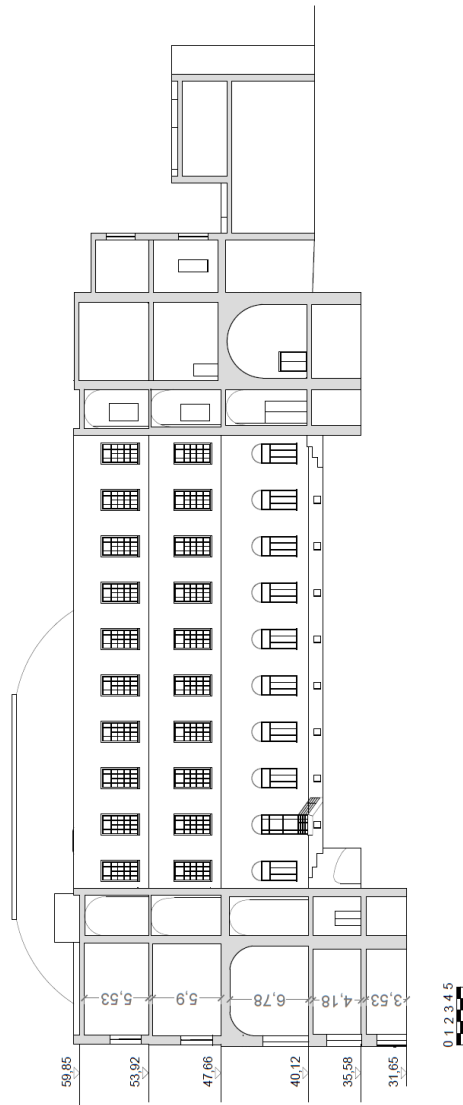
Figure A3.1. San Carlo all'Arena Convent in Naples.



(a)



(b)



(c)

Figure A3.2. Plan (a) and Cross-Sections A-A(b) and B-B (c).

The building case study is connected to a construction of varying height on its Eastern side and to a church that dates back to 1632, coinciding with the initial construction phase of the Convent, on its Western side (Figure A3.3).



Figure A3.3. Façade facing Via Foria: the adjacent constructions.

This church, designed by Fra Nuvolo, a Dominican architect, boasts an oval floor plan encircled by six chapels. Notably, its dome, as illustrated in Figure A3.4, features a lowered design akin to the Pantheon (Maio et al., 2016 [63]).



Figure A3.4. Dome of the church: internal (a) and external view (b).

The link between the Convent and the church is not only of historical significance but also physical, as highlighted in Figure A3.5.



Figure A3.5. Connection between the Convent and the Church.

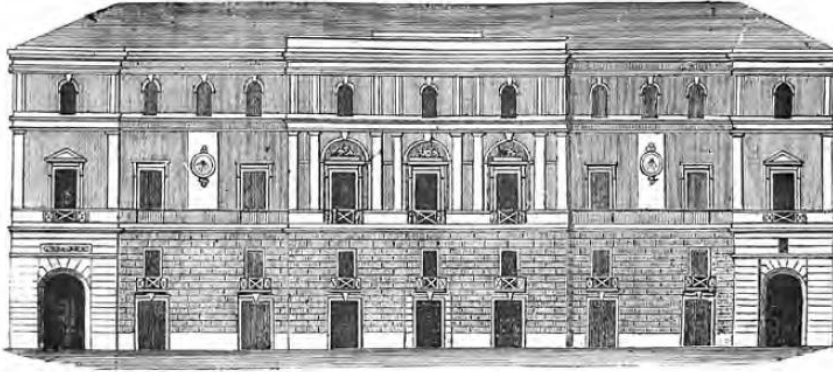
A3.2 Historical evolution of the Convent

This Section delves into the historical evolution of the convent, spanning from its initial construction in the 17th century to developments in the 20th century. Specifically, it provides a detailed account of the construction phases, as outlined in Polcari (2018 [63]), and documents the structural challenges the convent encountered following the 2016 Norcia Earthquake, which necessitated the closure of the Third level. Additionally, it offers an insight into the diverse functions and purposes the convent has served over time, a reflection of its complex evolution.

A3.2.1 The construction phases as outlined in Polcari (2018)

This section focuses on the construction phases as outlined in Polcari (2018 [63]). The origins of the convent can be traced back to the 17th century when the initial section was constructed under the auspices of the Cistercians. In 1681, a second segment was initiated, and by 1715, it had been completed. In 1755, a third portion of the cloister was erected, coinciding with the completion of the façade of the adjoining church. In 1792 the Cistercians left the church and the convent. During the ten years of French occupation, the church served as barn, and the convent was utilized as military garrison. The year 1836 marked a pivotal moment following a cholera outbreak, leading to a comprehensive restoration project supervised by Francesco De Cesare. This endeavour significantly transformed the convent. To mitigate the potential structural stresses from

the hilly terrain, the section facing Via Foria was advanced and separated from the rest of the complex. Additionally, the cloister courtyard received reinforcement via buttresses, and a third level was introduced (Figure A3.6).



(a)



(b)

Figure A3.6. Façade on via Foria (De Cesare F., 1837. *Sull'origine delle lesioni della chiesa di San Carlo Borromeo in Napoli e suo progetto di ricostruzione*) (a); Current state of the Facade on via Foria (b).

In 1861, the structure was provisionally occupied by the National Guards of General Cosenz, under the orders of Garibaldi. In 1867, due to the law of 7 July 1866, which suppressed the convents and churches of certain

religious orders, the convent was permanently closed, while the church remained open for worship, still officiated by the Piarist Fathers. The “Convitto Comunale Liceo Ginnasio Domenico Cirillo” (1869 - 1896) was established within the convent. In 1896, the “Giambattista Della Porta” Technical and Nautical Institute took over. The early 20th century ushered in further expansions, with notable renovations in 1904-06 and 1908, including the reconstruction of the staircase. A major turning point occurred in 1923 after a devastating church fire. During this period, a fourth and final level was incorporated into the convent’s architecture.

Figures A3.7a and A3.7b visually represent the historical analysis detailed in this section by employing distinct colours to demarcate the various construction phases.

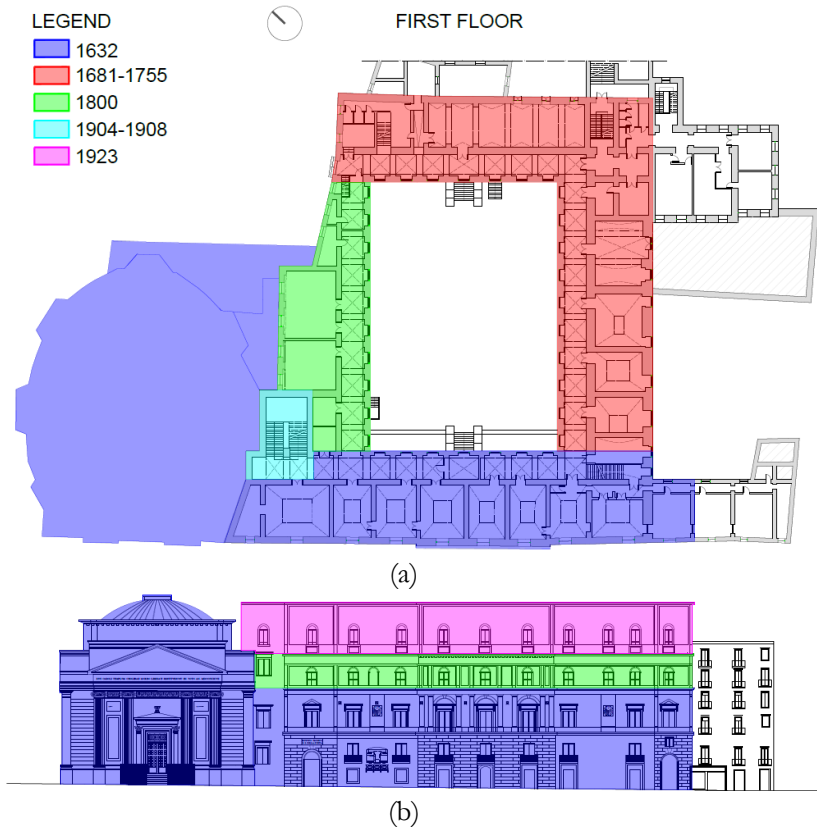


Figure A3.7. Historical evolution of the Convent: plan (a) and façade (b).

A3.2.2 The period following the 2016 Norcia Earthquake

Based on interviews with school staff and information from newspaper articles (Figure A3.8) conducted by the author during the survey, it becomes evident that the closure of the upper level of the facility, which houses Liceo Cuoco, occurred as a response to significant wall cracks following the 2016 Norcia earthquake. As reported by Metronapoli.it, the E-Magazine of the Metropolitan City of Naples, the extensive maintenance efforts directed at reopening the upper level of the facility began in December 2017 and were initially slated for completion by February 2018.



Figure A3.8. Newspaper articles: il Corriere del Mezzogiorno (8/11/2016) (a) Metronapoli.it (14/12/2017).

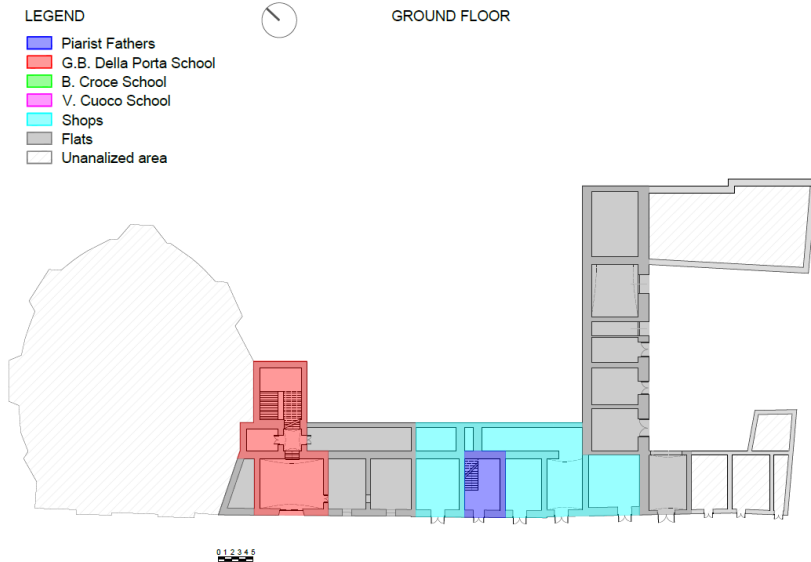
A3.2.3 The different occupancy of the Convent

As described in the previous Sections, over the years, St. Carlo all'Arena convent has undergone various changes in terms of its occupancy. Initially, it served as a Convent for the Cistercians. In 1792 the Cistercians left the church and the convent. During the ten years of French occupation, the church served as barn, and the convent was utilized as military garrison.

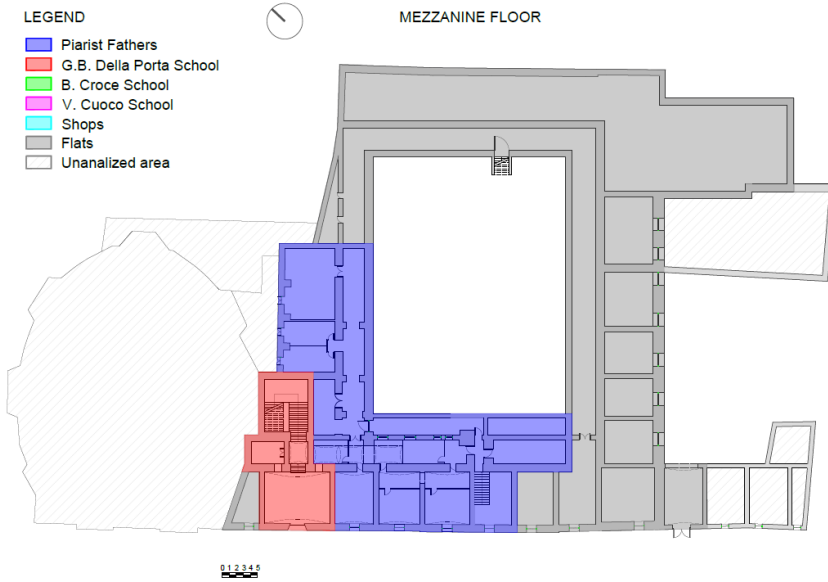
However, following the suppression of monasteries in 1865, the convent was partitioned among several different institutions. Nowadays, the convent continues to be occupied by various institutions, each serving distinct purposes. A graphical representation of the institutions occupying different floors within the convent is provided in Figure A3.9. As it can be observed, *Croce, Della Porta and Cuoco Schools* (depicted in green, red and pink, respectively) occupy a substantial portion of the architectural complex, extending their presence across the ground floor, the first, mezzanine, second, and third floors.

Piarist Father (highlighted in blue) maintain a significant area within the mezzanine floor. Furthermore, a portion of the ground floor and mezzanine floor is designated for *shops* (indicated in sky-blue) and *flats* (in grey).

Table A3.1 provides a comprehensive account of the area occupied by each institution on the various floors of the convent.

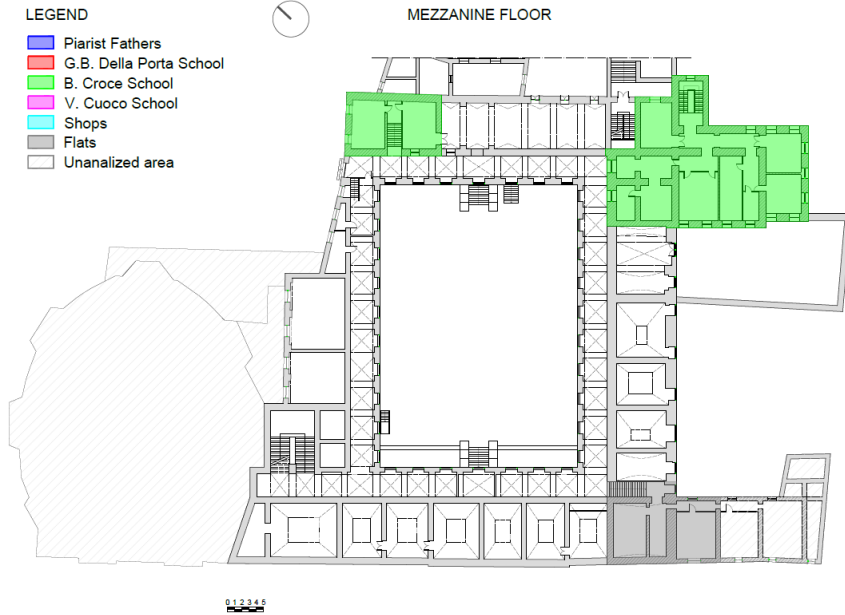


(a)



(c)

The Case Study of St. Carlo all'Arena Convent in Naples



(e)



(f)



(g)

Figure A3.9. Different occupancy: ground floor (a); mezzanine floor (b); first floor (c); mezzanine floor (d); second floor (e); third floor (f); and façade (g).

Table A3.1. Different occupancy of St. Carlo all'Arena convent.

Occupancy	Ground Floor	Mezzanine Floor	First Floor	Mezzanine Floor (2)	Second Floor	Third Floor
	[m ²]	[m ²]	[m ²]	[m ²]	[m ²]	[m ²]
Piarist Fathers	57	796	0	0	0	0
Croce School	0	0	2.034	544	0	0
Della Porta School	209	209	878	0	2.870	0
Cuoco School	0	0	0	0	0	2.730
Shops	341	0	0	0	0	0
Flats	652	1.767	0	165	0	0
TOT	1.259	2.772	2.912	708	2.870	2.730

A3.3 Preliminary considerations: the rules of art

A3.3.1 Structural system: preliminary considerations

About the structural system of the convent, the following observations are made.

- The building has rectangular plan, with maximum dimensions of 68 x 65 m, inclusive of a courtyard spanning 27 x 36 m.
- Its overall height varies due to its location near a hill, with the maximum height reaching 28.20 m and the minimum at 24 m. In particular, the Southern part facing via Foria and the Eastern part of the building are located at the lowest elevation. These two parts consist of four levels, one of which is a mezzanine level, resulting in an overall height of 28.20 m. The remaining parts, given the hilly terrain, have a lower height of 24.0 m, with three levels and a basement. The basement serves as a mezzanine for the Southern and Eastern parts. The structure is *not regular in height*.
- The thicknesses of the walls at various levels are respectful of the rules of arts, see Sections A3.3.2 and A3.3.3.
- The construction exhibits a regular arrangement of the openings with a vertical alignment, except for wall 18y where an irregular arrangement of openings is evident. This irregularity is believed to

have resulted from the addition of openings in subsequent years. See Section A3.3.4 for a detailed analysis.

- The transverse walls are arranged with regular spacing, not exceeding 10 m, especially on the ground floor, mezzanine floor and the first floor. Nevertheless, this spacing is exceeded on the second and third floor.
- The lowered cloister vaults of the first floor are not respectful of the rule suggested by Breyman [8] which recommends that they should remain unloaded. This is due to the addition of another level occupied by the Della Porta School in later years.
- The slabs with steel beams do not adhere to the historical practice, which prescribed that inter-spaces should be at least $L/30$, where L represents the span length.
- The walls facing the courtyard at the third level are made in airbrick, and they bear the vertical load and the horizontal thrust of tile vaults. This deviates from established architectural principles.

A3.3.2 On the stability of the masonry walls as suggested in Rondelet (1802)

Table A3.2 offers a comparative analysis of the slenderness of the walls of the analysed Convent in relation to the limit proposed by Rondelet for walls with low stability. Additionally, comparisons between the wall thicknesses and the minimum values suggested by Colombo in his Manual of Engineer are given. In particular, it can be observed that the slenderness of the walls on various floors is lower or equal to the value recommended by Rondelet for wall with low stability. However, only in few cases the values exceed this limit, specifically on the first floor without mezzanine (first floor (2)), second floor and third floor, standing at 15, 18 and 20 respectively (see Figure A3.10). Regarding wall thickness, distinctions are made between internal (t_{int}) and external walls (t_{ext}). In few instances, the thickness of walls is not respectful of the rules suggested by Colombo, with differences ranging from 5 cm (evident on the first floor) to 15 cm (found on the third floor).

Table A3.2. Comparison between wall thickness and the rules of art.

Level	San Carlo all'Arena Convent				Rondelet (1802)	Colombo (1877)	
	t_{int}	t_{ext}	h_0	h_0/t	$(h_0/t)_{low}$	t_{int}	t_{ext}
[-]	[cm]	[cm]	[cm]	[-]	[-]	[cm]	
Ground Floor	55-125	65-155	393	6-3		65	85
Mezzanine Floor	55-125	65-155	454	8-3		65	85
First Floor (1)	65-100	65-100	439	7-4		55	75
First Floor (2)	50-95	65-155	754	15-5	12	55	65
Mezzanine Floor	65-100	65-100	315	5-3		55	65
Second Floor	35-95	55-95	626	18-7		45	55
Third Floor	30-95	50-85	593	20-6		45	45

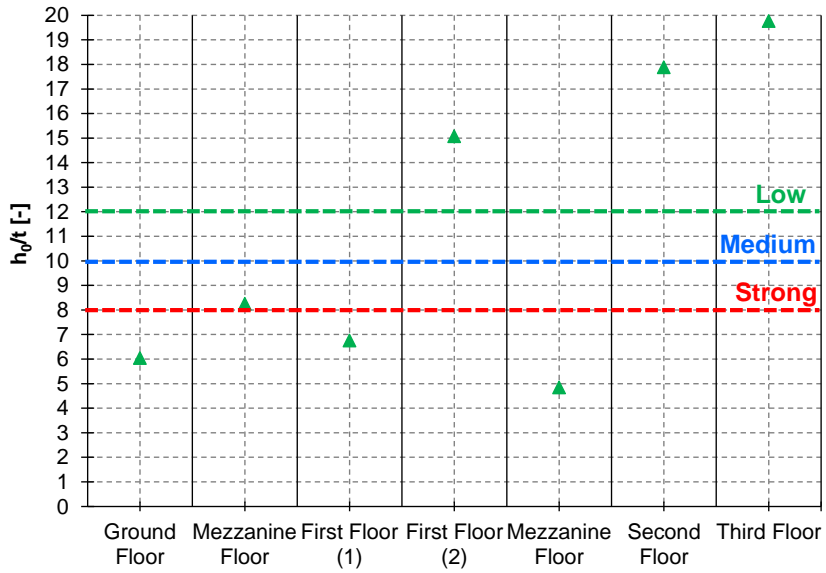


Figure A3.10. Comparison between maximum slenderness and the limit suggested by Rondelet (1802).

A3.3.3 In-plan area ratio A_w/A_{tot}

Figure A3.11 gives a histogram containing the values of the in-plan ratios A_w/A_{tot} , $A_{w,x}/A_{tot}$, $A_{w,y}/A_{tot}$ for each floor of the analysed structure. By comparing the ratios A_w/A_{tot} (in green) of the analysed structure with those computed by Rondelet for notable monuments, such as Bourse de Commerce, market grain, in Paris (8,4%), Notre Dames in Paris (14%), Basilica of S. Maria del Fiore (20%), the Pantheon (23%) and Dome of Les Invalides (27%), it becomes evident that the analysed construction is respectful of the rules of art. Additionally, the ratios $A_{w,x}/A_{tot}$ (in red) and $A_{w,y}/A_{tot}$ (in blue) exceed the minimum value prescribed by EC8 (2%) and NTC18 (3.5%). However, in some instances, these ratios fall below the minimum value suggested by Lourenco et al. (10%). Specifically:

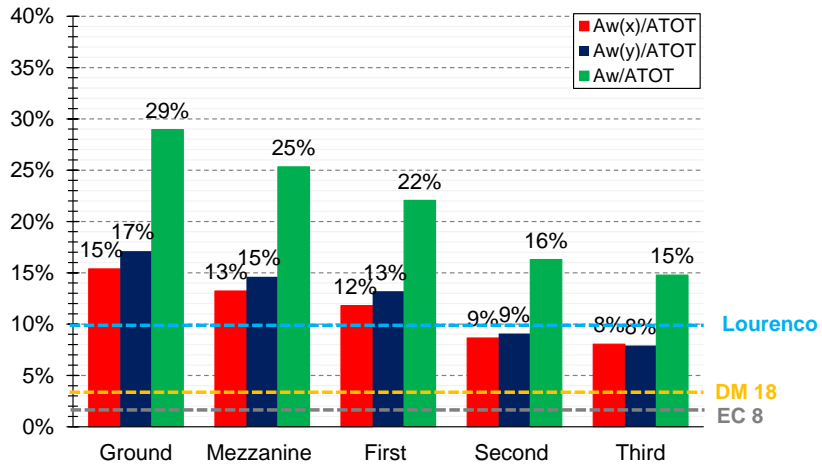
- The second floor exhibits values equal to 9% in both transverse and longitudinal directions;
- The third floor shows values of 8% in transverse direction $A_{w,y}/A_{tot}$ and in longitudinal direction $A_{w,x}/A_{tot}$.

These results are summarized in Table A3.3, which reports the values of the A_w/A_{tot} , $A_{w,x}/A_{tot}$, $A_{w,y}/A_{tot}$ ratios obtained for each floor. In addition, the values lower than the minimum prescribed by Lourenco et al. are highlighted in bold, while values lower than the minimum suggested by EC8 are in italic.

Table A3.3. In-plan ratios for the analysed structure.

Level	A_{tot}	A_w	A_w/A_{tot}	$A_{w,x}$	$A_{w,x}/A_{tot}$	$A_{w,y}$	$A_{w,y}/A_{tot}$
<i>[-]</i>	<i>[m²]</i>	<i>[m²]</i>	<i>[%]</i>	<i>[m²]</i>	<i>[%]</i>	<i>[m²]</i>	<i>[%]</i>
Ground	1259	365	29%	194	15%	215	17%
Mezzanine	2772	702	25%	367	13%	405	15%
First	2784	614	22%	328	12%	367	13%
Second	2761	450	16%	239	9%	251	9%
Third	2730	403	15%	220	8%	216	8%

The Case Study of St. Carlo all'Arena Convent in Naples



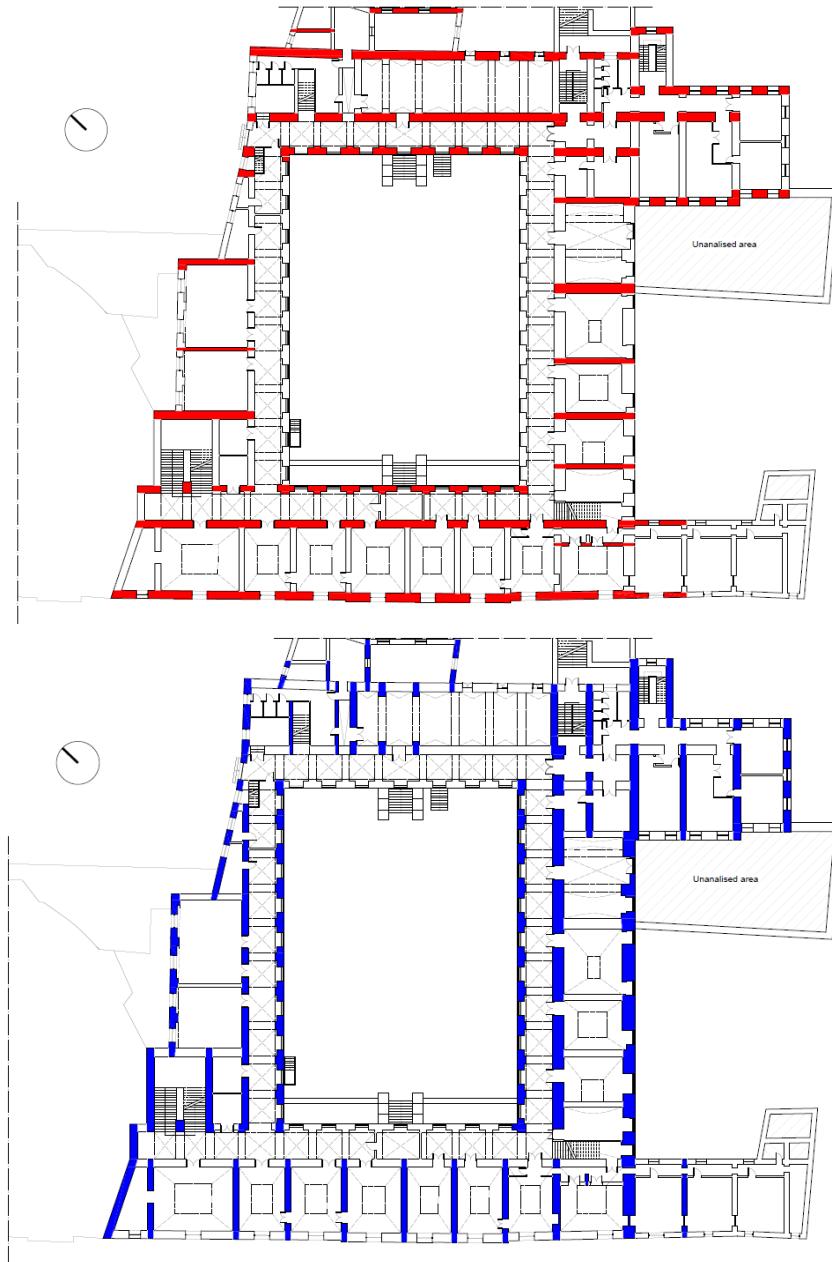


Figure A3.11. In-plan ratio.

A3.3.4 On the arrangement of the openings

In this Section some considerations regarding the arrangement of the openings of the extracted walls from the analysed structure are listed below. For visual references and detailed plans with labelled wall alignments, please refer to **Appendix 4**.

The masonry walls are characterized by regular arrangement of the openings, showcasing precise vertical alignment and equal horizontal distance between them. However, this regularity is disrupted in the case of wall 18y, where the presence of recesses on the ground floor (probably realized in subsequent years) creates misalignment with the openings on the upper levels (Figure A3.12). Furthermore, the openings are interspersed with larger-sized masonry piers, defining unreduced resistant sections.



Figure A3.12. Wall 18y: the issue of the added openings.

A3.4 Structural modelling of the convent

As mentioned in previous Section, the Convent case study consists of various portions, built over different periods, ranging from the 17th to the 20th century. Much like the approach taken with the St. Domenico Maggiore Convent, the analysis of St. Carlo all’Arena Convent will involve

non-linear static analysis. This analysis will consider two limit hypotheses: one assuming no interaction between the various constructions, and the other assuming perfect interaction among them.

A3.4.1 Simplifications introduced in the structural models

About the structural models of the Convent and of each construction, the following considerations have been applied:

- In the hypothesis where no interaction between the convent and the adjacent structures, the church and the adjacent building with different floor heights have been excluded from the analysis.
- The seismic zero has been positioned at the lower foundations, corresponding to the foundation level of the portion facing Via Foria.
- For areas on the ground floor and mezzanine floor that were not investigated, the same plan positioning and wall thickness as the first floor have been assumed.
- The contribution of the wall supported by vaults at various floors has been considered only in terms of vertical loads, through the application of vertical forces. However, their contributions in terms of stiffness and strength have been neglected.

A3.4.2 Mechanical properties of material

The mechanical properties of tuff have been determined with reference to Table C8.5.I of the current Italian Building Code NTC18, taking into account an intermediate knowledge level LC2. Specifically, the median values within the Table's range have been adopted, except for the specific weight, where the maximum value has been considered. The adopted values for the mechanical properties are given in Table A3.4. It is important to note that a FC value of 1.20 has been selected in alignment with the LC2 knowledge level.

Table A3.4. Mechanical properties of the tuff.

Elastic Modulus	Shear Modulus	Specific Weight	Compressive Strength	Shear Strength
$[kg/cm^2]$	$[kg/cm^2]$	$[kg/cm^3]$	$[kg/cm^2]$	$[kg/cm^2]$
10,800	3,600	1,600	15	0.28

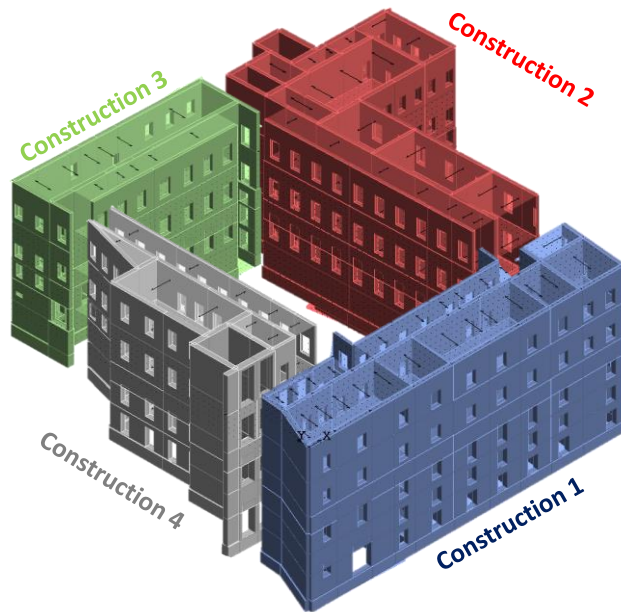


Figure A3.13. Structural models of each construction.

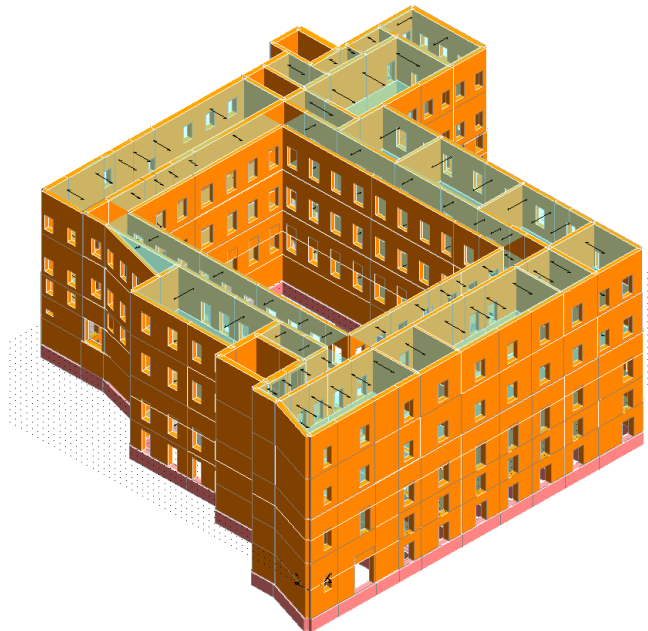


Figure A3.14. Structural model of the Convent.

A3.4.3 Reference system

The same reference system has been utilized in both the structural model of the individual constructions and the convent. For specific reference system locations, please refer to **Appendix 4**.

A3.5 Seismic vulnerability assessment

This section focuses on the seismic vulnerability assessment of St. Carlo all’Arena Convent in Naples. Similar to the methodology applied in the analysis of St. Domenico Maggiore Convent, the assessment of St. Carlo all’Arena Convent has been carried out under two distinct assumptions: one that considers no interaction between the individual constructions, and another that assumes perfect interaction among them. In this Section, the results of the non-linear static analyses conducted on each construction are presented. These results are compared with the analyses of the entire convent and include capacity curves and seismic vulnerability indexes. Additionally, 2D wall analyses have been performed using non-linear static analysis, with a distribution of forces proportional to the masses. The results of these analyses, presented in terms of capacity curves, are further compared to the capacity curve of the 3D structure.

A3.5.1 Capacity curves

Figures from A3.15 to A3.18 illustrate the capacity curves for each construction, comparing them with the capacity curve of the entire convent. Two different distributions of forces have been considered: one proportional to the masses and the other proportional to the first vibration mode of the structure. These curves are plotted in terms of (1) base shear vs displacement of the control point, and (2) base shear divided by the weight (F/w) vs displacement divided by the total height of the structure (d/H). It can be noted that, for both distribution of forces, in x direction the capacity curve of the convent exhibit a similar ultimate displacement as the capacity curves of the constructions 2 and 3. In terms of F/w , the curves show similar maximum values, with the exception for the capacity curve of construction 3, which features significantly higher values, nearly double that of the others. In y direction, the capacity curve of the complex has an ultimate displacement lower than the ultimate displacements of the individual constructions. In particular, for a distribution of forces

proportional to the masses, the curve of the convent reaches an ultimate displacement of 12 cm, while the other constructions curves range between 14 cm and 16 cm. With a distribution of forces proportional to the first vibration mode of the structure, the curve of the convent reaches an ultimate displacement of 10 cm, while the other constructions curves vary between 13 cm and 16 cm. In terms of F/w , the capacity curves of the complex exhibit a maximum value that falls between the values of the other construction curves.

To provide a comprehensive summary of the results, the maximum values of force and displacement and of base shear expressed as percentage of weight (F/W) and displacement expressed as a percentage of the height of the structure (d/H) in x and y direction for the two considered load patterns and for each construction are summarized in Table A3.5 and Table A3.6.

Table A3.5. *Distribution of forces proportional to the masses*: Maximum values of forces and displacement and of F/W and d/H ratios in x and y direction.

Construction	Direction	F_{\max}	d_{\max}	$(F/W)_{\max}$	$(d/H)_{\max}$
$[-]$	$[-]$	$[t]$	$[cm]$	$[\%]$	$[\%]$
C1	x direction	1055.54	25.07	8.6%	0.9%
	y direction	1012.94	16.73	8.2%	0.6%
C2	x direction	1080.07	15.09	7.3%	0.5%
	y direction	2137.66	14.74	14.5%	0.5%
C3	x direction	1087.23	14.82	15.5%	0.6%
	y direction	390.41	14.86	5.6%	0.6%
C4	x direction	652.53	18.13	8.6%	0.6%
	y direction	987.90	14.99	13.1%	0.5%
COMPLEX	x direction	3242.12	13.20	8.1%	0.5%
	y direction	4058.28	12.01	10.1%	0.4%

Table A3.6. *Distribution of forces proportional to the first vibration mode*: Maximum values of forces and displacement and of F/W and d/H ratios in x and y direction.

Construction	Direction	F_{\max}	d_{\max}	$(F/W)_{\max}$	$(d/H)_{\max}$
$[-]$	$[-]$	$[t]$	$[cm]$	$[\%]$	$[\%]$
C1	x direction	746.57	25.36	6.1%	0.9%
	y direction	528.60	16.47	4.3%	0.6%
C2	x direction	607.99	14.47	4.1%	0.5%
	y direction	1422.49	12.90	9.6%	0.4%
C3	x direction	687.78	13.64	9.8%	0.6%
	y direction	188.40	14.08	2.7%	0.6%
C4	x direction	362.40	14.72	4.8%	0.5%
	y direction	596.44	13.28	7.9%	0.5%
COMPLEX	x direction	2038.46	11.73	5.1%	0.4%
	y direction	2417.89	9.82	6.0%	0.3%

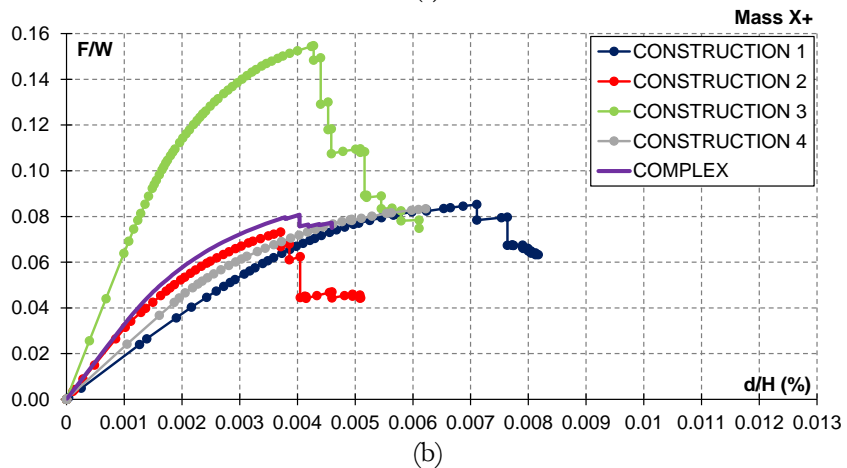
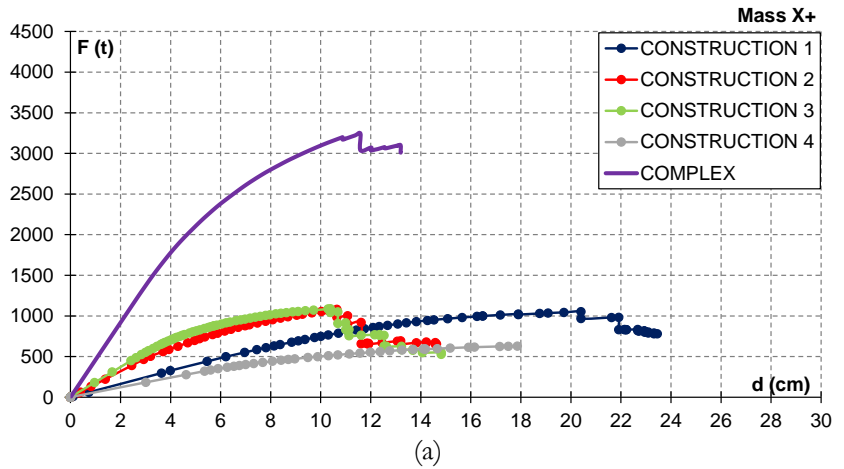


Figure A3.15. *Mass (x direction)*. Comparison between capacity curve of single construction and the entire convent in terms of (a) forces vs displacements; (b) Forces divided by weight vs displacements divided by total height of the structure.

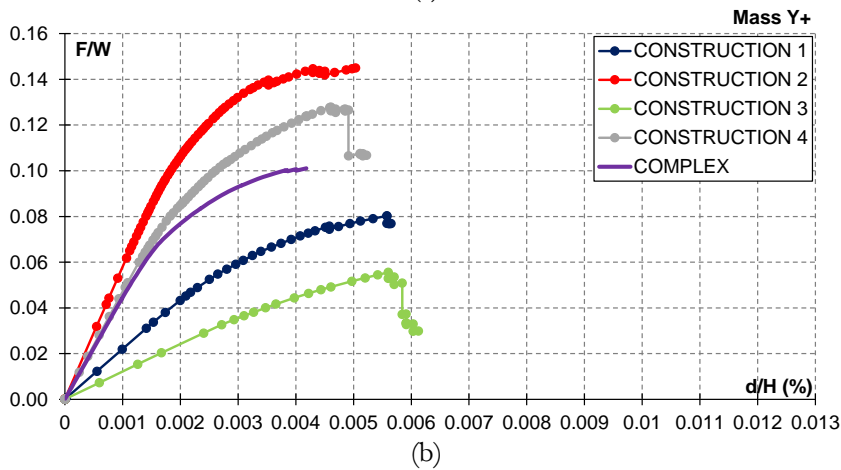
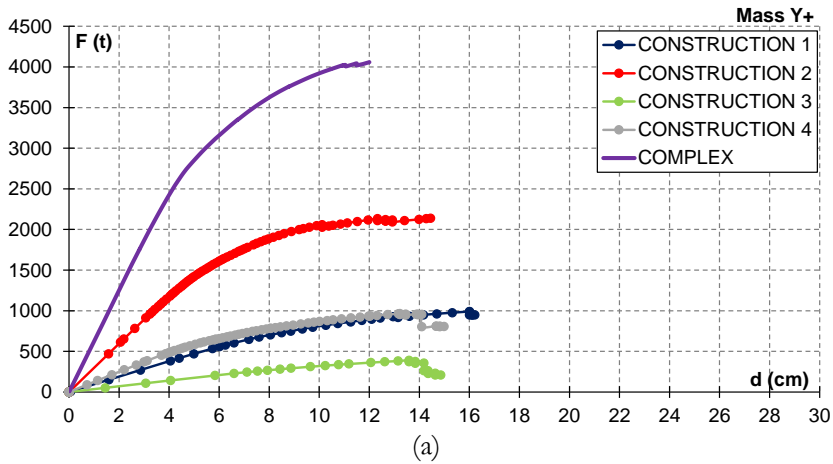


Figure A3.16. *Mass (y direction)*. Comparison between capacity curve of single construction and the entire convent in terms of (a) forces vs displacements; (b) Forces divided by weight vs displacements divided by total height of the structure.

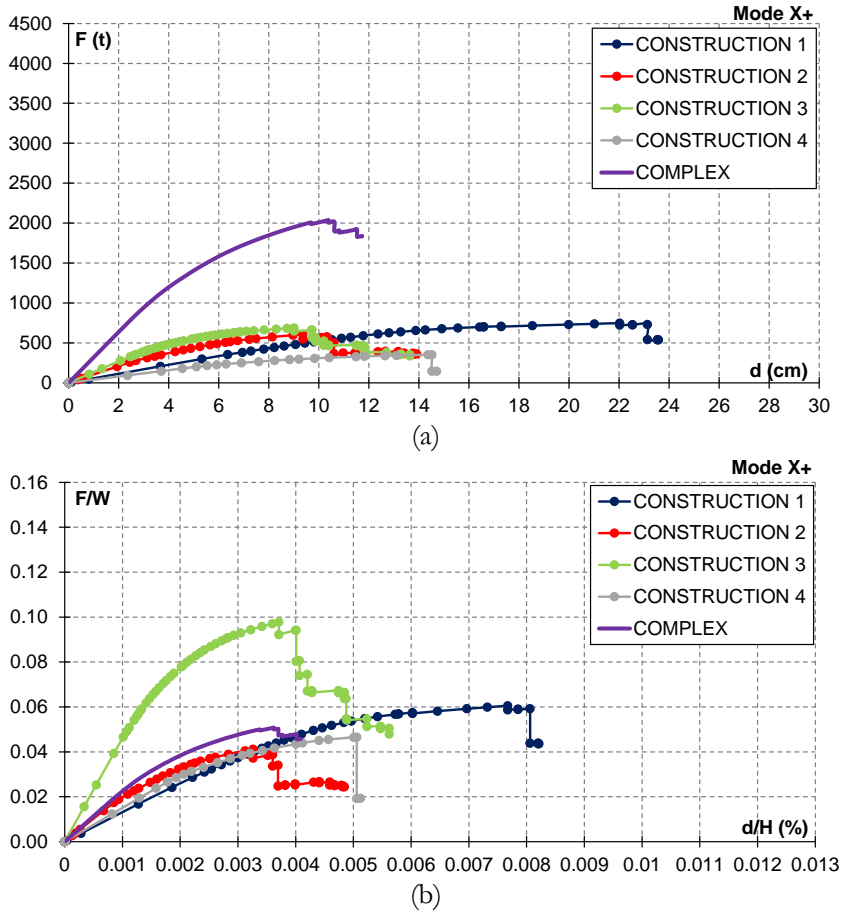


Figure A3.17. Mode (x direction). Comparison between capacity curve of single construction and the entire convent in terms of (a) forces vs displacements; (b) Forces divided by weight vs displacements divided by total height of the structure.

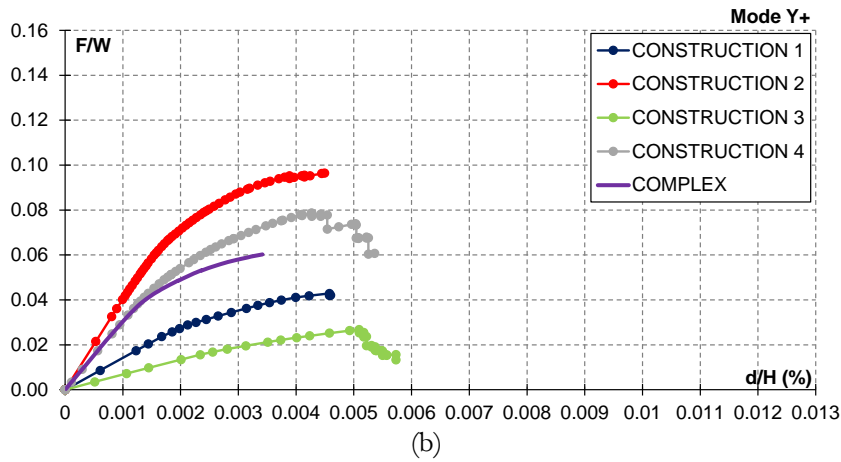
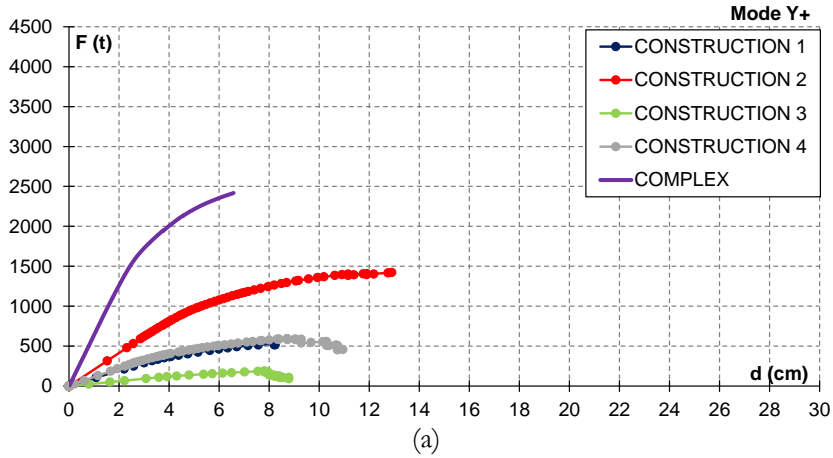


Figure A3.18. *Mode (y direction)*. Comparison between capacity curve of single construction and the entire convent in terms of (a) forces vs displacements; (b) Forces divided by weight vs displacements divided by total height of the structure.

A3.5.2 Seismic vulnerability indexes

In this Section, the application of N2 method is shown graphically and the seismic vulnerability indexes ζ_E are provided for the two limit hypotheses: for each construction individually and for the entire convent. Seismic vulnerability indexes for each construction and for the complex are visually presented in Figure A3.19 and summarized in Table A3.7. The results reveal that Constructions 1 and 3 exhibit higher values in x direction, while Constructions 2 and 4 demonstrate higher values in y direction. Interestingly, the complex displays comparable values of seismic vulnerability indexes in both orthogonal directions.

Table A3.7. Seismic Vulnerability Indexes.

Combination	ζ_E				
	C1	C2	C3	C4	COMPLEX
1 Mode X+	0.677	0.352	0.545	0.466	0.54
2 Mode X-	0.916	0.343	0.542	0.458	0.535
3 Mode Y+	0.512	0.797	0.389	0.644	0.531
4 Mode Y-	0.503	0.767	0.386	0.776	0.533
5 Mass X+	0.876	0.527	0.766	0.937	0.794
6 Mass X-	1.232	0.531	0.736	0.954	0.776
7 Mass Y+	0.859	1.221	0.617	1.089	0.855
8 Mass Y-	0.882	1.241	0.613	0.768	0.835
Max	1.232	1.241	0.766	1.089	0.855
Min	0.503	0.343	0.386	0.458	0.531

Figures from A3.20 to A3.24 depict the assessment of demand and capacity in both x and y directions using the Acceleration-Displacement Response Spectrum (ADRS), for cases with the lowest vulnerability indexes. It is important to note the following key observations:

- In the case of *Construction 1*, the capacity curves of the equivalent SDOF system in the two orthogonal directions are similar. They share similar values in terms of maximum strength and ultimate displacement.
- For *Construction 2*, the capacity curves of the equivalent SDOF system in the two orthogonal directions exhibit significant differences in terms of both maximum strength and ultimate

displacement. Specifically, the maximum strength and ultimate displacement in the y direction are double those in the x direction. These disparities result in seismic vulnerability indexes in the y direction being twice as high as those in the x direction.

- In the case of *Construction 3*, the capacity curves of the equivalent SDOF system in the two orthogonal directions show notable differences in maximum strength but not in terms of ultimate displacement. This leads to significantly different stiffness in the two orthogonal directions. In particular, the maximum strength value in the x direction is notably higher than the value in the y direction, influencing the stiffness in the x direction. Consequently, the seismic vulnerability indexes are considerably different, with a minimum value of 0.536 in the x direction and 0.302 in the y direction.
- For *Construction 4*, the capacity curves of the equivalent SDOF system in the two orthogonal directions differ in terms of maximum strength value but have comparable values in terms of ultimate displacement.
- In the case of the *Complex*, the capacity curves of the equivalent SDOF system in the two orthogonal directions have similar values in terms of maximum strength and ultimate displacement. This results in the seismic vulnerability indexes being comparable in both orthogonal directions.

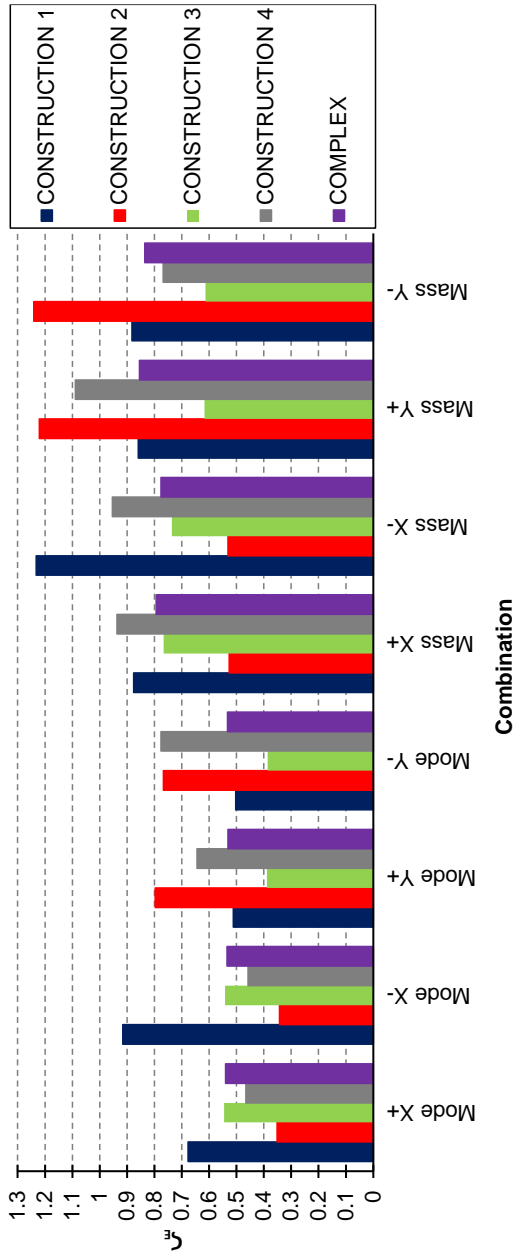
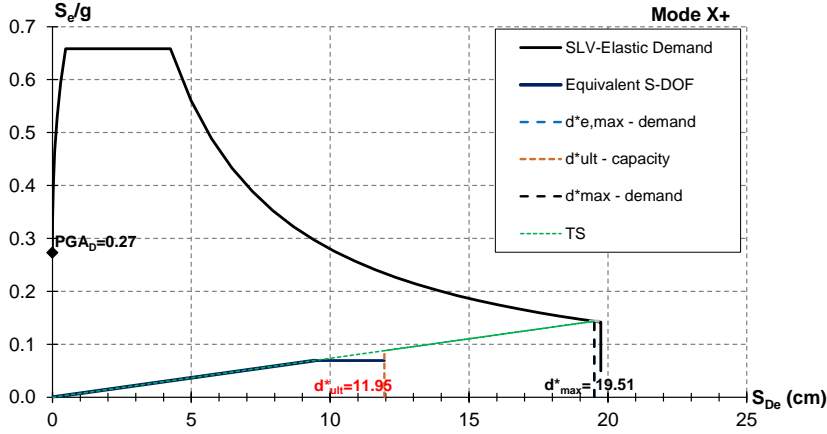


Figure A3.19. Comparison between Seismic Vulnerability Indexes of the single construction and the entire convent.

CONSTRUCTION 1

ADRS Spectrum

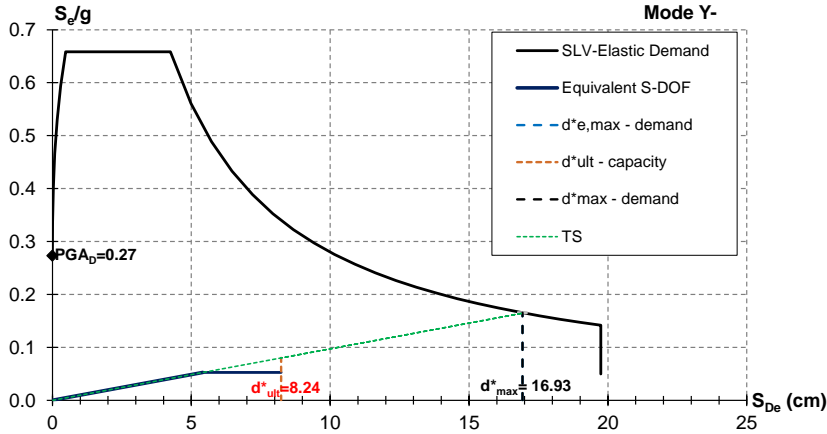
I.T.G. "Della Porta", Liceo "Cuoco"- Via Foria 65, Napoli



(a)

ADRS Spectrum

I.T.G. "Della Porta", Liceo "Cuoco"- Via Foria 65, Napoli



(b)

Figure A3.20. Construction 1. ADRS Spectrum in (a) x and (b) y direction.

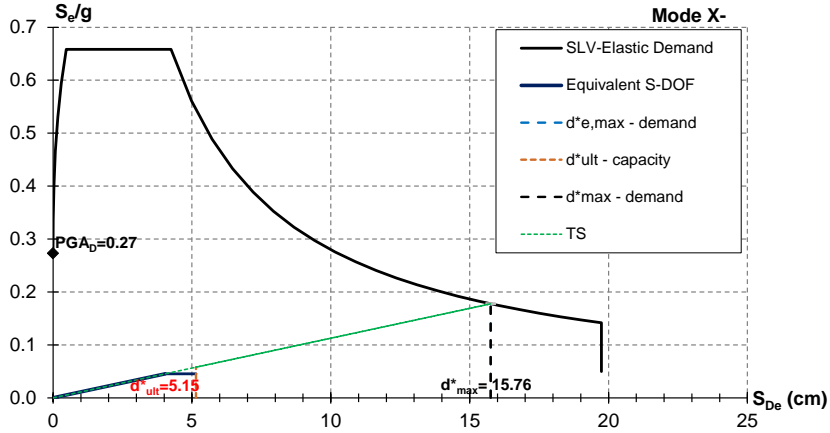
$$\zeta_{E,x} = \frac{11.95}{19.51} = 0.613$$

$$\zeta_{E,y} = \frac{8.24}{16.93} = 0.587$$

CONSTRUCTION 2

ADRS Spectrum

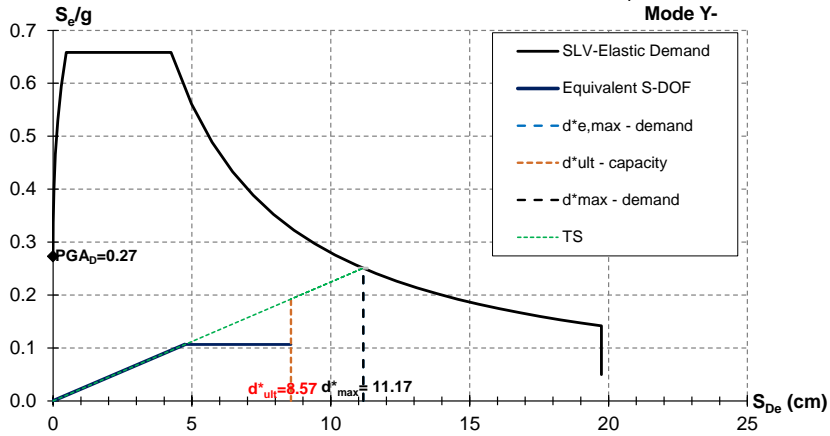
I.T.G. "Della Porta", Liceo "Cuoco"- Via Foria 65, Napoli



(a)

ADRS Spectrum

I.T.G. "Della Porta", Liceo "Cuoco"- Via Foria 65, Napoli



(b)

Figure A3.21. Construction 2. ADRS Spectrum in (a) x and (b) y direction.

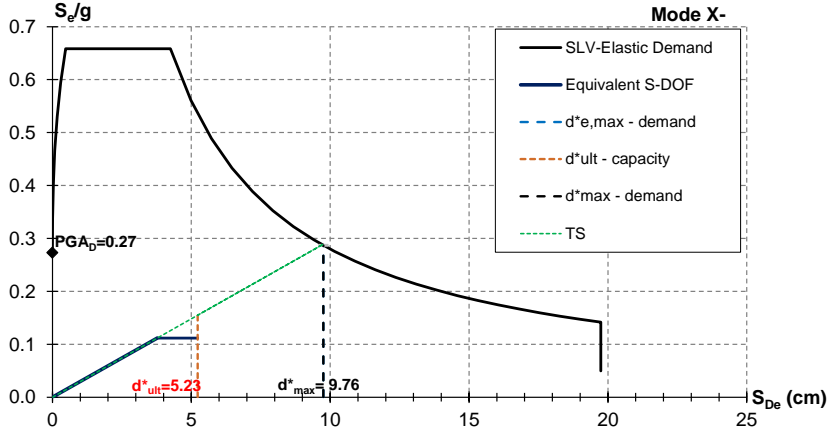
$$\zeta_{E,x} = \frac{5.15}{15.76} = 0.327$$

$$\zeta_{E,y} = \frac{8.57}{11.17} = 0.767$$

CONSTRUCTION 3

ADRS Spectrum

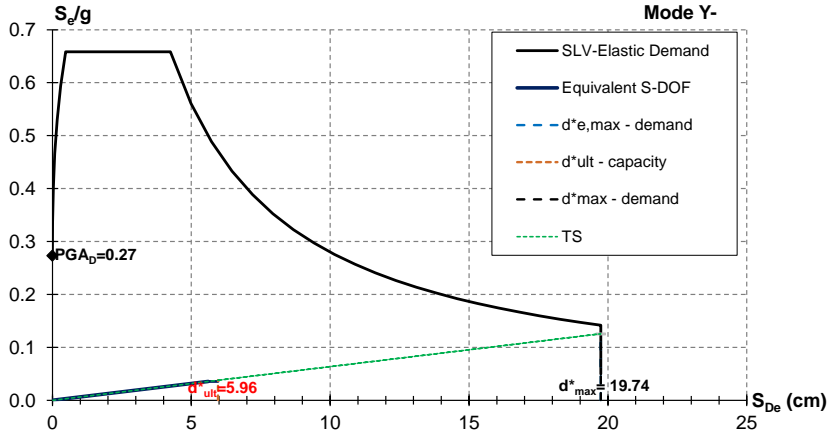
I.T.G. "Della Porta", Liceo "Cuoco"- Via Foria 65, Napoli



(a)

ADRS Spectrum

I.T.G. "Della Porta", Liceo "Cuoco"- Via Foria 65, Napoli



(b)

Figure A3.22. *Construction 3*. ADRS Spectrum in (a) x and (b) y direction.

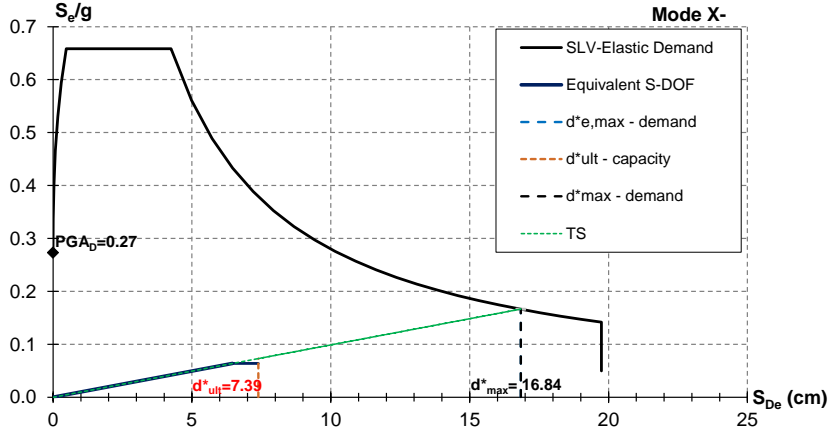
$$\zeta_{E,x} = \frac{5.23}{9.76} = 0.536$$

$$\zeta_{E,y} = \frac{5.96}{19.74} = 0.302$$

CONSTRUCTION 4

ADRS Spectrum

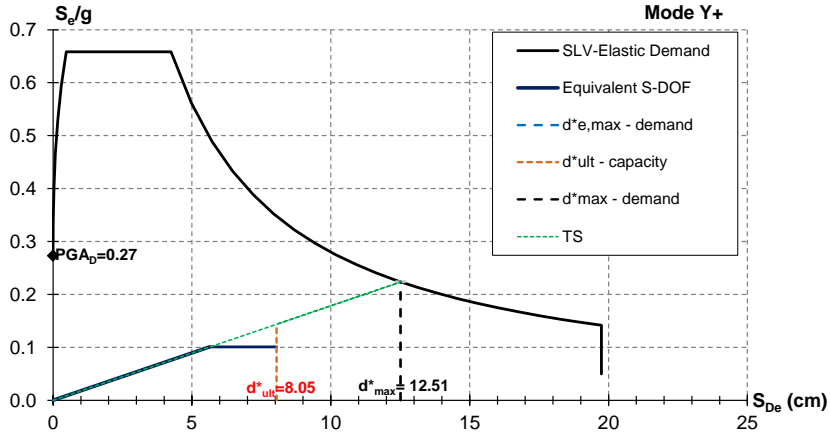
I.T.G. "Della Porta", Liceo "Cuoco"- Via Foria 65, Napoli



(a)

ADRS Spectrum

I.T.G. "Della Porta", Liceo "Cuoco"- Via Foria 65, Napoli



(b)

Figure A3.23. Construction 4. ADRS Spectrum in (a) x and (b) y direction.

$$\zeta_{E,x} = \frac{7.39}{16.84} = 0.439$$

$$\zeta_{E,y} = \frac{8.05}{12.51} = 0.643$$

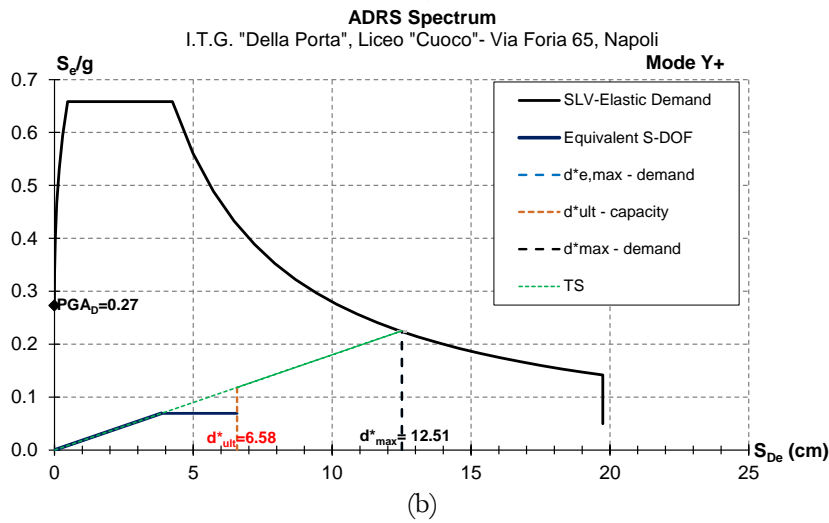
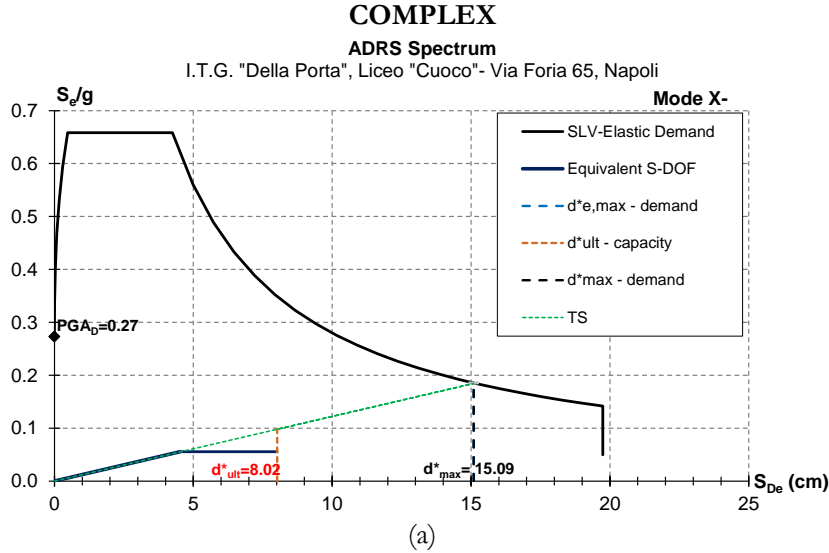


Figure A3.24. *Complex*. ADRS Spectrum in (a) x and (b) y direction.

$$\zeta_{E,x} = \frac{8.02}{15.09} = 0.531$$

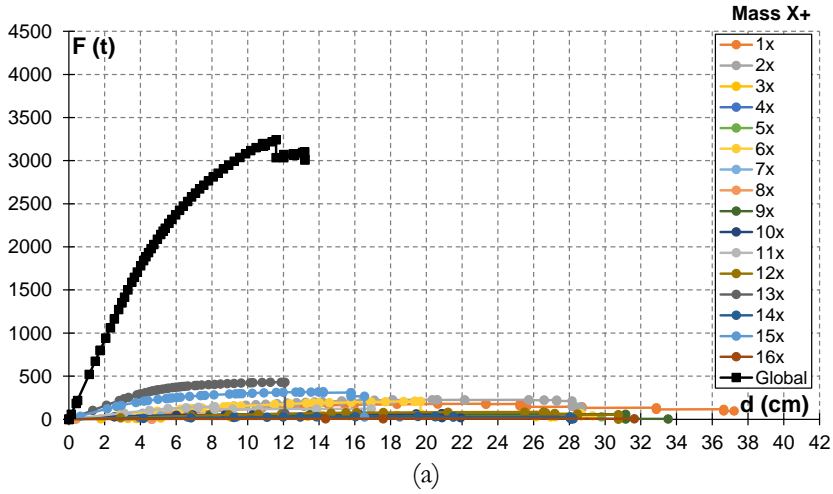
$$\zeta_{E,y} = \frac{6.58}{12.51} = 0.526$$

A3.5.3 Non-linear static analysis of 2D walls

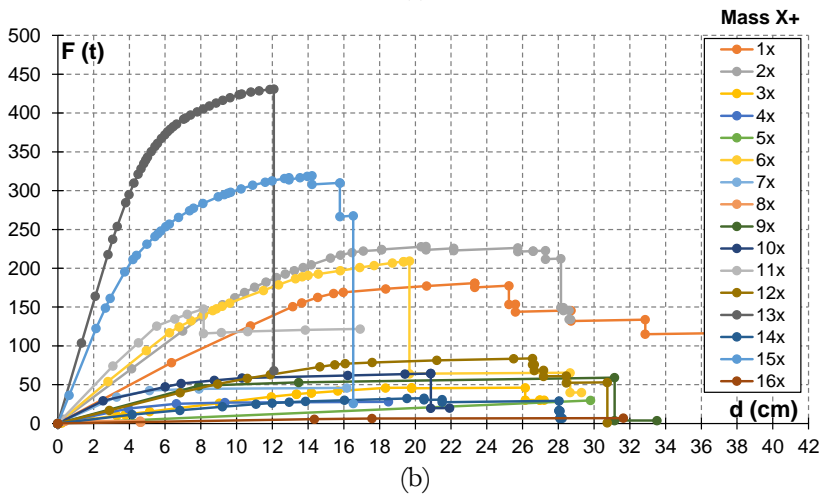
With the aim of identifying the weakest wall alignment that lead to the collapse of the structure, the analysis of 2D walls within each construction have been conducted via non-linear static analysis, assuming a distribution of forces proportional to the masses. For visual representations of the various alignments, please refer to **Appendix 4**. The results of this analysis are presented in terms of capacity curves, defined as (1) base shear vs displacement of the control point, and (2) base shear divided by the weight (F/w) vs displacement divided by the total height of the structure (d/H). In particular, Figures A3.25 and A3.26 illustrate the capacity curves of each 2D alignment, also offering a comparative analysis with the capacity curve of the 3D structure. Note that the analyses has been carried out with a multi-collapse assumption. The results of the analyses reveal that:

- In x direction, wall 13x stands out with the highest maximum base shear but a lower ultimate displacement. Conversely, the weakest alignment, featuring the minimum base shear, is wall 16x. It's worth noting that the 2D and 3D structural comparison highlights that it shares the same ultimate displacement of 12 cm with the complex.
- In y direction, wall 11y has the lowest ultimate displacement, measuring 4 cm. The weakest alignments include walls 3y, 5y, 14y, and 17y. Comparing the 3D structure with the 2D walls, it's observed that the 3D capacity curve shares the same ultimate displacement of 12 cm as wall 9y.

x direction



(a)



(b)

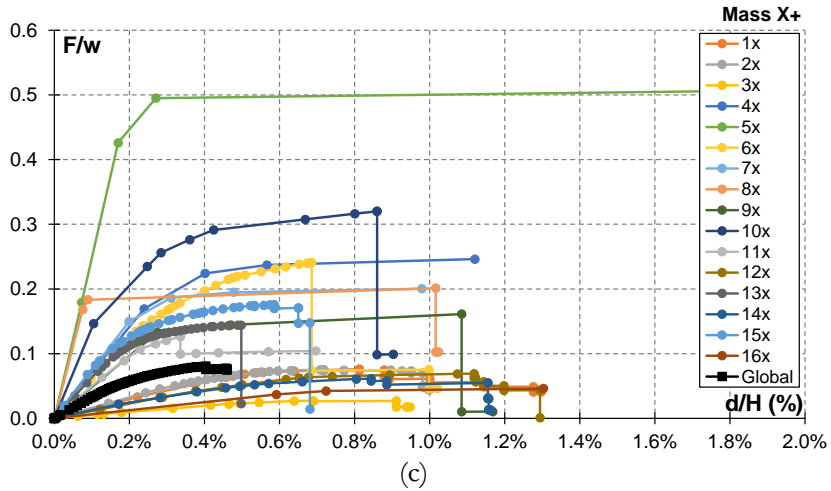
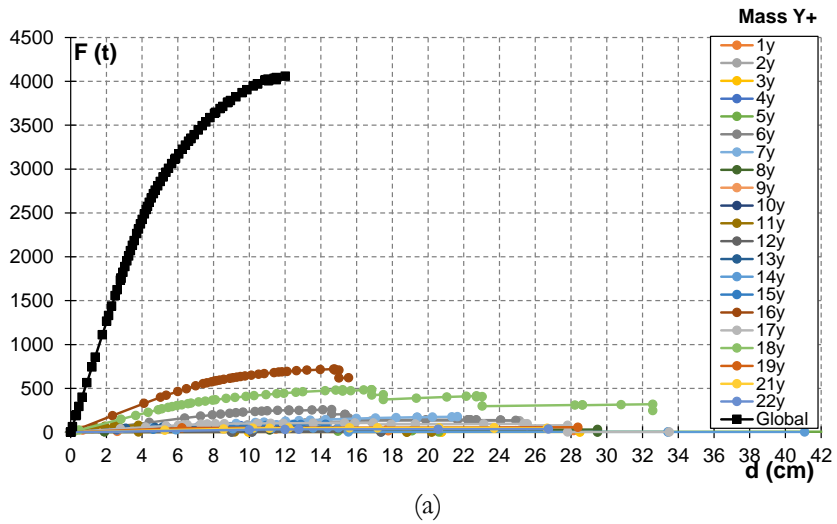
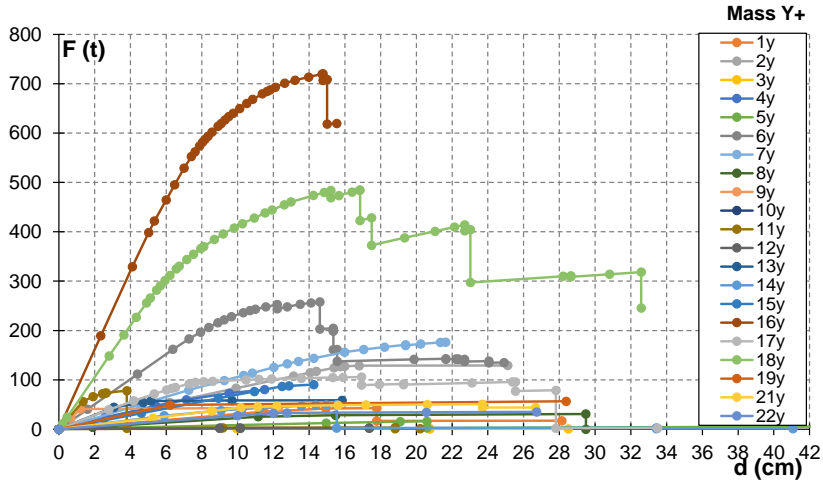


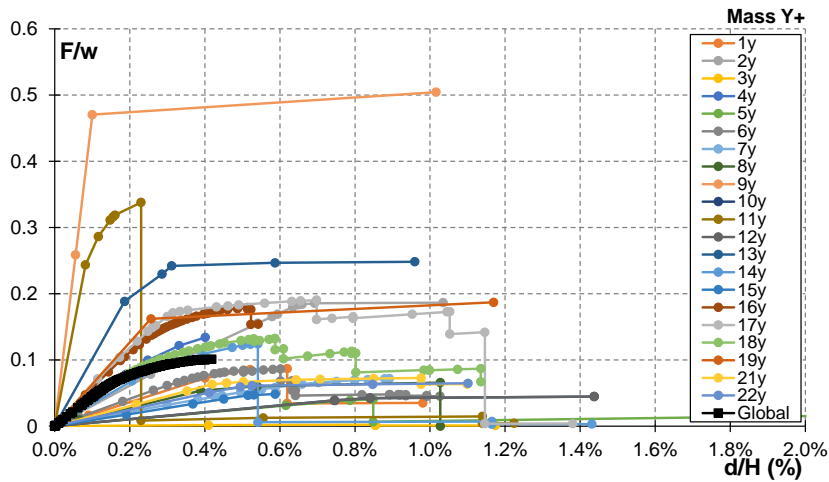
Figure A3.25. *X direction*: Capacity curve of 2D walls in terms of (a) forces vs displacements; comparison between capacity curve of 2D walls and 3D structure in terms of (b) forces vs displacements; (c) Forces divided by weight vs displacements divided by total height of the structure.

y direction





(b)



(c)

Figure A3.26. *Y direction*: Capacity curve of 2D walls in terms of (a) forces vs displacements; comparison between capacity curve of 2D walls and 3D structure in terms of (b) forces vs displacements; (c) Forces divided by weight vs displacements divided by total height of the structure.

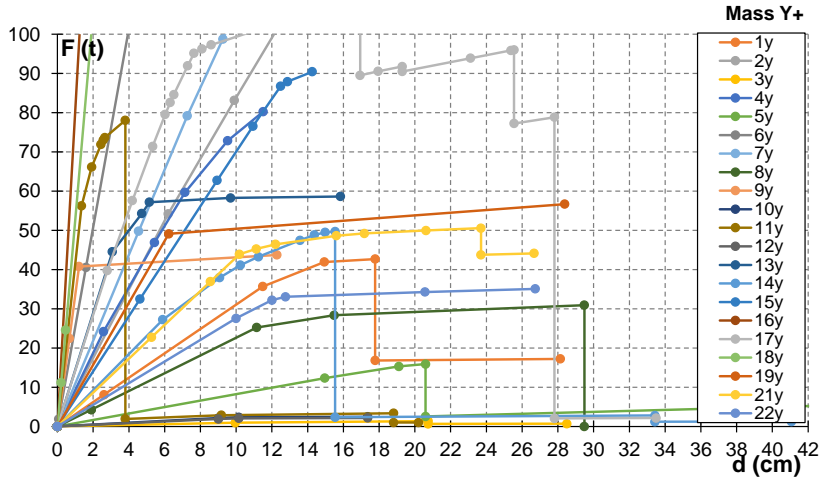


Figure A3.27. *Y direction*. Capacity curve of 2D walls in terms of forces vs displacements: zoom.

Appendix 4

St. Carlo all'Arena Convent: Wall alignments

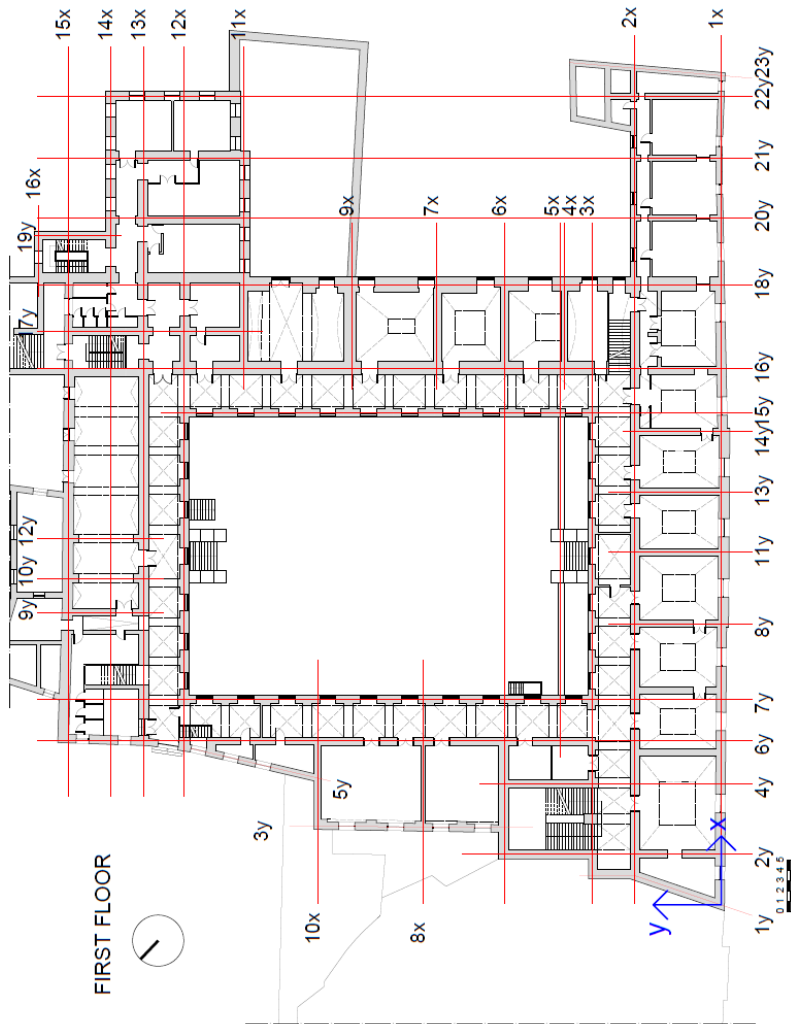
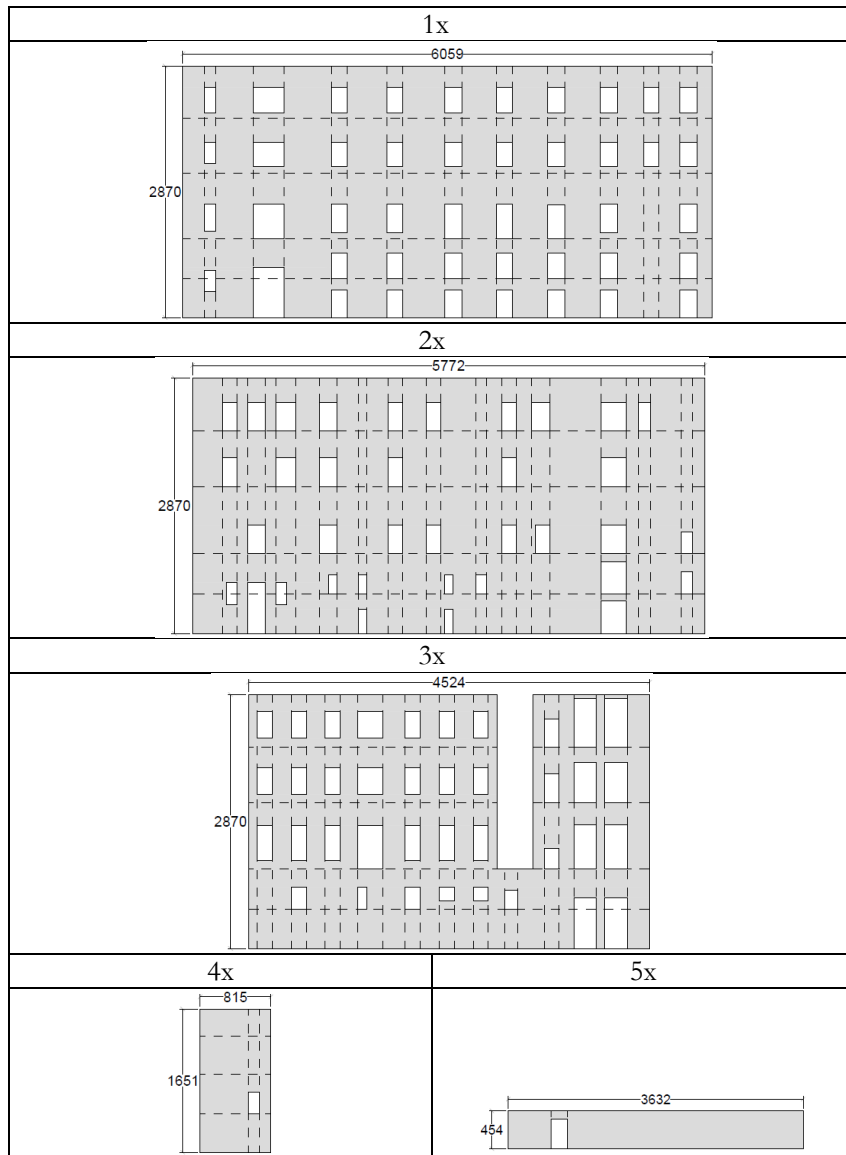
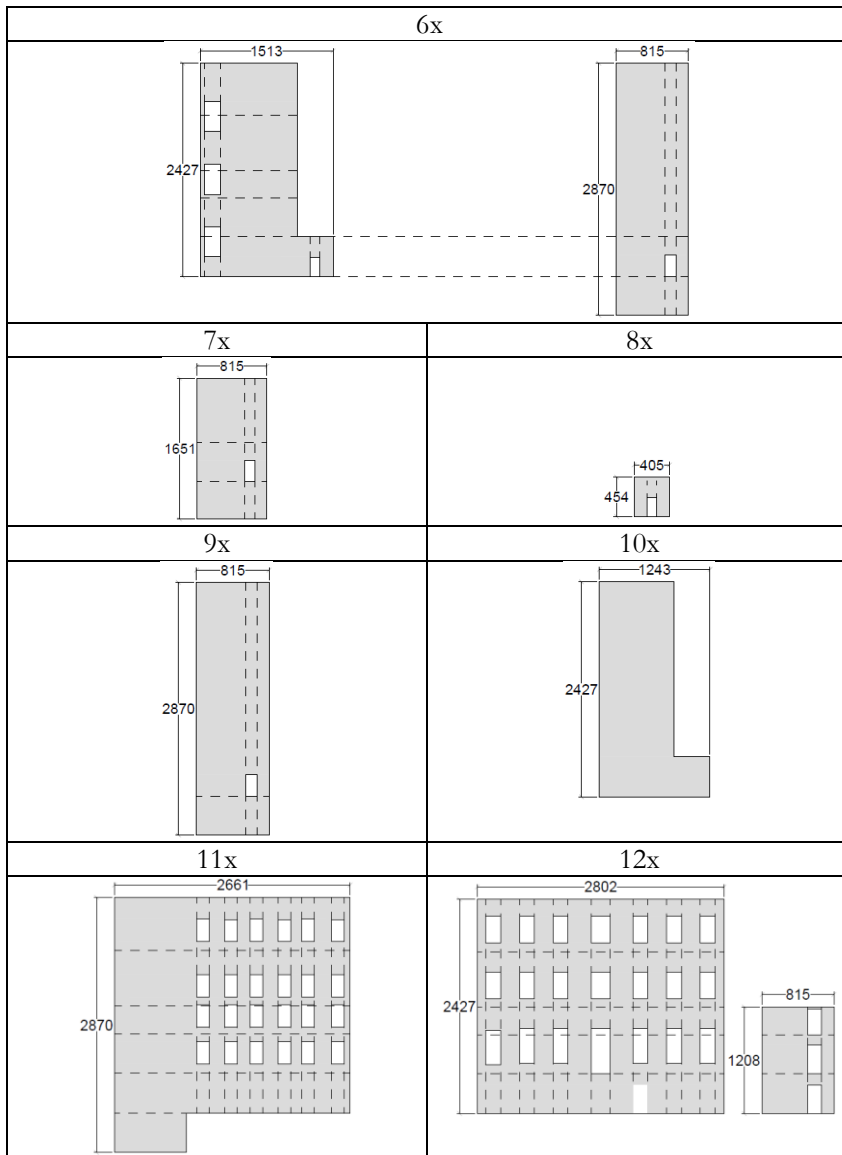


Figure A4.1. *San Carlo all'Arena Convent*: wall alignments – plan.

St. Carlo all'Arena Convent: Wall alignments



Appendix 4



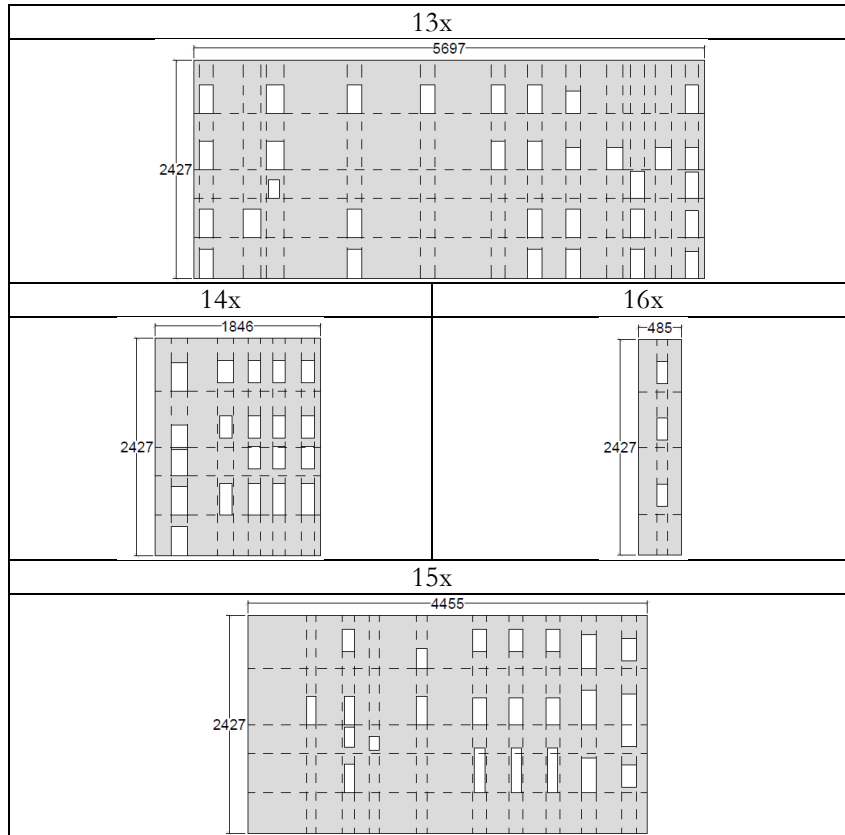
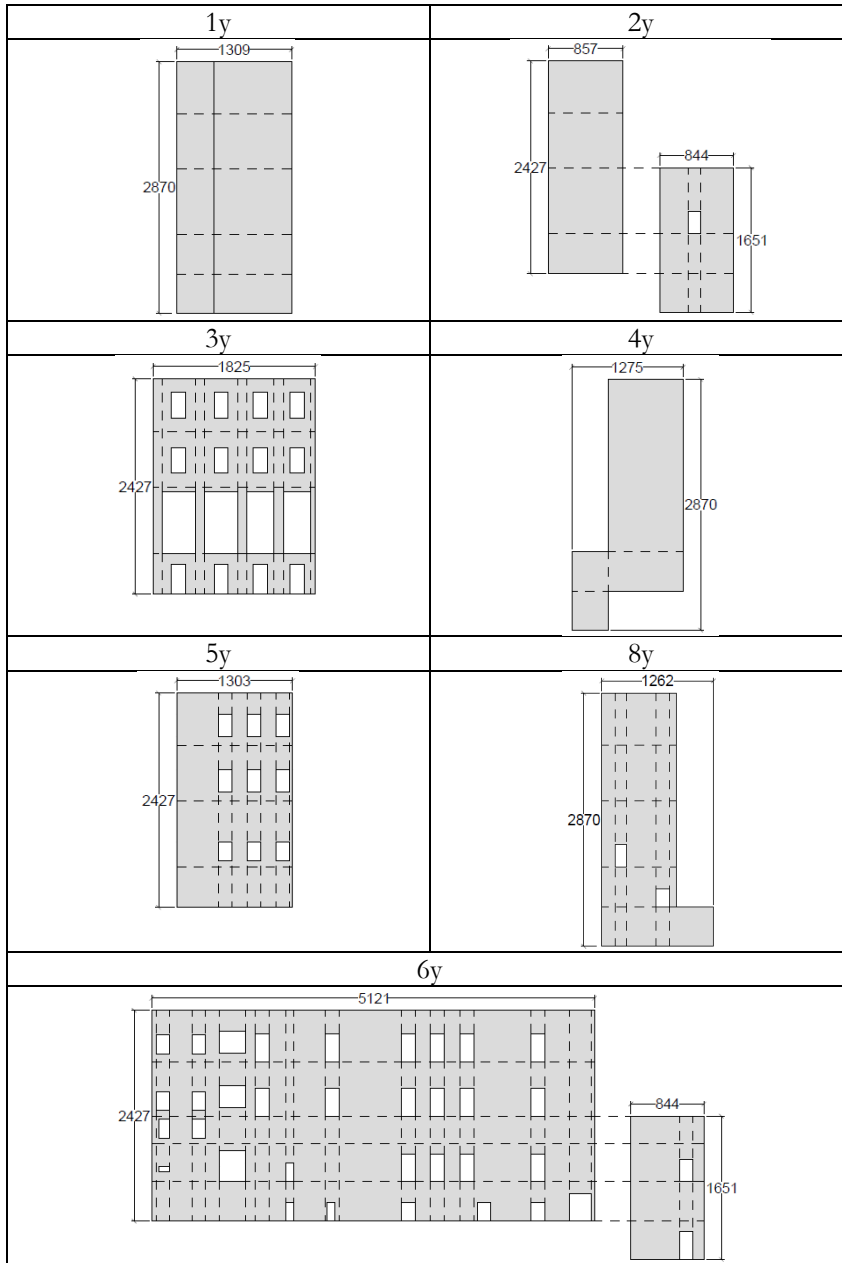
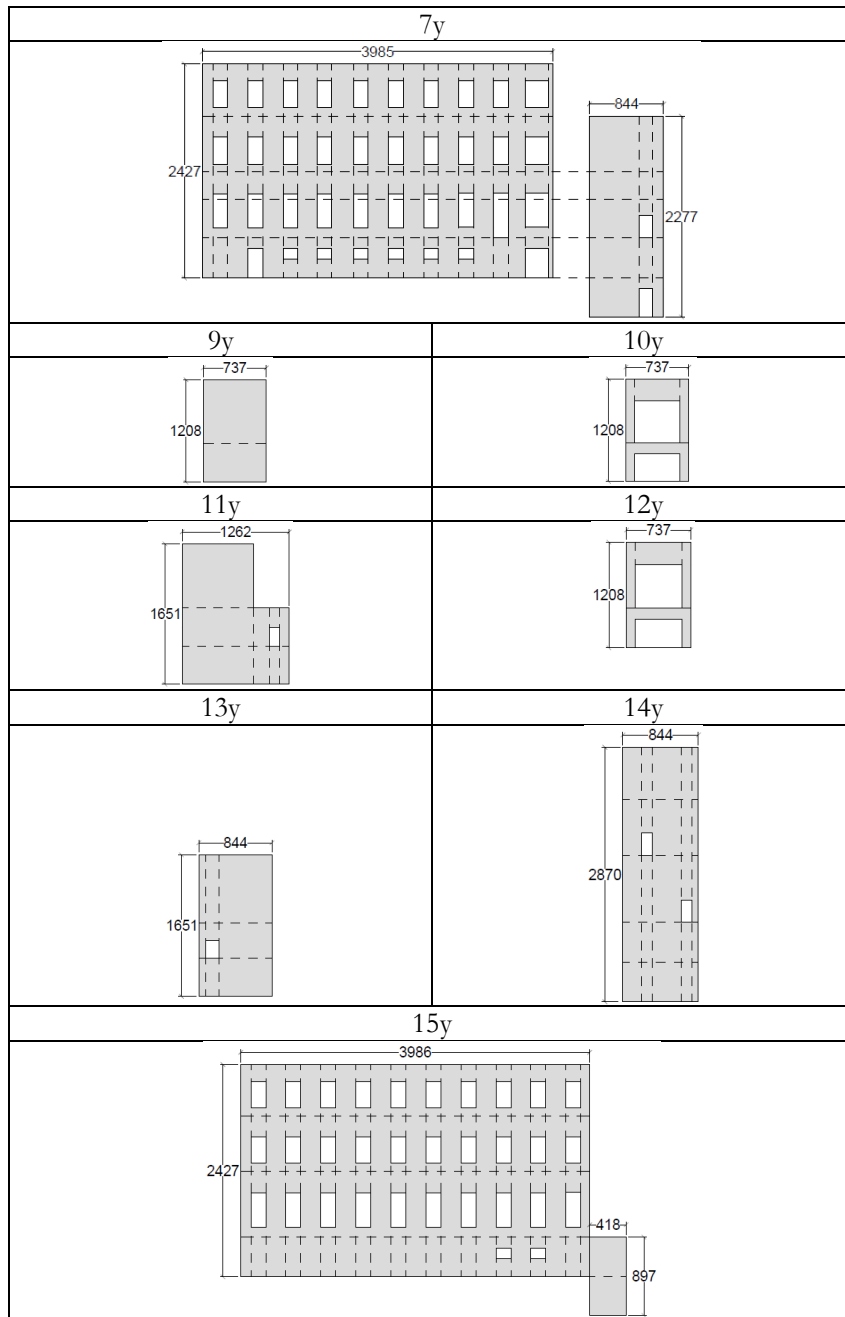


Figure A4.2. *San Carlo all'Arena Convent*: wall alignments – x direction.

Appendix 4



St. Carlo all'Arena Convent: Wall alignments



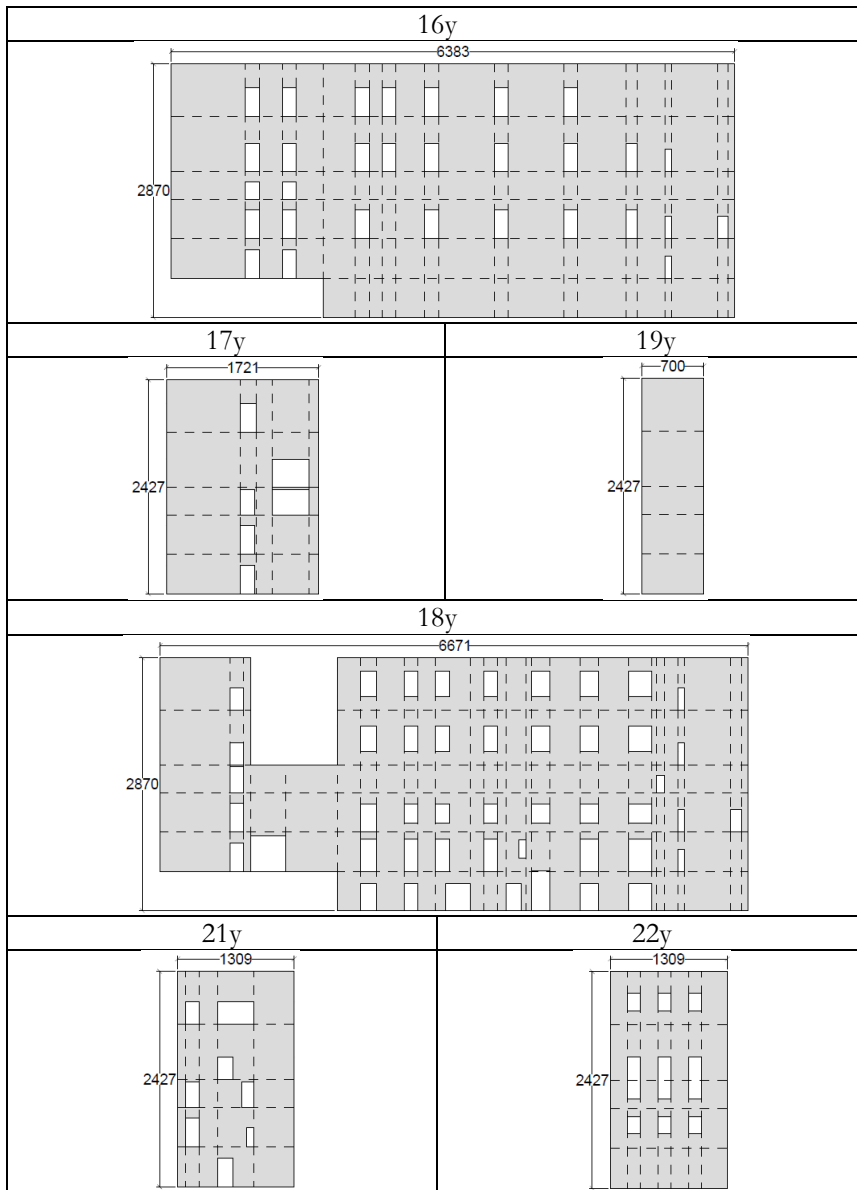


Figure A4.3. *San Carlo all'Arena Convent*: wall alignments – y direction.

Appendix 5

The application of L.A. to check non-linear analysis through SAM method

In this Chapter, the straightforward expression for predicting the horizontal capacity of multistorey unreinforced masonry frames, initially proposed in Lucibello (2013) and in Mazziotti (2015) in the framework of limit analysis approach, is explored. The formula derives from the extension of the single portal frame and multi-bay masonry portal, proposed by the research group and briefly outlined here. To test and discuss the formula, it has been first applied to a regular masonry wall, i.e. with a regular arrangement of the openings and similar pier widths. Nonlinear static analysis has been carried out assuming a proportional to mass distribution of forces and a high value of compressive strength of the material, align with Heyman's hypothesis of infinite compressive strength, which forms the basis for the derivation of the formula. The results have been systematically compared with the values provided by applying the proposed simple expression, which solely relies on geometrical parameters and external loads. A parametric analysis has been performed to assess the sensitivity of the results to the compressive strength of the material. At the end, the formula has been explored on the panels extracted from St. Domenico Convent and St. Carlo all'Arena Convent in Naples, featuring irregular arrangement of the openings and different pier widths. The results suggest that the values obtained with the proposed formula provide a good approximation of those from the pushover analysis for higher compressive strength values. The scatter tends to be larger when there is greater irregularity in the arrangement of openings in both the vertical and horizontal directions and when the failure mechanism differs from flexural failure.

A5.1 Application to a regular masonry wall

In this Section, the simplified formula is applied to a regular masonry wall. This wall features a regular arrangement of openings, with pier widths ranging from 97 cm to 261 cm, and a height of 19.71 m (Figure A5.1).

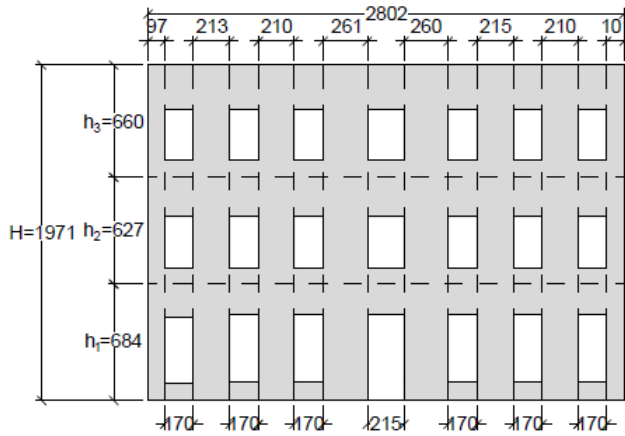


Figure A5.1. Analysed masonry wall.

The application of the formula is summarized in Table A5.1 and A5.2. Table A5.1 presents the pier width, with the minimum value in bold and the maximum in italics, along with the average value. Table A5.2 provides the results obtained using the simplified formula.

The proposed formula has been compared with the results obtained through the equivalent frame approach and pushover analysis. In particular, the pushover analysis has been carried out assuming a proportional-to-mass distribution of forces. Since the proposed formula is based on Heyman hypothesis of infinite compressive strength, a compressive strength of 100 kg/cm² has been assumed to approximate the infinite strength of the masonry. The mechanical properties of the masonry are detailed in Table A5.3. The pushover curve is illustrated in Figure A5.2, in terms of load multiplier F/w vs ratio between displacement and height of the wall d/H . This curve has been compared with the results obtained with the simplified formula (dashed red line), as well as the minimum (dashed blue line) and the maximum (dashed green line) ratios.

The application of L.A. to check non-linear analysis through SAM method

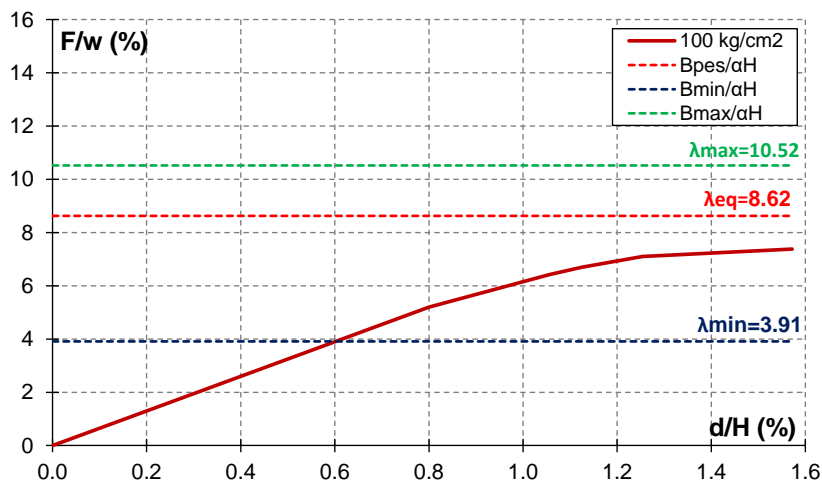


Figure A5.2. Pushover curves (continue red line) and comparison with the simplified formula (dashed red line), B_{\min}/H (dashed blue line) and B_{\max}/H (dashed green line): regular wall.

Table A5.1. Regular wall: width of pier (the minimum in bold and the maximum in italics) and weighted average of the width in meters.

B								B_{pes}
								$(\sum B_i^2 / \sum B_i)$
<i>[m]</i>								<i>[m]</i>
0.97	2.13	2.1	<i>2.61</i>	2.6	2.15	2.1	1.01	2.14

Table A5.2. Regular wall: weights expressed in tons, equivalent height in meters and the simplified proposed formula in comparison with the minimum and the maximum ratio.

W_1	W_2	W_3	α	H_{eq}	$B_{\min}/\alpha H$	$B_{\max}/\alpha H$	$B_{\text{pes}}/\alpha H$
<i>[t]</i>	<i>[t]</i>	<i>[t]</i>	<i>[-]</i>	<i>[m]</i>	<i>[%]</i>	<i>[%]</i>	<i>[%]</i>
288.81	254.66	194.57	1.26	12.40	3.9%	10.5%	8.6%

Table A5.3. Mechanical properties of the masonry.

Masonry	Elastic Modulus	Shear Modulus	Specific Weight	Compressive Strength	Shear Strength
	[kg/cm ²]	[kg/cm ²]	[kg/cm ³]	[kg/cm ²]	[kg/cm ²]
Tuff	10800	3600	1600	100	0.35

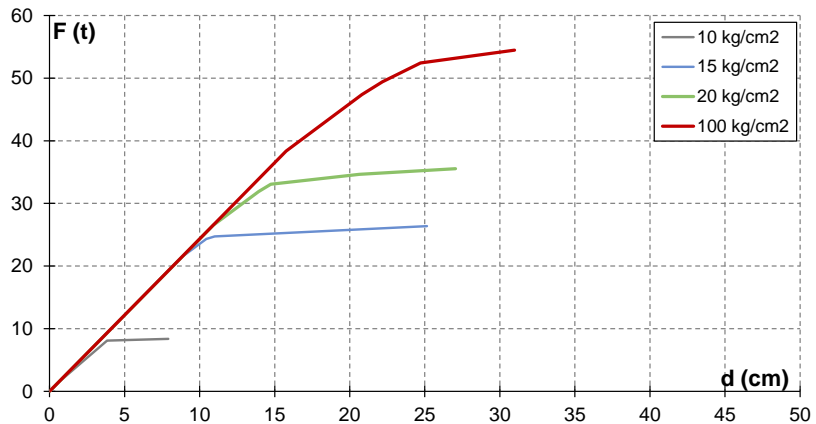
A5.2 Sensitivity analysis: compressive strength

The proposed formula is based on Heyman hypothesis of infinite compressive strength. In this Section, a parametric analysis has been performed to assess the sensitivity of the results to the compressive strength of the material. The pushover analysis of the wall analysed in the previous Section has been performed by assuming a proportional to the mass distribution of forces and the following values of compressive strength f_d :

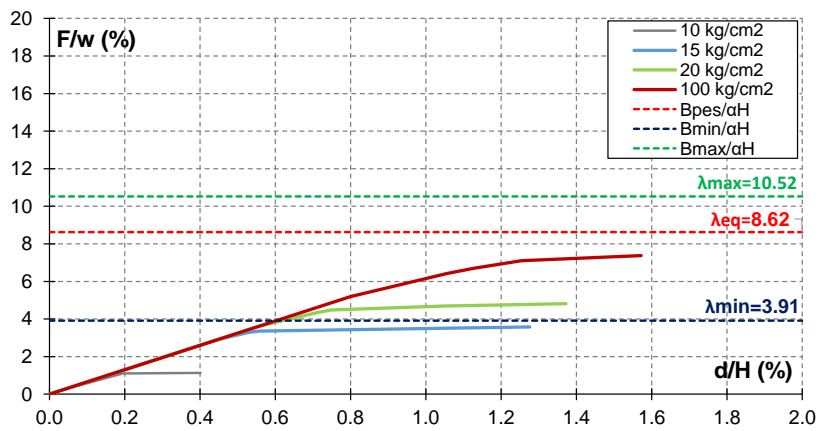
- (1) $f_d = 10 \text{ kg/cm}^2$;
- (2) $f_d = 15 \text{ kg/cm}^2$;
- (3) $f_d = 20 \text{ kg/cm}^2$;
- (4) $f_d = 100 \text{ kg/cm}^2$.

In Figure A5.3 the capacity curves of analysed wall for the different compressive strength values are depicted. These curves are presented in terms of base shear vs displacement and as load multiplier F/w vs the ratio between displacement and height of the wall d/H . The maximum base shear varies from 8 t for a compressive strength of 10 kg/cm² to 55 t for compressive strength of 100 kg/cm². In terms of F/w , the curves display maximum values ranging from 1.14% for the compressive strength of 10 kg/cm² to 7.38% for compressive strength of 100 kg/cm². The comparison between the capacity curves and the value obtained with the simplified formula reveals that, as the compressive strength increase, the deviation is drastically reduced. Figure A5.4 illustrates the scatter between the two values, as the compressive strength varies. It indicates that for lower compressive strength values, the scatter ranges from 659% (for a compressive strength of 10 kg/cm²) to 17% (for a compressive strength of 100 kg/cm²).

The application of L.A. to check non-linear analysis through SAM method



(a)



(b)

Figure A5.3. Pushover curves in terms of $F - d$ (a) and comparison between the pushover curves and the simplified formula (dashed red line), B_{min}/H (dashed blue line) and B_{max}/H (dashed green line) for different values of f_d .

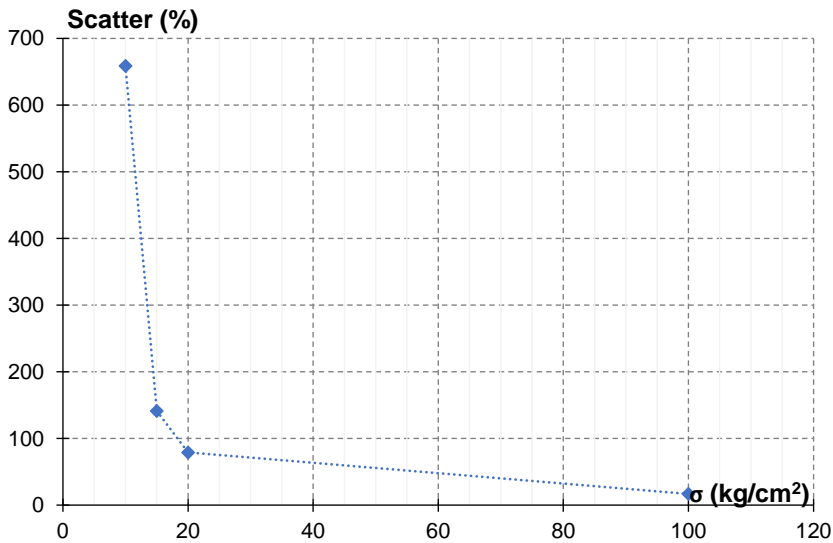


Figure A5.4. Scatter between the results obtained with the pushover analysis and the simplified formula.

A5.3 Application to generic masonry wall

To evaluate and discuss the formula, it has been applied to walls of St. Domenico Maggiore Convent and St. Carlo all’Arena Convent, and the results has been compared with the outcomes of the nonlinear static analysis. The nonlinear static analysis has been carried out using a proportional to the mass distribution of forces and assuming a tuff material with a compressive strength of 100 kg/cm². For the mechanical properties of the material, refer to Table A5.3. Figures from A5.5 to A5.7 depict the analysed walls, characterized by irregular arrangement of openings in both the vertical and horizontal direction, resulting in varying pier widths vertically. Tables from A5.4 to A5.6 provide the wall weights, the coefficient α , the overall height and the equivalent height. Tables from A5.7 to A5.9 present the minimum, the maximum and the weighted average values of the piers of the analysed walls, along with a summary of the outcomes obtained applying the simplified formula.

The application of L.A. to check non-linear analysis through SAM method

Table A5.4. *Construction 0*. Wall weights, coefficient α , overall height and equivalent height.

Wall	W_1	W_2	W_3	W_4	W_5	α	H	H_{eq}
$[-]$	$[t]$	$[t]$	$[t]$			$[-]$	$[m]$	$[m]$
3x	582.77	484.48	486.56	460.41	28.57	1.09	22.47	12.27
4x	1154.97	667.45	1038.87	601.24	611.90	1.18	22.47	13.27
5x	1153.75	631.36	1181.67	638.02	592.76	1.19	22.47	13.35
6x	910.63	740.26	848.66	607.69	61.19	1.08	22.47	12.13

Table A5.5. *Construction 1*. Wall weights, coefficient α , overall height and equivalent height.

Wall	W_1	W_2	W_3	α	H	H_{eq}
$[-]$	$[t]$	$[t]$	$[t]$	$[-]$	$[m]$	$[m]$
1x	200.83	129.79	104.29	1.22	16.15	9.89
2x	815.45	804.36	217.96	1.17	16.15	9.45
3x	222.76	303.43	388.65	1.49	16.15	12.06
4x	1160.00	863.44	240.13	1.11	16.15	8.98

Table A5.6. *San Carlo all'Arena*. Wall weights, coefficient α , overall height and equivalent height.

Wall	W_1	W_2	W_3	W_4	W_5	W_6	α	H	H_{eq}
$[-]$	$[t]$	$[t]$	$[t]$	$[t]$	$[t]$	$[t]$	$[-]$	$[m]$	$[m]$
1x	299.70	425.37	328.63	504.42	509.78	312.22	1.13	28.70	16.15
2x	382.82	510.97	320.20	796.59	616.68	406.91	1.43	28.70	16.29
3x	216.03	345.07	39.47	493.13	373.24	245.64	1.15	28.70	16.51
4x	27.61	33.89	27.04	25.31			1.28	16.51	10.59
12x	318.24	16.89	342.68	251.54	140.37		1.06	24.27	12.86
13x	581.06	343.09	786.75	744.08	535.51		1.15	24.27	13.99
14x	100.10	93.50	62.84	160.03	114.49		1.20	24.27	14.62
15x	393.11	243.15	478.07	450.92	249.63		1.09	24.27	13.26
16x	24.01	20.32	20.73	49.40	38.45		1.28	24.27	15.57

Table A5.7. *Construction 0*. Minimum, maximum and weighted average value and the outcomes of the simplified formula.

Wall	B_{\min}	B_{\max}	B_{pes}	$B_{\min}/\alpha H$	$B_{\max}/\alpha H$	$B_{\text{pes}}/\alpha H$
[-]	[m]	[m]	[m]	[%]	[%]	[%]
3x	0.73	3.98	2.78	3.0%	16.2%	11.3%
4x	0.35	12.84	5.03	1.3%	48.4%	19.0%
5x	0.25	3.58	2.05	0.9%	13.4%	7.7%
6x	0.50	4.15	2.92	2.5%	21.1%	14.8%

Table A5.8. *Construction 1*. Minimum, maximum and weighted average value and the outcomes of the simplified formula.

Wall	B_{\min}	B_{\max}	B_{pes}	$B_{\min}/\alpha H$	$B_{\max}/\alpha H$	$B_{\text{pes}}/\alpha H$
[-]	[m]	[m]	[m]	[%]	[%]	[%]
1x	0.6	8.4	7.88	3.0%	42.5%	39.8%
2x	0.9	3.37	2.66	4.8%	17.8%	14.1%
3x	2.31	13.4	5.52	9.6%	55.5%	22.9%
4x	1.23	3.55	2.80	6.9%	19.8%	15.6%

Table A5.9. *San Carlo all'Arena*. Minimum, maximum and weighted average value and the outcomes of the simplified formula.

Wall	B_{\min}	B_{\max}	B_{pes}	$B_{\min}/\alpha H$	$B_{\max}/\alpha H$	$B_{\text{pes}}/\alpha H$
[-]	[m]	[m]	[m]	[%]	[%]	[%]
1x	1.70	5.48	4.03	5.3%	17.0%	12.5%
2x	1.20	5.80	3.15	3.7%	17.8%	9.7%
3x	0.90	2.55	1.91	2.7%	7.7%	5.8%
4x	1.35	5.55	4.73	6.4%	26.2%	22.3%
12x	0.97	2.61	2.14	3.8%	10.1%	8.3%
13x	0.55	7.01	4.64	2.0%	25.0%	16.6%
14x	0.70	3.40	2.15	2.4%	11.6%	7.4%
15x	1.30	6.55	3.91	4.9%	24.7%	14.7%
16x	1.55	2.10	1.87	5.0%	6.7%	6.0%

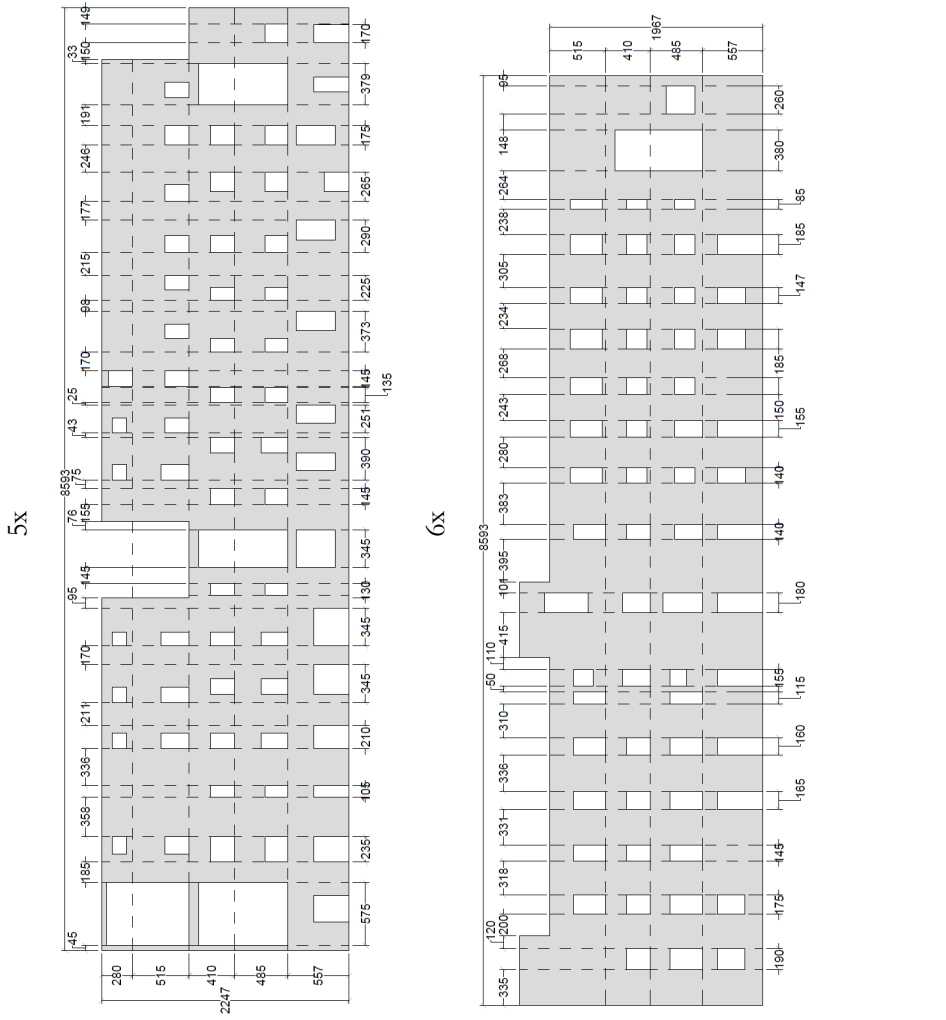
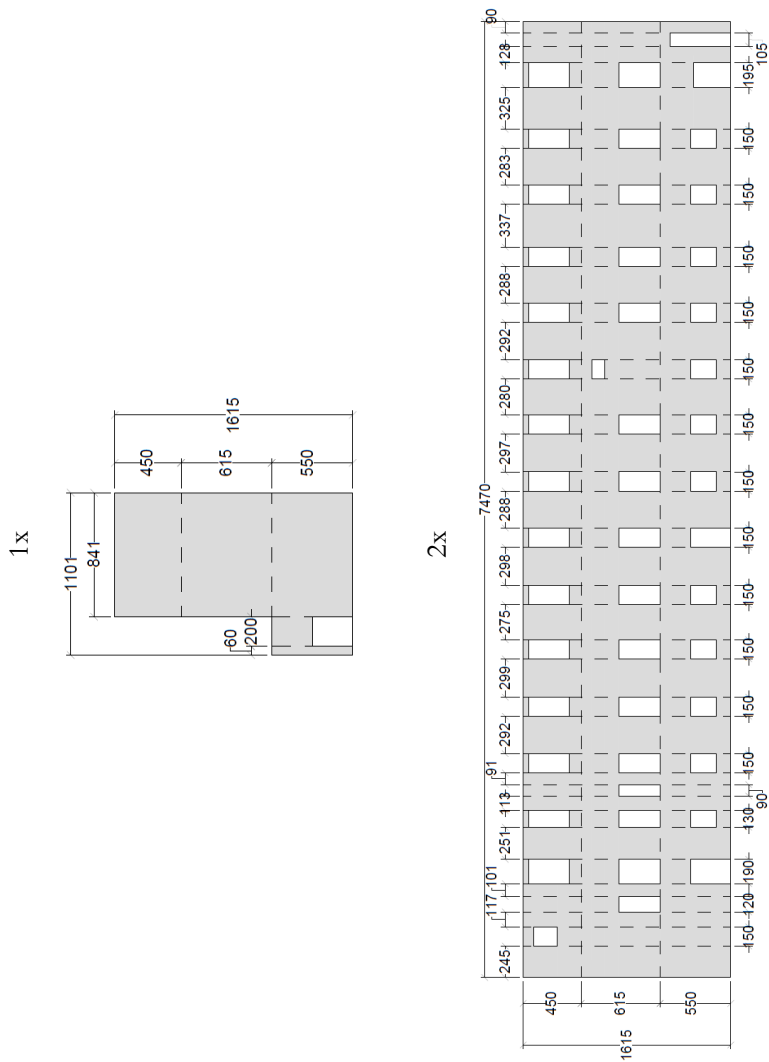


Figure A5.5. Analysed walls: San Domenico Maggiore – Construction 0.

SAN DOMENICO MAGGIORE - CONSTRUCTION 1



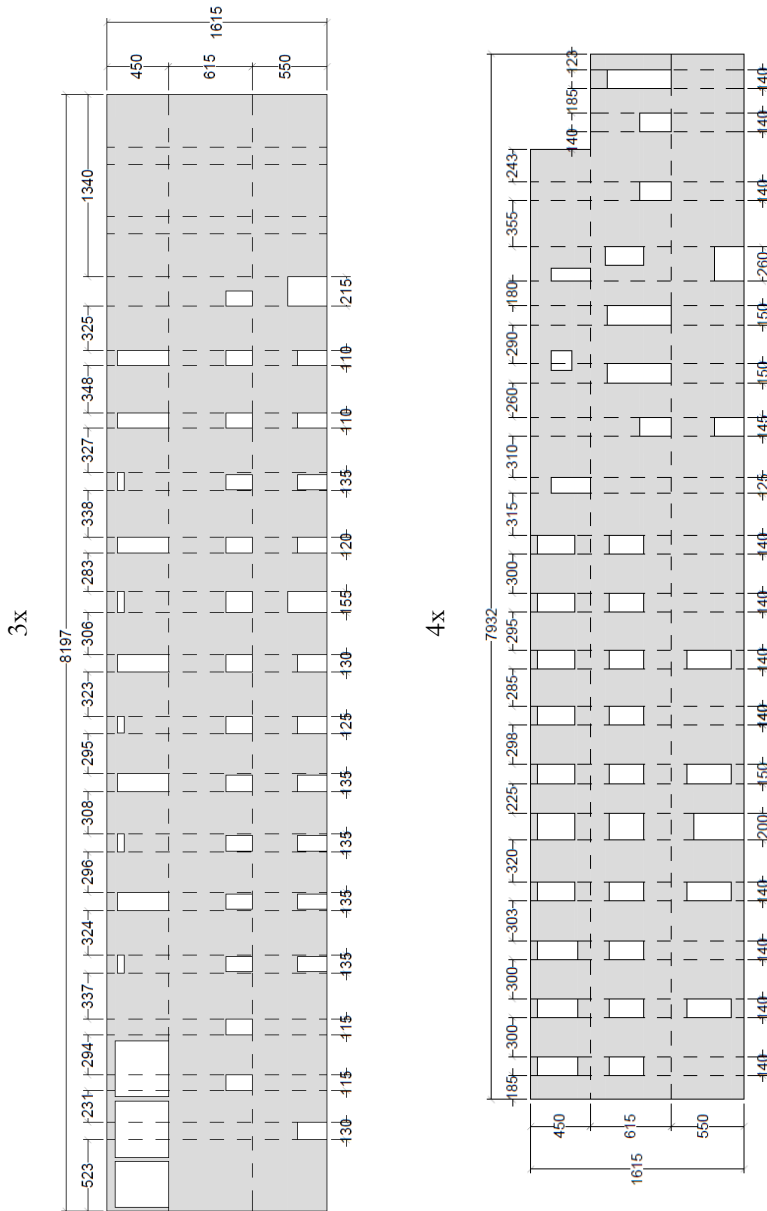
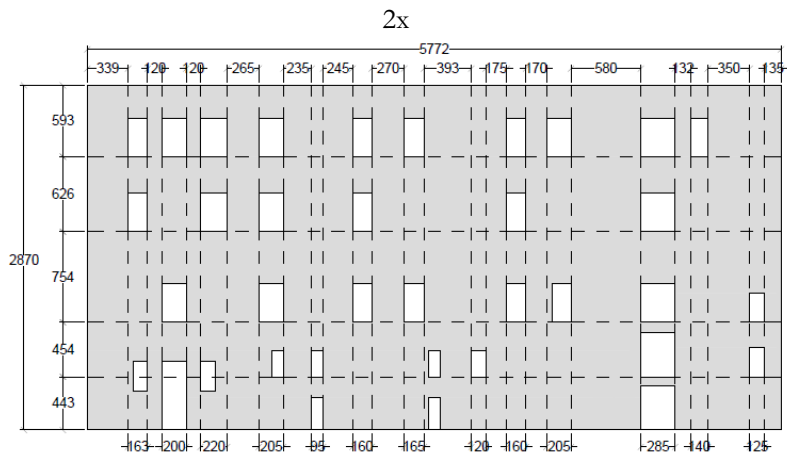
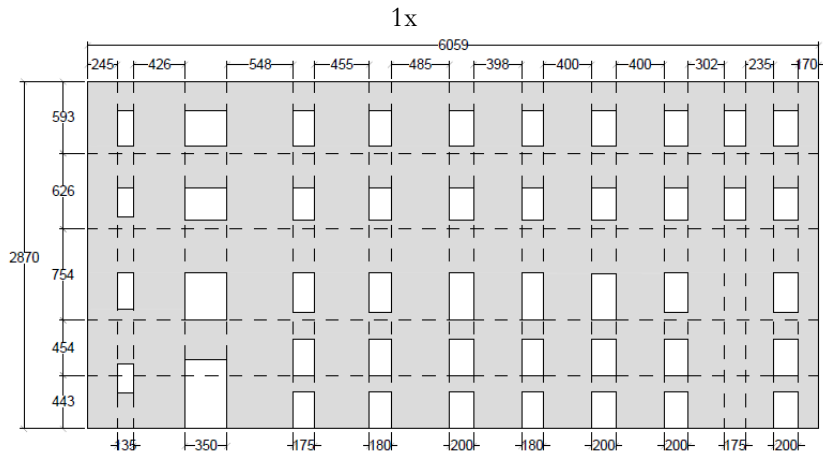


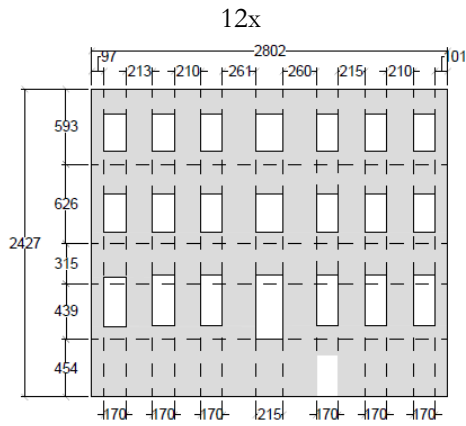
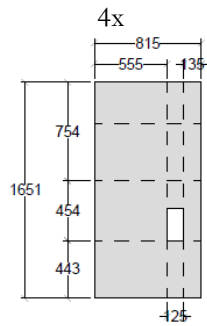
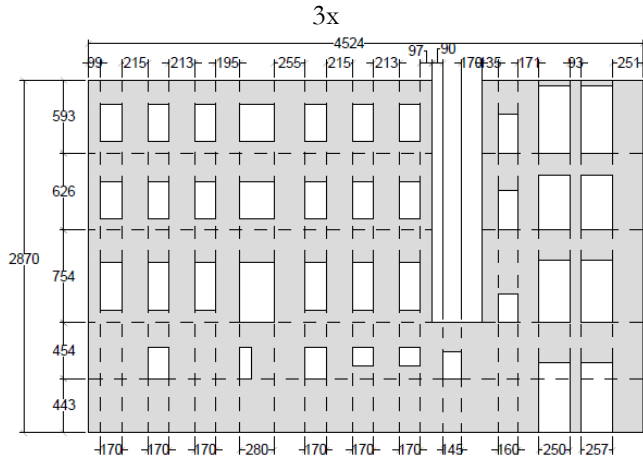
Figure A5.6. Analysed walls: San Domenico Maggiore – Construction 1.

The application of L.A. to check non-linear analysis through SAM method

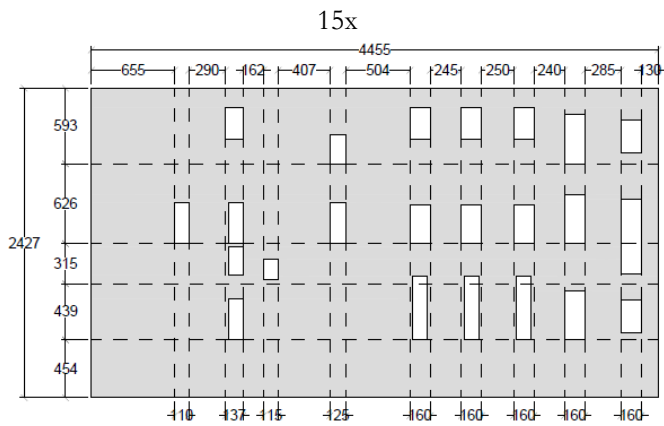
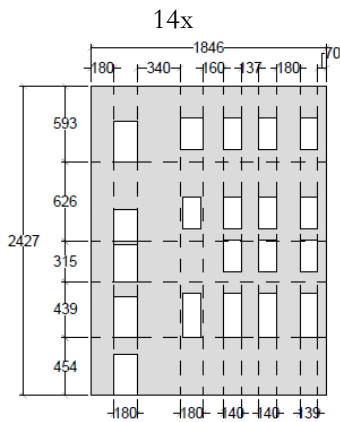
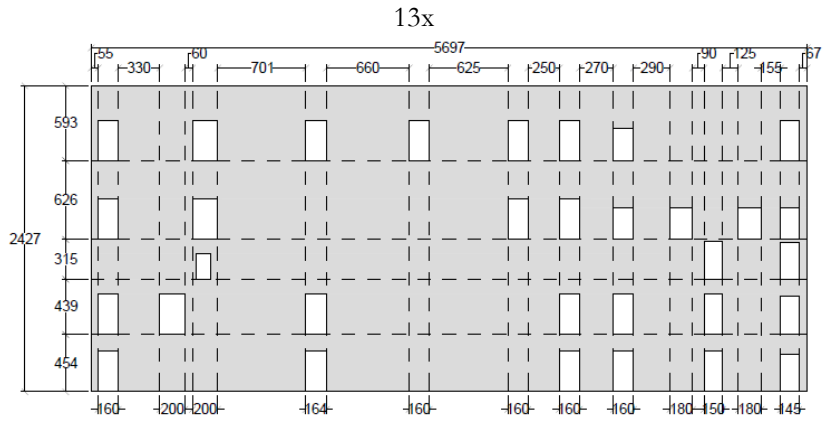
SAN CARLO ALL'ARENA



Appendix 5



The application of L.A. to check non-linear analysis through SAM method



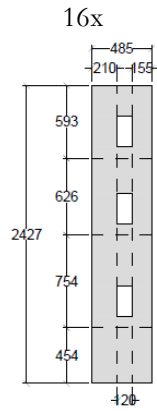
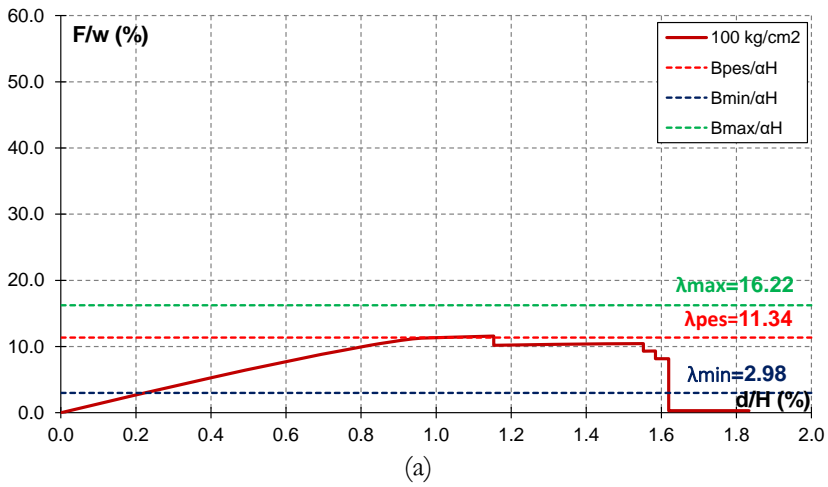
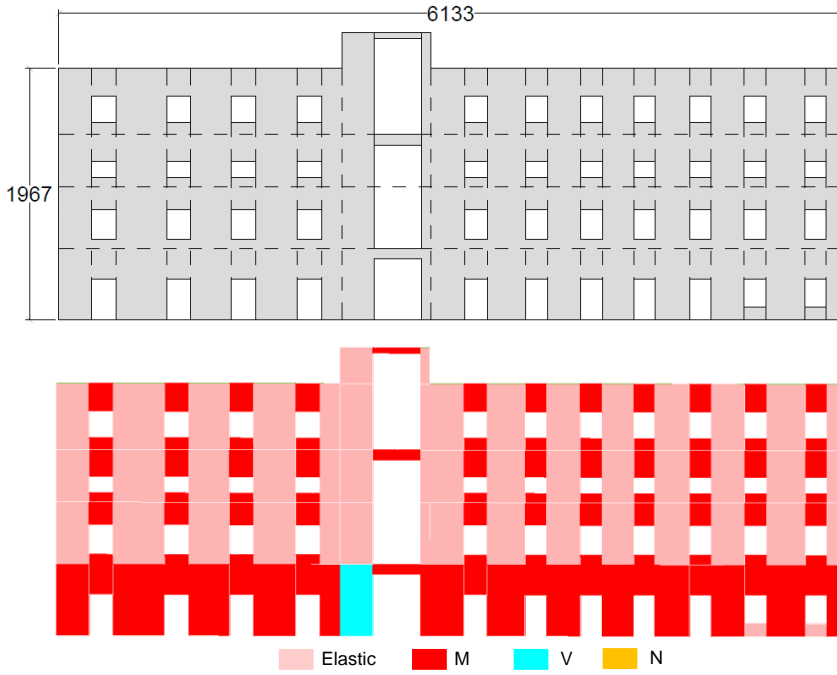
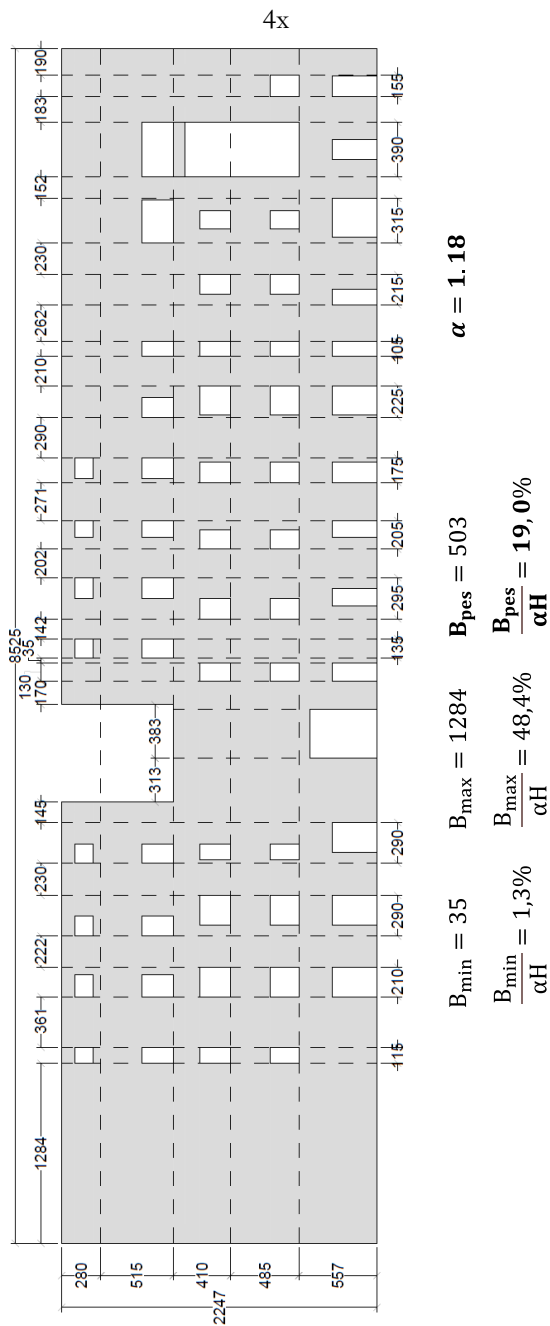
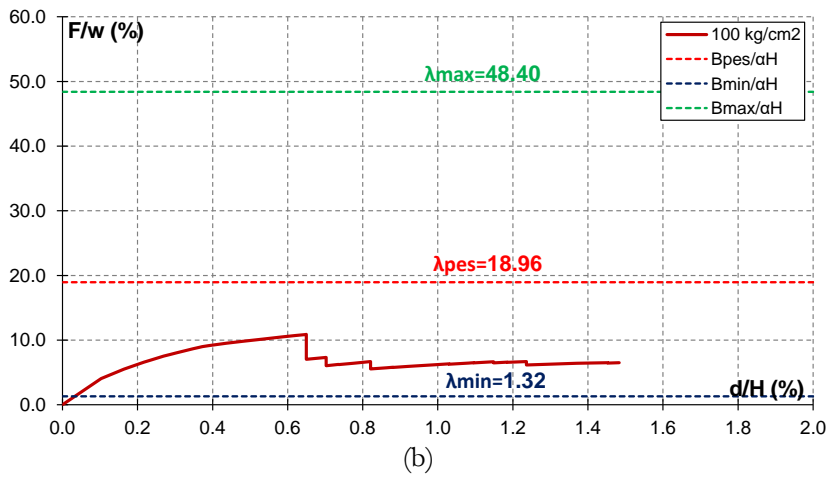
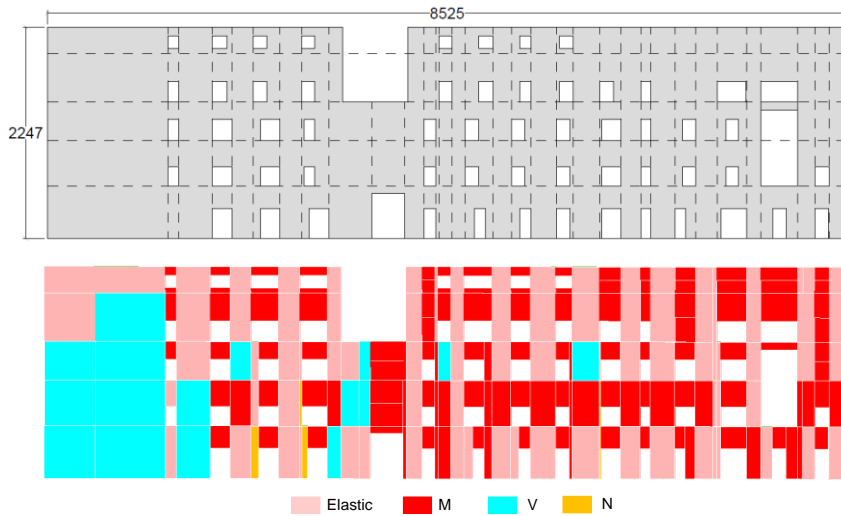


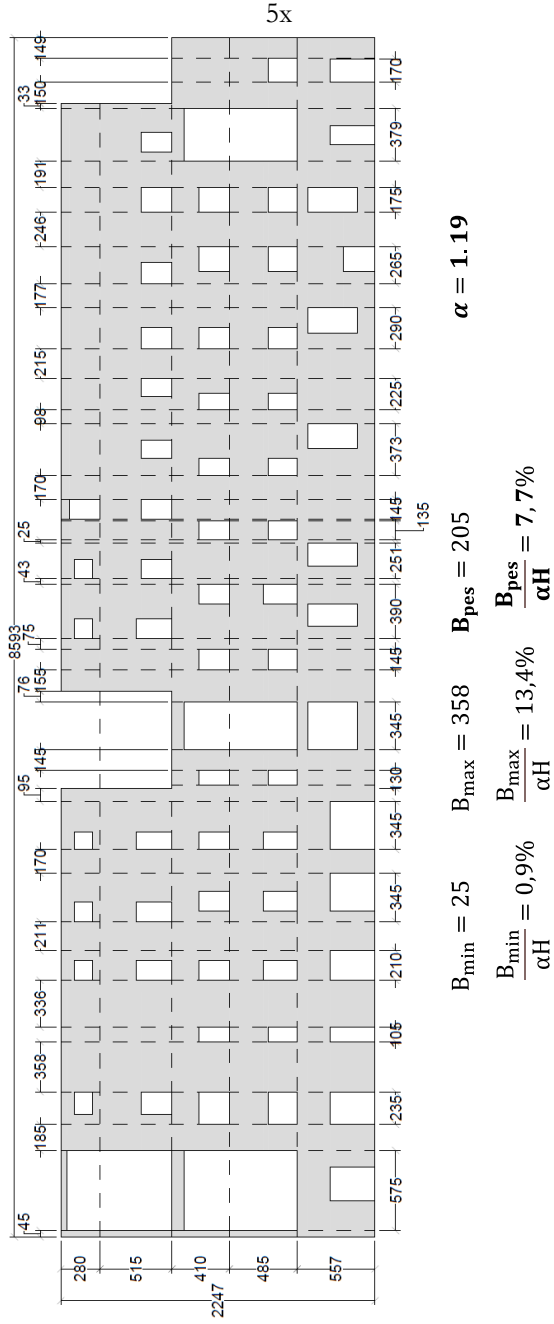
Figure A5.7. Analysed walls: San Carlo all’Arena.

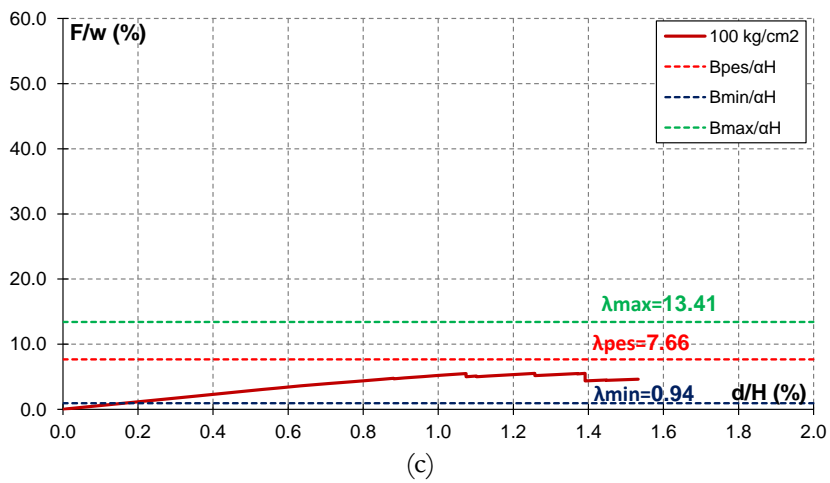
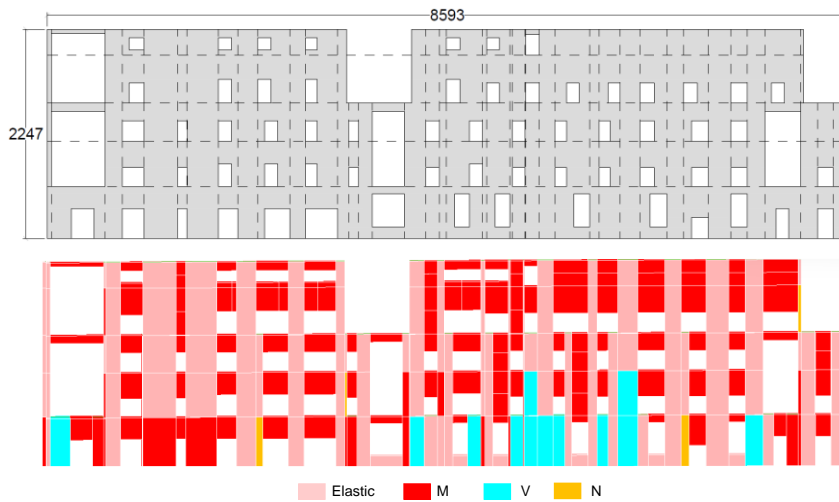


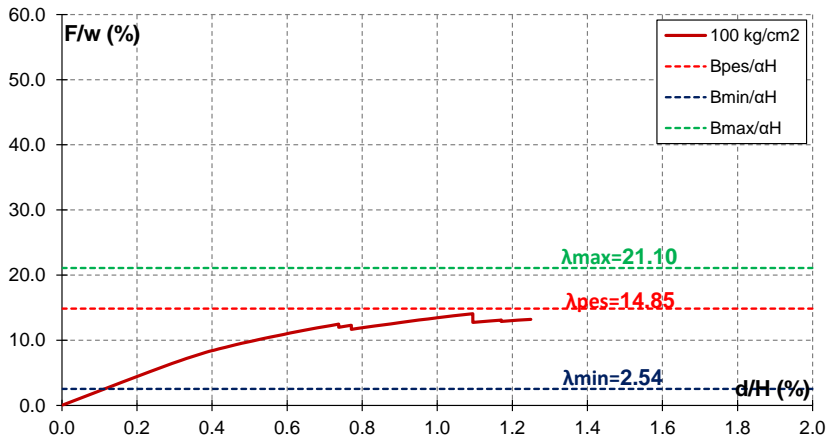
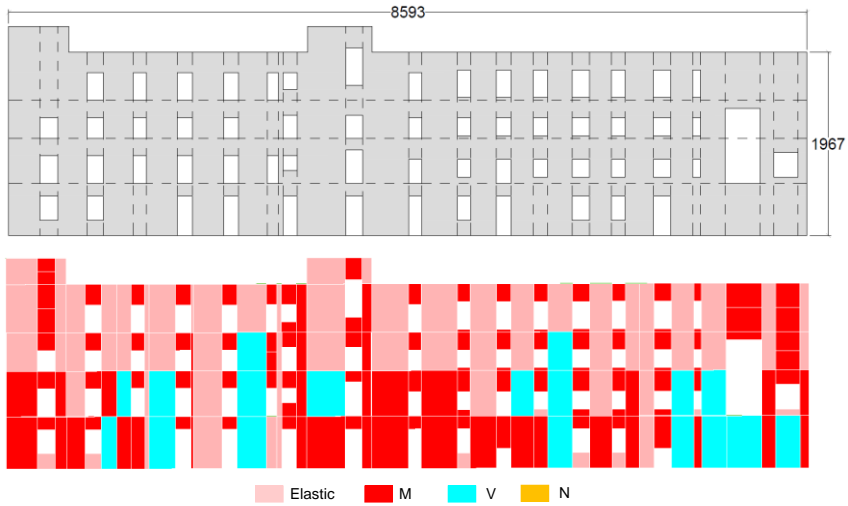


Appendix 5







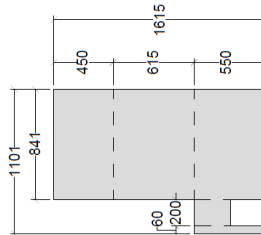


(d)

Figure A5.8. *Construction 0*. Pushover curves and comparison with the simplified formula (dashed red line), $B_{min}/\alpha H$ (dashed blue line) and $B_{max}/\alpha H$ (dashed green line): (a) 3x; (b) 4x; (c) 5x; (d) 6x.

SAN DOMENICO MAGGIORE - CONSTRUCTION 1

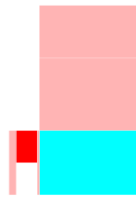
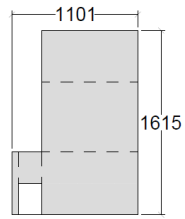
1x



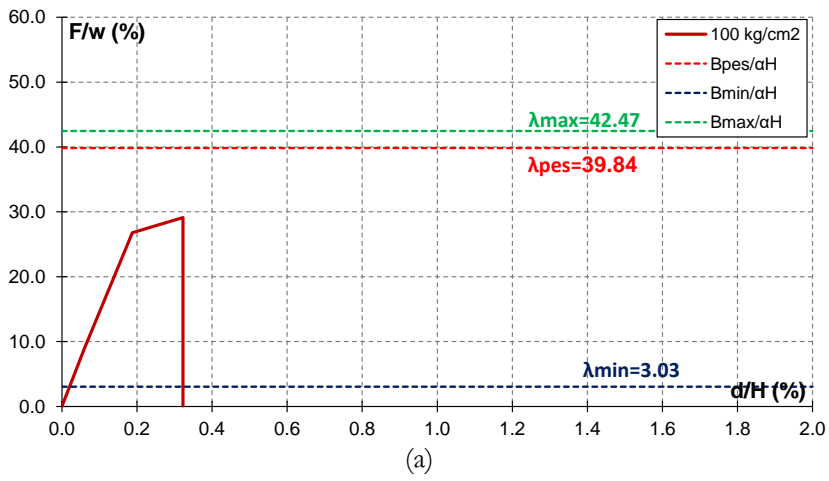
$$\alpha = 1.22$$

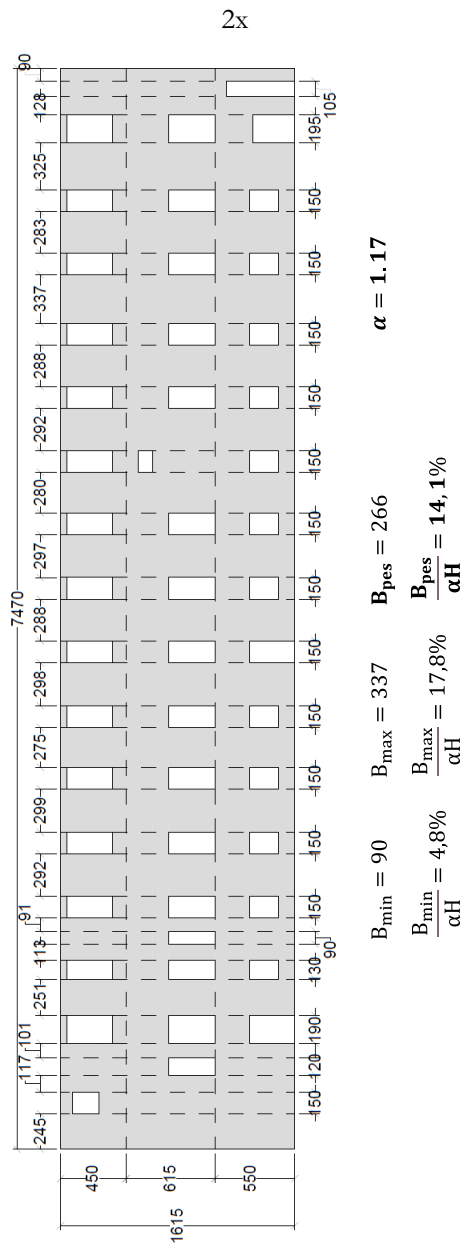
$$B_{\min} = 60 \quad B_{\max} = 840 \quad B_{\text{pes}} = 788$$

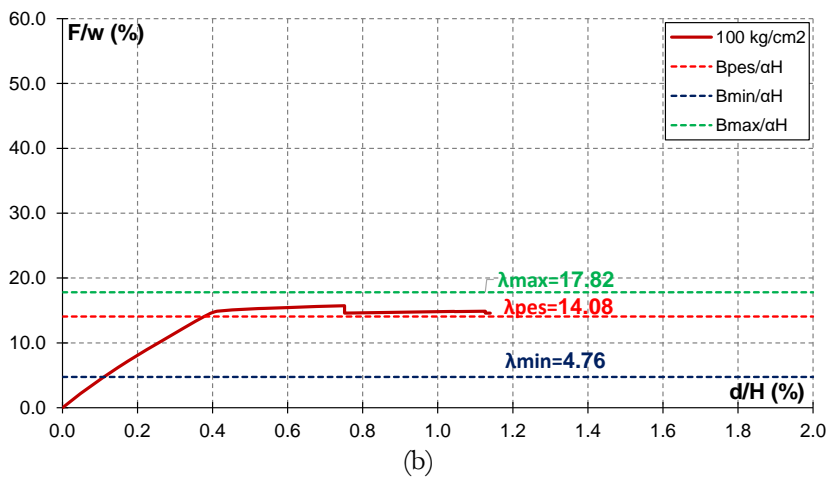
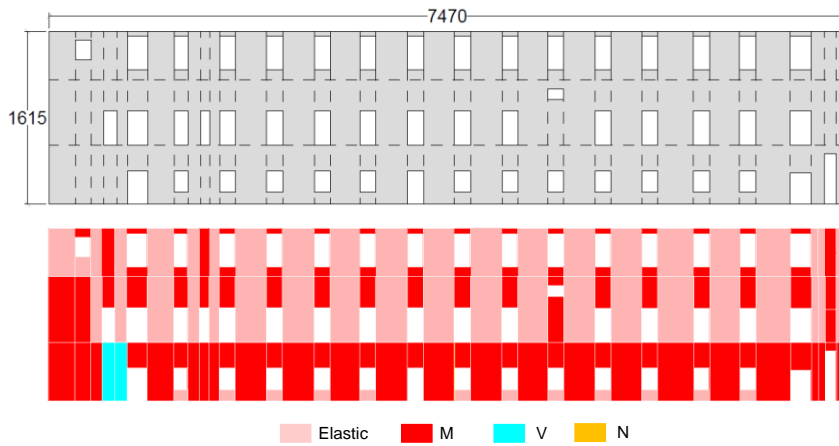
$$\frac{B_{\min}}{\alpha H} = 3,0\% \quad \frac{B_{\max}}{\alpha H} = 42,5\% \quad \frac{B_{\text{pes}}}{\alpha H} = 39,8\%$$

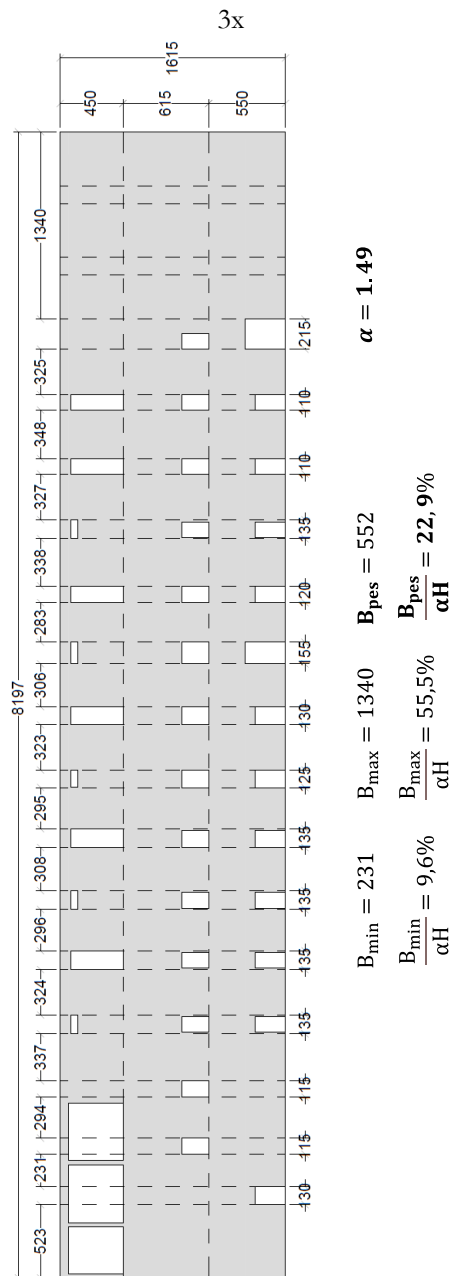


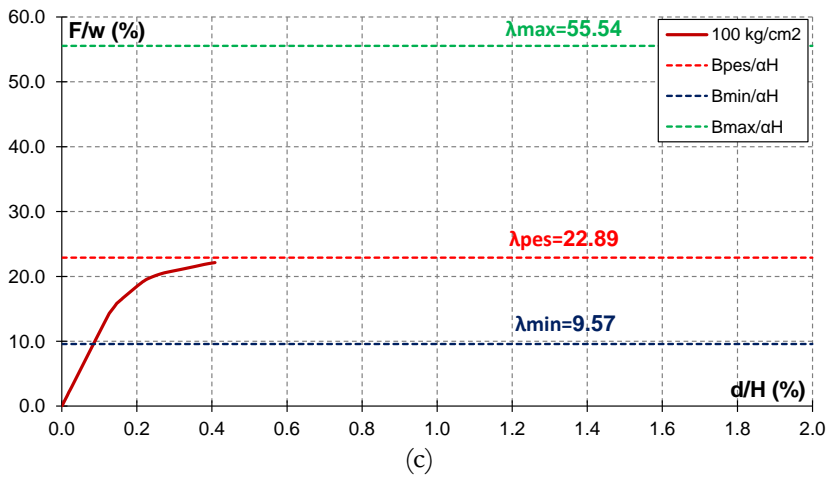
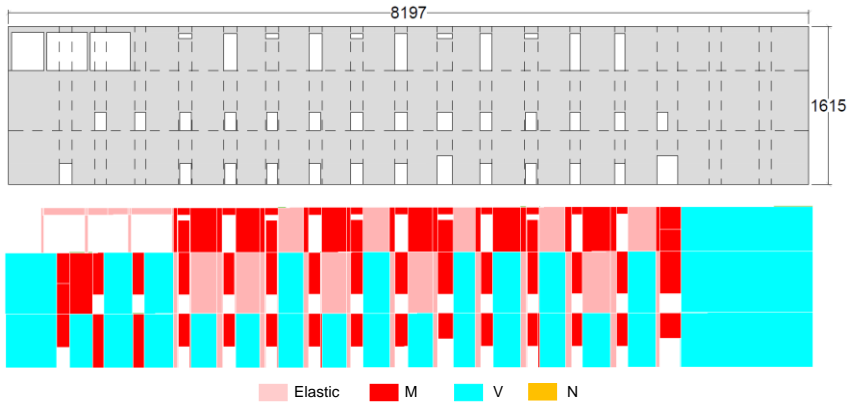
Elastic M V N

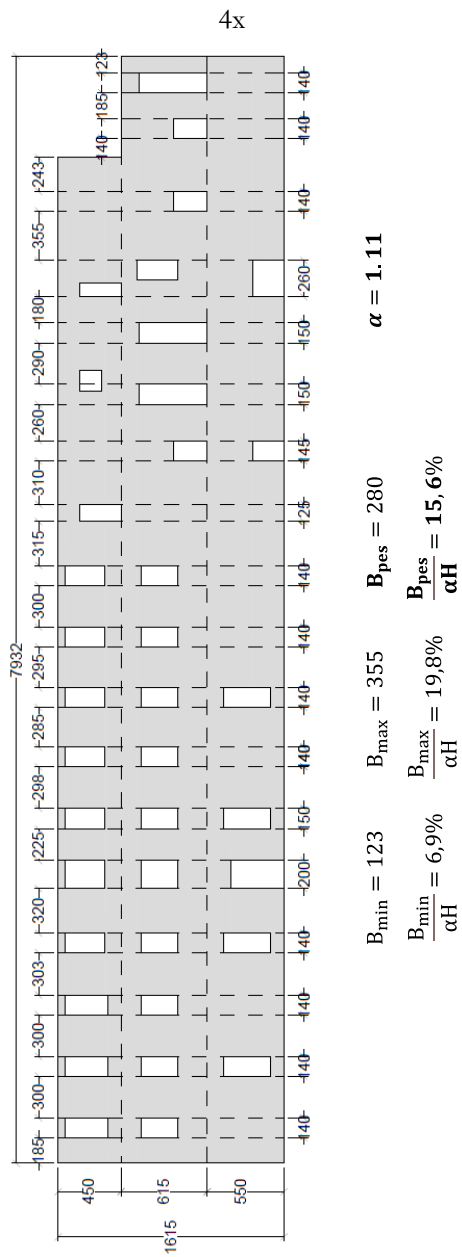












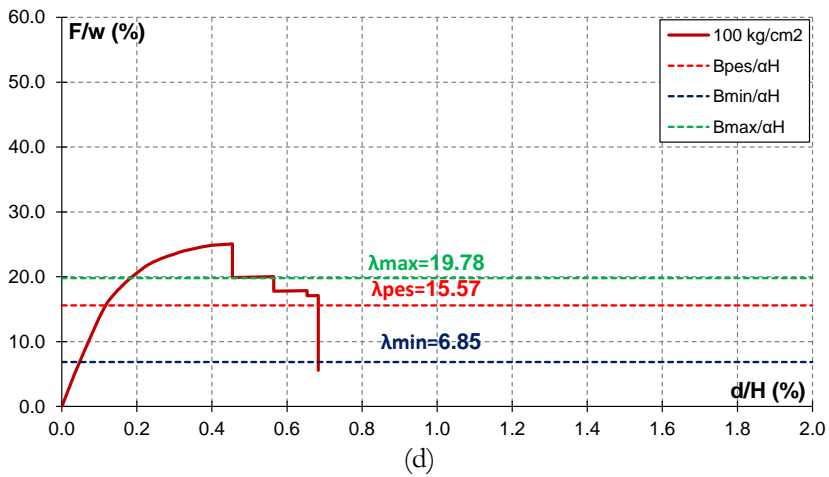
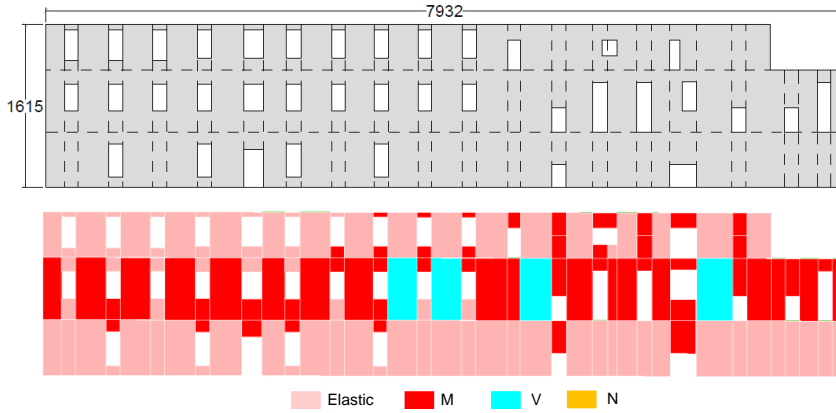
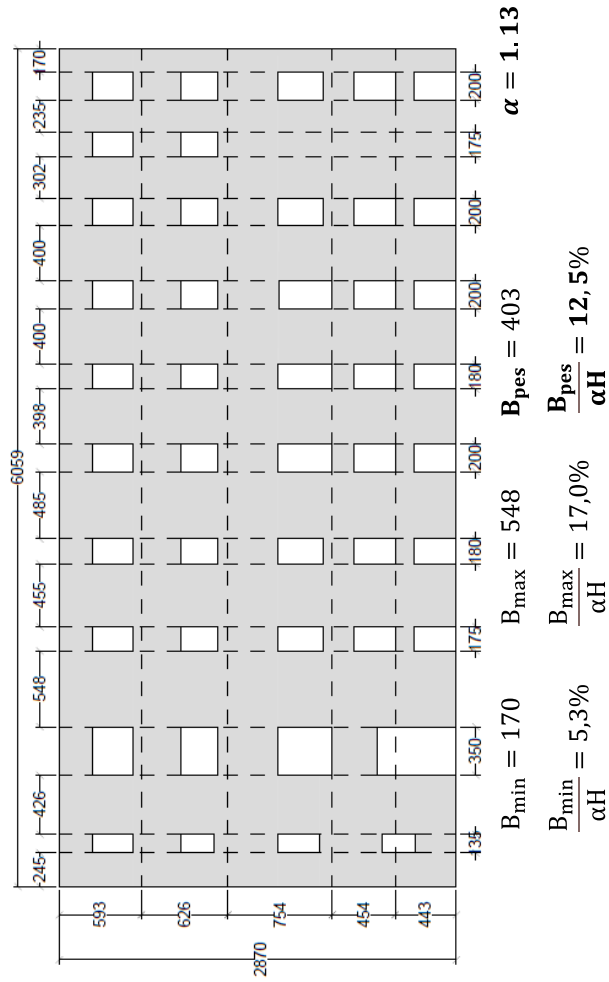
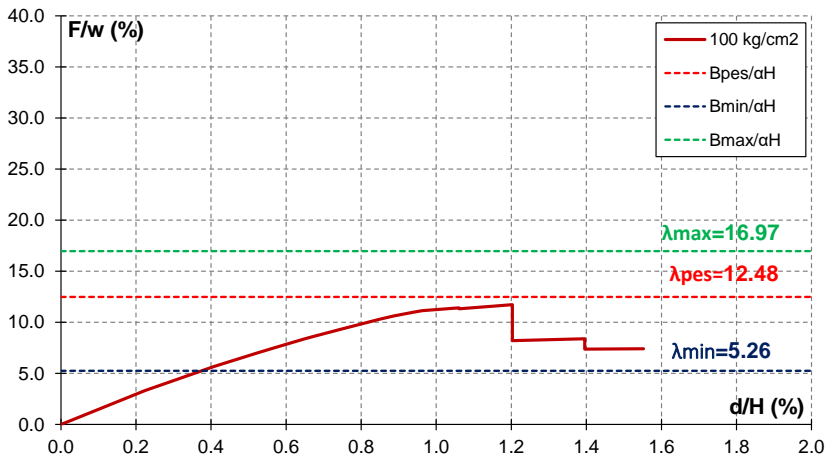
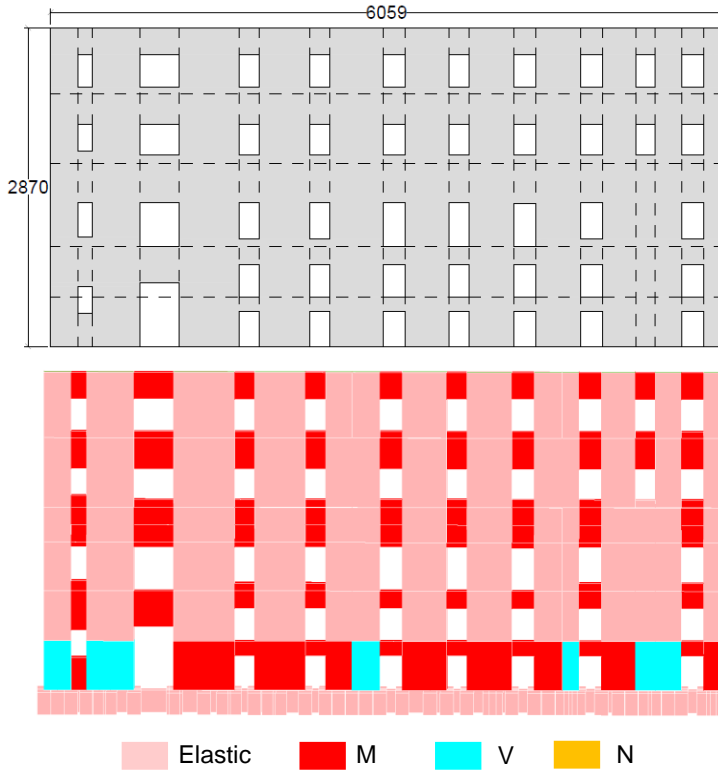


Figure A5.9. *Construction 1*. Pushover curves and comparison with the simplified formula (dashed red line), $B_{min}/\alpha H$ (dashed blue line) and $B_{max}/\alpha H$ (dashed green line): (a) 1x; (b) 2x; (c) 3x; (d) 4x.

SAN CARLO ALL'ARENA

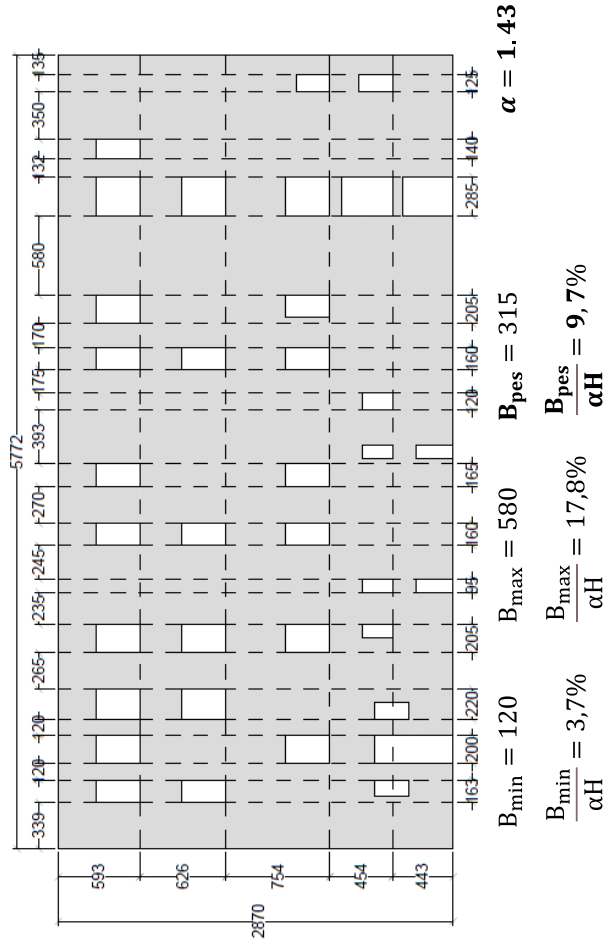
1x

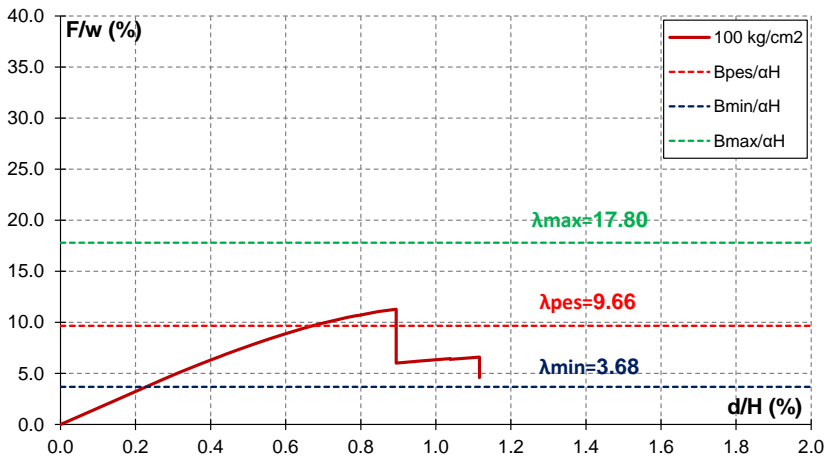
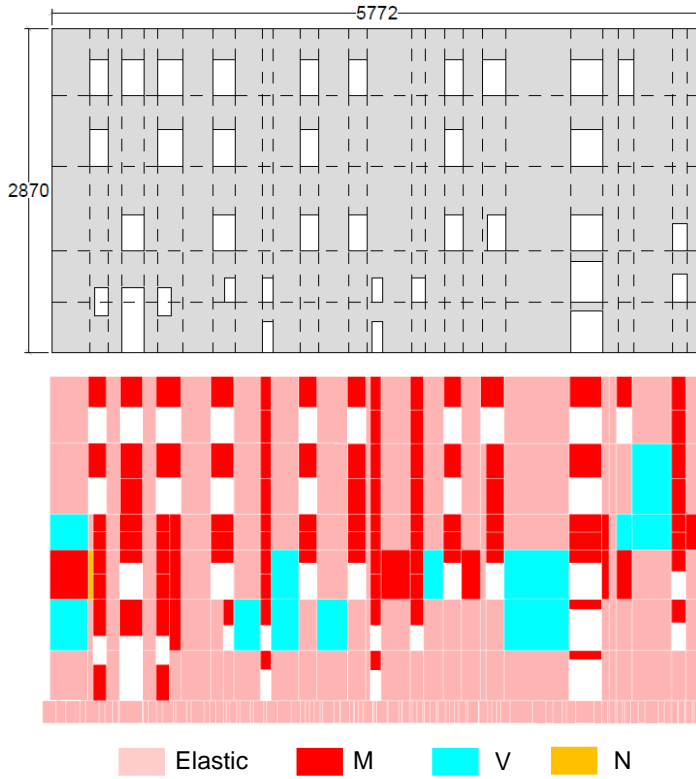




(a)

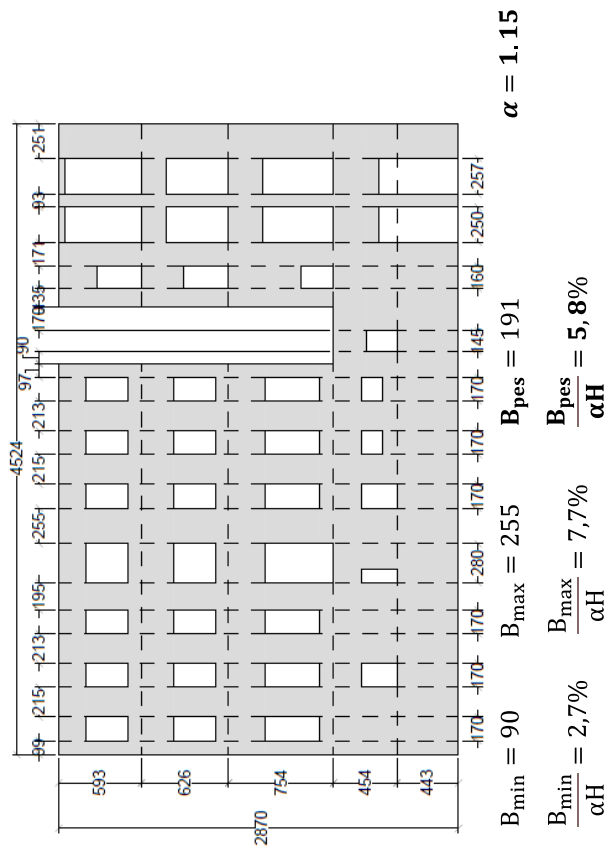
2x

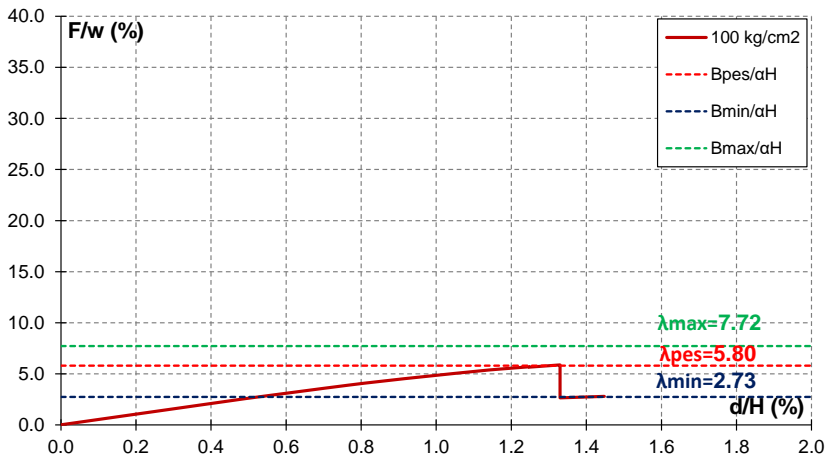




(b)

3x

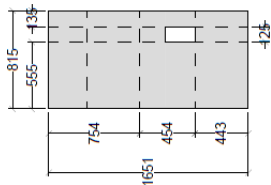




(c)

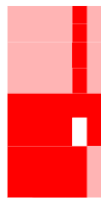
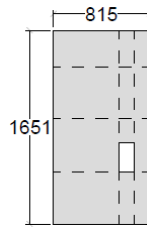
The application of L.A. to check non-linear analysis through SAM method

4x

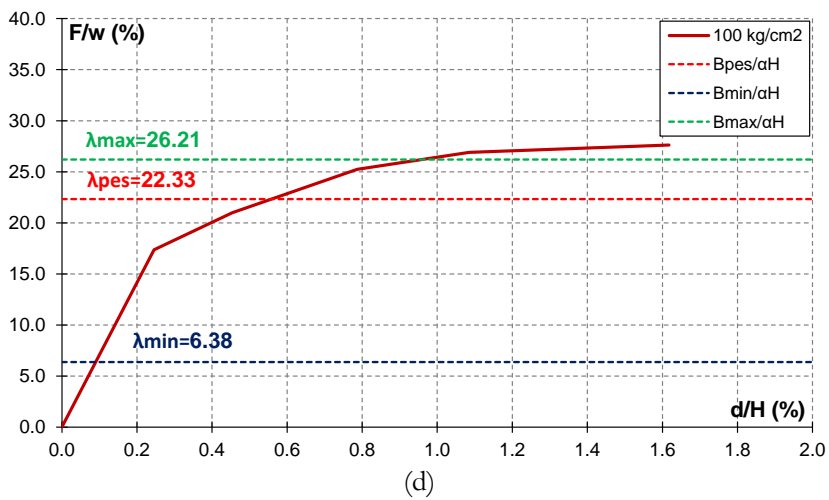


$$B_{\min} = 135 \quad B_{\max} = 555 \quad B_{\text{pes}} = 473 \quad \alpha = 1.28$$

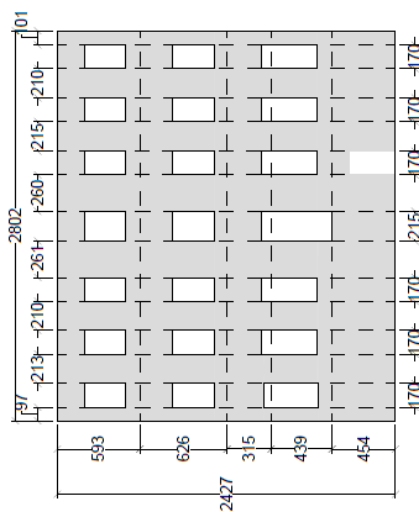
$$\frac{B_{\min}}{\alpha H} = 6,4\% \quad \frac{B_{\max}}{\alpha H} = 26,2\% \quad \frac{B_{\text{pes}}}{\alpha H} = 22,3\%$$



Elastic
 M
 V
 N



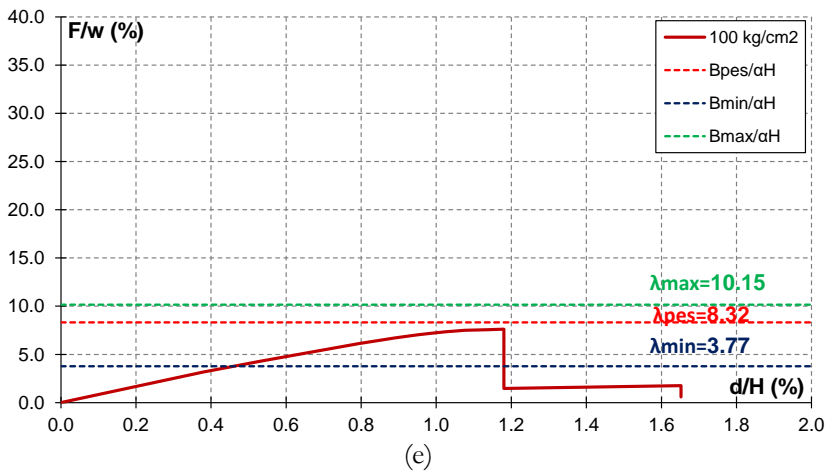
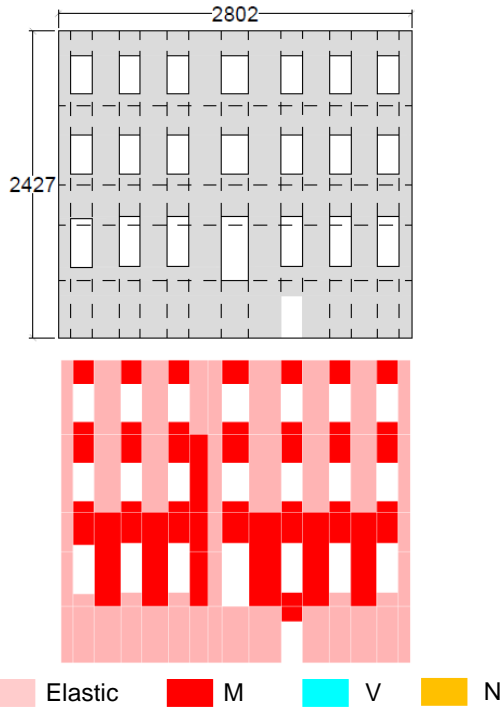
12x

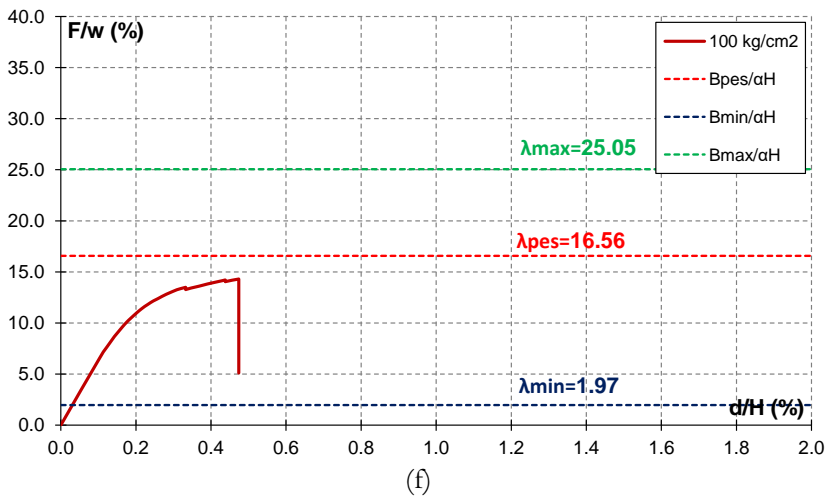
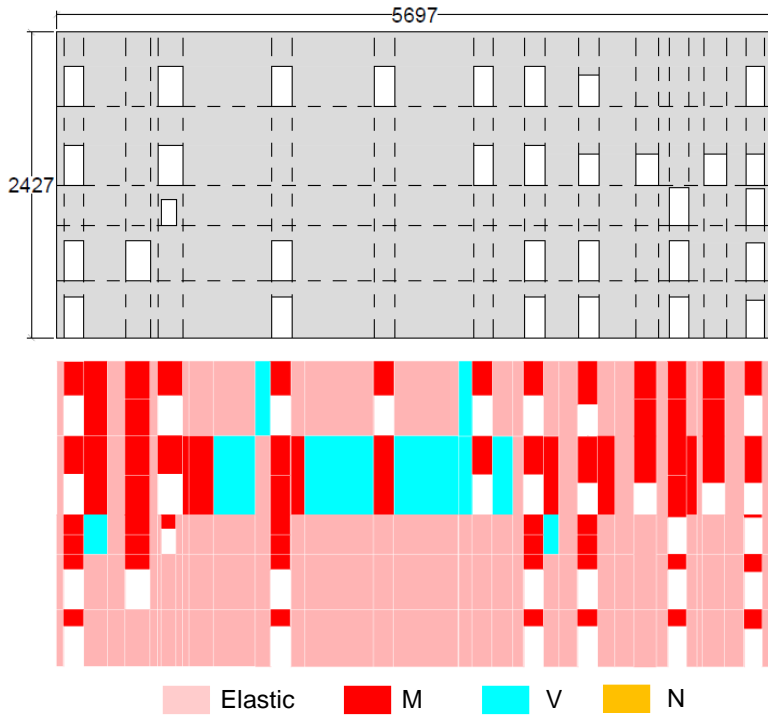


$$\alpha = 1.06$$

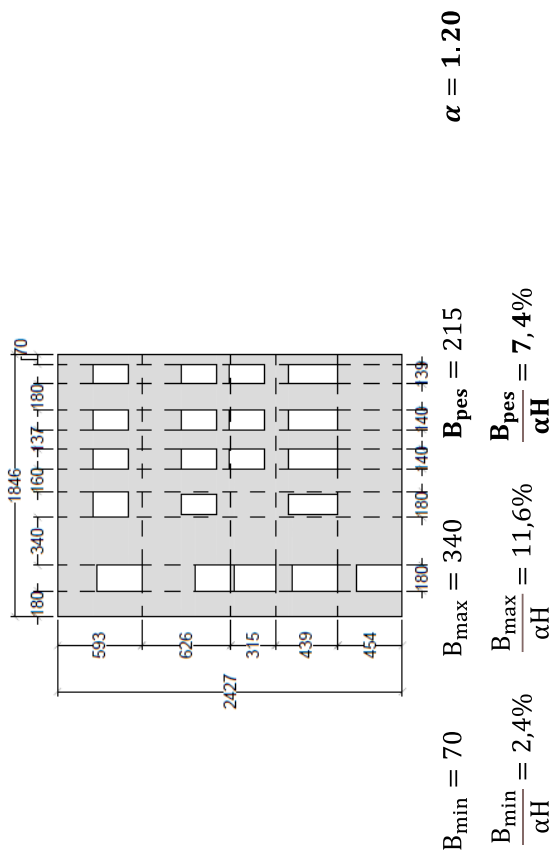
$$B_{\min} = 97 \quad B_{\max} = 261 \quad B_{\text{pes}} = 214$$

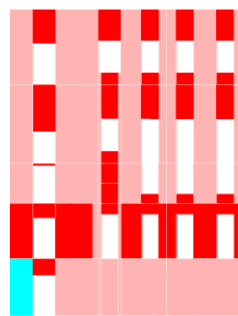
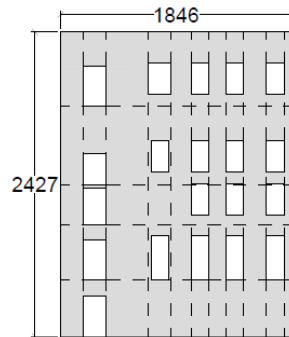
$$\frac{B_{\min}}{\alpha H} = 3,8\% \quad \frac{B_{\max}}{\alpha H} = 10,1\% \quad \frac{B_{\text{pes}}}{\alpha H} = 8,3\%$$



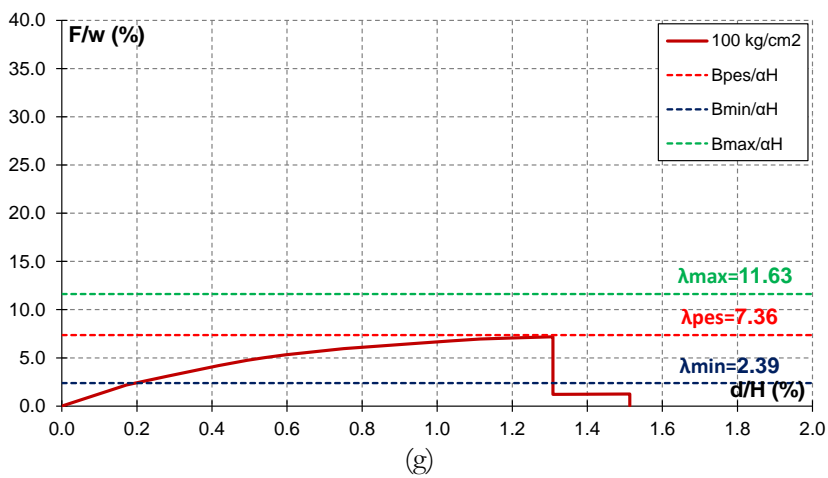


14x

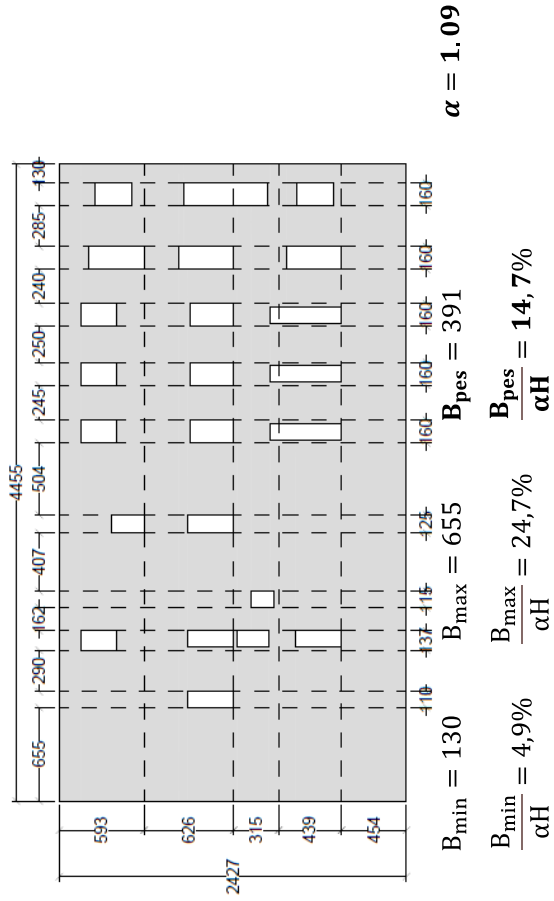


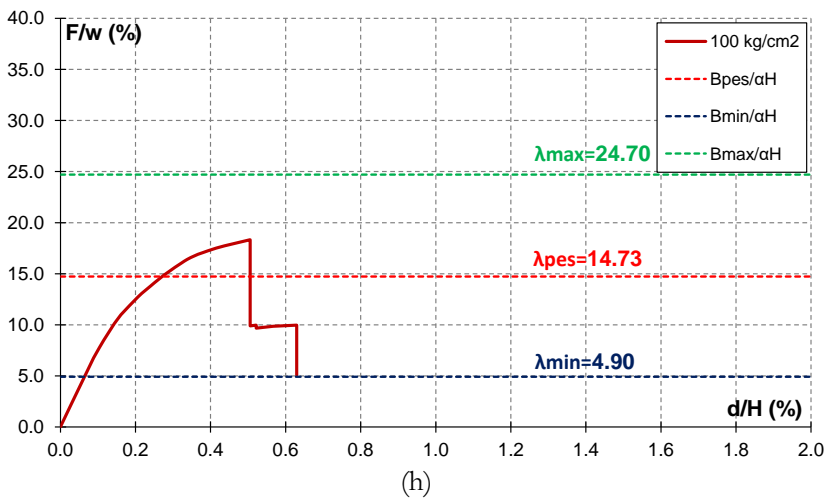
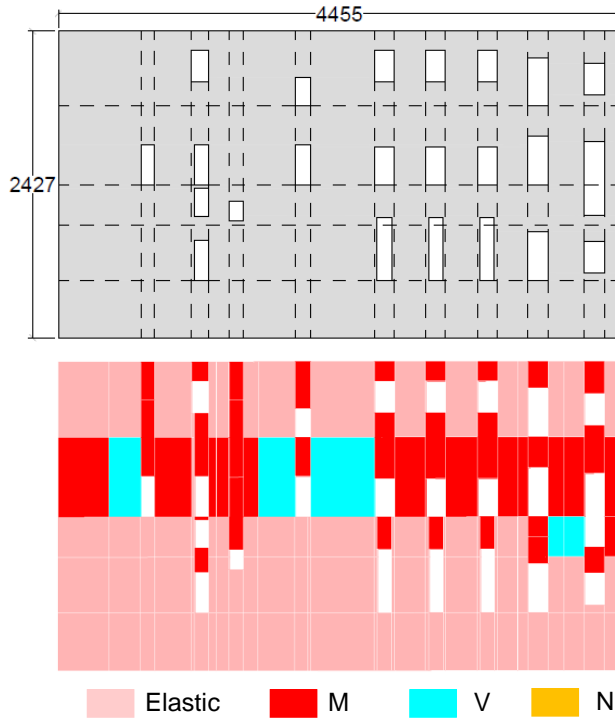


■ Elastic
 ■ M
 ■ V
 ■ N

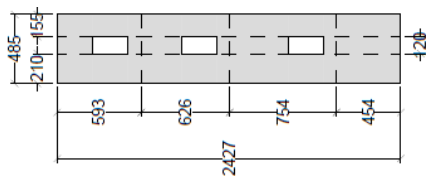


15x





16x



$$\alpha = 1.28$$

$$B_{pes} = 187$$

$$\frac{B_{pes}}{\alpha H} = 6,0\%$$

$$B_{max} = 210$$

$$\frac{B_{max}}{\alpha H} = 6,7\%$$

$$B_{min} = 155$$

$$\frac{B_{min}}{\alpha H} = 5,0\%$$

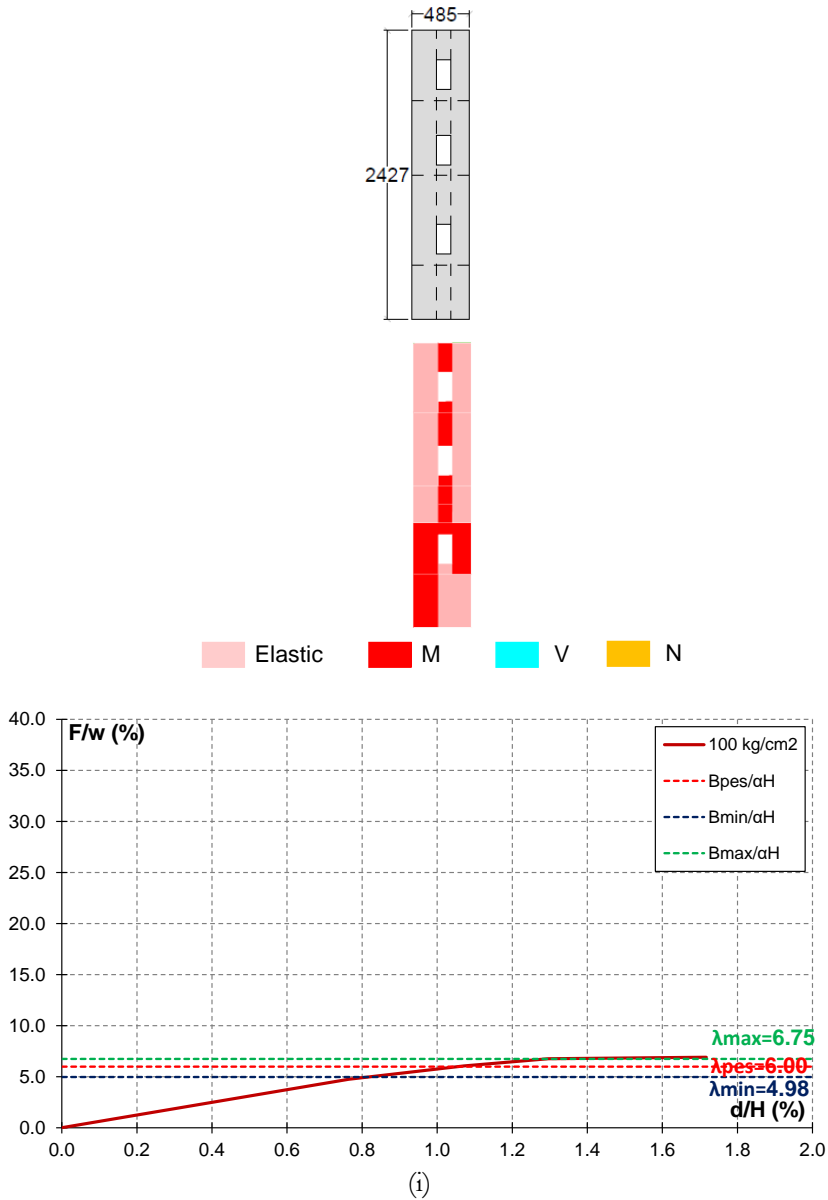


Figure A5.10. *San Carlo all' Arena*. Pushover curves and comparison with the simplified formula (dashed red line), $B_{\min}/\alpha H$ (dashed blue line) and $B_{\max}/\alpha H$ (dashed green line): (a) 1x; (b) 2x; (c) 3x; (d) 4x; (e) 12x; (f) 13x; (g) 14x; (h) 15x; (i) 16x.

Bibliography

- [1] Bianco, A., Foglia, O., Longobardi, G. (2016). Una lettura del palinsesto del convento sulla scorta dei recenti restauri. In: *La fabbrica di San Domenico Maggiore a Napoli*.
- [2] Bianco, A. (2012). Endoscopic analysis supporting issues of historic stratigraphic investigations: the case history of Saint Domenico Monastery in Naples-Italy. In *18th world conference on Nondestructive testing*.
- [3] Picone, R. (2016). Restauri e trasformazioni nel complesso domenicano di Napoli: dagli interventi del tardo Seicento ai ripristini ottocenteschi. In: *La fabbrica di San Domenico Maggiore a Napoli*.
- [4] Salerno, L. (1997). Il Convento di San Domenico Maggiore in Napoli.
- [5] Lumaga, B. Il restauro dello Studentato al secondo piano dell'Ala di San Tommaso del convento di San Domenico Maggiore in Napoli.
- [6] Foglia, O., Longobardi, G. (2016). I lavori di restauro e di rifunzionalizzazione. In: *La fabbrica di San Domenico Maggiore a Napoli*.
- [7] Italian ministry of infrastructures and transportations (2018). Nuove Norme tecniche per le costruzioni?. Decreto 17 Gennaio 2018 [in Italian].
- [8] Breymann, GA (1885). Trattato di Costruzioni civili. Archi, volte, cupole. Roma: Editrice Librerie Dedalo; 2003 [in Italian].
- [9] Rondelet, J. (1802). *Traite theorique et pratique de l'art de batir: Avec atlas de planches* (Vol. 1). L'auteur.
- [10] Cavalieri – San Bertolo N. (1839) Istituzioni di architettura statica e idraulica, Firenze: Batelli.
- [11] Colombo, G. (1877). *Manuale dell'ingegnere civile e industriale*. Hoepli.
- [12] Lourenço, P. B., & Roque, J. A. (2006). Simplified indexes for the seismic vulnerability of ancient masonry buildings. *Construction and Building Materials*, 20(4), 200-208.
- [13] Code, P. (2005). Eurocode 8: Design of structures for earthquake resistance-part 1: general rules, seismic actions and rules for buildings. *Brussels: European Committee for Standardization*.

- [14] Parisi, F., & Augenti, N. (2013). Seismic capacity of irregular unreinforced masonry walls with openings. *Earthquake Engineering & Structural Dynamics*, 42(1), 101-121.
- [15] Formenti, C. (1893). *La pratica del fabbricare*. Hoepli.
- [16] Méry, E. (1840). Sur l'équilibre des voûtes en berceau. *Annales des Ponts et Chaussées*, 19 (I Sem.), 50-70.
- [17] Heyman, J. (1982). The Masonry Arch.
- [18] Asteris, P. G., Sarhosis, V., Mohebkah, A., Plevris, V., Papaloizou, L., Komodromos, P., & Lemos, J. V. (2015). Numerical modeling of historic masonry structures. In *Handbook of research on seismic assessment and rehabilitation of historic structures* (pp. 213-256). IGI Global.
- [19] Lourenço, P. B. (2002). Computations on historic masonry structures. *Progress in Structural Engineering and Materials*, 4(3), 301-319.
- [20] Lagomarsino, S., Penna, A., Galasco, A., & Cattari, S. (2013). TREMURI program: an equivalent frame model for the nonlinear seismic analysis of masonry buildings. *Engineering structures*, 56, 1787-1799.
- [21] Como, M., Grimaldi, A. (1985). An unilateral Model for the Limit Analysis of Masonry Walls. In G. Del Piero & F. Maceri (Eds.), *International Congress On Unilateral Problems in Structural Analysis, CISM Courses and Lectures* (Vol. 288, pp. 25-45). Berlin: Springer.
- [22] Abruzzese, D., Como, M., Lanni, G. (1992). On the lateral strength of multistory masonry walls with openings and horizontal reinforcing connections. In *Earthquake Engineering, tenth world conference, Balkema-Rotterdam*.
- [23] Heyman J. (1966). The stone skeleton. *Int J Solids Struct* 1966;2:249-79.
- [24] Heyman J. (1995). The Stone Skeleton. *Structural Engineering of masonry*.
- [25] Roca, P., Cervera, M., Gariup, G., & Pela', L. (2010). Structural analysis of masonry historical constructions. Classical and advanced approaches. *Archives of computational methods in engineering*, 17, 299-325.
- [26] Calderoni, B., Cordasco, E. A., Lenza, P., & Pacella, G. (2011). A simplified theoretical model for the evaluation of structural behaviour of masonry spandrels. *International Journal of Materials and Structural Integrity*, 5(2-3), 192-214.
- [27] Bucchi, F., Arangio, S., & Bontempi, F. (2013, September). Seismic assessment of an historical masonry building using

- nonlinear static analysis. In *Proceedings of the 14th International Conference on Civil, Structural and Environmental Engineering Computing, Sardinia, Italy* (Vol. 36).
- [28] Tomazevic, M. (1978). The computer program POR, Report ZMRK, Institute for Testing and Research in Materials and Structures, Ljubljana, Slovenia.
- [29] Braga, F., & Dolce, M. (1982). Un metodo per l'analisi di edifici multipiano in muratura antisismici. *Proc. 6th IB Ma. C.*
- [30] Dolce, M.: Schematizzazione e modellazione degli edifici in muratura soggetti ad azioni sismiche. *L'Industria delle Costruzioni* **25**, 44–57 (1991). (in Italian)
- [31] Calderoni, B., Marone, P., & Pagano, M. (1987). Modelli per la verifica statica degli edifici in muratura in zona sismica.
- [32] Magenes, G., & Calvi, G. M. (1997). In-plane seismic response of brick masonry walls. *Earthquake engineering & structural dynamics*, *26*(11), 1091-1112.
- [33] Magenes, G., & Fontana, A. D. (1998, October). Simplified nonlinear seismic analysis of masonry buildings. In *Proc. Br. Masonry Soc. No. 8* (pp. 190-195).
- [34] Braga, F., & Liberatore, D. (1990, June). A finite element for the analysis of the response of masonry buildings. In *Proceedings of 5th North American masonry conference*.
- [35] D'Asdia, P., & Viskovic, A. (1995). Analyses of a masonry wall subjected to horizontal actions on its plane, employing a nonlinear procedure using changing shape finite elements. *WIT Transactions on Modelling and Simulation*, *12*.
- [36] Gambarotta, L., & Lagomarsino, S. (1996). Sulla risposta dinamica di pareti in muratura. *La meccanica delle murature tra teoria e progetto, Atti del Convegno Nazionale, Messina*, 18-20.
- [37] Gambarotta, L., & Lagomarsino, S. (1997). Damage models for the seismic response of brick masonry shear walls. Part I: the mortar joint model and its applications. *Earthquake engineering & structural dynamics*, *26*(4), 423-439.
- [38] Gambarotta, L., & Lagomarsino, S. (1997). Damage models for the seismic response of brick masonry shear walls. Part II: the continuum model and its applications. *Earthquake engineering & structural dynamics*, *26*(4), 441-462.
- [39] Caliò, I., Marletta, M., & Pantò, B. (2012). A new discrete element model for the evaluation of the seismic behaviour of unreinforced masonry buildings. *Engineering Structures*, *40*, 327-338.

- [40] S.T.S. S.r.l., (2022) Manuale d'uso. CDSWin + CDMaWin Strutture in c.a., acciaio, legno e muratura.
- [41] Dolce, M. (1989). *Schematizzazione e modellazione per azioni nel piano delle Pareti*. Ordine degli Ingegneri della Prov. di Potenza.
- [42] Como, M., & Grimaldi, A. (1983). *Analisi limite di pareti murarie sotto spinta*. Quaderni di Teoria e Tecnica delle Strutture, Università di Napoli, Istituto di Tecnica delle Costruzioni, Napoli.
- [43] Giordano, A., De Luca, A., Mele, E., & Romano, A. (2007). A simple formula for predicting the horizontal capacity of masonry portal frames. *Engineering structures*, 29(9), 2109-2123.
- [44] Brandonisio, G., De Luca, A., & Mele, E. (2009). Horizontal capacity of masonry portal frames under different loading conditions. In *Protection of Historical Buildings* (Vol. 2, pp. 1121-1126).
- [45] Giordano, A., De Luca, A., Cuomo, G., Mele, E., & Romano, A. (2006). Limit analysis of multiple span masonry portal frames. In *Possibilities of Numerical and Experimental Techniques* (pp. 1059-1066).
- [46] Lucibello (2013). Capacità sismica degli edifici in muratura. Doctoral Thesis.
- [47] Mazziotti (2015). Structural analysis of historical masonry buildings. Doctoral Thesis
- [48] Fajfar, P. (2021). The Story of the N2 Method. IAEE Monograph, Vol. 2. International Association for Earthquake Engineering.
- [49] Fajfar P., Fischinger M. (1987). Non-linear seismic analysis of RC buildings: Implications of a case study. *European Earthquake Engineering* 1(1):31-43.
- [50] Fajfar, P., & Fischinger, M. (1989). N2-A method for non-linear seismic analysis of regular buildings. In *Proceedings of the ninth world conference in earthquake engineering* (Vol. 5, pp. 111-116).
- [51] Saiidi, M., & Sozen, M. A. (1981). Simple nonlinear seismic analysis of R/C structures. *Journal of the Structural Division*, 107(5), 937-953.
- [52] Fajfar, P., & Gašperšič, P. (1996). The N2 method for the seismic damage analysis of RC buildings. *Earthquake engineering & structural dynamics*, 25(1), 31-46.
- [53] Kilar, V., & Fajfar, P. (1997). Simple push-over analysis of asymmetric buildings. *Earthquake engineering & structural dynamics*, 26(2), 233-249.

- [54] Fajfar, P., & Krawinkler, H. (eds.) (1997). Seismic design methodologies for the next generation of codes. In *Proceedings of the International Workshop on Seismic Design Methodologies for the Next Generation of Codes*, Bled, Slovenia, 24-27 June 1997. A. A. Balkema: Rotterdam, Brookfield.
- [55] Fajfar, P., & Gaspersic, P. (1998). A simplified nonlinear method for seismic evaluation of RC bridges [C]. Pro. In *6th US National Conference On Earthquake Engineering, Seattle, CD-ROM, EERI, Oakland*.
- [56] Fajfar, P. (1999). Capacity spectrum method based on inelastic demand spectra. *Earthquake Engineering & Structural Dynamics*, 28(9), 979-993.
- [57] Fajfar, P. (2000). A nonlinear analysis method for performance-based seismic design. *Earthquake spectra*, 16(3), 573-592.
- [58] Fajfar, P. (2002). Structural analysis in earthquake engineering—a breakthrough of simplified non-linear methods. In *12th European conference on earthquake engineering*.
- [59] Fajfar, P., Marušić, D., & Peruš, I. (2005). Torsional effects in the pushover-based seismic analysis of buildings. *Journal of earthquake engineering*, 9(06), 831-854.
- [60] Kreslin, M., & Fajfar, P. (2011). The extended N2 method taking into account higher mode effects in elevation. *Earthquake engineering & structural dynamics*, 40(14), 1571-1589.
- [61] Kreslin, M., & Fajfar, P. (2012). The extended N2 method considering higher mode effects in both plan and elevation. *Bulletin of Earthquake Engineering*, 10, 695-715.
- [62] Sorrentino, P., Brandonisio, G., & De Luca, A. (2022). Complex monumental buildings. Definition of complexities and structural implications. *Procedia Structural Integrity*, 44, 1664-1671.
- [63] Polcari, M. (2018). Il nodo, l'ordito, la trama. Breve nota per un inquadramento storico-urbanistico. In: Maio, Crovato, Palumbo (a cura di), "Atti di Convegno 7 maggio 2016. Dall'antico istituto di incoraggiamento all'istituto tecnico G.B. Della Porta" (2018).